

Jorun I. Marvik

# Fault Localization in Medium Voltage Distribution Networks with Distributed Generation

Thesis for the degree of Philosophiae Doctor

Trondheim, June 2011

Norwegian University of Science and Technology  
Faculty of Information Technology, Mathematics  
and Electrical Engineering  
Department of Electric Power Engineering



**NTNU – Trondheim**  
Norwegian University of  
Science and Technology

**NTNU**

Norwegian University of Science and Technology

Thesis for the degree of Philosophiae Doctor

Faculty of Information Technology, Mathematics and Electrical Engineering  
Department of Electric Power Engineering

© Jorun I. Marvik

ISBN 978-82-471-2913-5 (printed ver.)

ISBN 978-82-471-2914-2 (electronic ver.)

ISSN 1503-8181

Doctoral theses at NTNU, 2011:182

Printed by NTNU-trykk

## **ACKNOWLEDGEMENTS**

This research work was part of the project *Distribution 2020* at SINTEF Energy Research, Trondheim, Norway. The project was mainly financed by the Norwegian Research Council and ABB, but several Norwegian utility companies and some other industry partners also contributed in the project. I am grateful for the financial support provided for this PhD-project. Being part of the project *Distribution 2020* has been very valuable, and input and feedback provided by partners in the project during the work period is appreciated. The project leader for *Distribution 2020*, Senior Research Scientist Astrid Petterteig at SINTEF Energy Research has also been supervisor for my PhD-project. I am grateful for her involvement and support throughout the work.

The work was carried out at the Department of Electric Power Engineering at the Norwegian University of Science and Technology (NTNU). I wish to thank my supervisor Professor Hans Kristian Høidalen at NTNU for the guidance and support during the work on my PhD-project.

Finally, I wish to thank my family for continuous love and support.



## ABSTRACT

Being part of a larger research project named “Distribution 2020”, the focus of this work has been on increasing the automation of the fault handling in distribution networks, taking into consideration the increasing number of distributed generation (DG) units. The main goal of this work has been to investigate, and further develop methods for locating short circuit faults in distribution networks, with possible presence of DG-units. Also, the developed methods should be simple, and the use of measurements communicated from other locations than the substation should be kept at a minimum. Finally, the fault localization methods should be applicable for a general network. The development of such general methods is meant to be a step towards a more automated fault handling in distribution networks, leading to increased network reliability and reduced outage costs.

Fault data have been generated through simulations in the transient electromagnetic program PSCAD, where a simple model of a medium voltage (MV) distribution network was developed. Short circuit data from a real network was not available for this work. A distribution network may have various appearances, as the total length, number of branches, loading, short circuit capacity and other parameters may vary greatly, and generalizing the characteristics for a typical distribution network is not possible. The model parameters are chosen based on real network data, but the model is typically simplified compared to a real network.

This work has focused on short circuit faults. Fault simulations have been performed for a feeder without DG, with one DG- and with three DG-units. The impacts of various parameters on the distance estimate obtained by use of conventional distance relays have been investigated. Focus in the investigation was to find which parameters that impact most on the accuracy, and on quantifying the errors in the estimates. It is shown how load and DG introduce substantial errors in the distance estimates from traditional distance relays, and that there is a need for methods to compensate for these impacts in order to obtain a fault localization of sufficient accuracy.

Two methods for compensation of the impact from the load and DG-unit(s) on the distance estimates are presented. Both methods make use of pre-fault measurements from the DG-unit together with pre-fault substation measurements, and make rough estimations of the pre-fault load distribution on the feeder. In method 1 the required DG-quantities during fault are estimated, while in method 2 the DG voltage- and current- magnitude and the power factor angle are available from measurements. Requiring only magnitude values from the DG allows for simple communication solutions. In both method 1 and 2 a simple lumped feeder model is utilized for analytical estimation of unknown quantities. This includes estimation of the DG voltage phasor angle referred to the substation voltage.

The estimated DG currents during fault in method 1 are quite accurate, especially for two-phase short circuits, as seen in Ch. 6.2.5. For three-phase short circuits the estimated currents are generally a bit higher than the simulated. This results in overcompensation of the impact due to the DG in the distance-to-fault estimation. Despite of the overcompensation, the accuracy is improved with compensation 1 in most cases. The improvement is however dependent on the DG location. With a three-phase short circuit at the end of a 30 km long feeder, the largest improvement is seen when the DG is located close to (5 km) the substation, with a reduction of the error from +7.8 km to -1 km. The lowest accuracy of the compensated estimate is obtained when the DG is located at the middle of the feeder. The error is then -1.9

km, which still is an improvement compared to worst case without compensation. The estimates obtained at high load are only slightly more accurate than for low load, despite of the larger difference without compensation. If the DG location is fixed and the fault location is varied, the accuracy of the compensated estimate is decreasing as the fault is moved away from the substation, and the lowest accuracy is obtained when the fault is at the feeder-end. Generally, compensation method 1 results in larger improvement of the accuracy for two-phase short circuits, than for three-phase.

In method 2, measurements of the DG current- and voltage- magnitudes and the power factor angle during fault are utilized, and very accurate distance estimates are obtained for all cases (largest error with compensation 2 for the shown cases is 0.7 km). The DG-voltage phasor angle relative to the substation voltage is estimated from the lumped feeder model, like in the pre-fault state. The distance estimates are very accurate for all fault cases, so to have measurements from the DG during fault is very advantageous.

If the DG voltage magnitude is available during fault it can be utilized for finding the correct faulted branch if there is more than one candidate location. A method where the corresponding DG voltage is estimated for each possible fault location has been suggested. For the example feeder the smallest difference between the estimated and simulated voltage magnitudes corresponded to the correct fault location in all cases. Measurements from the DG-unit during fault result in both more accurate distance estimates and can be used to decide the correct faulted branch, and to have such measurements is therefore very beneficial.

## CONTENTS

Acknowledgements .....	I
Abstract .....	III
Contents .....	V
Symbols and notations .....	VIII
1 Introduction .....	1
1.1 Perspectives .....	1
1.2 Objectives and approach .....	2
1.3 Contribution .....	3
1.3.1 List of publications .....	4
1.4 Structure of the thesis .....	4
2 Protection and fault localization in distribution networks – state-of-the-art .....	6
2.1 Protection of distribution networks with DG .....	7
2.2 Fault localization in power systems – with focus on distribution networks .....	8
2.2.1 Fault localization based on power frequency quantities .....	9
2.2.2 Methods based on high frequency components .....	12
2.2.3 Knowledge based methods .....	13
2.3 Fault localization in networks with DG .....	13
3 Distribution system modeling .....	15
3.1 PSCAD simulation model .....	15
3.1.1 HV network .....	16
3.1.2 Substation transformer .....	17
3.1.3 Line .....	18
3.1.4 Load .....	19
3.1.5 DG-unit .....	21
3.1.6 Fault .....	24
3.1.7 “Measurements” in the PSCAD-model .....	25
3.2 Lumped model used for analytical calculations .....	26
3.2.1 Feeder with one DG-unit .....	27
3.2.2 Feeder with 3 DG-units .....	28
4 Conventional distance estimation .....	30
4.1 Conventional distance-to-fault estimation .....	30
4.2 Impact of fault resistance .....	32
4.2.1 Impact of fault resistance on feeder with one DG-unit .....	33
4.3 Conventional distance estimation in network without DG .....	34
4.3.1 Impact of load level on distance estimate .....	34
4.3.2 Impact of load distribution .....	35
4.3.3 Voltage dependency factor .....	36
4.4 Conventional distance estimation in network with one DG-unit .....	37
4.4.1 Impact of the location of the DG-unit .....	38
4.4.2 Impact of the fault location .....	38
4.4.3 Impact of generator rating .....	40
4.4.4 Size of the d-axis transient reactance .....	40
4.4.5 Impact of substation transformer rating .....	41
4.4.6 Impact of feeder length .....	42
4.5 Feeder with 3 DG-units .....	43
5 General method for compensation of load and DG on the distance estimation .....	45
5.1 Two compensation methods .....	45

Contents

5.2	General expression for the compensated distance estimate.....	47
5.3	Estimation of pre-fault load distribution .....	51
5.3.1	Pre-fault load estimation on a radial feeder with $N$ DG-units.....	52
5.3.2	Pre-fault load estimation on feeder with side-branches .....	55
5.3.3	Pre-fault estimation of load on last feeder section .....	56
5.4	Load estimation during fault.....	57
5.4.1	Estimation of load and voltages along a radial feeder during fault.....	58
5.4.2	Load estimation on feeder with side-branches.....	60
5.5	Estimation of fault current from a synchronous generator.....	61
5.5.1	Estimation of 3-phase short circuit current for DG.....	64
5.5.2	Estimation of 2-phase short circuit current for DG.....	65
6	Compensated distance estimate cases .....	67
6.1	Compensation cases for feeder without DG .....	67
6.1.1	Fault on the main branch.....	67
6.1.2	Fault on the side-branch .....	68
6.2	Compensation cases for feeder with one DG-unit.....	69
6.2.1	Pre-fault load estimation for feeder with one DG-unit .....	69
6.2.2	Fault on the main branch, before the $G$ -node.....	71
6.2.3	Fault on the main branch, after the $G$ -node.....	72
6.2.4	Fault on the side-branch before the $G$ -node .....	72
6.2.5	Calculation of DG-current during fault for feeder with one DG-unit.....	74
6.3	Compensation cases for feeder with 3 DG-units .....	75
6.3.1	Results of pre-fault load estimation for feeder with three DG-units.....	76
6.3.2	Fault cases for feeder with three DG-units.....	77
6.3.3	Fault located after branching node, and before the $G5$ -node .....	77
6.3.4	Fault located after the $G5$ -node.....	79
7	Compensated distance estimate results .....	80
7.1	Overview of compensation results cases .....	80
7.2	Results with compensation in network without DG .....	81
7.2.1	Load level on feeder without DG .....	81
7.2.2	Load distribution .....	83
7.2.3	Voltage dependency factor.....	84
7.3	Compensation results in network with 1 DG-unit.....	86
7.3.1	Impact of the location of the DG-unit .....	86
7.3.2	Impact of the location of the fault .....	88
7.3.3	Generator rating.....	89
7.3.4	Generator transient reactance .....	91
7.3.5	Substation short circuit capacity .....	92
7.3.6	Feeder length.....	92
7.4	Compensated distance estimate in network with 3 DG-units.....	93
8	Identification of the correct faulted branch .....	95
8.1	Comparison between measured and estimated DG voltage .....	95
8.1.1	Results with three-phase short circuits.....	96
8.1.2	Results with two-phase short circuits.....	97
8.2	Distance calculation from DG-measurements.....	99
9	Overcurrent protection in distribution network with DG.....	101
9.1	Blinding .....	101
9.1.1	Analytical analysis of three-phase short circuit .....	102
9.1.2	Analytical analysis of two-phase short circuit .....	106
9.2	Sympathetic tripping.....	110

Contents

10	Discussion .....	113
10.1	Conventional distance-to-fault estimation .....	113
10.2	Short circuit representation of the synchronous generator .....	115
10.3	Distance estimates with compensation .....	117
10.3.1	Feeder without DG .....	117
10.3.2	Feeder with one DG-unit.....	118
10.4	Finding the correct faulted branch .....	120
10.4.1	Comparison between measured and estimated DG-voltage.....	120
10.5	Distance calculation from DG measurements.....	121
10.6	Overcurrent protection and blinding.....	122
11	Conclusion.....	124
11.1	Further work.....	127
12	References .....	128

## SYMBOLS AND NOTATIONS

Upper case symbols (e.g.  $U, I$ ) denote rms values

Lower case symbols (e.g.  $u, i$ ) denote instantaneous values

Superscript *pre* denote pre-fault values ( $X^{pre}$ )

Superscript *nom* refer to nominal values ( $X^{nom}$ )

Subscript *d* and *q* refer to direct and quadrature axis components ( $X_d, X_q$ ).

Superscripts  $+, -$  and  $0$  refer to positive, negative and zero sequence components, respectively ( $X^+, X^-, X^0$ ).

Superscripts *A, B* and *C* refer to phase quantities ( $X^A, X^B, X^C$ ).

pu – per unit value

DG – distributed generation. Power generation unit connected at distribution network level.

Other authors may use embedded generation or dispersed generation.

*G*-node – the DG connection point, the node where the DG-unit is connected to the feeder

Power frequency and fundamental frequency is used to denote the 1. harmonic or 50 Hz (in a 50 Hz network) component of a quantity.

$U_S$	Substation voltage
$I_S$	Substation current
$Z_l$	Line impedance
$I_f$	Fault current
$I_L$	Load current
$U_G$	DG terminal voltage on MV-side of generator transformer
$I_G$	DG current on MV-side of generator transformer
$\varphi_G$	Phase angle of DG apparent power/Power factor angle
$\delta_{UG}$	Phasor angle of DG voltage
$Z_S$	Impedance to fault location calculated from substation voltage and current
$d_S$	Distance to fault location, calculated from substation voltage and current
$Z_C$	Compensated impedance estimate, from substation to fault location
$x_l$	Line reactance per unit of length
$Z_{G-f}$	Impedance to fault location, calculated from DG -voltage and -current
$d_{G-f}$	Distance to fault location, calculated from DG -voltage and -current

### Synchronous generator

$x_{G,d}, x'_{G,d}, x''_{G,d}$	d-axis synchronous, transient and subtransient reactance
$x_{G,q}, x'_{G,q}, x''_{G,q}$	q-axis synchronous, transient and subtransient reactance
$x_2$	Negative sequence reactance
$T'_d$	Short circuit d-axis transient time constant
$T'_{do}, T''_{do}$	Open-circuit d-axis transient and subtransient time constants
$T''_{qo}$	Open-circuit q-axis subtransient time constant
$T_a$	Armature winding time constant, giving the decay of the dc-current component

### Load

$P_L, Q_L$	Active and reactive power of load
$NP, NQ$	Voltage dependency factor for active and reactive power
$U_L$	Voltage across load

### Symbols and notations

$\varphi_L$	Load angle, $\cos(\varphi_L)$ is the power factor of the load
$S_{L\Sigma}$	Total feeder load
$R_L^{AB}, R_L^{BC}, R_L^{CA}$	Resistive component of load impedance between phases
$X_L^{AB}, X_L^{BC}, X_L^{CA}$	Reactive component of load impedance between phases



## 1 INTRODUCTION

In the conventional power system, the role of the distribution network is to carry (distribute) energy from the transmission network to the various customers. The distribution system usually operates at two voltage levels, medium voltage (MV) and low voltage (LV). The focus of this work is the MV voltage distribution network. These networks can be cable, overhead or mixed networks. Nominal voltages are ranging from 1 to 24 kV, where the highest voltages are used for overhead networks, and the lowest are used in cable networks [1]. Generally, urban networks are mainly cable networks with relatively short feeder lengths, while rural networks are mainly overhead networks with relatively long feeders [2]. In the conventional power system, power is mainly generated in large units connected to the transmission system.

### 1.1 Perspectives

During the last decade there has been a development towards building more small generation units which are connected directly to distribution networks, designated as distributed generation, DG. Although often associated with renewable and environmentally friendly energy, the term DG is independent of the type of energy source and simply means that the generation unit is connected to a distribution network. Still, the focus on increasing the amount of power generation from renewable sources has been one of the driving forces behind the development towards more DG. Both the political authorities and society support this kind of development. The energy consumption is growing, so the energy from the DGs is needed. Also, as electricity prices are increasing, building these small units become more profitable. Some energy sources are only profitable as small scale generation connected to the distribution network, and some energy sources can only be utilized where they are physically located. Thus DG is a possibility to utilize various energy sources, that otherwise might remain unexploited.

The developers of the DG units are commonly private individuals or companies that are not related to the distribution system operator (DSO). The DSO usually has no possibility to control the operation of the DG-units. To some degree the two parts have conflicting interests. Typically, the focus of the DG-owners is to generate power and obtain maximum profit, and to keep the costs of interconnection to the network low. On the other side, the main focus of the DSO is maintaining stability, high reliability and sufficient power quality in the network. The DSO must make interconnection requirements which ensure correct operation of the distribution system after connection of a DG-unit. From the DSO point of view it would be beneficial to utilize the possibility for controlling the voltage levels and reduction of losses in the distribution network through control of the reactive power generation/consumption of the DG-units. The DG-owners sees little benefit from generation or consumption of reactive power, and therefore the units are often operated at a constant power factor close to one. Often the generators are not dimensioned to have capacity for reactive power at nominal active power generation.

DG can be wind-, hydro- or solar- power, or it can be generated from biomass, fossil fuel or other energy sources. They can be connected directly to the distribution network, or through a converter. Units with rating 1-10 MW are generally connected at the MV distribution level [3], and only the smallest are connected at LV-level. In Norway, DG usually means small hydro power plants. Norway has large potentials for small hydro power, and The Norwegian Water Resources and Energy Directorate, NVE, has mapped at total potential of 25 TWh for

plants smaller than 10 MW [4]. Far from all of this potential will be released, but a large amount of plants have already been built, and there are lots of plans for new plants. The water resources are commonly located in rural areas. The distribution networks in these areas can be weak, and are mainly overhead or mixed networks. Often there can be many small hydro power plants within the same area. It is not uncommon to have many DG-units connected to the same feeder, or many feeders with DG connected to the same substation.

Generally, the solutions for fault handling in distribution systems are simple and cheap as compared to the transmission system, and the DSOs have been reluctant to invest very much in the distribution network. This should be kept in mind when suggesting new solutions for fault handling, and it is an advantage if the solutions are utilizing existing equipment in the distribution network. Conventional distribution networks are operated radially, although they may have a meshed structure allowing for reconfiguration of the network during interruptions. The planning and operation have conventionally been based on the assumption of unidirectional power flow from the substation to the loads [5]. In Norway, non-directional overcurrent relays with constant-current characteristics are normally used for short circuit protection. Sectioning of faults is done manually, which is very time-consuming. With DG in the network the power flow is no longer unidirectional, and the generated power on a feeder may exceed the load. This may cause problems for the protection. The present practice is to disconnect all DG-units when a fault is detected, allowing the protection to operate as in the conventional radial distribution networks without distributed generation. This is ok when there are few DGs in the network, but is not adequate when the penetration level becomes higher [6]. Then the DG should help support and restoring the network instead of being disconnected.

DG also affects the voltage in the point where it is connected and causes a change in the feeders' voltage profile. This can both be positive and negative seen from the perspective of the DSO. In addition, the generation from a DG may be variable and unpredictable. All together this may lead to power quality problems. As long as the penetration level is low, the DG-units can be fitted into the networks without large precautions. But as the penetration level is increasing the impact from the DG becomes more significant. For the protection this means that changes in the relay settings or even a different type of protection may become necessary. Regarding power quality the DG may for instance be required to have capacity for generation or consumption of reactive power. Parallel to the development towards more DG, the DSOs have increased their focus on power quality and on minimizing the interruption time for load customers. This is due to intensified regulations regarding power quality and increased penalty costs for non-supplied energy. Remote control of breakers is becoming more common. In one Norwegian utility a major decrease of outage times due to more efficient fault handling were obtained after systematic investments in remote control equipment [7].

## **1.2 Objectives and approach**

To minimize the interruption time, a fast and efficient fault handling is important. This can be achieved through introduction of more automation in the fault handling. The purpose of this thesis is to look into possibilities for precise localization of short circuit faults, utilizing fundamental frequency currents and voltages. The work is intended to be a step towards a more automated fault handling. By communicating data from the substation relays and DG-unit(s) to the control centre, distance-to-fault calculations can be performed there. In this way the presented methods can be used as tools for finding the correct fault location faster, and directing the repair crew to the correct fault location so that the fault restoration process can

be as fast as possible. Remote control of breakers opens possibilities for further automation of the fault handling by utilizing the information from the fault localization methods for opening the correct breaker.

The DSO typically employs a network information system (NIS) which is used for planning and documentation of the distribution network. It contains network data and load curves, and can perform steady-state power flow calculations. It may also have functionalities for reliability and fault calculations, and is based on RMS quantities. A modern NIS have a graphical interface with network maps on a geographical background [8]. A distribution management system (DMS) has many similarities with the NIS, but is intended for use in the control centre. It has a real-time connection to the network components via the supervisory control and data acquisition (SCADA) system. SCADA is a technology used for monitoring and control of the network equipment in real-time. In the DMS network information available from the NIS are combined with real-time status of the network components and control possibilities in the SCADA system. The fault location methods presented in this thesis can be implemented as a part of a DMS and be used in the utility control centre.

Another possibility would be to implement the proposed algorithms in a digital relay with communication directly from the DG-unit(s) to the substation relay.

Fault detection and classification, and protection schemes for distribution systems with DG are important issues, but this is not the main focus of this thesis. The issue of fault detection is however treated in Ch. 9 considering overcurrent protection.

The work is based on simulations in the transient simulation tool PSCAD. The PhD was a part of a larger project, Distribution 2020, where measurement equipment was installed in a real network with distributed generation. No short circuit faults occurred during the period of this PhD-work, and it was not possible to intentionally apply short circuit fault in order to obtain real fault data. During the period where this work was carried out there were also no suitable lab facilities available for practical experiments. Due to these all fault data are generated through simulations.

### **1.3 Contribution**

The main contribution of the thesis is two methods, method 1 and 2, for distance-to-fault estimation in a distribution network with DG. The methods are based on conventional distance fault localization utilising power frequency components, with compensation of the impact from load and DG.

The impacts from load and DG on the distance obtained using conventional reactance based fault localization have been investigated.

A simplified model with lumped line impedances and lumped loads intended for analytical calculations has been introduced. A method of estimating the size of the lumped loads from pre-fault measurements is presented. The required measurements are substation current and voltage, and DG connection point voltage magnitude. The lumped model can be used to estimate the phasor angles of measured quantities relative to the substation voltage.

A method 1, estimating the short circuit current of a synchronous generator from pre-fault measurements of DG current- and voltage- magnitudes and DG power factor angle is

presented. It allows for compensation of the fault current contribution from the DG even without any measurements available from the DG during fault.

A method 2, utilizing measurements from the DG location during fault in order to obtain a very accurate compensation of the impact from DG is presented. The phasor angles during fault are estimated from the lumped model. This means that only rms values needs to be communicated, and that very accurate time synchronization between the measurement in the substation and the DG location is not necessary.

A method of finding the correct faulted branch when there is more than one possible fault location on parallel branches in equal distance to the substation is introduced. The method compares the measured phasor magnitude values from the DG with corresponding values estimated from the lumped feeder model. The method thus requires measurements from the DG during fault.

A method for estimating the reduction of the fault current measured in the substation due to infeed from a DG-unit connected to the feeder is presented. The method requires pre-fault measurements from the substation and the DG-unit for estimation of loads and voltage in the fault location before the fault occurrence.

### 1.3.1 List of publications

Marvik, J.I. *Feilstrømmer og kortslutningvern i nett med distribuert produksjon*. 2007, NEF technical meeting (in Norwegian): Trondheim Norway. 7 p.

Marvik, J.I., Petterteig, A., and Høidalen, H.K. *Analysis of Fault Detection and Location in Medium Voltage Radial Networks with Distributed Generation*. 2007, IEEE Power Tech: Lausanne, Switzerland. 6 p.

Marvik, J.I., Høidalen, H.K., and Petterteig, A. *Evaluation of simple fault location on a MV feeder with DG, using fundamental frequency components*. 2009, Nordic Electricity Distribution and Asset Management Conference, NORDAC: Bergen, Norway. 7 p.

Marvik, J.I., Høidalen, H.K. and Petterteig, A. *Localization of Phase-to-Phase Faults on a Medium Voltage Feeder with Distributed Generation*. 2009, International Power System Transients Conference, IPST: Kyoto, Japan, 6 p.

Marvik, J.I., Høidalen, H.K., Petterteig, A. *Localization of short-circuits on a medium voltage feeder with distributed generation*. International conference on Electricity Distribution, CIRED: Prague, Czech Republic. 5 p.

### 1.4 Structure of the thesis

The thesis is divided into 11 chapters, and three additional appendix chapters. Short descriptions of each chapter are given here.

Chapter 2 puts the work of this thesis into context of previous research.

Chapter 3 presents the PSCAD simulation model and each of the components. The choices of models and corresponding parameters are justified. In addition a simplified model with lumped loads and line impedances are presented. The model is intended for analytical calculations.

## Chapter 1 – Introduction

Chapter 4 deals with conventional distance relays utilizing measurements from only one terminal, the substation. The impacts of various parameters on the accuracy of the estimated distance to the fault location are investigated. Plots of the distance estimate errors for the various cases are shown.

Chapter 5 describes two methods, 1 and 2, for compensation of the impacts from DG and load on the distance estimate, valid for a general distribution network. Estimation of the pre-fault load distribution utilizing pre-fault measurements from the substation and the DG(s) is shown. Estimation of the DG current during fault for method 1 is described. Flow charts are used to explain the methods.

Chapter 6 describes the compensation methods given for a general feeder in Chapter 5 for specific cases on the example feeder. The considered cases are for a feeder without DG, with one DG- and with three DG-units. Results of the pre-fault load estimation and the estimated DG currents during fault are shown.

Chapter 7 presents results using the compensation methods presented in Chapter 5 and described for the specific example feeder in Chapter 6. Results are presented as plots of distance estimate errors. The presented cases with compensation are on the whole the same as presented in Chapter 4 without compensation.

Chapter 8 deals with the challenge of deciding the correct fault location in a distribution network with tree structure. A method is presented where the measured and estimated DG voltage is compared in order to find the correct fault location. Another method suggested by other authors is also investigated. Both methods require measurements from the DG during fault.

Chapter 9 deals with the impact of DG on the feeder overcurrent protection. Two possible problems are discussed; blinding and sympathetic tripping. The emphasis is given to blinding, and it is shown how the reduction of the substation fault current due to infeed from the DG can be estimated using the lumped feeder model.

Chapter 10 contains discussion about the modelling and the results

Chapter 11 contains conclusions.

Chapter 12 contains a bibliography

Appendices A-C are found at the end of the thesis.

## 2 PROTECTION AND FAULT LOCALIZATION IN DISTRIBUTION NETWORKS – STATE-OF-THE-ART

Protection and fault localization are two different, but closely related topics within fault handling in power systems. A fault localization device has different requirements than a fault detection device [9]. While protection relays should detect faults within 10-50 ms, the speed requirement for the fault localization is less strict and may vary from a few seconds to minutes. This allows for utilizing additional information and slower numerical techniques in the fault localization. Low-speed data communication or SCADA can be used for transmission of data. Fault localization can be implemented as an additional function in a microprocessor based protection relay, in a digital fault recorder, as a stand-alone fault locator or it can be implemented in a post-fault analysis program [10]. If the fault locator is an additional functionality in the protection relay, different measurement windows may be used for the fault locator than for fault detection. The longer time window enables more accurate phasor calculations through use of digital filtering.

While distribution feeders are usually protected by a non-directional overcurrent relay in the substation, distance protection is the most common line protection at transmission level. In a meshed network each line section is protected by relays in both ends, allowing for fast disconnection of short circuits throughout the whole section length. It is also possible to establish a communication channel between the relays in the two line ends, to provide instantaneous clearing over the whole line section [11]. Different types of communication channels can be used, but the communication is usually simpler than that of the differential relays. There are generally no load taps or generation units connected to the line between the two terminals in a transmission network. For such networks fault localization based on reactance is relatively simple.

Distribution networks differ from transmission networks by some important characteristics, and this impacts the protection and fault localization [12], [13]. A typical distribution feeder may consist of both overhead lines and cable sections. The cross-sections are not constant throughout the feeder length, but are generally decreasing towards the feeder-end. Therefore the relationship between the measured impedance in the substation and the distance to the fault location is not linear. The resistive line losses are larger in distribution networks, so the angle of the short circuit current is typically not approximately  $90^\circ$ , as for a transmission line. Therefore the difference between the load current angle and the short circuit current angle is smaller for a distribution network. This leads to smaller margins when applying impedance protection. A very important difference between the two network levels is the network structure. As opposed to transmission lines, distribution networks typically have a tree-structure with several lateral branches. Faults in different geographical locations can generate the same currents and voltages in the substation. An estimated distance to the fault location may therefore correspond to several possible fault locations. In addition, load taps are typically found at irregular intervals on a distribution feeder. The current measured at the substation during a fault contains a load current component in addition to the fault current. The topology of a distribution network may be modified in different operating conditions. As a consequence it is important that updated information about the network topology is available for the protection and fault localization

[14] discusses the sources of inaccuracy when using distance relays for fault localization in distribution networks. In addition to the characteristics of distribution networks described

above, infeed from power plants along the line are mentioned as a source of error in the distance metering. This error depends on the ratio of the short circuit capacity of the feeding network to the short circuit capacity of the infeeding plant and also the geographic position of the infeeding plant in the network.

## **2.1 Protection of distribution networks with DG**

The influence DG has on fault detection and fault clearing, as well as an increased focus on minimizing the outage times, introduces need for changes in fault localization methods and equipment [15]. Whether traditional and inexpensive overcurrent protection can be used in networks with DG depend on how significant the influence from the DG is during faults. The impact of distributed generation on protection of distribution networks has been described in many papers and reports, e.g. [15], [16], [17], [6], [8], [18], [19]. Two frequently mentioned problems when using traditional non-directional overcurrent protection are blinding and sympathetic tripping. Problems can often be avoided through adjustments of the relay settings. In networks with DG, protection coordination is complicated, especially since there is a conflict between adjustment of settings required to avoid blinding and adjustments required to avoid sympathetic tripping. [8] presents a methodology for network planning and coordination when connecting a DG to a network. The necessary analyses before connection of a DG are presented as steps in an iterative procedure. It is suggested that the procedure is implemented as an additional functionality of the NIS. The blinding and sympathetic tripping phenomenons are discussed further in Ch. 9.

DG usually causes an increase of the fault current level in the fault location. This leads to larger stress on the network equipment. The generator type and connection to the distribution network is very important in this matter. Synchronous generators are the most common generator type in especially medium to large sized DG-units. This generator type contribute most to the fault current, and a separately excited synchronous generator can give 500-1000 % of the nominal current for the first few cycles before decaying to 200-400 % current. Induction generators are commonly used in smaller to medium sized DG-units. This generator type also has a large current immediately following a fault, and at the initial stage the contribution from an induction machine may be almost as large as from a synchronous machine of the same rating. However, the short circuit current is decreasing faster for an induction generator. The short circuit current can be 500-1000 % of the nominal current for the first few cycles, but are decaying to negligible amount within 10 cycles. The same characteristics are also true for induction motor loads and for self-excited synchronous generators. Generators connected via power electronic converters will have a limited capacity for fault current contribution, depending on the converter rating and controller settings. The fault current may be 100–400 % of the rated current. An example of inverter connected DG-units is photovoltaic cells. [20], [21], [22], [8], [23].

Automatic reclosing of the substation circuit breaker is usually employed in order to limit the interruption time for the customers. A major part of faults in the distribution network are of a transient nature, at least in overhead networks, and by de-energizing the system for a short time the fault arc will extinguish and the system may be restored to service [23]. If the DG unit remains connected to the network when the substation circuit breaker is opened, it continues to feed current to the fault. This means that the arc will not be extinguished, and the reclosing fails, [8], [3], [24], [18], [25]. In addition, synchro-check becomes necessary before reclosing the circuit breaker, in order to avoid a possible connection between two parts of the system which are out of phase [26]. Radial distribution system voltages are normally regulated using tap-changing in the substation transformer. Voltage regulation practice is

based on radial power flow from the substation to the loads, leading to a voltage drop downstream from the substation. The power flow measured in the substation will be reduced or even change direction when DG is connected to the network. If the infeed from DG is not taken into consideration the voltage adjustment performed by the tap-changer might become incorrect. This is also discussed in Appendix A.

Islanding operation occurs when a part of the distribution system becomes electrically isolated from the main power system, but continues to be energized by a DG connected to the isolated part of the system. Especially synchronous generators have the capability of sustaining the operation in islanding mode as long as there is approximately balance between load and generation. Unplanned islanding is not desirable since it can lead to safety problems for humans and power quality problems for the local loads. It is therefore important that an islanding condition is detected, and that all DG-units are disconnected within a few seconds [23]. Loss-of-mains protection is one of the most challenging protection issues related to distributed generation, [24]. Basic under/over voltage and under/over frequency relays may fail to operate if the power mismatch in the island is small [26]. Possible solutions are to use rate-of-change-of-frequency protection, ROCOF, [27] or vector shift protection, [28], [29]. If automatic reclosing is to be used, and all DGs are not disconnected when a disturbance occurs, synchronizing check is required before reclosing [30].

[31] suggests a new protection scheme for MV distribution networks based on distance relays. An 11 kV cable network with RMUs is studied, and the intention is to incorporate a distance relay in the RMU. To save cost the voltage measurement will be located on the low voltage side of the distribution transformer. Communication schemes were not considered due to limited availability of communication at this voltage level. The presented protection scheme is intended to allow for larger amounts of DG to be connected to the network than with the conventional overcurrent protection scheme. Distance protection is less sensitive to source impedance variation, it can operate correctly with bidirectional fault current flow and the fault clearing times become shorter.

[32] deals with using transient current signals for determining the fault current direction in distribution networks with DG. The advantage as compared to the conventional directional overcurrent relays is that installing voltage measuring transformers is not required. Transient directional relays are installed in all points where DG-units are connected, and an asynchronous data communication protocol is used for transmission of fault transient directional wave states.

Some possible positive impacts introduced by DG are mentioned in [20]. The DG may provide voltage support and contribute to improved power quality, and improved system reliability can be achieved. Losses in the distribution network may be reduced since the DG can feed local loads. If the reactive power of the DG can be controlled reactive losses can be reduced. This can lead to a release of transmission and distribution capacity, and deferment of new or upgraded network infrastructure. Achieving these benefits may however be difficult in practice.

## ***2.2 Fault localization in power systems – with focus on distribution networks***

Within the topic of fault localization, a major part of the research has been focusing on transmission networks. The consequences for the power system and the energy supply are much larger when a transmission line is lost than a distribution line. Fault location estimation

is considered essential in transmission networks, and due to this the use of advanced and expensive methods is economically justified. In distribution networks fault locators have been considered useful, but not necessary [33]. The IEEE Power System Relaying Committee has looked into various approaches to determine the fault location on both transmission and distribution lines [9]. Reviews of presented fault localization techniques for distribution networks have been presented in [33], [34], [35] and [36]. The Electric Power Research Institute, EPRI, has a project on fault localization in distribution systems, and different approaches are evaluated and the limitations of the different methods are identified [35].

Faults in distribution systems have up to now normally been located manually. Short circuit faults have traditionally been located by opening the main circuit breaker followed by opening a sectioning breaker, and then reclosing the circuit breaker. If the fault is still present after the breaker reclosing, the procedure is repeated by opening the next sectioning breaker. This is repeated until the fault is isolated. The sectioning breaker closest to the feeder end is opened first and the one closest to the substation is opened last. This way of finding the faulted feeder section may be time consuming, and expose network components to stress.

The focus on distribution networks has been increasing, and much literature can now be found on the topic fault localization in distribution networks. Many methods for locating phase-to-phase fault in networks without DG are presented in the literature, and some are implemented with good results. For fault localization in conventional distribution networks without DG, the main challenges are minimizing the impacts from load and fault resistance. The research focus in the present state seems to be on high impedance earth faults. Still, localization of phase-to-phase faults in networks with DG is not a solved case. Most of the literature related to this considers advanced methods utilizing high-frequency components of currents or voltage, or many measurements distributed on the feeder. Few references are found on simple, fundamental frequency based methods for networks with DG. General sources of error in fault localization mentioned in the literature include measurement errors, load currents and fault resistance. Measurement errors are usually small, but for faults close to the substation they can become notable since the high short circuit current may cause saturation of the current transformers [37].

Benefits obtained through automated fault localization are discussed by [12]. These include reduced downtime and outage costs as the maintenance crews can be directed to the fault location faster. Consumer satisfaction is assumed to be increased due to the reduced downtime. In addition transient faults may be located and analysed, and corrective maintenance work (e.g. cutting trees) may be done to avoid a later permanent fault in the same location. These can be assumed to be general benefits obtained by a more automated fault localization in distribution networks.

A method for calculational synchronization of measurements acquired at two line terminals are presented in [38]. The method is intended for use in fault localization applications, and provides a cost beneficial alternative to GPS synchronization.

### **2.2.1 Fault localization based on power frequency quantities**

Fault localization based on impedance is the most common method in use. The impedance is calculated from the fundamental frequency components of voltage and current, and the reactance part of the impedance is used for fault localization. Thus the same measurement transformers that are already installed for fault detection can also be used. At transmission level, the lines are protected by one relay in each end of the line, which means that

measurements can be available from both ends of the line [39]. Communication and synchronization of measurements from different locations are more likely to be economically justified at transmission- than at distribution- level. For conventional distribution networks only current measurements from the substation are available, and as a minimum, voltage measurement transformers have to be installed in the substation. Due to the general tree-structure of distribution feeders, fault localization becomes more complicated than for a masked transmission network.

The starting point for distance-based fault localization should be an approach utilizing measurements from one terminal only. Such a fault locator was introduced in [40]. In [41] the impacts of fault resistance and intermediate loads were taken into account. The loads were calculated using a load flow program. [42] presented a fault locator for transmission lines based on measurements from one terminal. A method for compensation of the apparent reactance of the fault resistance due to infeed from the remote terminal is presented. The infeed from the remote terminal of a transmission line is analogous with the case of infeed from DG on a distribution feeder. A similar approach intended for radial transmission lines were presented by [39]. Here, load flow is calculated from pre-fault voltages and currents, and is used to obtain corresponding load admittances at each network node.

In Finland the possibilities of utilizing modern numerical relays for faster fault localization were exploited at an early stage. A method of comparing the measured fault current magnitude value with corresponding computed values to find the fault location has been used since the beginning of the 1990s. [13] discusses the theoretical background and implementation of this type of calculational fault localization for radially operated distribution networks. The main sources of error in the method are fault resistance, and load current superimposed on the fault current. In addition the method is sensitive to variation of the short circuit level of the feeding network and the substation transformer tap position. The load current is compensated for, and the load current is calculated using models accounting for the voltage dependency of the loads. The big advantage is that this method only requires current measurements, so no extra measurement equipment needs to be installed. The disadvantage is that modern numerical relays are required in each feeder.

Reactance based fault localization in distribution networks is already used by utilities in some countries. An Austrian utility has utilized digital distance relays for fault localization in their network since 1990 [14]. The network is located in a mainly rural region, and the MV feeders are protected by distance relays. Like for the current based fault localization method described above, modern numerical relays are required in each feeder. Longer feeders have additional circuit breakers and overcurrent relays. A list of reactances must be created for each feeder, and every section of the feeder is a line in this list. A short circuit program is used for calculating reactance values corresponding to the different possible fault locations. The probable faulted line sections are selected by a computer program and displayed on a screen in the operation centre. If the measured reactance is between the reactance at the beginning and the end of a line section this section is a probable fault location. It is important to update the network impedances, but this is already being done for network planning purposes, and does not require additional work. The distance relays are used in combination with short circuit indicators, and the results from the practical experiences are good.

[43] presents an automatic computer model for localization and isolation of faults, and for supply restoration. The model is named FI/FL-model and is an integrated part of the SCADA and the distribution network automation system. The fault location is estimated by combining

information from three different techniques. These are distance to fault estimation by comparing the measured and computed fault current, fault locator in the branching points and statistical information about line section fault frequencies. The information is combined using fuzzy logic. The faulted section is isolated automatically by remote control of line switches. Experiences from trial use in a Finnish network are described in the paper.

The utility CP&L operates distribution networks in North and South Carolina, US, which are of largely rural character [44]. A GIS system was installed in the beginning of the 1980s, which was the first step towards a future distribution automation system. Since the end of the 1990s, automated outage management, SCADA and feeder monitoring systems have been used together to provide information about the health of the distribution system.

[45] and [46], [37] and [47] discuss a method for estimating the distance to the fault using distance relays. The technique is based on measured busbar voltages and feeding transformer primary currents only. This means that only one measuring device is needed per primary transformer, and not one per feeder as in previously presented methods [36]. The key of the technique is compensation of the load current to achieve better accuracy. Both load current flowing into the faulted feeder and into the non-faulted neighbour feeders are estimated and compensated for. The calculated distance to the fault might correspond to several possible candidate locations. To decide the correct fault location additional information from fault locators in the branching points and knowledge of fault frequencies of different line sections are utilized. Also, the method can only be used for two-phase and three-phase short circuits. [48] has a similar approach of estimating the load floating into the unfaulted parallel feeders during fault. The utilization of pre-fault measurements to minimize the impact from load on the distance estimate is also described in [49] and [50]. None of the described methods considers the presence of DG on the feeder.

[51] discusses the challenges in extracting fault data from power quality (PQ) monitoring data for fault localization. Fault type and current magnitude are extracted from the PQ database. A short circuit analysis program is used for pre-calculation of fault current magnitudes of different fault types at every feeder section. When a fault occurs the measured current is compared to the pre-calculated values in order to estimate the fault location.

[52] presents a fault localization algorithm utilizing voltage measurements in selected nodes along the feeder in addition to voltage and current measured in the substation. The method is based on apparent impedance, and loads are estimated from pre-fault measurements. To select the most likely fault location the mismatches between calculated and corresponding measured voltage sags are computed. In ideal conditions the voltage mismatches should be zero for the faulted node.

A method based on measurement provided by intelligent electronic devices, IED, on each feeder in the substation is presented in [12]. The IEDs are connected to database with updated information about the network topology and parameters. The pre-fault load currents and voltages at each node are estimated using a three-phase power flow. The distance to the fault is calculated from power frequency voltages and currents.

[53] presents an impedance-based method using single-end measurements. Loads, fault resistance and the tree-structure of the distribution network are taken into account. The load is represented as known constant shunt impedances. The algorithm shows robustness to uncertainty in the load impedance.

### 2.2.2 Methods based on high frequency components

Travelling wave based methods is an alternative to the methods based on power frequency quantities. The single and double end travelling wave methods of fault localization have been available for a long time. After a fault has occurred a wave will arrive at the line end. There it is reflected back to the fault location, and subsequently reflected back to the line end. In the single ended method, the distance to the fault is determined from the travel time between the first and second reflection in the measuring point at the line end. It can be difficult to detect the second reflection of the wave, and therefore this method may be unreliable, especially for distribution networks. In the double ended method the transient wave is received in each of the two line ends at different times. The time difference is used to calculate the distance from the fault from each line end. Communication between the two line ends and a very accurate GPS clock is required to assure time synchronization for this method. Even though the double ended method gives the most accurate results, the single ended method has been used more for economical reasons. A travelling wave single ended method is presented in [54].

For distribution systems these type of methods become more complex than for transmission lines. Distribution networks are characterised by a more complex structure and shorter line lengths than transmission networks. After a fault, travelling waves propagate along the network and are reflected at line terminations, junctions between feeders and laterals and in the fault location. Because the topology of the distribution network involves many reflections, it can be difficult to separate the wave reflected from the fault point from other reflected waves [33]. An important disadvantage with methods utilizing high frequency components is the possible need for installing new measurement equipment. Since the conventionally installed measuring transformers are intended for measuring power frequency quantities, it has to be checked whether the existing equipment can measure the required high frequency quantities with a sufficient accuracy.

[55] proposes a method based on current travelling waves, and state that current transformers can reproduce the required frequency signals on the secondary side. This means that the existing measuring equipment can be used in this method. The method is mainly intended for transmission networks. Result from testing of a variety of current transformers of different types have been reported, [56]. It is found that distribution system current transformers normally have a good accuracy in the frequency range from 1 kHz to 100 kHz, and it is concluded that the conventional transformers can be used for current transient based protection.

[57] presents a fault localization method for distribution networks based on fault generated voltage transients. The transient signals are analysed with the continuous wavelet transform, and a new mother wavelet is introduced. Each path for the travelling wave can be associated to a set of frequencies corresponding to the travelling wave propagation modes. These frequencies can be evaluated before any fault occurs.

[58] presents a fault localization technique utilizing arc-generated high frequency signals. A specially designed fault locator is used to extract the fault generated high frequency voltage signals, and the travelling time of the signal is used to determine the fault position. The impact of discrete loads along the line is taken into consideration. At moderately high frequencies the behaviour of the distribution transformers becomes dominated by their capacitance. The actual level of loading of the distribution transformers has little impact when using high frequency signals for fault localization, and the same applies to the short circuit level at the substation. The technique is tested in simulations, and shows very high accuracy.

An often mentioned problem using travelling wave methods is to locate faults occurring close to the substation. This is also handled by the suggested technique.

Methods using high frequency components often use the wavelet transform to analyse the recorded signals. This transform is an alternative to the windowed fourier transform, and is often stated to be better suited for this type of analysis since it employs short time windows at high frequencies and long windows at low frequencies [59]. The windowed Fourier transform employs a uniform window for all frequency components.

### **2.2.3 Knowledge based methods**

Knowledge based fault localization methods is another alternative approach. These methods can be based on neural networks, fuzzy logic or genetic algorithms. Some methods combine information from a multi-agent system and from SCADA, [60]. [61] proposes a method using a learning algorithm for multivariable data analysis (LAMDA) classification technique. The classification technique is combined with an impedance-based fault localization method. Only measurements of power frequency voltages and currents in the distribution substation are required, which means that implementation costs are fairly low.

[62] presents an artificial neural network (ANN) and support vector machine (SVM) approach for fault localization in distribution systems. The method utilizes measurements from the substation and knowledge of circuit breaker and relay statuses. The ANN and SVM are trained by simulating faults at each node of the network for all types of faults and the complete range of short circuit levels for the network. A conventional training algorithm is used. The suggested approach is a good way to extract the limited fault information available during a fault in a distribution network, and the fault localization results are stated to be accurate. A disadvantage of this approach is that the ANN has to be retrained if the network configuration is changed. [63] also uses an ANN based approach where the network is trained to map the non-linear relationship existing between fault location and the characteristic eigenvalue.

[64] presents a fault localization method for distribution networks based on fuzzy set theory. The method handles the knowledge and experience of the control center operators in combination with the network data base and information from the SCADA system. With fuzzy set theory the inexactness and uncertainty in decision making and human reasoning can be modeled. Under lack of statistical data to calculate the probabilities, an expert may instead be able to express the possibilities for various hypotheses based on experience. The determination of membership functions is an essential part of the method, and the expert knowledge can be quantified by membership functions of fuzzy sets. The most likely fault location is selected from the fuzzy set based on the grades of membership of alternative hypotheses. Different selection methods can be applied in the decision making. The membership functions can be changed dynamically due to for instance changed weather conditions or different network configurations.

## **2.3 Fault localization in networks with DG**

As penetration of DG into distribution networks is growing, an increasing number of literature considering fault localization in networks with DG can be found. Many of the presented methods are utilizing measurements, relays and breakers in several locations with communication between. Consequently implementation costs may become considerable. Other methods utilize transient signals instead or in addition to the power frequency signals. An important question is then whether the conventional measuring transformers will measure

the transient voltages and currents with an acceptable accuracy. Previously presented single-ended methods, intended for use in transmission networks with remote infeed, may also find a new application in distribution networks with DG.

[65] presents a hybrid compensation method for performing fault analysis in distribution systems. To handle unbalanced systems, short circuit analysis is performed from a three-phase representation instead of symmetrical components. The impacts of load, DG and fault impedance are taken into consideration. The compensation of loads is done utilizing results from a pre-fault power flow analysis. DG-units are assumed to have constant internal voltage during fault. The presented algorithm is stated to be robust and efficient, and suited for applications such as adaptive relaying and fault localization.

Fault localization in networks with DG using fundamental frequency measurements is treated in [66].

[67] presents a single-ended fault localization method considering the impact from both loads and remote infeeds. The developed algorithm determines the superimposed voltage at any assumed fault point based on pre-fault and post-fault measurements of current and voltage.

[15], [68], [69], [16], [70] and [71] propose more advanced methods based on fault transients, adaptive protection schemes and relay agents for more precise fault localization. These methods utilize collection and communication of information about the actual system state, as well as computational intelligence.

[72] presents a hybrid transient based technique intended for distribution networks with high penetration of DG. Only current signals are utilized, and the signals are analysed by means of wavelet coefficient processing. Since voltage measurements are not necessary, the cost of installing potential transformers is avoided. The phase currents are decomposed into the corresponding modal components, and the type of fault can be determined by observing presence of the different modal components. The hybrid algorithm handles earth faults and short circuits differently, but in both cases the faulted branch is determined through comparison between polarities of the initial peaks of different measurement points. Measurements are required in all branches. It is stated that only communication of logical signals between the relays (IEDs) are required, which is advantageous.

A method using neural networks for fault localization is presented in [73]. The general idea is to divide the network into zones, with one zone for each DG-unit. A new zone is started when the average load exceeds the generation capacity of the DG. Zones without DG can also exist. Remotely controlled circuit breakers with synchro-check relays are placed between the zones. The relay in the substation holds the main responsibility for the protection, and continuously monitors currents flowing through the substation and all circuit breakers, and from all DG-units. The fault localization method can only be used when there is DG connected to the network, and the accuracy increase with the number of DG-units, as the number of inputs to the neural network then grows.

### **3 DISTRIBUTION SYSTEM MODELING**

This chapter first presents the modelling of a distribution system in the transient simulation tool PSCAD (Ch. 3.1). The simulation model is intended for generating fault data, emulating measurement from a real distribution network. Secondly, a simplified way of modelling a distribution network with lumped parameters is presented (Ch. 3.2). The purpose of the lumped model is to perform analytical calculations of voltages and currents in the network.

#### ***3.1 PSCAD simulation model***

PSCAD (Power Systems CAD) is a graphical user interface to the EMTDC solution engine. EMTDC solves the system equations for each time step using the trapezoidal rule of integration. PSCAD enables the user to schematically construct a circuit, run a simulation, analyze the results, and manage the data in a completely integrated, graphical environment. PSCAD offers a large library of pre-defined and tested models, ranging from simple passive elements and control functions, to more complex models, such as electric machines, FACTS devices, transmission lines and cables. If a particular model does not exist, PSCAD provides the flexibility of building custom models, either by assembling them graphically using existing models, or by utilizing an intuitively designed Design Editor [74]. PSCAD 4.2.1 Educational version was used in this work. A solution time step of 50  $\mu$ s has been used. PSCAD/EMTDC is suitable for simulation time domain instantaneous responses (electromagnetic transients). However, the simulation time becomes large for a network with many nodes and components, and the program is therefore not very suitable for simulating large networks.

A simple MV distribution feeder with one lateral branch, as shown in Figure 3.1, is modelled in PSCAD. The objective of the simulations is to generate voltage- and current- quantities from different fault cases on the feeder, as the possibilities of doing short circuit tests on a real network are restricted. Simulations with one or three DG-units connected to the feeder have been carried out. Two of the units are shown with stippled lines, because the majority of the simulations are done with only one DG-unit.

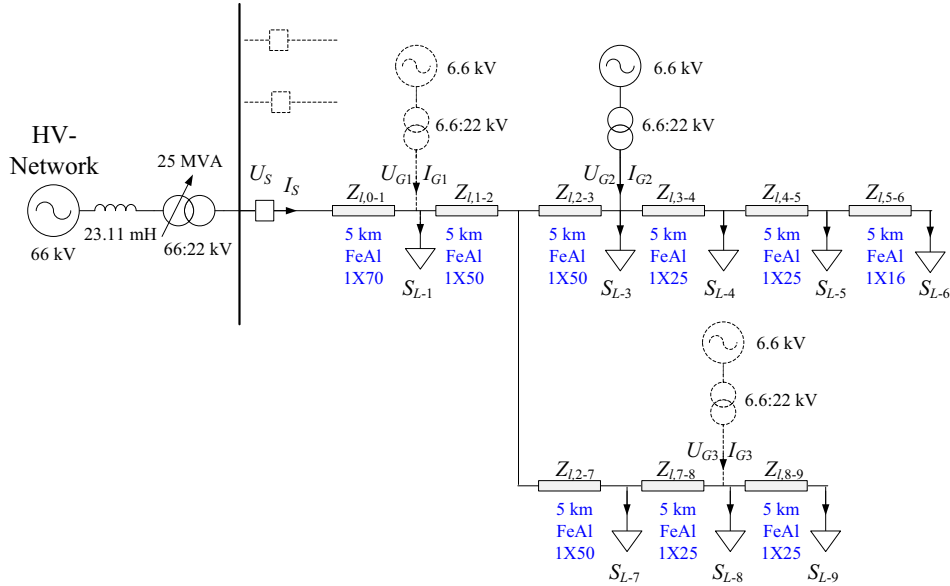


Figure 3.1: MV-voltage feeder simulated in PSCAD

The HV-network has an operating voltage of 66 kV. The operating voltage at MV-level is 22 kV. All line sections are 5 km long. The cross-section area of the line decreases from the substation towards the end of the feeder. High load for this feeder is 6 MVA. Low load is assumed to be 25 % of high load, 1.5 MVA. The DG-unit is a small hydro power plant with a synchronous generator.

The different model parameters can be varied in the simulations, but the starting point is always the same base case. In the base case the following applies:

- Active power is represented as constant current (NP = 1) and reactive power as constant impedance (NQ = 2). The loads are evenly distributed along the feeder, as described in chapter 3.1.4 below.
- There is no load on adjacent/neighbouring feeders.
- The fault resistance is equal to 0.01  $\Omega$ .

Generally only fundamental frequency components are considered in this study, and thus the high frequency behaviour of the components are not important. This allows for some simplifications in the modelling.

### 3.1.1 HV network

The HV-network has a short circuit capacity of 600 MVA. Since the main focus of this work is the distribution network, the HV feeding network is modelled in a very simple way by an ideal 66 kV voltage source behind an inductance. The short circuit capacity is chosen based on typical data for substations in the networks of a Norwegian utility company. In the network of one specific utility the short circuit capacity at the high voltage side of the substation transformer varies between 400 to 1000 MVA for most stations, while the largest substation has a short circuit capacity of 2000 MVA [75]. The simple modelling of the feeding network as a voltage source behind a reactance is done because the purpose is to study the distribution network. The model implies that all generators connected to the feeding network are located

far away from the substation, so that no transient responses from other generators than those connected to the distribution network are seen in the simulation results.

### 3.1.2 Substation transformer

The substation transformer is modelled using the component called 3-phase 2-winding transformer from the PSCAD library. The transformer rating is 25 MVA, and the nominal line to line voltages are 66 kV on winding 1 and 22 kV on winding 2. The leakage reactance is 0.1 pu, and copper losses are 0.005 pu referred to the transformer rating. It is assumed that more than one feeder is connected to the same substation transformer, and the rating is chosen according to the maximum total load of all feeders connected to the transformer. This maximum load is typically 50-60 % of the transformer rating [1]. It has been assumed here that the total load at high load is 14 MVA, corresponding to a transformer loading of 56 %. At present, there is a tendency to increase the loading of the transformers in the distribution networks. For the type of study performed here the ratio of the primary and secondary voltages and the short circuit characteristics are most important. Only fundamental frequency components are studied, and thus the high frequency behaviour is considered not important. Core losses and saturation have been neglected.

The transformer has a tap changer on winding 1 (on the high voltage side). The tap position is adjusted manually for low load and high load respectively. The regulations state that the voltage should be within  $\pm 10\%$  of the nominal voltage in all customer load points at the low voltage level [76]. [5] suggests narrower limits for the voltage: + 8% to – 6.5%. Limits for the medium voltage level are not stated by the regulations, so the limits for the low voltage level have been used as a guideline. The tap position is adjusted without any DG connected to the feeder, since this gives the lowest voltage at the feeder-end. The transformer is assumed to not have an automatic tap changer, and thus the same tap position is kept when the DG is connected and the voltage profile is changed. For a transformer without automatic tap changing in a real network, it can be expected that the tap position is changed only a few times per year due to varying load levels as the seasons change. Table 3.1 shows the tap positions that have been used for the low load and high load cases, respectively. Also shown are the corresponding maximum (in the substation) and minimum (at the feeder end) voltage values.

**Table 3.1: Tap positions for the substation transformer tap changer, and corresponding maximum and minimum voltages on the feeder at steady-state**

Load level	Tap position [pu]	$U_{\max}$ [pu], no DG	$U_{\min}$ [pu], no DG
Low load	0.98	1.02	0.99
High load	0.922	1.07	0.95

Setting the tap position to a value lower than 1 results in a voltage higher than the nominal operating voltage of 22 kV on the medium voltage side of the transformer. Voltage profiles at steady-state are shown in Appendix A.

The short circuit capacity of the transformer is calculated by setting the impedance equal to the leakage reactance (neglecting the copper losses), and is equal to 250 MVA. The short circuit capacity on the 22 kV side of the transformer is calculated by taking the short circuit capacities of the 66 kV feeding source and the transformer in parallel [77], and becomes 176.5 MVA. Thus the transformer is limiting the available short circuit capacity from the substation significantly as compared to the capacity available from the HV feeding network.

### 3.1.3 Line

The feeder consists of only overhead lines, and the lines are assumed to be symmetrical and transposed. The line sections are modelled using the coupled pi-equivalent model from the PSCAD library. The model is formed by using lumped R, L and C elements, with the R and L represented in matrix format and thereby providing coupling between the three phases. It provides correct fundamental frequency impedance, but it will not accurately model properties at other frequencies. Other line models which correctly represent the line at other frequencies than the power frequency are also provided by the PSCAD library. These models are based on travelling wave theory, and can thus only be used when the travel time is larger than the time step [74]. For a 50  $\mu$ s simulation time step the corresponding minimum line length is approximately 15 km. Use of a travelling wave based line model for modelling of shorter line sections thus requires a reduction of the simulation time step, which has the disadvantage of increasing the total simulation time. Only fundamental frequency components are considered in this thesis, and thus the high frequency behaviour of the line is considered not to be important. The use of the pi-equivalent line model can therefore be justified.

The feeder is made up of 9 pi-sections, each of 5 km length, and the name and conductor type for each section are shown in Table 3.2. The cross sections are reduced down the radial due to decreasing load current.

**Table 3.2: Line section name, conductor type and length**

Section	Impedance	Conductor type	Length [km]
0-1	$Z_{l,0-1}$	FeAl 1X70 26/7	5
1-2	$Z_{l,1-2}$	FeAl 1X50 6/1	5
2-3	$Z_{l,2-3}$	FeAl 1X50 6/1	5
3-4	$Z_{l,3-4}$	FeAl 1X25 6/1	5
4-5	$Z_{l,4-5}$	FeAl 1X25 6/1	5
5-6	$Z_{l,5-6}$	FeAl 1X16 6/1	5
2-7	$Z_{l,2-7}$	FeAl 1X50 6/1	5
7-8	$Z_{l,7-8}$	FeAl 1X25 6/1	5
8-9	$Z_{l,8-9}$	FeAl 1X25 6/1	5

Positive- and zero- sequence impedances for the different conductors used in the simulation model are given in Table 3.3. Positive- and negative- sequence impedances are equal.

**Table 3.3: Positive- and zero –sequence for the conductors used in the simulation model**

Conductor type	$R_+$ [ $\Omega$ /km]	$X_+$ [ $\Omega$ /km]	$X_{C,+}$ [k $\Omega$ ·km]	$R_0$ [ $\Omega$ /km]	$X_0$ [ $\Omega$ /km]	$X_{C,0}$ [k $\Omega$ ·km]
FeAl 1X70 26/7	0.257	0.362	315.471	0.404	1.600	645.659
FeAl 1X50 6/1	0.359	0.373	325.138	0.506	1.611	656.309
FeAl 1X25 6/1	0.721	0.395	345.238	0.868	1.633	675.817
FeAl 1X16 6/1	1.126	0.409	358.054	1.273	1.647	688.982

The positive sequence resistance and reactance values are taken directly from the manufacturer data [1]. The zero sequence parameters are calculated based on known geometry and assumed ground conditions, as shown in Appendix A.

### 3.1.4 Load

Loads are distributed along the feeder, and are concentrated in five load points on the main branch and three load points on the side branch. At nominal voltage, the apparent power of the five loads on the main branch is 1/6 of the total feeder load each. The remaining 1/6 of the load is made up by the three loads on the side-branch. These three loads are of equal size, so the size of each load is 1/18 of the total. The sizes of the loads in each load point are given in Table 3.4 for high load and low load.

**Table 3.4: Feeder loads at high and low load**

[MVA]	$S_{L\Sigma}^{nom}$	$S_{L-1}^{nom}$	$S_{L-2}^{nom}$	$S_{L-3}^{nom}$	$S_{L-4}^{nom}$	$S_{L-5}^{nom}$	$S_{L-6}^{nom}$	$S_{L-7}^{nom}$	$S_{L-8}^{nom}$	$S_{L-9}^{nom}$
Low load	6	1	0	1	1	1	1	0.333	0.333	0.333
High load	1.5	0.25	0	0.25	0.25	0.25	0.25	0.083	0.083	0.083

Where superscript *nom* means nominal values

The load in a distribution network consists of numerous nonlinear and switching loads with different characteristics, and many load models have been suggested. Utilities make tests and measurements to determine the load parameters in their network. Static response type models have been found to be adequate for modelling of large composite loads [78]. Static load models express the active and reactive power as a function of voltage and/or frequency at an instant of time. This type of models are used both for static load components and as an approximation for dynamic load components, [79]. Such a static load model has been used in this thesis, where the voltage dependency of the active and reactive power are given by the factors NP and NQ respectively [80]. The loads are assumed to be independent of frequency variations. Equal models have been used to model the voltage dependency of loads in e.g. [46], [36] and [52].

$$P_L = P_L^{nom} \left( \frac{|U_L|}{|U_L^{nom}|} \right)^{NP}, \quad Q_L = Q_L^{nom} \left( \frac{|U_L|}{|U_L^{nom}|} \right)^{NQ} \quad (3.1)$$

$U_L$  is the voltage across the load. In the simulation, the voltage magnitude across each line-to-line load is obtained separately using the “Single Phase RMS meter” from the PSCAD library.

The example network is not a model of a real network, and measured load characteristics from a specific network were not available. Therefore it has been chosen to model the loads using some general voltage dependency factors. With lack of more specific load data, constant current characteristics for active power loads and constant impedance characteristics for reactive power loads are commonly accepted characteristics, [79], [80]. The voltage dependency factors are summarised in Table 3.5, and these factors are used in most cases throughout this thesis. Characteristics of different load classes are shown in Appendix A.

**Table 3.5: Load characteristics used in most of the cases**

NP	NQ	$\text{Cos}(\varphi_L^{nom})$
1	2	0.9

Some simulations have been done to investigate the impact of using other load characteristics, and results are shown in Ch. 4.3.3.

Expressions for the load resistance and reactance as a function of the voltage across the load with NP =1 and NQ =2 are shown in (3.2).

$$R_L = R_L^{nom} \cdot \frac{|U_L|}{|U_L^{nom}|}, \quad X_L = X_L^{nom} \quad (3.2)$$

The load resistance is proportional to the voltage, while the load reactance is independent of the voltage. When the voltage is below half of the nominal value, constant impedance characteristics is also used for the active power. It is assumed that the load cannot maintain the constant current characteristics when the voltage is at such a low level.

In each load connection point, the loads are coupled between the phases (in delta) as shown in Figure 3.2. In reality the load would be connected to the feeder via a transformer, at low voltage level. These distribution transformers are for simplification and simulation speed not included in the simulation model. The transformers would, if included, represent additional losses in the load taps, but this is assumed to not be important for the type of fault studies carried out in this work.

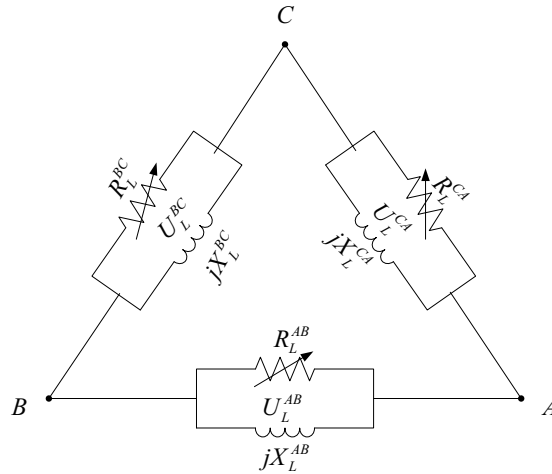


Figure 3.2: Delta coupled loads as in the PSCAD-model

The size of the resistance is controlled externally to take the voltage dependency of the loads into account. The relations between resistance and active power and between reactance and reactive power of the load between phase a and b are given in (3.3).

$$R_L^{AB} = \frac{|U_L^{AB}|^2}{P_L^{AB}}, \quad X_L^{AB} = \frac{|U_L^{AB}|^2}{Q_L^{AB}} \quad (3.3)$$

The dynamic response of the load during a transient is handled in a very simplified way by the static load model. In addition there is a time constant involved in the calculation of the RMS voltage, leading to a time-delay in the calculation of the variable load resistance in PSCAD. Due to this the characteristics given by the voltage dependency factor cannot be maintained completely in transient states. The voltage dependency factor is in reality not necessarily a constant value. Induction machine loads will for instance respond to a short circuit in a similar way as a synchronous machine, with an initial high current, decreasing with a time-constant determined by the machine characteristics. With many induction motors connected to the feeder, the short circuit current contribution from the loads would be larger than obtained using the static load model. Setting NP = 0 is a way to obtain a load characteristics approximate to that of an induction machine in steady-state, while NP = 2 is more suited to represent the machine in a transient state. In the simulation, measured values are read 50 ms

after fault inception, and it is expected that the transient short circuit currents from induction motors have died out to a large extent at this time. For the type of study based on power frequency components carried out here, the static load model is considered to be satisfactory. To get a more realistic behaviour during fault a detailed model of each load type would be required. This is considered out of the scope of this work.

More details regarding the load modeling are shown in Appendix A.

### 3.1.5 DG-unit

DG-units are modelled as synchronous generators. This generator type is the most common in small hydro power plants with active power rating of 1 MW or higher. The synchronous machine component from the PSCAD library is used. This model is programmed in state variable form, using generalized machine theory and the dq0-transformation. Data can be entered to the synchronous machine model in PSCAD on either generator format or equivalent circuit format. Usually generator data are given on generator format from the manufacturer, and this format has also been used here. In this work, all DG-units have the same parameters in per unit referred to the generator rating. This means that the generator with the highest rated power has the smallest impedance in ohm. The data used in the PSCAD-model on generator data format are given in Table 3.6. It is intended to represent “typical” data for synchronous generators used in small hydro power plants. In reality the parameter values for the generators can vary considerably, but it has been observed that synchronous generators used in small hydro power plants generally have larger reactance values in pu than what is common for the larger units.

**Table 3.6: Synchronous generator data on generator format**

Reactances [pu]		Time constants [sec]	
$x_d$	2	$T_a$	0.1
$x'_d$	0.22	$T'_{do}$	4
$x''_d$	0.2	$T''_{do}$	0.025
$x_q$	1.4	$T''_{qo}$	0.1
$x''_q$	0.2		

Since  $x_d > x_q$ , the generator has a rotor with salient poles. In the PSCAD model it is chosen to have one q-axis winding, which is used for representing salient pole machines. The inertia constant is set to  $H=1$  s. The PSCAD model requires that a value for the parameter potier reactance is entered. It is used to account for the difference between load saturation and open-circuit characteristics [80]. This parameter is usually not given on the generator data sheet, but should be a bit larger than the leakage reactance. It has here been chosen to set  $x_p=0.18$  pu.

The rated voltage on the generator terminals are 6.6 kV (line-to-line voltage). The generator transformer is modelled using the 3-phase 2-winding transformer model from the PSCAD library. Nominal line to line voltages are 6.6 kV on winding 1 and 22 kV on winding 2. The leakage reactance is 0.075 pu referred to the transformer rating. Transformer ratings for three corresponding generator ratings are given in Table 3.7. The synchronous machine model takes two inputs; mechanical torque  $T_m$  and field voltage  $E_f$ . A constant mechanical torque equal to 0.85 pu is applied to the input  $T_m$ . 0.85 is the nominal power factor of the generator, and this torque gives nominal active power generation. Rated active power is generated in all simulations. The calculation of the short circuit capacities can be found in Appendix B. Generator ratings and corresponding ratings for the generator transformer, and calculated

short circuit capacities are given in Table 3.7. The data concerns the base case and two other simulated cases.

**Table 3.7: Generator ratings used in the simulations**

Generator rating		Rated current	Generator s.c. capacity	Transformer rating	Transformer s.c. capacity	Resultant s.c. capacity on 22 kV side
[MW]	[MVA]	[kA]	[MVA]	[MVA]	[MVA]	[MVA]
3	3.57	0.31242	17.3	3.6	48	12.7
6	7.14	0.62484	34.6	7.2	96	25.4
7.5	8.93	0.78105	43.3	9	120	31.8

In Ch. 3.1.2 the short circuit capacity on the 22 kV side of the substation transformer was found to be 176.5 MVA. Comparing to the last column in Table 3.7, it is seen that the available short circuit capacity from the substation is much larger than the short circuit capacity from the generator for all three generator ratings.

The generators are assumed to have brushless excitation, which is represented by the IEEE AC8B exciter model in the simulations. The block diagram for this type of exciter is shown in Figure 3.3. An AC8B exciter model is available from the PSCAD-library, and has been used in this work.

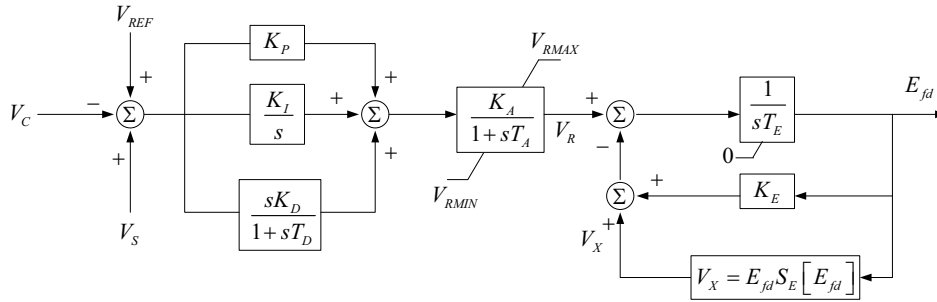


**Figure 3.3: IEEE AC8B exciter model for brushless exciter [81]**

The generator can be controlled to generate or consume a specified amount of reactive power by a VAR controller, The controller is implemented as a slow PI controller, and the voltage forms the inner loop implemented as a fast controller [82]. Block diagram representation of a VAR controller is shown in Figure 3.4.

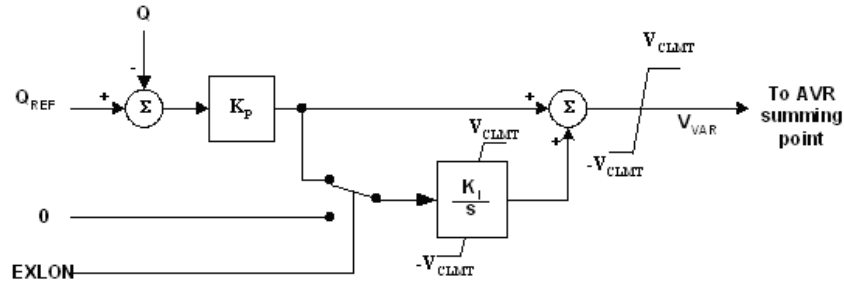


Figure 3.4: Block diagram for VAr controller type II model [82]

Reactive power ( $Q$ ) is measured on the 22 kV side of the generator transformer, and fed back to the PI-controller.  $Q_{REF}$  is set to 0, to obtain a power factor of 1. The controller is meant to control the reactive power to zero in steady-state, but have little impact during the transient state.

The parameters of the inner voltage control loop are chosen so that the requirements from transmission system operator, Statnett, as given in the FIKS document [83] are met. FIKS states the following requirements to the open-circuit response of a 5 % voltage step with brushless excitation:

- The voltage should reach 90 % of the final value within 1 s (1.045 pu within 1 s for a step from 1 to 1.05 pu).
- Maximum overshoot should be less than 15 % of the step (maximum value 1.0575 pu for a step from 1 to 1.05 pu).
- The response should be non-oscillatory.

A response fulfilling these requirements is shown in Figure 3.5, and corresponding exciter parameters are shown in Table 3.8.

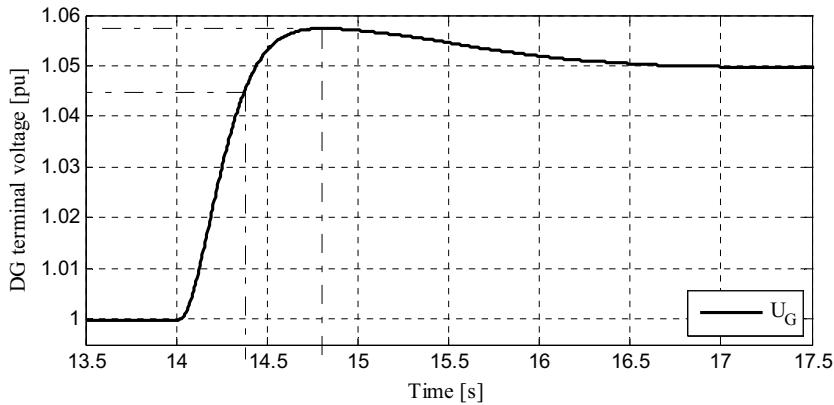


Figure 3.5: Open circuit voltage step response with exciter parameters as given in Table 3.8. Without outer VAr-controller loop.

Figure 3.6 shows the response in reactive power generated when a step from 0 to 0.1 pu is applied in  $Q_{REF}$ . The generator is operating at nominal active power. It can be seen that it takes 2.5-3 s before the new steady-state reactive power level is reached.

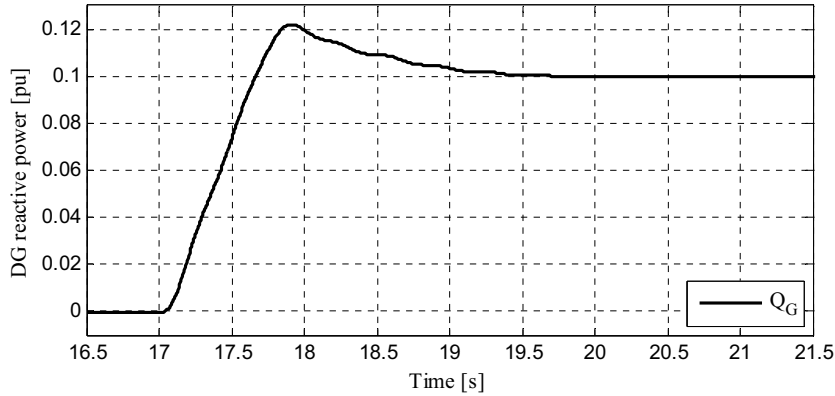


Figure 3.6: Step-response of reactive power with outer VAr-controller loop.

Table 3.8: Exciter and controller parameters

AC8B Regulator Constants		AC8B Exciter Parameters	
$K_P$	39	$T_E$ [s]	0.5
$K_I$ [pu]	45	$K_E$ [pu]	1.0
$K_D$ [pu]	73	$S_{E1}(E_{fd1})$ [pu]	1.5
$T_D$ [s]	0.09	$E_{fd1}$ [pu]	4.5
$K_A$ [pu]	1	$S_{E2}(E_{fd2})$ [pu]	1.36
$T_A$ [s]	0	$E_{fd2}$ [pu]	3.38
$V_{RMAX}$ [pu]	10		
$V_{RMIN}$ [pu]	0		
VAr Controller Parameters			
$K_P$ [pu]	1	$V_{CLMT}$ [pu]	0.1
$K_I$ [pu]	1		

The reason for choosing a power factor of 1 is that small hydro power generators commonly operate at power factors close to unity. The generator rating is in reality often chosen to be close to the turbine rating, and thus the generator has no capacity to generate or draw reactive power when operating at nominal active power. The reason for not choosing a larger generator is probably to minimize investment costs, and the fact that the plant owner sees no economical benefits related to reactive power generation or consumption.

### 3.1.6 Fault

Faults are applied using the “Faults” and “Timed Fault Logic” components. The “Faults” component is used for generating faults on a three phase AC circuit. The fault is applied via an external connection to the “Timed Fault Logic” component, which declares the time for the fault to occur and the duration of the fault. The fault type has to be declared inside the “Faults” component. The fault type can be three-phase, two-phase, two-phase-to-ground or phase-to-ground. Only three-phase and phase-to-phase short circuits are investigated in this thesis. The resistance between the phases in the normal un-faulted state is  $1 \cdot 10^6 \Omega$ , and  $0.01 \Omega$  in the faulted state.

### 3.1.7 “Measurements” in the PSCAD-model

Instantaneous currents and voltages are read in the measuring points in the PSCAD-model. For the protection and fault location phasor values are required. The conversion from an instantaneous value to a phasor is done using the fast Fourier transform (FFT) component from the PSCAD library. One FFT component is used for the conversion of each voltage and current in each of the three phases. All the FFT components are collected in a self-made block, “Fourier transform blocks”, shown in Figure 3.7 (a). The FFT component for converting the instantaneous current in phase A to a phasor is shown in Figure 3.7 (b).

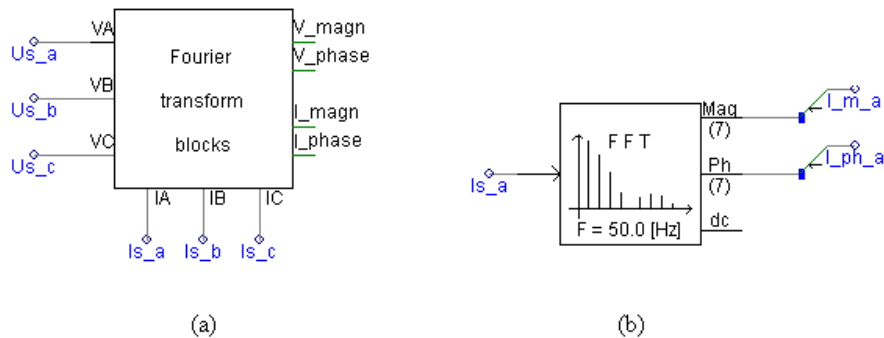


Figure 3.7: (a) “Fourier transform blocks” component, and (b) one “FFT” component from the PSCAD library, for conversion from instantaneous to phasor quantities

The FFT-block takes an instantaneous value as input, and outputs the magnitude- and phase-value of the harmonic contents of the input signal. The first harmonic (50 Hz) component is used in the fault localization. It is assumed that the dc offset is removed from the measured signal in conventional relays. Figure 3.8 shows the instantaneous DG-current,  $i(t)$ , and the first harmonic RMS current obtained from the FFT-block,  $I_{FFT,RMS}$ , in one phase, measured on the 22 kV-side of the generator transformer. The case is a three-phase short circuit occurring at  $t = 0.0$  s. at the end of the feeder in Figure 3.1, with one DG-unit located in point 3 (15 km).

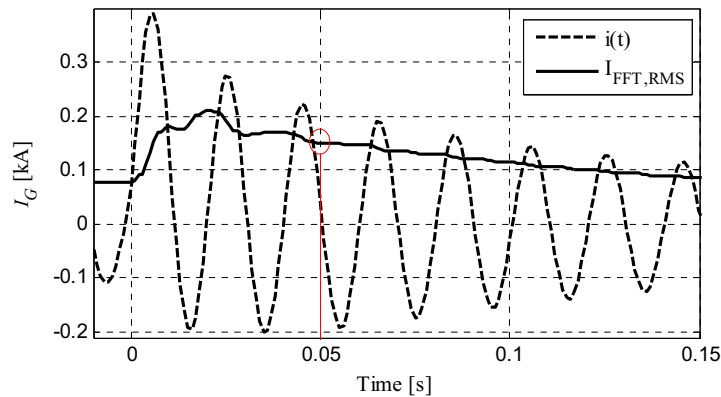


Figure 3.8: DG current on 22 kV level shown as instantaneous value,  $i(t)$ , and RMS-value obtained from the FFT-block,  $I_{FFT,RMS}$ .

The values denoted as “during fault” are read 2.5 cycles (50 ms at 50 Hz) after fault inception on the  $I_{FFT,RMS}$ -curve. In a simulation it is simple to read the fault data at a certain time after

the fault inception. In reality however, the fault inception time is not known, only the instant when the fault is detected. Thus in a practical case, the data have to be sampled a certain time after the fault detection. This requires a criterion for detection of the fault, which e.g. can be a current level or an impedance value. For simplicity this has not been done here. In another thesis [49] the data were collected three cycles after the fault is detected. The reason for this choice was to minimize the effect of current infeed by motors. The time for sampling the data should thus be a compromise between the desire to reduce the impact from infeed by motors and generators, and that the data has to be read before the feeder is disconnected.

See Appendix C for more details on the conversion between instantaneous values and phasors.

### 3.2 Lumped model used for analytical calculations

A simplified lumped feeder model is introduced in Figure 3.9. It is a general feeder model with two parallel branches (branch 1 and 2). The feeder can have one or more DG units connected on each branch. The feeder is divided into pi-equivalent sections. A section is a part of the feeder between two succeeding nodes. Feeder points classified as nodes are the substation, DG connection points, the branching point and the two feeder-end points.

The motivation for introducing this model is to have a generalized model for performing simple analytical calculations of voltages and currents on the feeder. Also the model is necessary for analytical estimation of loads. It is a lumped parameter model, with lumped load and line impedances. All series line impedances of a section are merged into one lumped impedance. Similarly all loads of a section are merged into two loads connected in shunt on each side of the line impedance. In the pre-fault steady-state operation, the apparent powers of the two loads of a section are assumed to be equal. This way of modelling the load implies that the load is evenly distributed within the section.

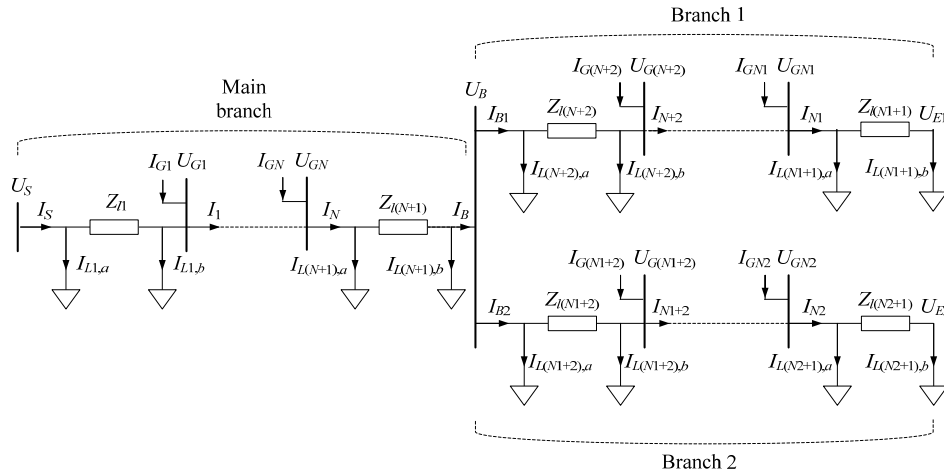


Figure 3.9: General feeder model with parallel branches and one or more possible DG-units

The number of sections and DG-units on each branch expressed by the constants by  $N$ ,  $N1$  and  $N2$  are summarized in Table 3.9. The number of sections on a branch is decided by the number of DG-units connected to the branch, and generally there is one more section than DG-units on each branch.

**Table 3.9: Number of sections and DG-units on the branches**

	Main branch	Branch 1	Branch 2
Number of DG-units	$N$	$N1-N-1$	$N2-N1-1$
Number of branches	$N+1$	$N1-N$	$N2-N1$

There are several advantages with using the simplified feeder model. The simplified model has less unknown parameters (loads, voltages, currents) that need to be estimated. Approximate calculations can be done on the feeder without an advanced simulation model and -tool available.

PSCAD simulations are performed on two types of feeders; a feeder with one DG-unit, and a feeder with three DG-units of which two are located on parallel branches. The corresponding lumped feeder models for these specific cases are described in the following sub-chapters.

### 3.2.1 Feeder with one DG-unit

The lumped model for a feeder with one DG-unit is shown in Figure 3.10. The model is valid for the pre-fault steady-state, indicated by the superscript *pre*.

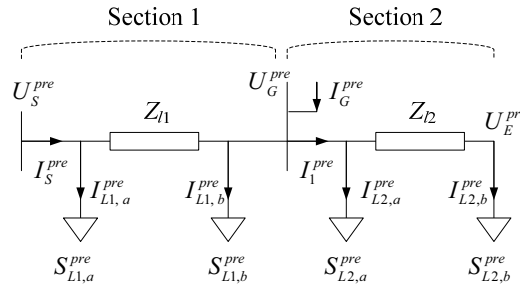


**Figure 3.10: Simplified lumped feeder model for the case when the DG-unit is connected in point 3, 15 km from the substation on the main branch**

The feeder part between the substation (node  $S$ ) and the DG connection point (node  $G$ ) is section 1. The total load of section 1 in the pre-fault state is  $S_{L1}^{pre}$ . The part of the load connected in the substation is named  $S_{L1,a}^{pre}$  and the load connected in the  $G$ -node is  $S_{L1,b}^{pre}$ . The section between the DG connection point and the feeder end is section 2, with the total load  $S_{L2}^{pre}$ . The part of the load connected in the  $G$ -node is  $S_{L2,a}^{pre}$  and the load connected in the feeder end is  $S_{L2,b}^{pre}$ . It is assumed that in the pre-fault state, the load on each side of the line impedance is equal. This implies:

$$S_{L1,a}^{pre} = S_{L1,b}^{pre} = \frac{S_{L1}^{pre}}{2} \quad S_{L2,a}^{pre} = S_{L2,b}^{pre} = \frac{S_{L2}^{pre}}{2} \quad (3.4)$$

The feeder has one side-branch, but the branching point is not treated a separate node in this case. This is done because no measurements are assumed to be available from the branching point, and there are no DG-units connected to the side-branch. In the load estimation, loads connected to a side-branch are included in the total load of the section.

As an example it can be assumed that only the DG-unit  $G2$  in Figure 3.1 is present. In the lumped model, the line impedances between the substation and the DG-node are merged into the impedance  $Z_{L1}$ , and the line impedances between the DG connection point and the feeder-end are merged into the impedance  $Z_{L2}$ . The line impedances on the side branch are neglected.

In this case the following relations between the line impedances in the two models are found in the pre-fault state:

$$\begin{aligned} Z_{l1} &= Z_{l,0-1} + Z_{l,1-2} + Z_{l,2-3} \\ Z_{l2} &= Z_{l,3-4} + Z_{l,4-5} + Z_{l,5-6} \end{aligned} \quad (3.5)$$

In a similar way the load between the substation and the DG-node is merged into two loads on each side of the lumped line impedance  $Z_{l1}$ , and the load between the DG-node and the feeder end is merged into two loads on each side of  $Z_{l2}$ . The load connected to the side branch is included in the load of the section between the substation and the DG-node. The load of section 1 can be estimated if the voltage magnitude in the DG-node is known from measurements.

### 3.2.2 Feeder with 3 DG-units

In the same way as for the feeder with one DG-unit, a simplified model for analytical calculations on the feeder with three DG-units is presented. The feeder modelled in PSCAD was presented in Figure 3.1, and the simplified model is presented in Figure 3.11. In this case, the feeder can be divided into three parts with one DG-unit connected in each. The first part is from the substation to the branching node, the second part is from the branching node to the end of the main branch, and the third is from the branching node to the end of the side-branch. This division into three parts is convenient in the analysis of the feeder during fault.

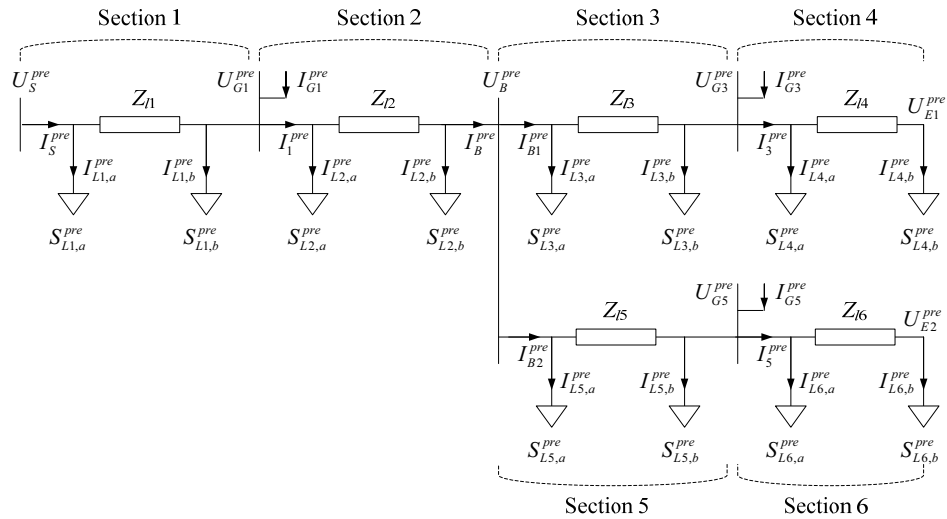


Figure 3.11: Simplified feeder model for feeder with 3 DG-units

In this case the branching point is treated as a separate node, and the feeder is divided into 6 sections. As the figure shows, the simplified model becomes much more complex in this case than for the feeder with only one DG-unit. Still, for a real MV feeder with longer lines and many side-branches this model will be a useful simplification, reducing the number of variables that needs to be estimated.

If all three DG-units are present in Figure 3.1, the relations between the line impedances in the PSCAD model and the simplified model are:

$$\begin{aligned}
Z_{l1} &= Z_{l,0-1} \\
Z_{l2} &= Z_{l,1-2} \\
Z_{l3} &= Z_{l,2-3} \\
Z_{l4} &= Z_{l,3-4} + Z_{l,4-5} + Z_{l,5-6} \\
Z_{l5} &= Z_{l,2-7} + Z_{l,7-8} \\
Z_{l6} &= Z_{l,8-9}
\end{aligned} \tag{3.6}$$

In a similar way the load between the substation and the DG1-node is merged into two loads on each side of the lumped line impedance  $Z_{l1}$ . The load between the DG1-node and the branching node is merged into two loads on each side of  $Z_{l2}$ , the load between the branching node and the DG2-node into two loads on each side of  $Z_{l3}$ , and the same way for the remaining feeder line sections.

The simplified lumped model will be used later for analytical estimation of the feeder load, and load estimation for a general feeder is described in Ch. 5.3. More specific descriptions are given in Ch. 6.2.1 for a feeder with one DG-unit, and in Ch. 6.3.1 for a feeder with 3 DG-units.

## 4 CONVENTIONAL DISTANCE ESTIMATION

This chapter deals with the use of conventional distance to fault locators on distribution feeders. Measurements from only one location, the substation, are utilized, and the distance from the measuring point to the fault location is estimated. The accuracy is influenced by several quantities, and the impacts of various parameters and components on the distance estimate are investigated. These include load (level, distribution, characteristics), DG (location, rating, parameters), fault location and type, and short circuit capacity of the source the feeder is connected to (substation transformer rating, short circuit capacity of high voltage network). The worst case in the sense of largest error in the distance estimate is found.

The feeder modelled in PSCAD introduced in Ch. 3 is shown in Figure 4.1. Initially, results without any DG connected to the feeder are shown. Most presented results are for a feeder with only one DG-unit, and the location of this unit varies. Results for a feeder with three DG-units located as shown below are presented in Ch. 4.5.

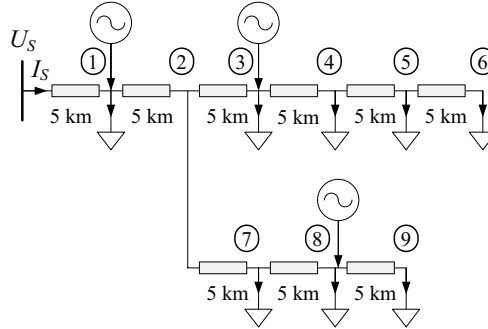


Figure 4.1: MV-feeder modelled in PSCAD

General abbreviations used in the figure legends in the following subchapters are given in Table 4.1.

Table 4.1: Abbreviations used in the figure legends

Legend	Explanation
3 $\phi$	Three-phase short circuit
2 $\phi$	Two-phase short circuit
LL	Feeder at low load
HL	Feeder at high load
1	With compensation 1
2	With compensation 2

The plots start at 5 km on the x-axis. This means that the fault location or DG-connection point is varied from 5 to 30 km. The 0 km point is omitted because it corresponds to the substation, and a DG located there is not assumed to be connected to the feeder, but instead directly to the substation.

### 4.1 Conventional distance-to-fault estimation

Impedance relays are the most common line protection at transmission level, and in meshed networks. They respond to the impedance between the measurement point and the fault

location [84]. For a fault between two phases, the impedance can be obtained from the substation voltages and currents in the two phases involved. The difference between the two phase-voltages is divided by the difference between the two phase-currents, and this can be written in a simpler form using the  $\Delta$ -symbol as shown in (4.1). For a three-phase short circuit the voltages and currents in any pair of phases can be used to calculate the distance. The equation is thus valid for both two-phase and three-phase short circuits [11], [85].

$$Z_S = \frac{U_S^B - U_S^C}{I_S^B - I_S^C} = \frac{\Delta U_S}{\Delta I_S} \quad (4.1)$$

Where  $Z_S$  is the impedance between the measuring point and the fault location

A single line diagram illustrating the impedance  $Z_S$  is shown in Figure 4.2. Possible loads or DG-units connected to the feeder are ignored.

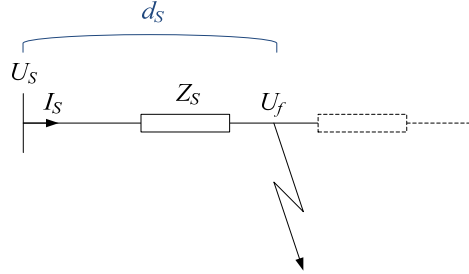


**Figure 4.2: Simplified model showing the distance to the fault location obtained from substation measurements only**

Relays energized by delta voltages and currents respond to the positive sequence impedance between the measurement point and the location of a multiphase fault. A complement of three phase-distance relays covers the seven possible multi-phase faults. These faults are double phase, double phase to ground and three phase faults [11]. Using delta voltages and currents thus has a practical justification, as the number of relays required to cover all multiphase faults are minimized, which is a great advantage.

The impact of the fault resistance is neglected in (4.1). The impedance in (4.1) can be used for fault localization. The reactance (imaginary) part of the measured impedance is then normally used [86]. In this way, the impact from a possible fault resistance is eliminated or reduced. The impedances per unit of length of each feeder line section are assumed to be known, and the distance to the fault location can be estimated by the following equation:

$$d_S = \frac{\text{Im}(Z_S)}{x_l} = \frac{X_S}{x_l} \quad (4.2)$$

$d_S$ : distance from measuring point to fault location [km]  
 $x_l$ : line reactance per unit of length [ $\Omega$ /km]

A distribution feeder will generally not have lines with constant cross-section area, and thus the parameter  $x_l$  will not be a constant throughout the feeder length. This means that the relationship between the reactance  $X_S$  and the distance to the fault is not linear, as on transmission level. The algorithm for the conversion from impedance to distance for a feeder with various cross-section areas is shown in the flow chart in Appendix, Figure C.3. The flow chart shown corresponds to the main branch of the feeder presented in Figure 3.1. The distance obtained is used as a starting point for the calculations in both compensation methods

described in the next chapter. Figure 4.3 shows a graphical representation of the relation between the distance and the impedance seen from the substation. From the calculated impedance to the fault location, the corresponding distance can be read out of the curve in Figure 4.3. If the reactance input is  $Z_{in} = Z_S$ , then the distance output is  $d_{out} = d_S$ .

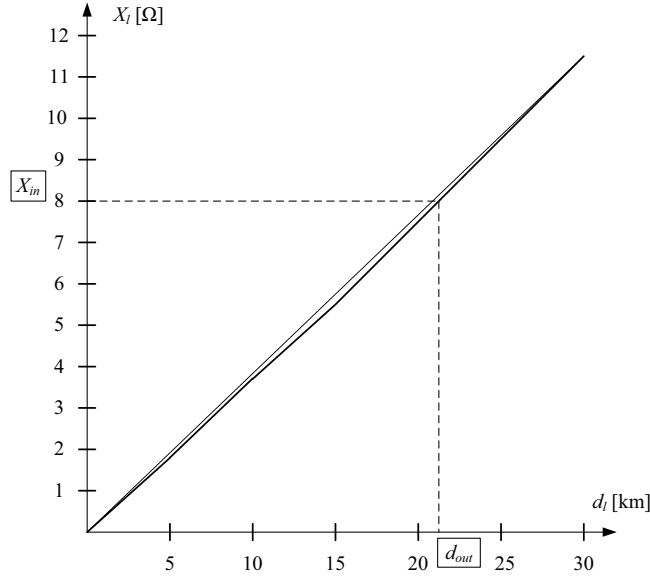


Figure 4.3: Estimated reactance to the fault location,  $X_{in}$ , and the corresponding distance,  $d_{out}$

As an example, one reactance and the corresponding distance are shown in the figure. A reactance  $X_{in} = 8 \Omega$  corresponds to a distance to the fault location,  $d_{out} = 21.3$  km. The non-constant cross-sections have been taken into account, but it can be seen that there is very little difference between the reactance values of the line sections as the curve is increasing approximately linearly. It is first and foremost the resistive part of the line impedance that is changed when the cross-section is changed, and a linear approximation could have been used. The curve with a linear relation between distance and reactance is shown with a stippled line, using the average line reactance for the feeder.

## 4.2 Impact of fault resistance

In Ch. 4.1 it was stated that the reactance part of the impedance is commonly used for fault localization, with the intention of avoiding impact from fault the resistance. The purpose of this chapter is to justify this choice. In phase-to-phase faults the fault resistance is due to the arc-resistance. This arc resistance is dependent on the magnitude of the fault current, thus in reality it will not be constant for the different fault locations. The fault resistance for this fault type is generally much smaller than for phase-to-earth faults. One empirical formula for calculation of the arc resistance  $R_{arc}$  is Van Warringtons [87] formula:

$$R_{arc} = \frac{28700 \cdot l_{arc}}{I_{sc}^{1.4}} \quad (4.3)$$

$l_{arc}$  is the length of the arc in meter  
 $I_{sc}$  is the short circuit current in ampere

A larger short circuit current means a smaller arc resistance, so the arc resistance will be smallest for a fault close to the substation. In addition, the short circuit currents will increase

with distributed generation on the feeder, and this will result in reduced arc resistances. [88] presented an alternative approach for calculating the arc resistance based on experimental tests, intended for MV networks. The method takes the impact from DG on the fault current level into account.

The arc-resistances for three-phase short circuits at different fault locations have been calculated using an iterative approach in MATLAB. Cases without DG and with a 3 MW DG-unit connected at 5 km or 30 km from the substation have been considered, and results are shown in Table 4.2. The arc length has been set equal to the distance between the phases.

**Table 4.2: Arc resistances [ $\Omega$ ] for different fault locations**

Fault location	[km]	5	10	15	20	25	30
No DG	[ $\Omega$ ]	0.358	0.621	0.945	1.518	2.204	3.339
3 MW DG in 1	[ $\Omega$ ]	0.367	0.621	0.946	1.527	2.230	3.395
3 MW DG in 6	[ $\Omega$ ]	0.367	0.637	0.971	1.562	2.273	3.449

It can be seen that the fault resistances are quite small for this feeder, and the largest value is 3.45 Ohm. When the DG-unit is connected to the feeder, the fault resistance values are slightly increased.

#### 4.2.1 Impact of fault resistance on feeder with one DG-unit

For a feeder without DG it is assumed that the impact of the fault resistance on the distance estimate obtained from the reactance is negligible. Simulations have been done to find out if this assumption is valid also for a feeder with DG. If the currents fed to a fault from the substation and from the DG is not in phase, the fault resistance could have an impact also on the reactance part of  $Z_s$ . It is expected that worst case would be when the DG-unit is connected at the feeder end, so the results from this case are shown in Figure 4.4. Results are shown for three fault resistance values:  $R_f = 0.01$ , 1 and 5  $\Omega$ . The values are chosen based on the resistances in Table 4.2. In each case the same fault resistance has been used in all fault locations. This is not quite in accordance with reality where the fault resistance would depend on the short circuit current, e.g. as described by (4.3), but is done here for simplicity.

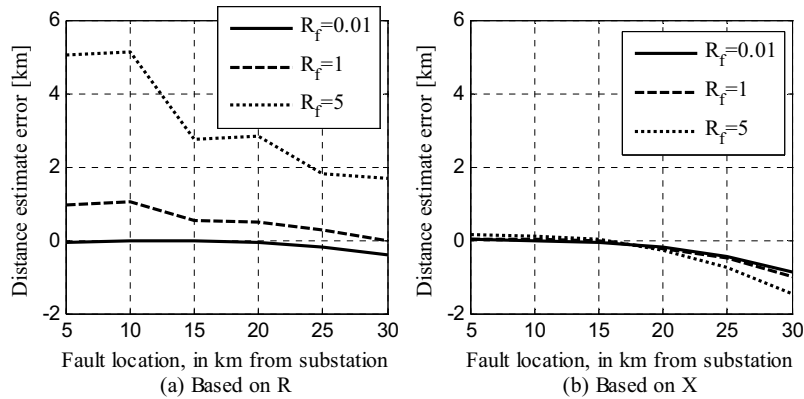


**Figure 4.4: Distance estimate errors when estimated from (a) resistance and (b) reactance, with low load. The DG is located at the end of the feeder (30 km from the substation), and all faults are 3-phase short circuits.**

For the distance estimate based on resistance, shown in Figure 4.4 (a), the fault resistance impacts on the estimate, especially when the fault is located close to the substation. Figure 4.4 (b) shows that the distance estimated from the reactance is little dependent on the size of the fault resistance, even with a DG-unit feeding current to the fault from the end of the feeder. Some impact from the fault resistance is seen when the fault is also at the end of the feeder. Still, the results shown in Figure 4.4 justify the use of the reactance part of  $Z_S$  for distance estimation.

### 4.3 Conventional distance estimation in network without DG

In a network without any DG, the error in the distance estimate is mostly due to loads connected along the feeder. The load generally cause a negative error in the estimate, and thus makes the fault appear to be located closer to the substation than it is in reality. The distance estimate error is expected to increase (become more negative) as the load level is increased. The voltage dependency characteristic and distribution of the loads is also expected to be of importance, and this is investigated in the following.

#### 4.3.1 Impact of load level on distance estimate

On medium voltage level, there can be loads connected through distribution transformers along the whole feeder length. Generally the load cause a negative distance estimate error, and thus faults appear to be located closer to the substation than they are in reality. The distance estimate errors for low load and high load, and for three-phase and two-phase short circuits at varying locations are shown in Figure 4.5.

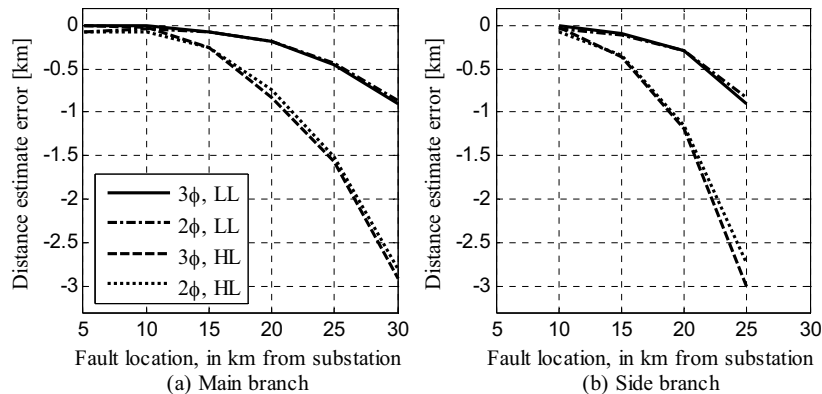


Figure 4.5: Impact of load level on the distance estimate errors for low load and high load. 3-phase and 2-phase short circuits at varying locations on (a) the main branch and (b) the side branch.

The load current causes a negative error in the impedance. The error is proportional to the load current, and thus it is larger for the high load cases than for low load. The error is also proportional to the line impedance between the load connection point and the fault location. This impedance is increasing with the distance to the fault location and is larger for a line with small cross-section area. This is most clearly seen on the curves for high load in Figure 4.5 (a), where the slope of the curves are steepest between 25 and 30 km, which is the line section with the smallest cross-section.

The errors are a bit larger for three-phase than two-phase short circuits, but generally the differences between the results for the two fault types are very small. Worst case is a three-

phase short circuit at the end of the side branch when the feeder is at high load. For fault at the end of the main branch the largest error is -2.9 km or -9.7 %, while for a fault at the end of the side branch the largest error is -3.0 km or 10 %.

### 4.3.2 Impact of load distribution

The normal load distribution, L-N, was described in chapter 3, and means that loads are evenly distributed along the feeder as shown in Figure 4.6 a). (This is the default load distribution, used unless something else is mentioned.) Load distribution L-1 is shown in b), and means that the entire load is connected in point 1, 5 km from the substation. Load distribution L-6 is shown in c), and means that the entire load is connected in point 6, 30 km from the substation, on the main branch.

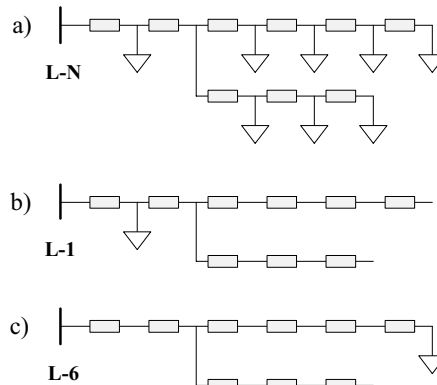


Figure 4.6: Illustration of the three load distribution L-N, L-1 and L-6

A comparison between the distance estimate errors for these three load distributions are shown in Figure 4.7.

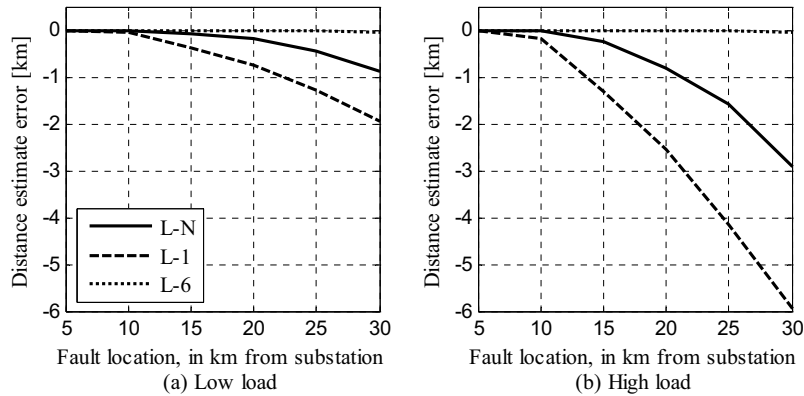


Figure 4.7: Impact of load distribution on distance estimate errors on a feeder without DG. With 3-phase short circuits located on the main branch for (a) low load and (b) high load.

The distance estimate error is largest when the entire load is located 5 km from the substation, which is as expected since all of the load will be between the substation and the fault location for all fault locations except the one 5 km from the substation. Thus the total load impacts on

the distance estimate in all cases. Worst case appears when the fault is located at the feeder end. The error is then -1.9 km or -6.5 % for low load and -6 km or -19.9 % for high load.

If the load is concentrated in point 6, the load has no impact on the distance estimate, and the error is close to zero for all fault locations. This is also as expected, since the load is not located between the substation and the fault location.

### 4.3.3 Voltage dependency factor

Since the feeder voltage decreases when there is a short circuit the voltage dependency of the loads is of importance. The default voltage dependency factor for the active power of the load is  $NP = 1$ , which means that the current drawn by the load is constant as described in chapter 3.5. The active power is then proportional to the voltage across the load.  $NP = 0$  means that the active power is independent of the voltage, and the load draws a constant active power.  $NP = 2$  means that the load has a constant impedance characteristics, and the power drawn by the load is proportional to the voltage squared. The three characteristics are summarized in Table 4.3.

**Table 4.3: Three voltage dependency factors and corresponding active power load characteristics**

$NP = 0$	constant active power load
$NP = 1$	active power is a constant current load (default)
$NP = 2$	active power is a constant impedance load

The impact of the voltage dependency factor  $NP$  on the distance estimate error is studied in this chapter. Figure 4.8 shows the errors for the three different factors at (a) high load and (b) low load level. The plots are obtained from PSCAD simulations with loads with three different voltage dependency factors for the active power. In each of the cases all loads on the feeder had the same voltage dependency factor.

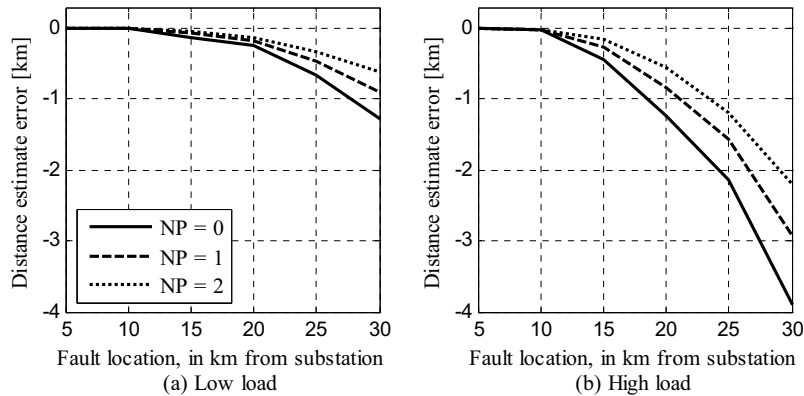


**Figure 4.8: Distance estimate errors for three different voltage dependency factors for the load. 3-phase short circuits at varying locations on the main branch.**

The largest errors occurs when the active power is independent of the voltage ( $NP = 0$ ). This is as expected since the active power drawn by the load is not reduced during short circuit. The smallest errors occurs when the active power is proportional to the voltage squared ( $NP = 2$ ). This is also as expected since it is the case with the largest decrease of the power drawn by

the load during a short circuit. The largest distance estimate errors for the three voltage dependency factors are given in Table 4.4 for low load and high load.

**Table 4.4: Worst case distance estimate errors for three voltage dependency factors for active power**

	Low load		High load	
	[km]	[%]	[km]	[%]
NP = 0	-1.3	-4.2	-3.9	-13.0
NP = 1	-0.9	-3.0	-2.9	-9.7
NP = 2	-0.6	-2.1	-2.2	-7.4

#### 4.4 Conventional distance estimation in network with one DG-unit

A feeder with DG and one side-branch was shown in Figure 3.1. The connection point of the DG-unit can be moved along the main branch of the feeder, which means that it can be connected in point 1 (5 km) to point 6 (30 km). The fault location can be in all load points along the main branch or the side-branch. The DG generally causes a positive error in the distance estimate when it has a common path with the main feeding source, [21]. The fault location then appears to be farther away from the substation than it is in reality. As the load and DG have opposite impacts on the distance estimate, they to some degree counterbalance each other. This means that the distance estimate error on a feeder with DG is largest at low load. Figure 4.9 shows the feeder with one DG-unit that can be connected in one of the 6 load points on the main feeder branch. In most cases the DG is generating rated power of 3 MW. The faults are 2-phase (2 $\phi$ ) or 3-phase (3 $\phi$ ) short circuits at the end of the main branch.

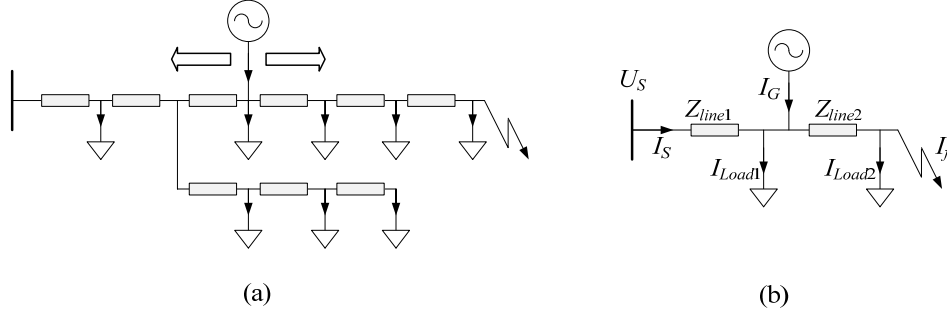


**Figure 4.9: (a) Feeder simulated in PSCAD with short circuit at the end of the main branch and (b) simplified model for approximated view. The DG-unit can be located in one of the 6 load points on the main branch.**

Referring to Figure 4.9 (b), the following approximate expression for the error in the impedance seen from the substation to the fault location,  $\varepsilon_Z$ , can be found for a three-phase short circuit:

$$\varepsilon_Z = \frac{1}{I_S} \left( -Z_{line1} I_{Load1} + Z_{line2} (I_G - I_{Load}) \right) \quad (4.4)$$

Where  $I_{Load} = I_{Load1} + I_{Load2}$

This expression can be used to make some simplified considerations about the size of the error. If the load currents are increased while  $Z_{line1}$  and  $Z_{line2}$  are held constant, the first term in (4.4) is increased in magnitude and the second term is decreased. Increasing the load thus corresponds to moving the distance estimate curve downwards. Further, a DG connected close

to the substation corresponds to a relatively small  $Z_{line1}$  and a large  $Z_{line2}$ , and a large influence from the term containing the DG-current.

#### 4.4.1 Impact of the location of the DG-unit

How much impact the DG-unit has on the distance estimate depends on where on the feeder it is connected. The distance estimate errors for the various DG-locations are shown in Figure 4.10.

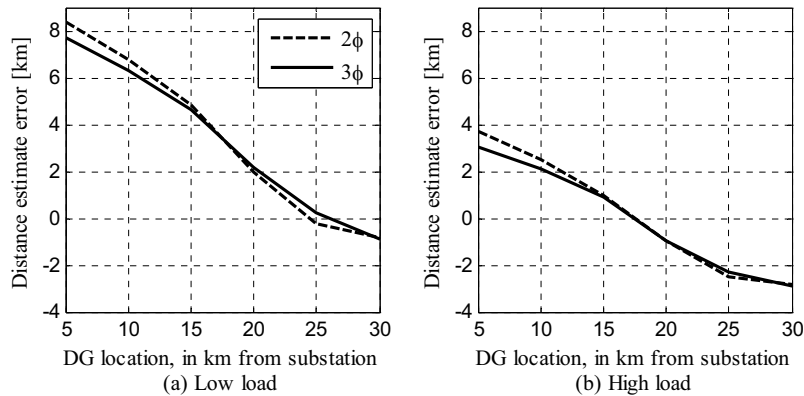


**Figure 4.10: Distance estimate errors for short circuits at the end of the main feeder branch. The connection point of the DG is varied along the main branch. (a) Low load and (b) high load.**

It can be seen that the largest error occurs for a two-phase short circuit at low load when the DG is connected 5 km from the substation. The error is then 8.4 km. The difference between the results for three-phase and two-phase short circuits are minor. The load level appears to be very important, and the largest error at high load is 3.7 km. The errors are decreasing as the DG connection point is moved from the substation to the feeder end. For low load the error is close to zero when the DG is connected at 25 km and becomes negative when the DG is connected at the feeder end. For high load the error goes from positive to negative as the DG is moved from 15 to 20 km.

A positive error means that the impact from the DG is larger than the impact from load during fault. The error is largest in the low load case, since load and DG has opposite impacts on the distance estimate, and lesser load means larger impact from the DG. When the DG is connected at the feeder end it has no impact on the distance estimate, and only load contribute to the distance estimate error. Referring to (4.4), with a fixed fault location, the sum of the currents in the second term can be assumed to be equal to a constant value ( $I_G - I_{Load} = \text{constant}$ ). Moving the DG connection point from the substation to the feeder end corresponds to increasing the first term ( $Z_{line1}$  and  $Z_{Load1}$  are increased), and decreasing the second term ( $Z_{line2}$  is decreased). The curves cross zero when the two terms become equal in magnitude. As increasing the load level means lowering the entire curve according to (4.4), the curves cross zero for a DG connection point closer to the substation for high load than for low load.

#### 4.4.2 Impact of the fault location

The impact of the location of the fault on a feeder with one 3 MW DG-unit connected 5 km from the substation is shown in Figure 4.11. Curves for low load are plotted in (a) and curves for high load are plotted in (b). Figure 4.12 shows the impact of the load when the same DG-

unit is connected 15 km and 30 km from the substation and the feeder is at low load. The fault location is varied along the main branch (a) and the side branch (b).

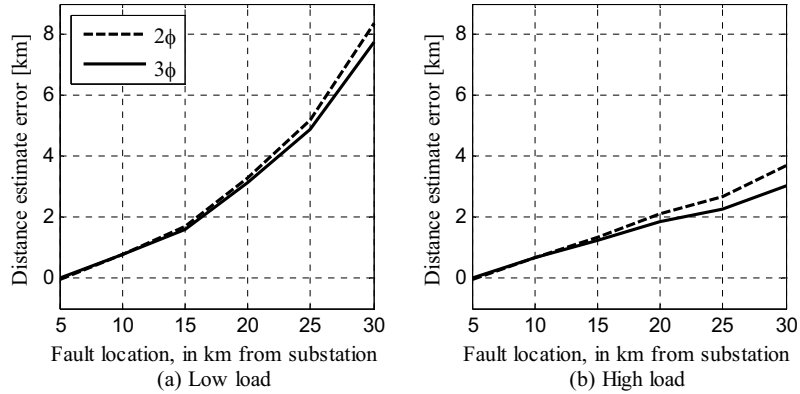


**Figure 4.11: Distance estimate errors when the DG is located 5 km from the substation and the fault location is varied along the main branch. 3-phase and 2-phase short circuits at (a) low load and (b) high load**

The distance estimate error increases as the fault location is moved from 5 to 30 km. The error is larger for low load than high load, approximately doubled. Two-phase short circuits cause larger errors than three-phase short circuits, [21]. However, the differences between the two fault types are not very large. The largest distance estimate error is 8.4 km.

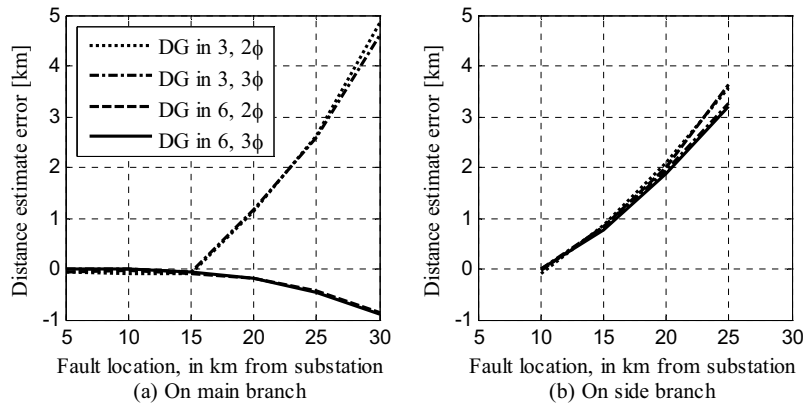


**Figure 4.12: Distance estimate errors when the DG is located 15 or 30 km from the substation for low load. 3-phase and 2-phase short circuits on (a) main branch and (b) side branch**

Figure 4.12 (a) shows that the DG only impacts on the distance estimate when the fault is located after the DG-connection point. When the DG is connected in point 3 the error is close to zero for faults located between the substation and 15 km, while for faults located after 15 km the error is positive and increasing as the fault is moved towards the feeder end. When the DG is connected in point 6 it has no impact for faults on the main branch. The error is due to load, and is negative and increasing in magnitude as the fault location is moved towards the feeder end. The difference between three-phase and two-phase faults are minor. Figure 4.12 (b) shows that the DG impacts on the distance estimate error for all fault locations on the side branch. This is due to side infeed from the generator to the fault. Two-phase short circuit at

the end of the side branch (25 km) give the largest error. For three-phase short circuits the errors are slightly smaller. The side infeed depends very little on how far from the faulted branch the DG is located. The impact from the DG for a fault on the side branch between the substation and the DG is in principle the same as the impact for a fault located after the DG, and originates from the common path of the fault currents from the substation and the DG to the fault location.

#### 4.4.3 Impact of generator rating

The effect of increasing the rating of the DG-unit is shown in Figure 4.13 for (a) low load and (b) high load. The DG is connected 15 km from the substation, and generates rated power in all cases.

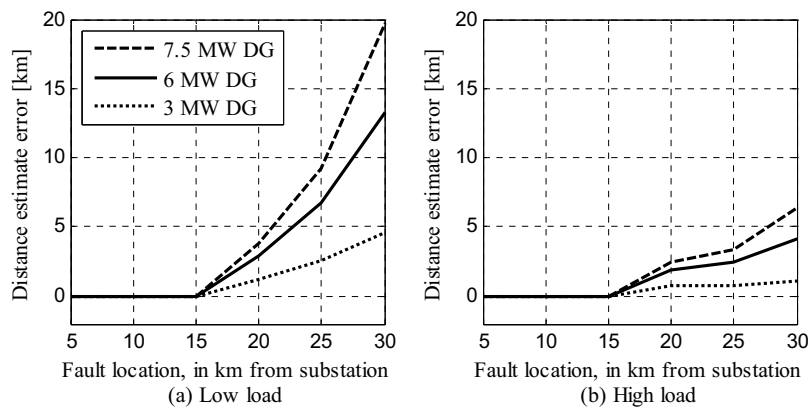
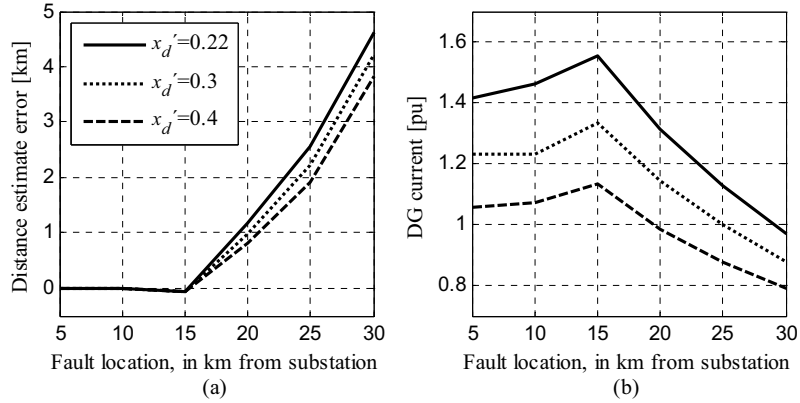


Figure 4.13: Distance estimate errors for 3-phase short circuits at varying locations along the main feeder-branch for (a) low load and (b) high load. DG connected at 15 km, generating 3, 6 or 7.5 MW

It can be seen that the DG has no impact on the distance estimate for faults located before the DG connection point, independently of the generation level. Maximum error occurs when the fault is located at the feeder end and at low load. Maximum error with 3 MW DG is 4.6 km, 13.3 km with 6 MW DG and 19.75 km with 7.5 MW DG. This means that doubling the generation from 3 to 6 MW results in almost a tripling of the maximum error. A 2.5 times increase from 3 to 7.5 MW results in a 4.3 times increase of the maximum error. That is, the level of generated power from the DG is significant for the accuracy of the distance estimation. Maximum errors at high load are approximately one fourth of those at low load, and thus the load level is very important.

#### 4.4.4 Size of the d-axis transient reactance

The short circuit current of the generator is dependent of the generator impedance and the loading of the generator prior to the fault. For the transient part of the short circuit current, the size of the transient reactance is most important. Figure 4.14 (a) shows the distance estimate error and (b) the short circuit current magnitude for three different d-axis transient reactance values as a function of the fault location. The DG is generating nominal power (3 MW), and is connected at 15 km. The reactance values are in pu referred to the generator rating.



**Figure 4.14: (a) Distance estimate errors and (b) DG short circuit current with 3-phase short circuits at varying locations along the main feeder branch at low load. 3 MW DG-unit connected in point 3 (15 km)**

0.22 is the reactance value normally used throughout this work. The distance estimate error is largest for the smallest reactance value. A decrease of the transient reactance causes a decrease also in the transient internal emf. Still, a smaller reactance leads to a higher short circuit current and a larger distance estimate error, as can be seen from Figure 4.14 (b). The short circuit current from the DG-unit is also largest when the fault is located close to the connection point, and decreases when the fault location is farther away.

In the simulations, only the d-axis transient reactance was changed. For a real generator a different transient reactance would cause changes in other generator parameters, since they are not independent.

#### 4.4.5 Impact of substation transformer rating

The available short circuit capacity from the substation depends on the capacity of the high voltage feeding network, the substation transformer rating and the loading of the neighbouring feeders. In this subchapter the effect of decreasing the substation transformer rating is examined, as a decrease of the transformer rating results in a decrease of the available short circuit power from the substation. Figure 4.15 shows a comparison of the distance estimate error when the transformer rating is 25 MVA and 12 MVA. There is a 3 MW DG connected at 15 km.

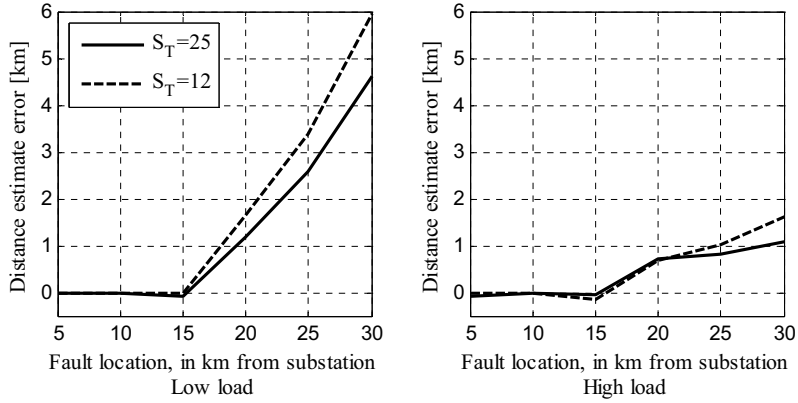


**Figure 4.15: Distance estimate errors for two different substation transformer ratings for (a) low load and (b) high load. 3 MW DG at 15 km and 3-phase short circuit at varying locations along the main branch.**

The errors are largest for the lowest transformer rating. With less short circuit power available from the substation, the DG will have more impact. When the transformer rating is approximately halved from 25 to 12 MVA the largest error is increased by 28.5 %, from 4.6 km to 6 km. A reduction of the 66 kV feeding source short circuit capacity will have the same impact as the reduction of the substation transformer, but generally the transformer capacity is the limiting factor.

Usually there will be more than one feeder connected to the substation. Some of the available short circuit power from the substation is consumed by the load on the neighbouring feeders. This will become more noticeable if the fault is located far from the substation, so that the voltage in the substation remains at a relatively high level during fault. Also the voltage dependency characteristics of the loads on the neighbouring feeders are of importance. The load on the adjacent feeder seems to have a negligible impact on the distance estimate error for the low load case, but some more impact for high load.

#### 4.4.6 Impact of feeder length

The feeder length is expected to be important for the accuracy of the distance estimate. A feeder with a total length of 60 km for the main branch is shown in Figure 4.16. The feeder is equal to the 30 km long feeder, but the length of each line section is doubled.

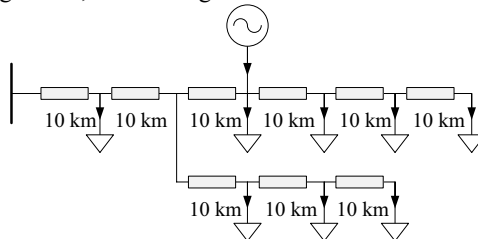


**Figure 4.16: Feeder with 10 km line sections, and total length of the main feeder branch equal to 60 km**

Results are shown for 3 MW DG-unit located in two different locations for the two feeder lengths in Figure 4.17 (a) for low load and (b) for high load. The plot legends are explained in Table 4.5.

**Table 4.5: Explanation of plot legends for Figure 4.17**

DG in 1, 60 km	DG located 10 km from the substation, total feeder length is 60 km
DG in 3, 60 km	DG located 30 km from the substation, total feeder length is 60 km
DG in 1, 30 km	DG located 5 km from the substation, total feeder length is 30 km
DG in 3, 30 km	DG located 15 km from the substation, total feeder length is 30 km

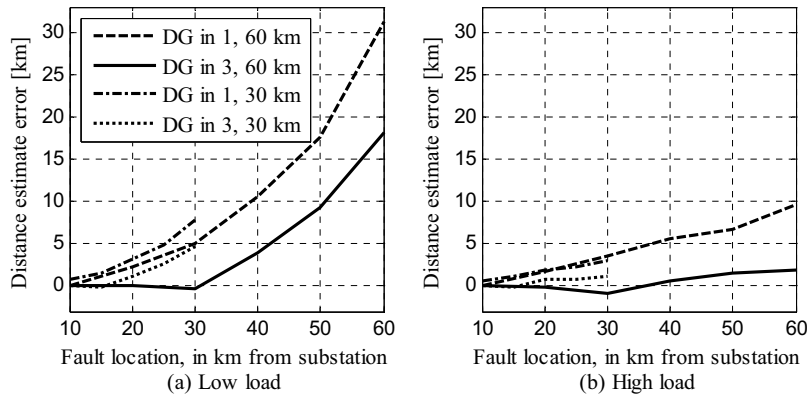


**Figure 4.17: Distance estimate errors for two feeder lengths, 60 and 30 km at (a) low load and (b) high load. 3 MW DG-unit located at 5 or 15 km for the 30 km feeder, and at 10 or 30 km for the 60 km feeder.**

It can be seen that for the low load cases there is a large increase of the distance estimate error as the fault location is moved towards the end of the 60 km feeder. For high load the increase is smaller, and the curve is not so steep. Referring to (4.4), the DG- and load- currents can be assumed to remain approximately unchanged when the feeder length is doubled, even though the voltages in the load and DG connection points during fault are a bit higher for the longer feeder. This implies that a doubling of the feeder length would lead to a doubling of the errors. As seen from Figure 4.17 (a), the errors are more than doubled, and this is because the substation fault current is reduced. With the DG connected at the middle of the feeder and the fault located at the feeder end at low load, the substation current is more than halved from 3 pu for the 30 km to 1.4 pu for the 60 km feeder. A doubling of the total feeder impedance and halving of the substation current is thus expected to result in a four times larger error. This corresponds quite well with the results seen in the plot, at least for low load. For high load, the small decrease in the DG short circuit current, and the small increase of the load currents during fault when the feeder length is doubled become more important. The errors were quite small for the 30 km feeder, and are not increased much when the feeder length is doubled.

The largest error is 31.2 km for a fault at the feeder end (60 km) and the DG connected 10 km from the substation at low load. Largest error for a fault at the end of the 30 km feeder with the DG connected 5 km from the substation was 7.7 km. For high load the largest error is 9.6 km for a fault at the 60 km feeder, and 3.1 km for the 30 km feeder.

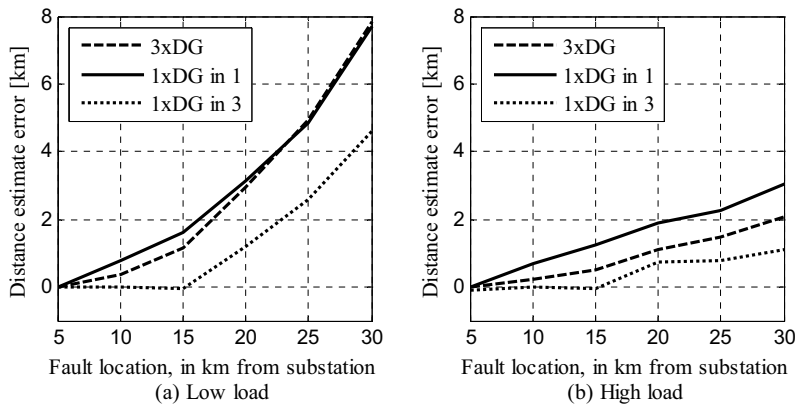
#### 4.5 Feeder with 3 DG-units

Figure 4.1 showed a feeder with 3 DG-units, and in this subchapter each unit is assumed to generate nominal power of 1 MW each. This means that the total generation is 3 MW, which is the same level as in previously shown cases for a feeder with one DG-unit. The case with three DG-units is compared to the case with one unit with equal total generated power, with

three-phase short circuits at varying locations along the main feeder branch. Results are shown in Figure 4.18 (a) for low load and (b) for high load, and the plot legends are explained in Table 4.6, referring to Figure 4.1.

**Table 4.6: Explanation of plot legends for feeder with 3 DG-units**

3xDG	3 DG units generating 1 MW each. Connected in point 1 and 3 on the main branch, and point 8 on the side branch
1xDG in 1	1 DG unit generating 3 MW. Connected in point 1 on the main branch
1xDG in 3	1 DG unit generating 3 MW. Connected in point 3 on the main branch



**Figure 4.18: Comparison between distance estimate errors for a feeder with three DG-units, generating 1 MW each and one unit generating 3 MW. 3-phase short circuits along the main branch for (a) low load and (b) high load.**

For low load the errors are approximately equal with one DG-unit located 5 km from the substation as with three DG-units. With one DG-unit connected at 15 km errors are smaller. It can be concluded that DG-units connected close to the substation contribute most to the distance estimate error. For high load one DG-unit located 5 km from the substation is worst case, but overall errors are generally lower than for the low load cases. In a simplified study it can be desirable to represent a number of DG-units connected to the same feeder by one big aggregated DG-unit. It can be concluded that this aggregated unit should be located in the same point as the unit closest to the substation or closer, in order to study the worst cases.

## 5 GENERAL METHOD FOR COMPENSATION OF LOAD AND DG ON THE DISTANCE ESTIMATION

Conventional distance to fault locators can be used to estimate the distance to a fault on a distribution feeder. The distance to the fault is estimated from the substation voltage and current, utilizing knowledge of the impedance per unit of line length. Chapter 5 showed how different parameters impact on the accuracy of this distance estimation. Load and DG-units connected along the feeder were seen to cause substantial errors in the distance estimate. Loads reduce the estimated distance compared to the real, while DG-units have the opposite impact and increase the estimated distance compared to the real. In order to use distance to fault locators on distribution feeders with sufficient accuracy, these errors should be compensated for. This chapter presents two methods for calculation of compensated distance estimates. Through these new methods more accurate distance estimates can be obtained by compensating for the impacts from load and DG.

The estimation of the compensated impedance ( $Z_C$ ) seen from the substation to the fault location is explained in the following subchapters. The equations used in the process are valid for both three-phase and two-phase short circuits. The estimated distance to the fault location after the impacts from load and DG are compensated for, is calculated using known feeder impedances as shown in Figure 5.3. Input to the algorithm in this case is the calculated impedance  $Z_C$ , and output is the distance to the fault,  $d_C$ .

The main challenge in the distance estimation in a distribution system, compared to a transmission network is the large number of load taps, and lack of measurement along the feeder. Typically, the actual size of the loads is unknown, at least for the fault handling system. Only the location and installed capacity of distribution transformers are known. In many networks also the DG-unit operating conditions may be unknown. This will have to change in the future, and here the pre-fault operating conditions of DG-units are assumed to be known. Besides, the responses of both loads and DG-units during fault have to be considered.

An important objective when developing the compensation methods has been to keep the use of measurements from locations outside the substation at a minimum. In case of utilizing measurements from the DG-units, only magnitude value measurements are required in the algorithms. The advantage of not requiring phasors is that the time-synchronization between measurements from the DG and the substation does not need to be as accurate as if instantaneous measurements were used.

### 5.1 Two compensation methods

Two methods for calculations of compensated distance estimates are presented. Both methods make use of pre-fault measurements from the DG-unit(s) together with pre-fault substation measurements to establish the pre-fault load distribution. The use of pre-fault substation measurements for estimation of the pre-fault load has been suggested by other authors,[39], [78], [65], [47], [89], [48], [12], [52]. The difference between the two methods is the measurements which are used. The presented methods are not two alternative ways to calculate the compensated distance estimate, and choice of method can be done from the actual data available for the protection system during fault. Method 1 is used if only pre-fault measurements are available from the DG-unit(s), while method 2 is used if also measurements during the fault are available. The available measurements are always utilized, and method 1

will not be used if DG measurements are available during the fault. Method 1 is easiest to implement for a feeder with only a few DG-units. If DG-units are connected to parallel branches, pre-fault measurements from the branching node are required. For a feeder with many DG-units it is a great advantage to have measurements from the DG-units also during fault.

The necessary input data and measurement for both methods and additional required measurements in method 2 are summarized in Table 5.1. All line impedances of the feeder,  $Z_{ln}$ , are assumed to be known. The distance from the substation to all DG-units,  $I_{Gn}$ , are known. Also common power factor angles of the load in each section,  $\varphi_{Ln}^{pre}$ , are assumed to be known. The pre-fault measurements available from the DG are voltage- and current- phasor magnitude values,  $|U_{Gn}^{pre}|$  and  $|I_{Gn}^{pre}|$ , and the angle between the voltage and the current phasors,  $\varphi_{Gn}^{pre}$ . The substation voltage and current, including their phasor angles are known from both the pre-fault and faulted states. The additional measurements in method 2 are DG voltage- and current- phasor magnitude values,  $|U_{Gn}|$  and  $|I_{Gn}|$ , and the angle between the voltage and the current phasors,  $\varphi_{Gn}$ , during fault. The phasor angle of the  $G$ -node voltage referred to the substation is not known, and has to be estimated both in the pre-fault state and during the fault.

**Table 5.1: Common input data and measurements for method 1 and 2 and additional measurements in method 2**

	Common for method 1 and 2	Additional for method 2
Input data	$Z_{ln}, I_{Gn}, \varphi_{Ln}^{pre}$	
Pre-fault measurements	$ U_S^{pre} ,  I_S^{pre} $ $ U_{Gn}^{pre} ,  I_{Gn}^{pre} , \varphi_{Gn}^{pre}$	
Measurements during fault	$U_S, I_S$	$ U_{Gn} ,  I_{Gn} , \varphi_{Gn}$

Where superscript *pre* means pre-fault measurements

Bold font means a vector of parameters or measurements, e.g.  $Z_{ln} = [Z_{l1} Z_{l2} Z_{l3} \dots]$

Both methods require voltage- and current- phasors from the DG-unit during fault. If no measurements are available (method 1), the voltage and current has to be estimated. The DG-voltage estimation is described in Ch. 5.4 and the estimation of the DG-current is described in Ch. 5.5. If magnitude values of voltages and currents are available (method 2), only the phasor angles have to be estimated. The voltage estimation is done as described in Ch. 5.4, like for method 1, but only the phasor angle of the estimated voltage is used further in the calculation. The phasor angle of the estimated voltage in each node is combined with the measured voltage magnitude, (5.1), to form the DG voltage phasor. The DG current phasor is estimated by first calculating the apparent power from the measured quantities, (5.2), and then estimating the current phasor, (5.3).

$$(U_{Gn})_{m-e} = |U_{Gn}|_m \cdot e^{j(\delta_{VGn})_e} \quad (5.1)$$

$$(S_{Gn})_m = |U_{Gn}|_m \cdot |I_{Gn}|_m \cdot e^{j(\varphi_{Gn})_m} \quad (5.2)$$

$$(I_{Gn})_{m-e} = \frac{(S_{Gn})_m^*}{(U_{Gn})_{m-e}^*} = |I_{Gn}|_m \cdot e^{j((\varphi_{Gn})_m - (\delta_{VGn})_e)} \quad (5.3)$$

Subscript  $m$  means measured value and subscript  $e$  means estimated value.

Subscript  $m-e$  means combination of measured magnitude value and estimated phasor angle.

There are many common steps in the calculations of the compensated impedance for the two methods. When the DG- and load currents during fault are established, the final calculation of the compensated impedance to the fault, as shown in Ch. 5.2, is the same for the two methods.

## 5.2 General expression for the compensated distance estimate

The starting point for the compensation algorithms is the simplified lumped model, introduced in Ch. 3.2. The model for a general feeder was shown in Figure 3.9. The simplified model enables estimation of voltages and currents through analytical calculations.

The flow chart in Figure 5.1 shows the logic of the compensation algorithms. Initially, two independent estimations are carried out, step **(1)** and **(2)**. The first is to estimate the distance to the fault location using substation measurements only. This means conventional distance estimation with no information about load and generation on the feeder, (4.1). The conversion from impedance ( $Z_S$ ) to distance estimate ( $d_S$ ) is done using known line impedance per unit of length for the different cross-sections, as shown in Figure 4.3. Subsequently this estimate is used to assume on which section the fault is located, which means to assume the faulted section  $F$ . The distance estimate is also utilized to estimate the amount of the total load on the faulted section which is connected between the substation and the fault location. The second initial estimation is the pre-fault load distribution, which is described in Ch. 5.3. The order in which steps **(1)** and **(2)** are performed can be reversed. The next step is to choose method 1 or method 2 for calculation of the compensated impedance. If measurements from the DG-unit are available during fault method 2 is chosen, and if not method 1 has to be used, as explained in Ch. 5.1. In both methods the next step is successive estimation of loads and DG-voltages in each section starting from the substation and stopping at the faulted section ( $F$ ), as explained in Ch. 5.4, step **(3A)** and **(3B)**. In method 1 the DG-currents have to be estimated in each DG-node, and this estimation is described in Ch. 5.5. In method 2 the angle of the estimated DG-node voltage is combined with the measured magnitude, and the DG-current is calculated from the measured quantities and the estimated voltage phasor. When the load- and DG- currents during fault are estimated together with the voltage in the last node before the fault location, node  $F$ , the compensated impedance ( $Z_C$ ) can be calculated according to (5.7), step **(4)**. The calculation of the compensated impedance is common for both methods, and for two-phase and three-phase short circuits. The final step is to calculate the distance ( $d_C$ ) corresponding to the calculated impedance, step **(5)**, using the relation between impedance and distance shown in Figure 4.3. The distance estimate  $d_C$  is the new estimated distance to the fault location, and should be closer to the true distance than the initial estimate,  $d_S$ . Results are shown in Ch. 7.

If the initial distance estimate  $d_S$  corresponded to more than one possible faulted section, separate calculations are done for each possible fault location. The result will be more than one compensated distance estimate  $d_C$  as output, and the correct location has to be found by some other method. Possible solutions for this are discussed in Ch. 8, and a new method is also presented there.

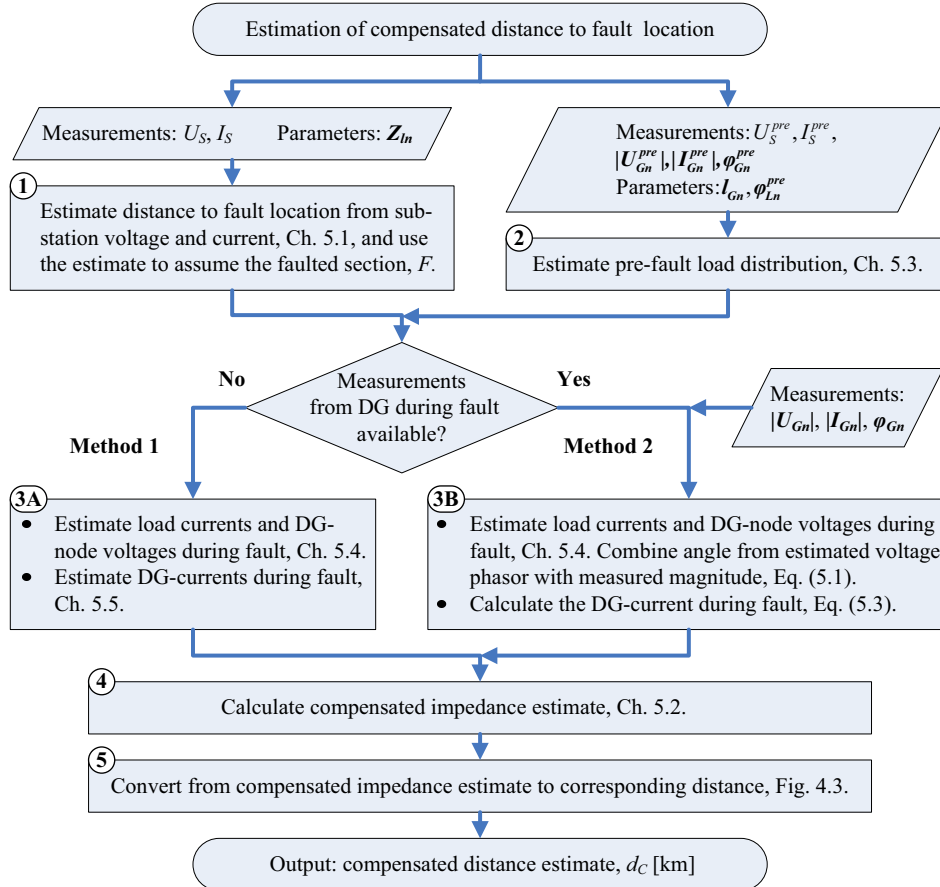


Figure 5.1 Flow chart for the fault location process

The calculations can be repeated with the compensated distance estimate  $d_C$  as input for the next iteration instead of  $d_S$ .

It is desirable to have a general expression for calculation of the compensated impedance instead of having different expressions for the various fault locations and fault types. Such an expression is derived in the following, and corresponds to step (4) in the flow chart in Figure 5.1. Generally, the compensated distance estimate can be derived from the equivalent shown in Figure 5.2. Node  $F$  is the last node before the assumed fault location. Nodes were explained in the introduction to Ch. 3.2, and node  $F$  can be the substation node, a DG connection point or a branching-node.

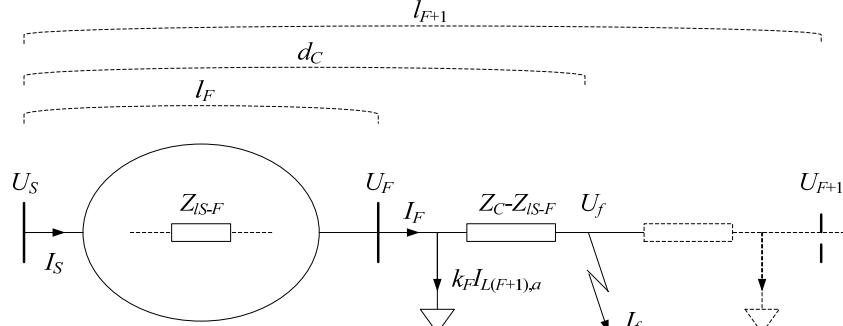


Figure 5.2: Feeder model showing the faulted section  $F$ , for calculation of the compensated impedance

The estimation of the pre-fault load of the section between node  $F$  and  $F+1$  is shown in Ch. 5.3, and the calculation of the load during fault is shown in Ch. 5.4. To estimate the amount of load between the  $F$ -node and the assumed fault location, a fractional constant  $k_F$  is calculated. This constant is equal to the initially assumed distance between the  $F$ -node and the fault location, divided by the length of the assumed faulted section:

$$k_F = \frac{d_s - l_F}{l_{F+1} - l_F} \quad (5.4)$$

$l_F$  and  $l_{F+1}$  are known distances from the substation to the nodes  $F$  and  $F+1$

The impedance  $Z_{IS-F}$  is the sum of the line impedances along the path from the substation to the  $F$ -node.

$$Z_{IS-F} = \begin{cases} 0 & F = 0 \\ \sum_{n=1}^F Z_{In} & F \geq 1 \end{cases} \quad (5.5)$$

In the special case where the  $F$ -node is the substation,  $l_F = 0$  and  $Z_{IS-F} = 0$ .

For an unsymmetrical fault as a two-phase short circuit, negative sequence currents and voltages will be present in addition to the positive sequence quantities. The sequence network for a two phase short circuit is shown in Figure 5.3 (a). The line impedances are equal in the positive and negative systems. For the symmetrical three-phase short circuit fault, only positive sequence quantities are present, and the impedance to the fault location can be found from the equivalent shown in Figure 5.3 (b), or a corresponding equivalent showing phases  $A$  and  $B$  or phases  $A$  and  $C$ .

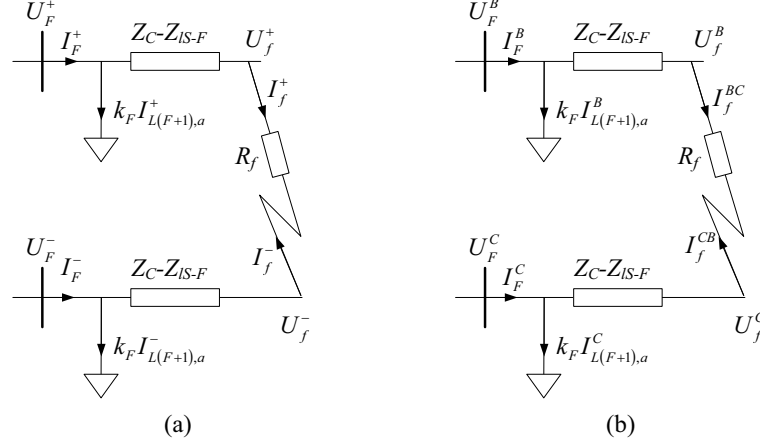


**Figure 5.3: (a) Symmetrical components representation for 2-phase short circuits and (b) phase components representation for short circuit involving phases B and C.**

From Figure 5.3 (a), an expression for the compensated impedance estimate ( $Z_C$ ) can be obtained. The transformation from positive and negative sequence quantities to phase quantities is shown in Appendix C. For a three-phase short circuit, as shown in Figure 5.3 (b), the final equation in (5.6) can be obtained directly, since only positive sequence components exist for such a fault.

$$\begin{aligned}
 Z_C &= Z_{IS-F} + \frac{(U_F^+ - U_F^-) - \frac{R_f}{2}(I_f^+ - I_f^-)}{(I_F^+ - I_F^-) - k_F(I_{L(F+1),a}^+ - I_{L(F+1),a}^-)} \\
 &= Z_{IS-F} + \frac{(U_F^B - U_F^C) - \frac{R_f}{2}(I_f^{BC} - I_f^{CB})}{(I_F^B - I_F^C) - k_F(I_{L(F+1),a}^B - I_{L(F+1),a}^C)} \\
 \Rightarrow Z_C &= Z_{IS-F} + \frac{\Delta(U_F)}{\Delta(I_F - k_F I_{L(F+1),a})} - \frac{R_f}{2} \cdot \frac{\Delta(I_f)}{\Delta(I_F - k_F I_{L(F+1),a})}
 \end{aligned} \tag{5.6}$$

The  $\Delta$ -symbol is used to indicate a difference between two phase quantities.

Only the reactance part of the impedance  $Z_C$  is used in the distance calculation. This is to avoid influence from the fault resistance, as explained in Ch. 4. Looking at the last term in (5.6), it might have a reactance component if the currents in the denominator and nominator are not in phase. However, it is assumed that the last term in (5.6) has a negligible imaginary part, and is thus removed from the equation. This is further examined in Appendix C. The general expression for the compensated impedance then becomes:

$$Z_C = Z_{C(3\phi)} = Z_{C(2\phi)} = Z_{IS-F} + \frac{\Delta U_F}{\Delta(I_F - k_F I_{L(F+1),a})} \tag{5.7}$$

$Z_{C(3\phi)}$ ,  $Z_{C(2\phi)}$  is compensated impedance to fault location for three-phase and two-phase short circuits

The calculation of the distance corresponding to the impedance is done referring to Figure 4.3. The calculation of the necessary load and DG-currents are explained in the following sub-chapters.

For a three-phase short circuit the phase –voltages and –currents are symmetric. The compensated impedance can be calculated from quantities of one of the phases instead of using delta quantities:

$$Z_{C(3\phi)} = Z_{IS-F} + \frac{U_F}{I_F - k_F I_{L(F+1),a}} \quad (5.8)$$

### 5.3 Estimation of pre-fault load distribution

The first step in finding a compensated distance estimate is to estimate the distribution of loads between the sections in the simplified feeder model presented in Ch. 3.2. This chapter deals with estimation of the load distribution in the pre-fault steady state. Generally, the load in each load tap is unknown, or real-time data is not available for protection purposes. Information about the load composition may be collected by the utilities for load forecasting, [79]. Load data might also be available as hourly data for consumer billing through automatic meter reading, but normally there is no connection between the metering system or and the feeder protection system. Consequently, real time load data is usually not available for the protection system, and thus have to be estimated. By connecting the two systems, the pre-fault load estimation could be avoided and the distance estimation improved.

The total pre-fault load flow to or from the feeder is known through measurements of substation voltage and current, (5.9). In addition it is assumed that pre-fault apparent power of all DG-units connected to the feeder are available through measurements of voltage and current magnitude values, together with the angle between the voltage and current, (5.10).

$$S_S^{pre} = U_S^{pre} (I_S^{pre})^* = |U_S^{pre}| \cdot |I_S^{pre}| \angle \varphi_S^{pre} \quad (5.9)$$

$$S_{Gn}^{pre} = |U_{Gn}^{pre}| \cdot |I_{Gn}^{pre}| \angle \varphi_{Gn}^{pre} \quad (5.10)$$

Utilizing the measured pre-fault load flow in the substation to compensate for the load current during fault have been done in fault localization methods presented earlier, [36].

To be able to estimate the pre-fault load distribution, it is assumed that all loads in one section of the feeder have the same power factor, and that this power factor is known. In addition to measurements and feeder data, other information can also be utilized in the load estimation:

- Typical load profiles for the feeder based on data and experience from the past can be used to assume how the load is distributed in the present state.
- Knowing the nominal power rating and location of installed distribution transformers, the total (measured) load can be distributed on each transformer according to the rating.
- Knowledge of load types and characteristics in the different feeder sections can be utilized.

The utilities are expected to have this kind of information available. However, the actual load might deviate considerably from typical loads. This makes measurements preferable.

Depending on the number of DG-units and their position along the feeder, the pre-fault load distribution among the feeder sections can be estimated. For a radial feeder the load estimation can in principle be made for a feeder with an infinite number of DG-units connected to it. The following subchapter (Ch. 5.3.1) describes how the measured voltage magnitude in the DG connection point can be utilized for estimating the distribution of loads between the sections before and after the DG-connection point. The load estimation becomes more difficult if there are DG-units connected on different branches. In this case it is

necessary to have current measurements in each branch in order to estimate the load. This is shown in Ch. 5.3.2.

### 5.3.1 Pre-fault load estimation on a radial feeder with $N$ DG-units

This subchapter describes how the pre-fault loads in the simplified feeder equivalent can be estimated for a radial feeder. In the outlined method the load within each section is assumed to have a common power factor, which must be known. The utilities are assumed to have knowledge about this power factor. Different load power factors in the different sections can also easily be implemented in the model.

The total power flow to the load including line losses can be calculated, since the apparent power fed from the substation and the DG-units are known through measurements:

$$\sum_{n=1}^{N+1} S_{Ln}^{pre} + \sum_{n=1}^{N+1} S_{In}^{pre} = S_S^{pre} + \sum_{n=1}^N S_{Gn}^{pre} \quad (5.11)$$

Even if the total pre-fault load is known from (5.11), it remains to decide how the load is distributed along the feeder. A generalized line section between two nodes,  $n-1$  and  $n$ , is shown in Figure 5.4. This section can be one out of several sections on a radial feeder with a number of DG-units connected to it. Two loads  $S_{Ln,a}^{pre}$  and  $S_{Ln,b}^{pre}$  are connected on each side of the series line impedance  $Z_{ln}$ . When the voltage and current phasors in node  $n-1$  are known, the voltage magnitude in node  $n$  can be utilized for estimating the shunt load in node  $n-1$ ,  $S_{Ln,a}^{pre}$ . In this way it is possible to estimate the load distribution along any feeder with several DG-units (or other points where the voltage magnitude is measured).

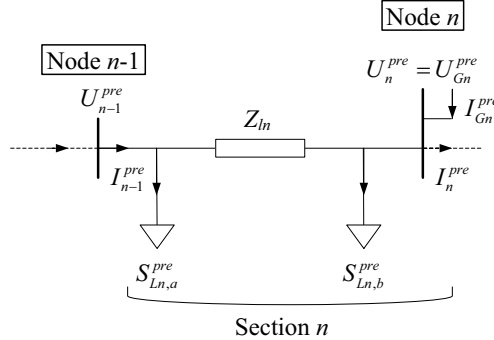


Figure 5.4: Line section model for estimation of pre-fault load on radial feeder

Any loads connected to a side-branch between node  $n-1$  and  $n$  is treated as if it was connected to the main branch, and is included in the estimated shunt loads. If the load on a side-branch were to be estimated separately, measurements in the branching node would be required. Such measurements are not expected to be available in a distribution network. An alternative solution could be to disperse the estimated total load according to the known ratings of the distribution transformers. For a side-branch with DG-units connected to it, measurements in the branching node are required, as further discussed in Ch. 5.3.2.

It is assumed that in the pre-fault state, the apparent power of the loads on each side of the lumped line impedance are equal:  $S_{Ln,a}^{pre} = S_{Ln,b}^{pre}$ . The magnitude value of the load in node  $n-1$  in Figure 5.4 can be estimated from a second order equation, (5.15). The starting point is the expression for the voltage in node  $n$ , (5.12). Since only the magnitude value of the voltage is

measured, the equation cannot be used directly. Taking the absolute value of the voltage and reorganizing the equation results in a second order equation for the load magnitude. More details can be found in Appendix C. For simplification of the expression, a complex variable  $K_n$  is introduced, (5.14).

$$U_n^{pre} = U_{n-1}^{pre} - Z_{ln} \left( I_{n-1}^{pre} - \left( \frac{S_{Ln,a}^{pre}}{U_{n-1}^{pre}} \right)^* \right) \quad (5.12)$$

$$\left| S_{Ln,a}^{pre} \right|^2 + (K_n + K_n^*) \left| S_{Ln,a}^{pre} \right| + K_n K_n^* - \frac{\left| U_{n-1}^{pre} \right|^2 \left| U_n^{pre} \right|^2}{\left| Z_{ln} \right|^2} = 0 \quad (5.13)$$

$$K_n = \left( \frac{\left| U_{n-1}^{pre} \right|}{Z_{ln}} - \left| I_{n-1}^{pre} \right| e^{-j\varphi_{n-1}^{pre}} \right) \left| U_{n-1}^{pre} \right| e^{j\varphi_{Ln}^{pre}} \quad (5.14)$$

$$\left| S_{Ln,a}^{pre} \right| = -\text{Re}(K_n) \pm \sqrt{-(\text{Im}(K_n))^2 + \frac{\left| U_{n-1}^{pre} \right|^2 \left| U_n^{pre} \right|^2}{\left| Z_{ln} \right|^2}} \quad (5.15)$$

$\varphi_{n-1}^{pre}$  is the angle between the voltage  $U_{n-1}^{pre}$  and the current  $I_{n-1}^{pre}$ .

$\varphi_n^{pre}$  is the common phase angle of the load on section  $n$

The phasor angles of the voltage and current in node  $n-1$  are eliminated from the equation, and only the angle between the two phasors ( $\varphi_{n-1}^{pre}$ ) is required for estimating the load. After the magnitude value of the apparent power is estimated, the next step is to combine it with the known power factor, (5.16). The load in node  $n$ ,  $S_{Ln,b}^{pre}$  is assumed to be equal to the load in node  $n-1$  in the pre-fault state.

$$S_{Ln,a}^{pre} = S_{Ln,b}^{pre} = \left| S_{Ln,a}^{pre} \right| e^{j\varphi_{Ln}^{pre}} \quad (5.16)$$

When the load  $S_{Ln,a}^{pre}$  is estimated, the voltage phasor in node  $n$  can be calculated, (5.17). Then the phasor-angle of the estimated voltage is combined with the measured voltage magnitude, (5.18). To estimate the load in the next section, section  $n+1$ , the current floating into the section from node  $n$  ( $I_n^{pre}$ ) has to be known. The pre-fault power from the DG-unit is known through measurements. The DG-current phasor can then be calculated once the voltage in node  $n$  is estimated, (5.19). The current floating into the next section is calculated in (5.20).

$$\left( U_n^{pre} \right)_e = U_{n-1}^{pre} - Z_{ln} \left( I_{n-1}^{pre} - \left( \frac{S_{Ln,a}^{pre}}{U_{n-1}^{pre}} \right)^* \right) \quad (5.17)$$

$$\left( U_n^{pre} \right)_{m-e} = \left| U_{Gn}^{pre} \right|_m \angle \left( \delta_{Un}^{pre} \right)_e = \left( U_{Gn}^{pre} \right)_{m-e} \quad (5.18)$$

$$\left( I_{Gn}^{pre} \right)_{m-e} = \left( \frac{\left( S_{Gn}^{pre} \right)_m}{\left( U_n^{pre} \right)_{m-e}} \right)^* = \left( \frac{\left| U_{Gn}^{pre} \right|_m \cdot \left| I_{Gn}^{pre} \right|_m \angle \left( \varphi_{Gn}^{pre} \right)_m}{\left( U_n^{pre} \right)_{m-e}} \right)^* \quad (5.19)$$

$$I_n^{pre} = I_{n-1}^{pre} - \left( \frac{S_{Ln,a}^{pre}}{U_{n-1}^{pre}} \right)^* - \left( \frac{S_{Ln,b}^{pre}}{\left( U_n^{pre} \right)_{m-e}} \right)^* + I_{Gn}^{pre} \quad (5.20)$$

Subscript  $m-e$  means combination between measured ( $m$ ) and estimated ( $e$ ) values.

If measured values are available, they are always utilized in the further calculations, but the subscript  $m-e$  is removed from the equations.

When the voltage in both node  $n-1$  and  $n$  are known the line losses in section  $n$  can be calculated:

$$S_{ln}^{pre} = \frac{(U_{n-1}^{pre} - U_n^{pre})(U_{n-1}^{pre} - U_n^{pre})^*}{Z_{ln}} \quad (5.21)$$

The calculations presented here are repeated for all sections on the feeder. A flow chart illustrating the iterative estimation of the load of each section on a radial feeder with  $N-1$  DG-units is shown in Figure 5.4.

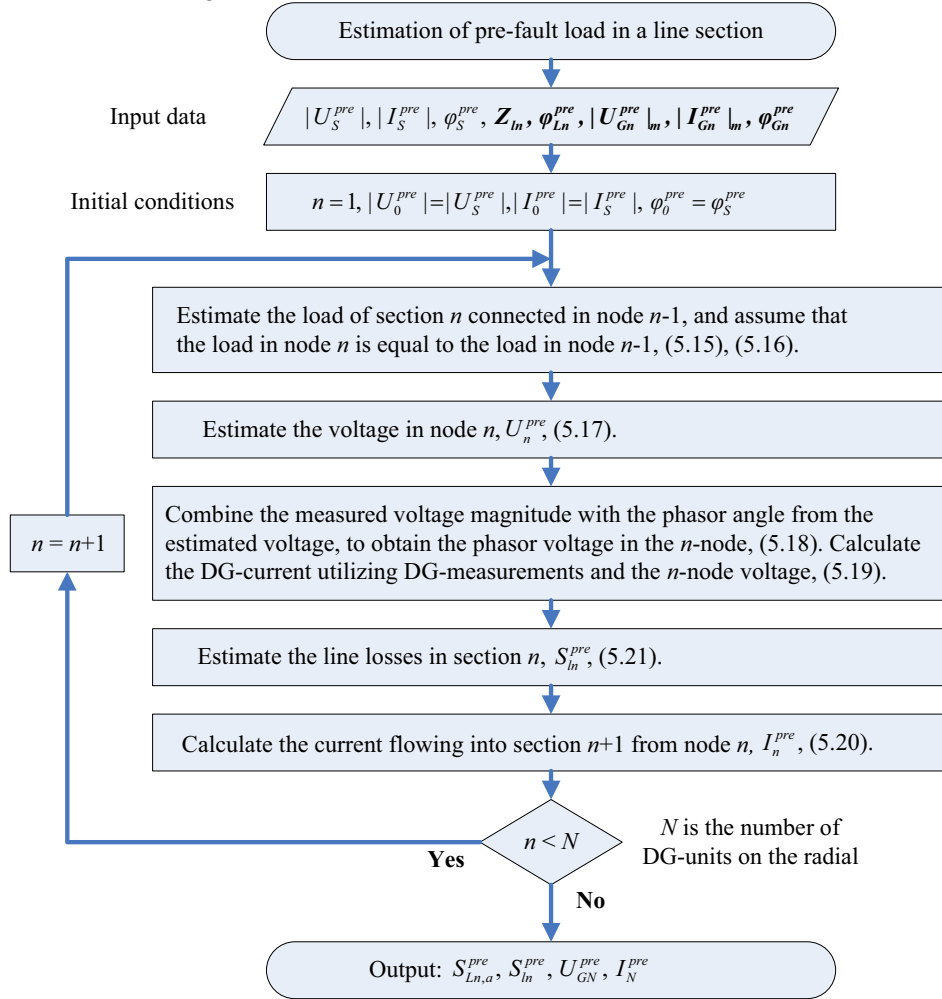


Figure 5.5: Flow chart for estimation of pre-fault load distribution for a radial feeder with  $N$  DG-units

The loads on the end sections of the two branches are calculated as described in Ch. 5.3.3.

### 5.3.2 Pre-fault load estimation on feeder with side-branches

As stated earlier, a load connected to a side-branch without any DG-units is treated as if it was connected to the main branch, and is included in the total load of the section. This is the way side-branches without any DG is handled. DG-units connected to side-branches could possibly be treated similarly, by assuming that they are connected to the main branch in the branching node. Alternatively the load can be estimated utilizing the DG-voltage measurement, in a similar way as for a radial feeder. This however becomes much more complicated for a feeder with DG-units connected to parallel branches than for a strictly radial feeder, and measurements from the branching node are required.

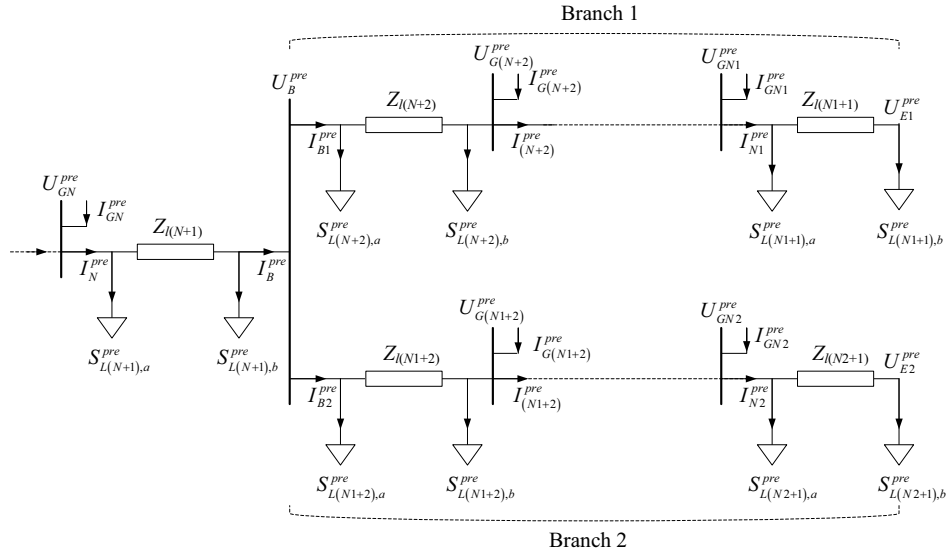


Figure 5.6: Feeder with two branches with DG-units in the pre-fault state

To be able to estimate the load in the last section before the branching node, section  $N+1$ , the voltage magnitude in the  $B$ -node,  $|U_B^pre|$ , must be measured. Then the load can be estimated like for a radial feeder, as described in Ch. 5.3.1. If only the current magnitude,  $|I_B^pre|$ , is measured, the load cannot be calculated analytically due to too many unknown parameters. The phasor angle of the voltage in the  $B$ -node is found by estimating the voltage:

$$U_B^pre = U_{GN}^pre - Z_{L(N+1)} \left( I_N^pre - \left( \frac{S_{L(N+1),a}^pre}{U_{GN}^pre} \right)^* \right) \quad (5.22)$$

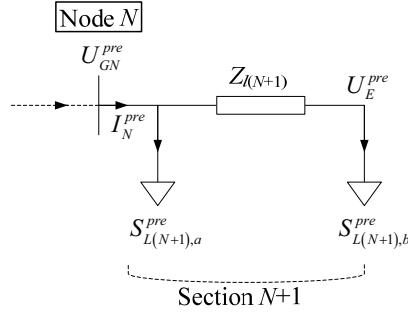
The angle of the estimated voltage is then combined with the measured voltage magnitude. To estimate the pre-fault load on one of the branches, the branching current magnitude together with the angle between the branching node voltage and current must be measured. Then the load distribution can be estimated like for a radial feeder, as was shown in the flow chart in Figure 5.5. The initial and ending conditions for the iteration on the two branches are summarized in Table 5.2. The loads on the end sections of the two branches are calculated as described in Ch. 5.3.3.

**Table 5.2: Initial conditions for estimation of pre-fault load distribution on two parallel branches**

	Branch 1	Branch 2
Required input data	$ U_B^{pre} ,  I_{B1}^{pre} , \phi_{B1}^{pre}$	$ U_B^{pre} ,  I_{B2}^{pre} , \phi_{B2}^{pre}$
Start of iteration	$n = N+2$	$n = N1+2$
End of iteration	$n = N1$	$n = N2$
Initial conditions	$ U_{N+1}^{pre}  =  U_B^{pre} $ $ I_{N+1}^{pre}  =  I_{B1}^{pre} $ $\phi_{N+1}^{pre} = \phi_{B1}^{pre}$	$ U_{N1+1}^{pre}  =  U_B^{pre} $ $ I_{N1+1}^{pre}  =  I_{B2}^{pre} $ $\phi_{N1+1}^{pre} = \phi_{B2}^{pre}$

### 5.3.3 Pre-fault estimation of load on last feeder section

Finally, after iteratively calculating the pre-fault load on all sections with DG-units connected at the section end, the load between the last DG-unit on the radial and the feeder end has to be estimated. The last section before the feeder end is shown in Figure 5.7.


**Figure 5.7: Feeder end section in the pre-fault section**

The power flowing into the feeder from the substation and the power generated in the DG-units in the pre-fault state are known from measurements. The load and losses on all sections between the substation and the last DG-unit have been calculated. Then the remaining power is assigned to the load and losses of the last section of the feeder. The total load and line losses on the last section,  $S_{N+1}^{pre}$ , are given by (5.23).

$$S_{N+1}^{pre} = S_{L(N+1),a}^{pre} + S_{L(N+1),b}^{pre} + S_{l(N+1)}^{pre} = S_S^{pre} + \sum_{n=1}^N S_{Gn}^{pre} - \sum_{n=1}^N S_{Ln,a}^{pre} - \sum_{n=1}^N S_{Ln,b}^{pre} - \sum_{n=1}^N S_{ln}^{pre} \quad (5.23)$$

The load is defined to be equal on both sides of the lumped line impedance, and it can be calculated by a second order equation. The line losses in the end-section is expressed by (5.24), and the voltage at the end of the radial is expressed by (5.25). The expression for the voltage is inserted into the loss equation, and the feeder-end voltage is eliminated.

$$U_E^{pre} = U_{GN}^{pre} - Z_{l(N+1)} \left( I_N^{pre} - \left( \frac{S_{L(N+1),a}^{pre}}{U_{GN}^{pre}} \right)^* \right) \quad (5.24)$$

$$\begin{aligned}
 S_{L(N+1)}^{pre} &= \frac{(U_{GN}^{pre} - U_E^{pre})(U_{GN}^{pre} - U_E^{pre})^*}{(Z_{l(N+1)})^*} \\
 &= Z_{l(N+1)} \left( I_N^{pre} - \left( \frac{S_{L(N+1),a}^{pre}}{U_{GN}^{pre}} \right)^* \right) \left( (I_N^{pre})^* - \frac{S_{L(N+1),a}^{pre}}{U_{GN}^{pre}} \right)
 \end{aligned} \tag{5.25}$$

The expression for the line losses, (5.25), is inserted into (5.23), and the 2. order equation in (5.26) is obtained. A complex constant  $K_E$  is introduced for simplification. The magnitude value of the load on the last feeder section connected in node  $N$  is then calculated by solving (5.27).

$$\left| S_{L(N+1),a}^{pre} \right|^2 + K_E \left| S_{L(N+1),a}^{pre} \right| + \left| U_{GN}^{pre} \right|^2 \left( \left| I_N^{pre} \right|^2 - \frac{S_{N+1}^{pre}}{Z_{l(N+1)}} \right) = 0 \tag{5.26}$$

$$\text{With } K_E = \left( \frac{2 \cdot \left| U_{GN}^{pre} \right|^2}{Z_{l(N+1)}} - I_N^{pre} (U_{GN}^{pre})^* \right) e^{j\varphi_{l(N+1)}^{pre}} - (I_N^{pre})^* U_{GN}^{pre} e^{-j\varphi_{l(N+1)}^{pre}}$$

$$\left| S_{L(N+1),a}^{pre} \right| = -\frac{K_E}{2} \pm \sqrt{\left( \frac{K_E}{2} \right)^2 - \left| U_{GN}^{pre} \right|^2 \left( \left| I_N^{pre} \right|^2 - \frac{S_{N+1}^{pre}}{Z_{l(N+1)}} \right)} \tag{5.27}$$

The estimated amplitude value is then combined with the known phase angle:

$$S_{L(N+1),a}^{pre} = S_{L(N+1),b}^{pre} = \left| S_{L(N+1),a}^{pre} \right| e^{j\varphi_{l(N+1)}^{pre}} \tag{5.28}$$

Alternatively, the losses on the end-section, section  $N+1$ , can be neglected, and all of the load can be assumed to be connected in the last DG-node before the feeder-end:

$$S_{L(N+1),a}^{pre} = S_{L(N+1),b}^{pre} = \frac{S_{N+1}^{pre}}{2} \tag{5.29}$$

#### 5.4 Load estimation during fault

The load during fault is estimated using the same static load model as in the PSCAD-model described in Ch. 3.1.4, but with nominal values of voltage and power replaced by pre-fault values. Referring to Figure 5.4, the active and reactive power during fault are calculated as functions of the pre-fault values of voltage and power (superscript *pre*):

$$S_{Ln,a} = P_{Ln,a}^{pre} \left( \frac{|U_{n-1}|}{|U_{n-1}^{pre}|} \right)^{NP} + jQ_{Ln,a}^{pre} \left( \frac{|U_{n-1}|}{|U_{n-1}^{pre}|} \right)^{NQ} \tag{5.30}$$

$$S_{Ln,b} = P_{Ln,b}^{pre} \left( \frac{|U_n|}{|U_n^{pre}|} \right)^{NP} + jQ_{Ln,b}^{pre} \left( \frac{|U_n|}{|U_n^{pre}|} \right)^{NQ} \tag{5.31}$$

$S_{Ln,a}$ ,  $S_{Ln,b}$  is apparent power of the load on each side of the line impedance in section  $n$  during fault

$S_{Ln,a}^{pre}$ ,  $S_{Ln,b}^{pre}$  is active and reactive power of the load on each side of the line impedance in

section  $n$  in the pre-fault state

$U_{n-1}$ ,  $U_n$  is the voltage across the load during fault

$U_{n-1}^{pre}$ ,  $U_n^{pre}$  is the voltage across the load in the pre-fault state

NP, NQ is voltage dependency factor for active and reactive power.

NP = 1 and NQ = 2 are used in the algorithms, but with specific information about the load available other factors can be used.

Generally, the loads currents in section 1 during fault can be expressed by (5.32) for the load in node  $n-1$  and (5.33) for the load in node  $n$ .

$$I_{Ln,a} = \left( \frac{S_{Ln,a}}{U_{n-1}} \right)^* \quad (5.32)$$

$$I_{Ln,b} = \left( \frac{S_{Ln,b}}{U_n} \right)^* \quad (5.33)$$

To estimate the apparent power of the load, the voltage magnitude in the connection node of the load must be known. This voltage magnitude can be available from measurement if it is a DG-connection point, or it must be estimated. To calculate the load current the voltage phasor must be known and the voltage phasor angles must be estimated in all cases. The estimation of loads and voltages has to be done successive, starting from the substation and towards the feeder-end.

The voltage in node  $n$  is estimated in a similar way as for the pre-fault case, (5.34). The current flowing into section  $n+1$  from node  $n$  is given by (5.35).

$$U_n = U_{n-1} - Z_{ln} \left( I_{n-1} - \left( \frac{S_{Ln,a}}{U_{n-1}} \right)^* \right) \quad (5.34)$$

$$I_n = I_{n-1} - \left( \frac{S_{Ln,a}}{U_{n-1}} \right)^* - \left( \frac{S_{Ln,b}}{U_n} \right)^* + I_{Gn} \quad (5.35)$$

#### 5.4.1 Estimation of load and voltages along a radial feeder during fault

The loads and DG-voltages during fault are estimated section for section, starting in the substation and ending in the last DG-node before the assumed fault location. One section of the radial feeder during fault is shown in Figure 5.8.

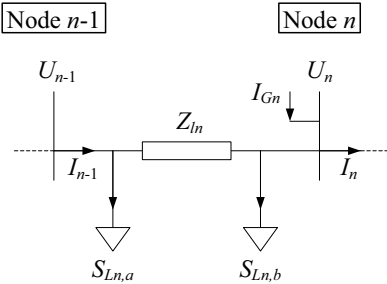


Figure 5.8: Feeder model for successive estimation of loads and voltages during fault for a radial feeder

A flow chart illustrating the process of estimating loads and voltages during fault is shown in Figure 5.9. The iteration runs from  $n = 1$  to  $n = F$ . Node 0 is the substation, so initial conditions for the estimation are:  $U_0 = U_S$ ,  $I_0 = I_S$ ,  $U_0^{pre} = U_S^{pre}$ ,  $I_0^{pre} = I_S^{pre}$

The first step is to estimate the load of section 1, connected in node 0 (the substation), using (5.30). Then the voltage in the next node (node 1) is estimated with (5.34). Next method 1 or 2 is chosen according to available measurements from the DG-unit(s) during fault. In method

1 the DG-current is estimated assuming constant transient internal emf, as explained in Ch. 5.5. In method 2 the phasor angle of the estimated voltage in node 1 is combined with the measured voltage magnitude. The DG-current is calculated using the available measurements from the DG, (5.3). The next step is common for both methods, and is to estimate the load of section 1 connected in node 1 with (5.31), and the current flowing into section 2 from node 1 using (5.35). The described steps are repeated through iteration until node  $F$  is reached. Finally the load current of section  $F+1$  connected in node  $F$  is estimated, and this is the output of the algorithm together with the voltage in node  $F$  and the current flowing into section  $F+1$ .

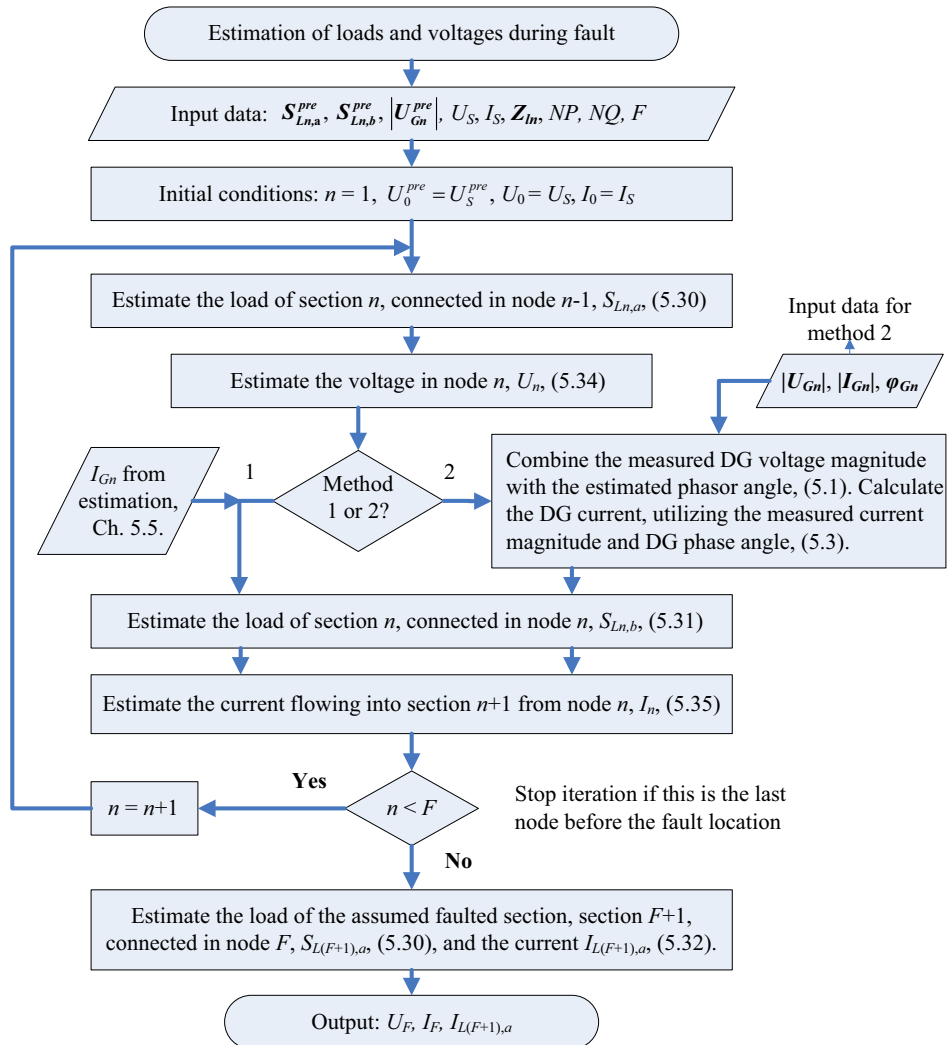
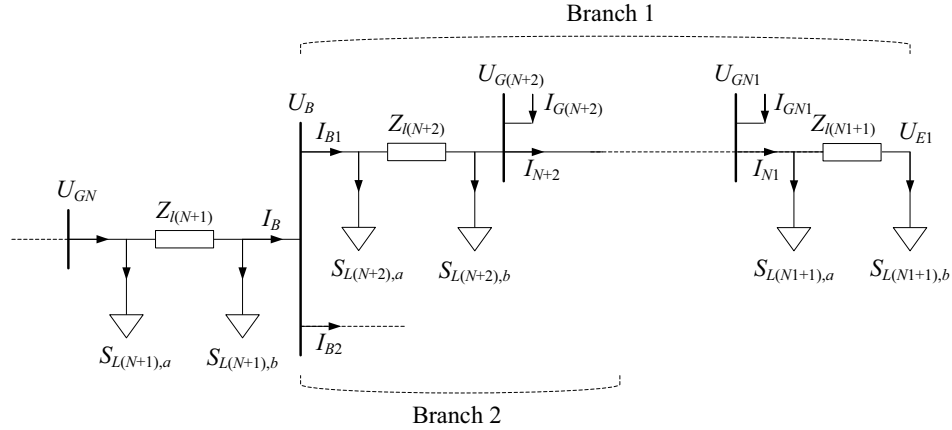


Figure 5.9: Flow chart for successive estimation of loads and voltages during fault

Separate calculations have to be done for two phases involved in the short circuit fault. The output data  $U_F$ ,  $I_F$  and  $I_{L(F+1),a}$  are put into (5.7), and the compensated distance estimate can be calculated.

### 5.4.2 Load estimation on feeder with side-branches

A feeder with two parallel branches with one or more DG-units connected to each branch was shown in Figure 3.11. If the fault is assumed to be located on branch 2, the current on the unfaulted branch, branch 1, can be estimated from Figure 5.10.



**Figure 5.10: Feeder model for estimation of the current on the unfaulted branch 1 during fault, with a fault on the parallel branch 2.**

The iterative estimations of loads and voltages from the substation to the last DG-node before the branching node (node  $N$ ) are done as shown in the flow chart in Figure 5.9. The next step is to estimate the branching node voltage,  $U_B$ , (5.36). Then the current floating into the branching node is estimated, (5.37).

$$U_B = U_{GN} - Z_{I(N+1)} \left( I_N - \left( \frac{S_{L(N+1),a}}{U_{GN}} \right)^* \right) \quad (5.36)$$

$$I_B = I_N - \left( \frac{S_{L(N+1),a}}{U_{GN}} \right)^* - \left( \frac{S_{L(N+1),b}}{U_B} \right)^* \quad (5.37)$$

The current floating from the unfaulted branch 1 must be estimated. The total apparent power of the load and DG-units connected to branch 1,  $S_{B1}$ , is equal to:

$$S_{B1} = \sum_{n=N+2}^{N+1} (S_{Ln,a} + S_{Ln,b}) - \sum_{n=N+2}^{N1} S_{Gn} \quad (5.38)$$

The loads are estimated from (5.30) and (5.31).

If no measurements are available during fault (method 1), the branching node voltage is used instead of the node voltages in the calculations. The pre-fault voltage magnitudes are available from measurements in all nodes. This means that all loads and DG-units connected to branch 1 are handled as if they were connected in the branching node, and line losses on branch 1 are neglected.

If the voltage magnitudes are measured in the DG-nodes during fault (method 2), these measurements are used in the estimation of apparent power of loads. The apparent power from the DG-units are calculated from (5.2). The voltage in the end of branch 1 is assumed to be equal to the voltage in the last DG-node:  $U_{E1} = U_{GN1}$ .

In the calculation of the currents, the voltage phasor angles are also required, not only the magnitude values. The total current on branch 1 is expressed by:

$$I_{B1} = \sum_{n=N+2}^{N1+1} \left( \left( \frac{S_{Ln,a}}{U_{n-1}} \right)^* + \left( \frac{S_{Ln,b}}{U_n} \right)^* \right) - \sum_{n=N+2}^{N1} \left( \frac{S_{Gn}}{U_n} \right)^* \quad (5.39)$$

If the voltage magnitudes are measured, all loads and DG-units on the branch can be assumed to be connected in one of the DG-nodes on branch 1. In the following it is assumed to be connected in the first node after the branching node. The voltage in this node can be estimated, and utilized for estimating the current on branch 1,  $I_{B1}$ .

$$\begin{aligned} U_B &= U_{G2} + Z_{l1} I_{B1} \\ &= U_{G(N+2)} + \frac{Z_{l(N+2)}}{\left( U_{G(N+2)} \right)^*} \left( \sum_{n=N+2}^{N1+1} \left( \left( S_{Ln,a} \right)^* + \left( S_{Ln,b} \right)^* \right) - \sum_{n=N+2}^{N1} \left( S_{Gn} \right)^* \right) \\ \Rightarrow U_{G(N+2)} &= \frac{|U_{G(N+2)}|}{\left( U_B \right)^*} + \left( \frac{Z_{l(N+2)}}{U_B} \right)^* \left( \sum_{n=N+2}^{N1+1} \left( S_{Ln,a} + S_{Ln,b} \right) - \sum_{n=N+2}^{N1} \left( S_{Gn} \right) \right) \end{aligned} \quad (5.40)$$

After having estimated the total current on branch 1, estimation of loads and voltages on the faulted branch 2 are done as shown in the flow chart in Figure 5.9. The iteration goes from the branching node,  $n = N1+1$ , to the last node before the fault location (node  $F$ ),  $n = F$ . Initial conditions for the estimation of loads on branch 2 are:  $U_{N1+1} = U_B$ ,  $I_{N1+1} = I_{B2}$ . With these initial conditions,  $U_F$ ,  $I_F$  and  $I_{LF,1}$  can be estimated, as shown in Figure 5.9. Finally, the compensated impedance to the fault location can be calculated using (5.7), and the corresponding distance is calculated as shown in Figure 4.3.

In the pre-fault load estimation explained in Ch. 5.3.2, loads on branches without DG were handled as if they were connected to the main feeder branch. This means that line losses on these side-branches are neglected. If the fault location is assumed to be on a branch without DG, no measurements from the branching node are assumed to be available. The branching node voltage is estimated both in the pre-fault and faulted states. Referring to Figure 5.10, only the total pre-fault load of section  $N+1$  and  $N+2$  can be estimated, since the branching node voltage is not measured. Half of the total load of the sections is assumed to be connected in the branching node, on the faulted branch 2. In this case node  $F$  is the branching node, and the current  $I_F = I_{B2}$ . The estimation of the currents on branch 1 is done in a similar way as for a fault on the side branch with DG. The case with a fault on a side branch without DG is shown for a specific feeder in Ch. 6.2.4.

### 5.5 Estimation of fault current from a synchronous generator

In method 1 the DG current during fault is estimated. The DG-unit is a synchronous generator, and the short circuit response can be calculated by representing the machine by equivalent circuits for the subtransient and transient states in the same way as for the steady-state [90]. In the subtransient state, the generator can be represented by a constant subtransient internal emf behind the subtransient reactance. In the transient state, the generator can be represented by a constant transient internal emf behind the transient reactance. When the machine is loaded, the subtransient, the transient and the steady-state internal emfs are not equal to each other. The three internal emfs can be calculated using the pre-fault terminal current and voltage. The subtransient emf is calculated using the subtransient reactance, the transient emf is calculated using the transient reactance and the steady-state emf is calculated using the synchronous reactance of the generator. The pre-fault current- and voltage-

magnitudes at the generator terminal are assumed to be known from measurements in all cases, and thus the internal emfs can be calculated. The subtransient emf can be assumed to remain constant and equal to the pre-fault value in the subtransient state, and the transient emf can be assumed to remain constant and equal to the pre-fault value in the transient state. Thus, when the pre-fault values of the internal emfs are known, the short circuit current response from the generator can be calculated. Since representing the synchronous generator in the way described above is a simplification, reduced accuracy in the short circuit current estimate is expected. A flow chart for the process of estimating the DG-current is shown in Figure 5.11.

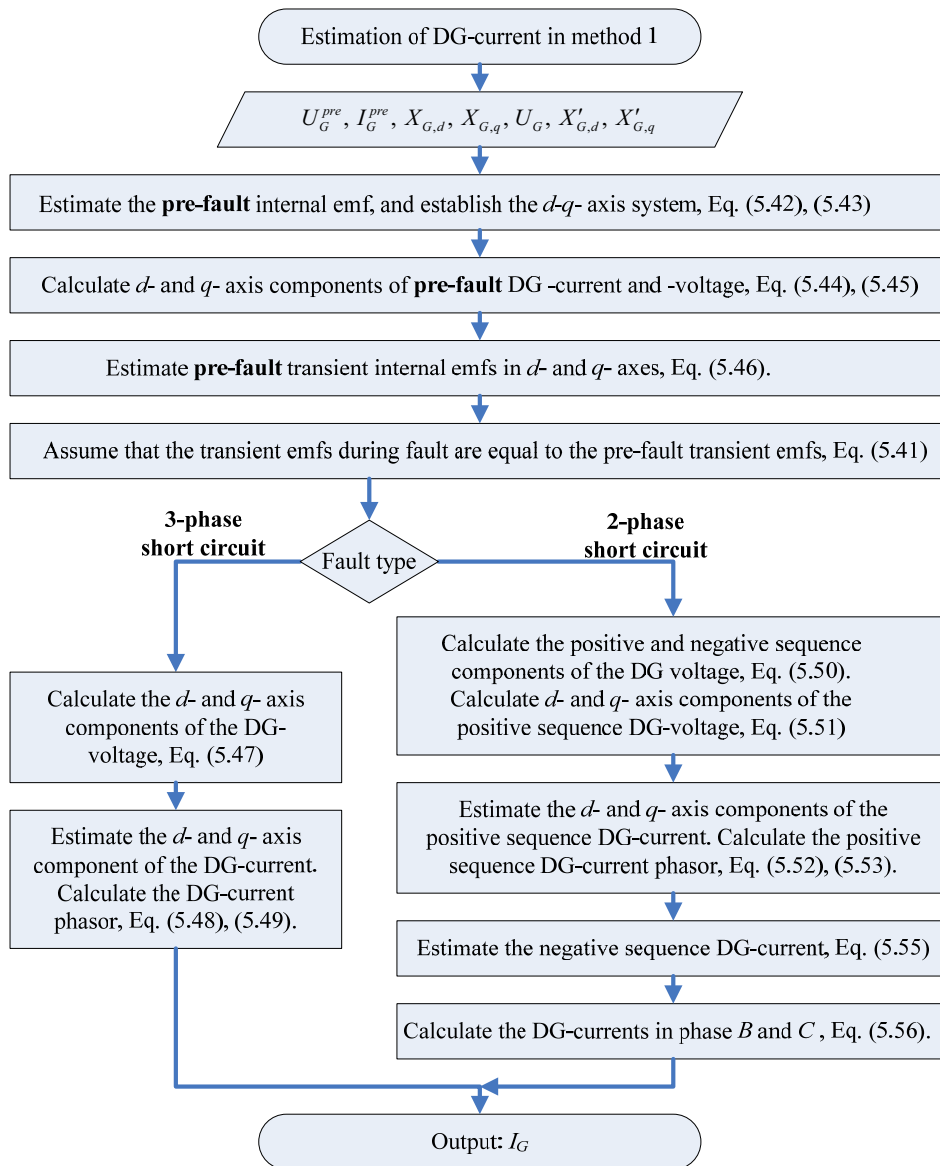


Figure 5.11: Flow chart for estimation of DG-current

The first step is to establish the  $d$ - $q$  axis system, and this is done by calculating the  $q$ -axis steady-state emf, using (5.42) if the generator has a round rotor, and using (5.43) if it is a salient pole generator. In steady-state the internal emf is equal to the  $q$ -axis internal emf,  $E'_{G,q}{}^{pre}$  ( $E'_{G,d}{}^{pre} = 0$ ). The  $q$ -axis is oriented in phase with the calculated emf, and the  $d$ -axis leads the other axis by  $90^\circ$ . Next the pre-fault DG current and voltage are decomposed to the  $d$ - and  $q$ -axes, (5.44), (5.45), and the transient internal emfs in both axes are calculated, (5.46). It is chosen to represent the generator by its transient state equivalent circuit. The generator is then represented by constant  $d$ - and  $q$ -axis transient emfs  $E'_{G,q}$  and  $E'_{G,d}$  behind the transient reactances  $X'_{G,d}$  and  $X'_{G,q}$ , respectively. The rotor flux linkages in both axes can be assumed to remain constant during the transient state, and the internal emfs corresponding to these linkages can also be assumed to remain constant, and equal to the pre-fault values as described above:

$$E'_{G,d} = E'_{G,d}{}^{pre} \quad \wedge \quad E'_{G,q} = E'_{G,q}{}^{pre} \quad (5.41)$$

This property is utilized for calculating the DG-current during fault.

The pre-fault DG-voltage phasor,  $U_G{}^{pre}$ , is estimated from the lumped feeder model as in (5.17) and (5.18). The pre-fault DG-current phasor,  $I_G{}^{pre}$ , is estimated from (5.19). The DG voltage during fault,  $U_G$ , can be estimated from the simplified feeder equivalent, with the load calculated as showed in Ch. 5.4. To calculate the pre-fault transient internal emfs, the angle between a reference axis and the  $q$ -axis,  $\theta_{EG,q}^{pre}$ , has to be found. The angle is shown in Figure 5.12. Phase  $A$  is used as the reference-axis that gives the reference angle for all measurements on the feeder. The  $d$ -axis is leading the  $q$ -axis by  $90^\circ$ .

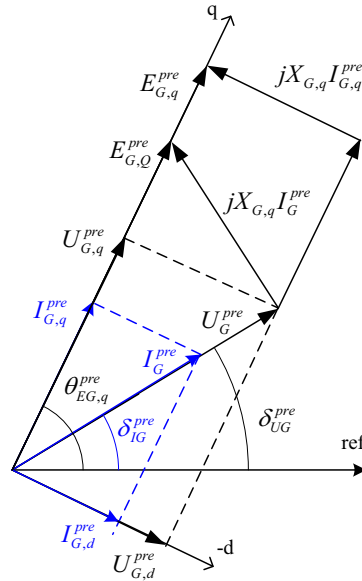


Figure 5.12: Phasor-diagram for the DG-unit, in the pre-fault state. Generator with salient pole rotor.

A phasor diagram for a generator with round rotor is shown in Appendix, Figure B.6.

$$E'_{G,q}{}^{pre} = U_G{}^{pre} + j \cdot X_{G,d} I_G{}^{pre} \quad (5.42)$$

$$E'_{G,d}{}^{pre} = U_G{}^{pre} + j \cdot X_{G,q} I_G{}^{pre} \quad (5.43)$$

$\theta_{EG,q}^{pre}$  is the angle of the emf in (5.42) or (5.43) referred to the reference axis.

The pre-fault current and voltage is resolved into  $d$ - and  $q$ -axis components, (5.44), (5.45). Then the internal transient emf can be calculated using the pre-fault voltages and currents, (5.46).

$$\begin{aligned} I_{G,d}^{pre} &= -|I_G^{pre}| \cdot \sin(\theta_{EG,q}^{pre} - \delta_{IG}^{pre}) \\ I_{G,q}^{pre} &= |I_G^{pre}| \cdot \cos(\theta_{EG,q}^{pre} - \delta_{IG}^{pre}) \end{aligned} \quad (5.44)$$

$$\begin{aligned} U_{G,d}^{pre} &= -|U_G^{pre}| \cdot \sin(\theta_{EG,q}^{pre} - \delta_{UG}^{pre}) \\ U_{G,q}^{pre} &= |U_G^{pre}| \cdot \cos(\theta_{EG,q}^{pre} - \delta_{UG}^{pre}) \end{aligned} \quad (5.45)$$

$$E'_{G,d} = U_{G,d}^{pre} + (X'_{G,q} \cdot I_{G,q}^{pre}) \quad (5.46)$$

$$E'_{G,q} = U_{G,q}^{pre} - (X'_{G,d} \cdot I_{G,d}^{pre})$$

The reactances  $X'_{G,d}$ ,  $X'_{G,q}$  include the transformer reactance in addition to the transient reactances of the generator.

### 5.5.1 Estimation of 3-phase short circuit current for DG

Only positive sequence components are present during a three-phase short circuit, and the amplitude values are equal in all three phases. The DG can be represented by the equivalent circuit shown in Figure 5.13, which is the same as the positive sequence equivalent. Since it is a symmetrical fault, all quantities have the same magnitude value in all three phases. The phase angles of the voltages and currents in the three phases are  $120^\circ$  apart. Thus the calculations are only shown for one phase, but will be similar in all three phases.

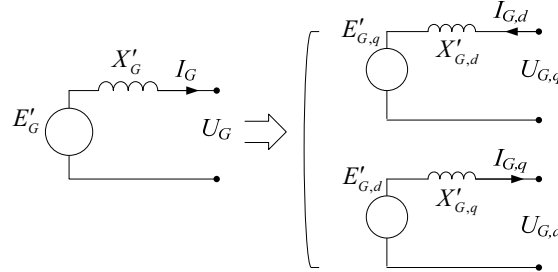


Figure 5.13: Positive sequence equivalent circuit for the transient state

The DG-voltage during fault is resolved into  $d$ - and  $q$ -axis components:

$$\begin{aligned} U_{G,d} &= -|U_G| \cdot \sin(\theta_{EG,q}^{pre} - \delta_{UG}) \\ U_{G,q} &= |U_G| \cdot \cos(\theta_{EG,q}^{pre} - \delta_{UG}) \end{aligned} \quad (5.47)$$

The  $d$ - and  $q$ -axis components of the currents are:

$$\begin{aligned} I_{G,q} &= \frac{E'_{G,d} - U_{G,d}}{X'_{G,q}} \\ I_{G,d} &= -\frac{E'_{G,q} - U_{G,q}}{X'_{G,d}} \end{aligned} \quad (5.48)$$

The DG-current phasor during fault is:

$$\begin{aligned}
 |I_G| &= \sqrt{(I_{G,d})^2 + (I_{G,q})^2} \\
 \delta_{IG} &= \theta_{EG,q}^{pre} - \arctan\left(-\frac{I_{G,d}}{I_{G,q}}\right) \\
 \Rightarrow I_G &= |I_G| \cdot \angle \delta_{IG}
 \end{aligned} \tag{5.49}$$

### 5.5.2 Estimation of 2-phase short circuit current for DG

For a two-phase short circuit the generator has to be represented by a negative sequence equivalent in addition to the positive sequence equivalent shown in Figure 5.13. The positive and negative sequence representations of the feeder are connected in parallel at the fault location [91]. The chosen positive and negative sequence representations of the DG are shown in Figure 5.14.

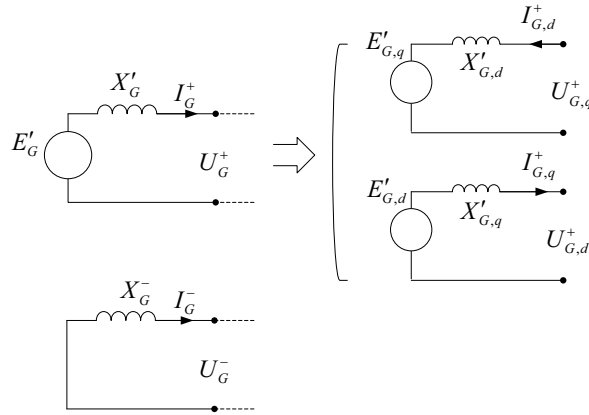


Figure 5.14: Positive and negative sequence equivalent circuits for the transient state

The positive and negative sequence components, with  $h = e^{j2\pi/3}$ , are equal to:

$$\begin{aligned}
 U_G^+ &= \frac{1}{3} \cdot (U_G^A + hU_G^B + h^2U_G^C) \\
 U_G^- &= \frac{1}{3} \cdot (U_G^A + h^2U_G^B + hU_G^C)
 \end{aligned} \tag{5.50}$$

The positive sequence voltage is resolved into its  $d$ - and  $q$ -axis components:

$$\begin{aligned}
 U_{G,q}^+ &= |U_G^+| \cdot \cos(\theta_{EG,q}^{pre} - \delta_{UG}^+) \\
 U_{G,d}^+ &= -|U_G^+| \cdot \sin(\theta_{EG,q}^{pre} - \delta_{UG}^+)
 \end{aligned} \tag{5.51}$$

Then the  $d$ - and  $q$ -axis components of the positive sequence DG-current are estimated from:

$$\begin{aligned}
 I_{G,q}^+ &= \frac{E'_{G,q} - U_{G,q}^+}{X'_{G,q}} \\
 I_{G,d}^+ &= -\frac{E'_{G,d} - U_{G,d}^+}{X'_{G,d}}
 \end{aligned} \tag{5.52}$$

The positive sequence DG-current during fault is:

$$\begin{aligned}
 |I_G^+| &= \sqrt{(I_{G,d}^+)^2 + (I_{G,q}^+)^2} \\
 \delta_{IG}^+ &= \theta_{EG,q}^{pre} - \arctan\left(\frac{I_{G,d}^+}{I_{G,q}^+}\right) \\
 \Rightarrow I_G^+ &= |I_G^+| \cdot \angle \delta_{IG}^+
 \end{aligned} \tag{5.53}$$

The negative sequence reactance is expressed by (5.54) [90], and the negative sequence DG-current during fault by (5.55).

$$X_G^- = \sqrt{X_{G,d}'' X_{G,q}''} \tag{5.54}$$

$$I_G^- = -\frac{U_G^-}{j \cdot X_G^-} = -\frac{U_G^-}{j \cdot \sqrt{X_{G,d}'' X_{G,q}''}} \tag{5.55}$$

When the positive and negative sequence current components are known, the phase currents can be calculated:

$$\begin{aligned}
 I_G^B &= h^2 I_G^+ + h I_G^- + I_G^0 \\
 I_G^C &= h I_G^+ + h^2 I_G^- + I_G^0
 \end{aligned} \tag{5.56}$$

The zero sequence component,  $I_G^0$ , is equal to zero.

## 6 COMPENSATED DISTANCE ESTIMATE CASES

Chapter 6 showed how compensated distance estimates can be found on a general feeder, presenting general equations and algorithms. This chapter presents the same equations and algorithms applied on specific cases. The intention is to further explain the general equations and show examples of using them. On the presented cases, the algorithms have been tested through PSCAD-simulations and analytical calculations on the feeder presented in Ch. 3. PSCAD-simulations have been performed for three different feeder cases:

- feeder without DG,
- feeder with one DG-unit
- feeder with three DG-units

In the cases with one DG-unit the location of the DG can be varied along the main branch. In the cases with three DG-units they are located at fixed locations, in point 1, 3 and 8 referring to Figure 3.1. This means that two of the DGs are located at parallel branches. It is believed that these two specific feeders with DG can be used for representing common real distribution feeder cases.

The calculation of the compensated distance estimates for the different fault cases are explained in this chapter. Plots showing the uncompensated distance estimates were shown in Chapter 5, and plots showing the compensated estimates are shown in Chapter 7.

### 6.1 Compensation cases for feeder without DG

Compensation based on the lumped feeder model can also be done on a feeder without DG. Without any DG, no measurements can be expected to be available from other locations than the substation. This means that the feeder load is divided into two loads of equal apparent power in the pre-fault state. One load is located in the substation and the other at the feeder end. This is a very simple representation of the feeder, and the accuracy is not expected to be very high. General expressions for estimation of the load during fault were given in Ch. 5.4.

#### 6.1.1 Fault on the main branch

The lumped feeder model without DG for a fault on the main branch is shown in Figure 6.1.

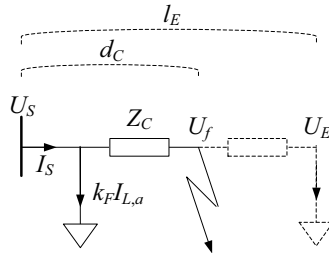


Figure 6.1: Lumped model for feeder without DG for a fault on the main branch

Line losses are neglected, and in the pre-fault state the total load is assumed to be equal to the load flow in the substation. The voltage and current in the substation are measured, and the pre-fault load in the substation is given by:

$$S_{L,a}^{pre} = \frac{1}{2} \cdot U_S^{pre} \cdot (I_S^{pre})^* \quad (6.1)$$

Only the load connected in the substation is compensated for. The compensated distance estimate is given by (5.7), with the load factor  $k_F$  calculated as shown in (6.3).

$$Z_C = \frac{\Delta U_S}{\Delta(I_S - k_F I_{L,a})} \quad (6.2)$$

$$k_F = \frac{d_S}{l_E} \quad (6.3)$$

If there is a breaker with voltage and current measurements somewhere on the feeder, this measurement location can be treated as a node, like a DG-connection point. Then the feeder can be divided into two sections, one before and one after the measurement point. Alternatively, the feeder can be divided into two sections even without additional measurements on the feeder. A fictitious node can e.g. be defined after half of the feeder length, resulting in two sections. Then the load can be evenly distributed between the four shunt loads, and the voltage in the fictitious node is estimated both in the pre-fault and the faulted state. This is expected to improve the accuracy of the load compensation.

### 6.1.2 Fault on the side-branch

If the fault is assumed to be on the side-branch, the feeder is represented as shown in Figure 6.2 during fault.

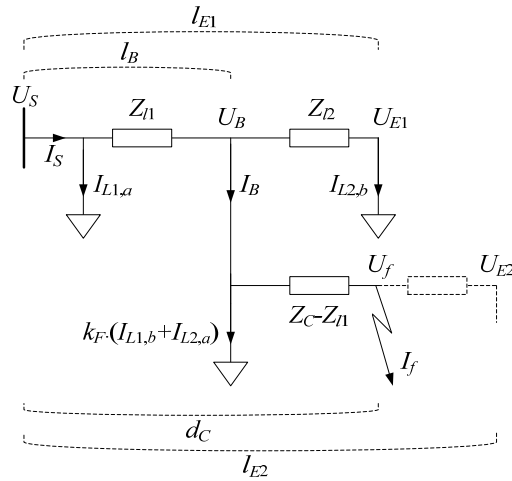


Figure 6.2: Feeder representation during fault when the fault is located on the side-branch.

The feeder is divided into two sections, divided by the branching node,  $B$ . The load is divided between the two sections according to their length.

$$S_{L1,a}^{pre} = S_{L1,b}^{pre} = \frac{l_B}{2 \cdot l_E} \cdot U_S^{pre} \cdot (I_S^{pre})^* \quad (6.4)$$

$$S_{L2,a}^{pre} = S_{L2,b}^{pre} = \frac{l_E - l_B}{2 \cdot l_E} \cdot U_S^{pre} \cdot (I_S^{pre})^*$$

During fault, the load at the end of the main branch,  $S_{L2,b}$ , is assumed to be connected in the branching node, which means that the voltage drop across the line impedance  $Z_{l2}$  is neglected.

The voltage in the branching node is estimated both in the pre-fault and the faulted state:

$$\begin{aligned} U_B^{pre} &= U_S^{pre} - Z_{l1} (I_S^{pre} - I_{L1,a}^{pre}) \\ U_B &= U_S - Z_{l1} (I_S - I_{L1,a}) \end{aligned} \quad (6.5)$$

The compensated distance estimate is given by (6.6), and the load factor by (6.7).

$$Z_C = Z_{l1} + \frac{\Delta(U_B)}{\Delta(I_S - I_{L1,a} - I_{L2,b} - k_F(I_{L1,b} + I_{L2,a}))} \quad (6.6)$$

$$k_F = \frac{d_S - l_B}{l_{E2} - l_B} \quad (6.7)$$

## 6.2 Compensation cases for feeder with one DG-unit

The simplified feeder model for the feeder with one DG-unit for the pre-fault case is shown again in Figure 6.3. The DG-unit can be connected in one of the load points along the main feeder branch. Only loads are connected to the side-branch.

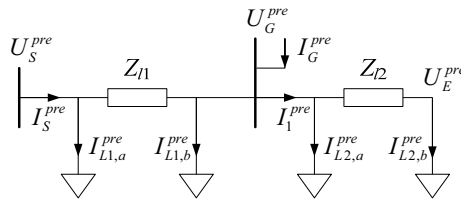


Figure 6.3: Simplified lumped model for feeder with one DG-unit

The impedance from the substation to the fault location  $Z_C$  is the unknown parameter that should be estimated. To be able to do calculations on the circuit, an initial assumption of the fault location is done according to the estimate  $d_S$ . Three different fault cases are considered, according to the assumed location of the fault. The fault can be on the main branch, either before or after the  $G$ -node. These two cases are shown in Figure 6.4 and Figure 6.5. The third possible case is to have a fault on the side-branch. The side-branch can either be located in front of or after the  $G$ -node. The case where the side-branch is located after the  $G$ -node is not treated separately, since the available measurements cannot be used to decide whether the fault is on the main- or the side-branch in that case.

Summary of the three possible fault cases:

- Fault located before the  $G$ -node on the main branch
- Fault located after the  $G$ -node on the main branch
- Fault located on the side-branch before the  $G$ -node

In Chapter 9 a method for utilizing the difference between the estimated and simulated DG voltage magnitudes for finding the faulted branch is introduced. Estimations of the DG – current and voltage are therefore required, even though it is not required for estimating the compensated impedance.

### 6.2.1 Pre-fault load estimation for feeder with one DG-unit

The general equations for estimation of the pre-fault loads were given in Ch. 5.3.1. The pre-fault load of section 1, connected in the substation,  $S_{L1,a}^{pre}$ , is estimated from (6.8). The variable  $K_1$  is given by (6.9). To be able to solve the equation, the common phase-angle of the loads in section 1,  $\varphi_{L1}^{pre}$ , must be known. The estimated magnitude value of the apparent power is finally combined with the known power factor in (6.10).

$$|S_{L1,a}^{pre}| = -\text{Re}(K_1) \pm \sqrt{-(\text{Im}(K_1))^2 + \frac{|U_S^{pre}|^2 |U_G^{pre}|^2}{|Z_{l1}|^2}} \quad (6.8)$$

$$K_1 = \left( \frac{U_S^{pre}}{Z_{l1}} - I_S^{pre} \right) (U_S^{pre})^* e^{j\varphi_{L1}^{pre}} \quad (6.9)$$

$$S_{L1,a}^{pre} = S_{L1,b}^{pre} = |S_{L1,a}^{pre}| e^{j\varphi_{L1}^{pre}} \quad (6.10)$$

Once the load is known, the voltage phasor in node  $G$  can be estimated from (6.11). The phasor-angle of the estimated voltage is combined with the measured voltage magnitude, as in (5.1).

$$U_G^{pre} = U_S^{pre} - Z_{l1} \left( I_S^{pre} - \left( \frac{S_{L1,a}^{pre}}{U_S^{pre}} \right)^* \right) \quad (6.11)$$

To estimate the load in section 2 the current  $I_1^{pre}$  has to be known. The DG-current phasor is calculated as in (5.3), with  $|U_G^{pre}|$ ,  $|I_G^{pre}|$  and  $\varphi_G^{pre}$  known from measurements. Then  $I_1^{pre}$  can be calculated from (6.12).

$$I_1^{pre} = I_S^{pre} - \left( \frac{S_{L1,a}^{pre}}{U_S^{pre}} \right)^* - \left( \frac{S_{L1,b}^{pre}}{U_G^{pre}} \right)^* + I_G^{pre} \quad (6.12)$$

The load is defined to be equal on both sides of the lumped line impedance of section 2, and it can be calculated by a second order equation, as expressed generally by (5.26). The specific equation for calculation of the pre-fault load of section 2 connected in the  $G$ -node is given by (6.13), with the variable  $K_2$  given by (6.14). The common phase-angle of the loads in section 2,  $\varphi_{L2}^{pre}$ , must be known. The estimated magnitude value of the apparent power is finally combined with the known power factor in (6.15).

$$|S_{L2,a}^{pre}| = -\frac{K_2}{2} \pm \sqrt{\left( \frac{K_2}{2} \right)^2 - |U_G^{pre}|^2 \left( |I_1^{pre}|^2 - \frac{S_2^{pre}}{Z_{l2}} \right)} \quad (6.13)$$

$$K_2 = \frac{2 \cdot |U_G^{pre}|^2}{Z_{l2}} e^{j\varphi_{L2}^{pre}} - I_1^{pre} (U_G^{pre})^* e^{j\varphi_{L2}^{pre}} - (I_1^{pre})^* U_G^{pre} e^{-j\varphi_{L2}^{pre}} \quad (6.14)$$

$$S_{L2,a}^{pre} = S_{L2,b}^{pre} = |S_{L2,a}^{pre}| e^{j\varphi_{L2}^{pre}} \quad (6.15)$$

Results of pre-fault load estimation for all possible locations of the DG-unit along the main branch are shown in Table 6.1. Total load at nominal voltage is 1.5 MVA for low load and 6 MVA for high load. As previously stated, the apparent power is assumed to be equal on each side of the line impedance in the pre-fault state. An additional condition is that the total load of the section has to be less than the sum of the apparent power fed from the substation and DG-unit, minus the line losses. If this condition is not met with equal load on each side of the line impedance, the load  $S_{L1,b}^{pre}$  is instead calculated from:

$$S_{L1,b}^{pre} = S_S^{pre} + S_G^{pre} - S_{l1}^{pre} - S_{L1,a}^{pre} \quad (6.16)$$

The total estimated feeder load shows good agreement with the total simulated load. The pre-fault load estimation utilizing measured voltage magnitude in the DG-node thus works with an adequate accuracy. It can be observed that the total load is increasing as the DG connection point is moved towards the feeder-end. The line losses are relatively small compared to the loads, and neglecting these losses would cause only a minor error. Still, line losses have been taken into account in this work.

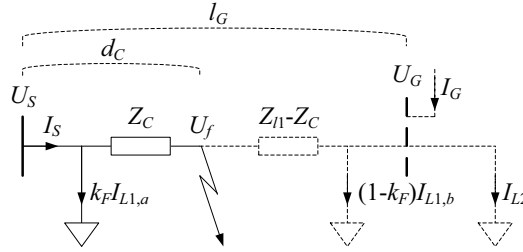
**Table 6.1: Estimated and simulated pre-fault loads in [MVA] at low load (LL) and high load (HL) for various DG-locations.**

DG location [km]	Estimated						Simulated	
	$S_{L1}^{pre}$		$S_{L2}^{pre}$		$S_{L1}^{pre} + S_{L2}^{pre} = S_L^{pre}$		$S_L^{pre}$	
	LL	HL	LL	HL	LL	HL	LL	HL
5	0.004	0.003	1.444	5.887	1.448	5.890	1.474	5.974
10	0.268	1.195	1.197	4.809	1.464	6.004	1.490	6.039
15	0.507	2.294	0.975	3.799	1.482	6.093	1.503	6.011
20	0.859	3.832	0.644	2.359	1.503	6.191	1.520	6.165
25	1.154	5.111	0.362	1.147	1.516	6.258	1.531	6.212
30	1.528	6.343	0	0	1.528	6.343	1.538	6.241

Loads during fault are estimated using (5.30) - (5.33). The same voltage dependency characteristics have been used for loads in both sections. The estimation of the DG-current during fault is performed as described in Ch. 5.5.

### 6.2.2 Fault on the main branch, before the G-node

If the fault according to the estimate  $d_s$  can be assumed to be located between the substation and the G-node, the feeder can be represented by the equivalent shown in Figure 6.4.


**Figure 6.4: Simplified lumped circuit for a fault on the main feeder branch before the G-node**

Only the load between the substation and the assumed fault location is compensated for. This load is assumed to be split into two equal loads on each side of the line impedance  $Z_C$ . The load fractional factor  $k_F$  is equal to the initial estimated distance  $d_s$  divided by the distance to the G-node,  $l_G$ :

$$k_F = \frac{d_s}{l_G} \quad (6.17)$$

The distance from the substation to the G-node is assumed to be known.

$$Z_C = \frac{\Delta U_s}{\Delta(I_s - k_F I_{L1,a})} \quad (6.18)$$

The network after the fault location has no influence, and thus the number of DG-units and branches in the rest of the network is not important. The rest of the network will contribute to the fault current, but will only contribute to a voltage drop over the fault resistance. This has no influence on the distance estimate, since it is calculated from the reactance part of  $Z_C$ . Since the load current is only dependent on the substation voltage, there is no difference between method 1 and 2 for this case.

The DG current and load currents  $I_{L1,b}$  and  $I_{L2}$  during fault are estimated under the assumption that the DG voltage during fault is equal to the voltage in the fault location,  $U_G \approx U_f$ . Once these currents are estimated, the voltage drop over the impedance ( $Z_{l1} - Z_C$ ) can be calculated, and a new DG voltage estimated.

$$U_G = U_f + (Z_{l1} - Z_C)(I_G - (1 - k_F)I_{L1,b} - I_{L2}) \quad (6.19)$$

The magnitude of this estimated voltage is used for finding the faulted branch in the method introduced in Ch. 9.

### 6.2.3 Fault on the main branch, after the G-node

The equivalent circuit for the case where the fault appears to be located after the G-node is shown in Figure 6.5.

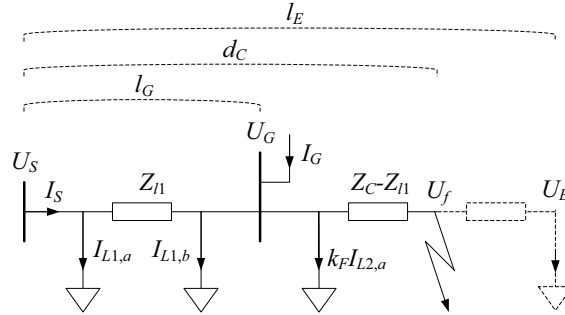


Figure 6.5: Simplified lumped circuit for a fault on the main feeder branch after the G-node

The fractional factor  $k_F$  is:

$$k_F = \frac{d_S - l_G}{l_E - l_G} \quad (6.20)$$

The voltage in the G-node during fault is estimated in (6.21).

$$U_G = U_S - Z_{l1}(I_S - I_{L1,a}) \quad (6.21)$$

In method 1 the estimated DG voltage during fault is utilized. In method 2 the voltage magnitude during fault is available from measurements, and is combined with the phasor angle of the estimated voltage, as in the pre-fault state. Impacts from both load and DG have to be compensated for, and the compensated impedance is calculated from (6.22).

$$Z_C = Z_{l1} + \frac{\Delta U_G}{\Delta(I_S - I_{L1,a} - I_{L1,b} + I_G - k_F I_{L2,a})} \quad (6.22)$$

### 6.2.4 Fault on the side-branch before the G-node

The case where the fault is located on the side-branch before the G-node is shown in Figure 6.6. The feeder section between the substation and the G-node is in this case split into the two sections 11 and 12. The location of the branching node is known, and the distance  $l_B$  and the line impedances  $Z_{l11}$  and  $Z_{l12}$  are considered as known.



### 6.2.5 Calculation of DG-current during fault for feeder with one DG-unit

Figure 6.7 and Figure 6.8 shows comparisons between estimated and simulated DG-currents. The curves show the magnitude values of the difference between the current phasors in phases B and C. The reason for plotting the difference between the two phase currents instead of simply plotting the magnitude values of each phase is that the impedance to the fault location is expressed as a function of difference between phase quantities.

The fault is located at the feeder end, 30 km from the substation, while the location of the DG is varied from 5 to 30 km from the substation on the main branch. Figure 6.7 shows the results for three-phase short circuits, while Figure 6.8 shows the results for two-phase short circuits.

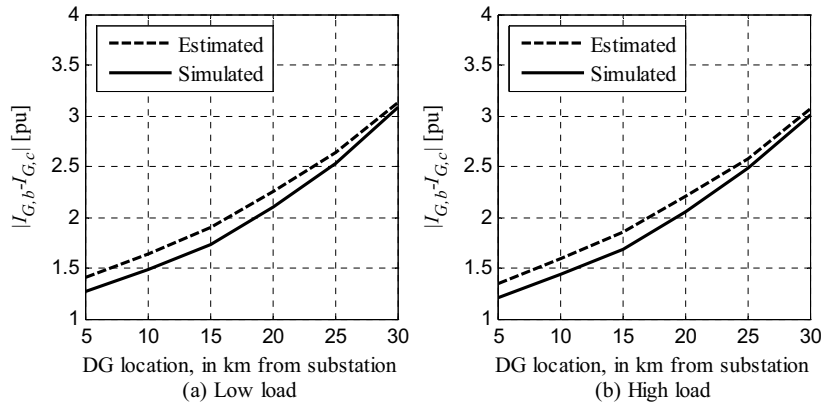


**Figure 6.7: Magnitude of the difference between the DG-currents in phases B and C. Estimated and simulated DG-currents for 3-phase short circuits at the feeder end for (a) low load and (b) high load. The DG-connection point is varied along the main branch.**

For three-phase faults the estimated values are larger than the simulated in all cases. The difference between the two values is approximately constant for all DG locations, except when the DG is located at the feeder end, where the difference between the two values is minor.

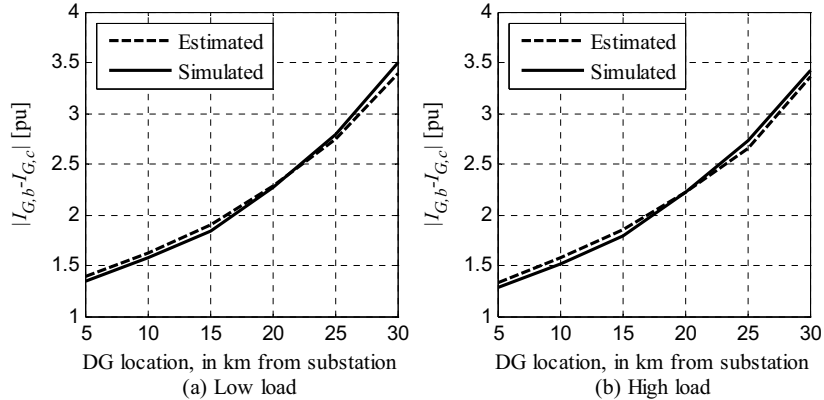


**Figure 6.8: Magnitude of the difference between the DG-currents in phases B and C. Estimated and simulated DG-currents for 2-phase short circuits at the feeder end for (a) low load and (b) high load. The DG-connection point is varied along the main branch.**

For two-phase faults the estimated values are close to the simulated, and thus the estimates are more accurate than for three-phase faults. When the DG is located 5 to 15 km from the substation the estimated values are a bit too large, and when it is located 25 to 30 km from the substation the estimated values are a bit too small. The negative sequence reactance of the generator, unlike the positive sequence reactance, is constant through the short circuit course. For a three-phase fault it is important for the accuracy of the estimation that the chosen simplified representation of the DG-unit (transient reactance behind transient internal emf) corresponds to the time after fault occurrence on which the substation fault data are sampled. Since the negative sequence current is constant, this is less important for a two-phase fault, and this can explain why the current estimates are closest to the simulated values for two-phase short circuits.

Figure 6.9 shows comparison between estimated and simulated DG current magnitudes as functions of the fault location when the DG is connected 5 km from the substation. Plot (a) show results for three-phase short circuits and (b) shows results for two-phase short circuits, both at low load.

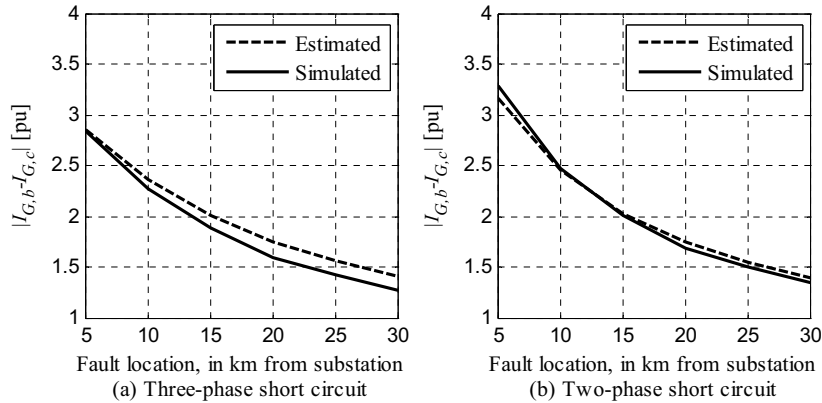


**Figure 6.9:** Magnitude of the difference between the DG-currents in phases *B* and *C* at low load. Estimated and simulated DG-currents for (a) 3-phase and (b) 2-phase short circuits at varying locations. The DG is located 5 km from the substation.

The results show the same tendency as the plots with fixed fault location and varying DG locations. The estimated current magnitudes are larger than the simulated for all fault locations when the fault is a three-phase fault. For two-phase faults the estimated DG currents are larger than the simulated for fault locations 15 to 30 km from the substation, but the difference between estimated and simulated values are much less than for three-phase faults. When the fault is located 5 km from the substation the estimated current is slightly smaller than the simulated. It can be concluded that the estimated currents generally are larger than the simulated for three-phase short circuits, while for two-phase faults the estimated values are approximately equal to the simulated.

### 6.3 Compensation cases for feeder with 3 DG-units

In addition to the feeder with one DG-unit, a feeder with 3 DG-units and with generation on two parallel branches has been considered. Simulations are done in PSCAD, and compensated distance estimates are found through analytical calculations. The simplified lumped feeder model is shown in Figure 6.10 (repeated from Ch. 3). In the following subchapters different

fault cases are presented, and assuming a faulted section corresponds to selecting one of the fault cases.

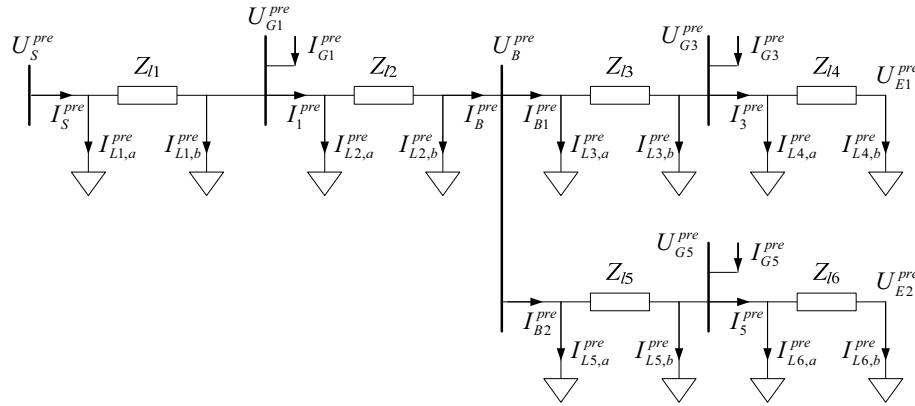


Figure 6.10: Simplified model of feeder with 3 DG-units and one side-branch

For both compensation method 1 and 2, pre-fault measurements from the branching node are necessary. The required measurements are the branching node voltage magnitude and current magnitudes on both branches, and the phase angle between the voltage and current, as shown in Table 5.2.

### 6.3.1 Results of pre-fault load estimation for feeder with three DG-units

Table 6.2 shows results of pre-fault load estimation when DG-1 is located in point 1, DG-2 located in point 3 and DG-3 located in point 8, referring to Figure 3.1. The total load at nominal voltage is 1.5 MVA for low load and 6 MVA for high load.

Table 6.2: Load for feeder with 3 DG-units, results from estimation and from PSCAD-simulation.

[MVA]	Estimated load		[MVA]	Simulated/Actual load	
	Low load	High load		Low load	High load
$S_{L1}^{pre}$	0.004	0.009	$S_{L-1}^{pre}$	0.249	1.063
$S_{L2}^{pre}$	0.241	1.050	$S_{L-3}^{pre}$	0.249	1.009
$S_{L3}^{pre}$	0.003	0.001	$S_{L-4}^{pre}$	0.247	0.979
$S_{L4}^{pre}$	0.980	3.931	$S_{L-5}^{pre}$	0.246	0.959
$S_{L5}^{pre}$	0.098	0.426	$S_{L-6}^{pre}$	0.245	0.945
$S_{L6}^{pre}$	0.147	0.605	$S_{L-7}^{pre}$	0.083	0.342
			$S_{L-8}^{pre}$	0.084	0.340
			$S_{L-9}^{pre}$	0.084	0.339
$S_L^{pre}$	1.466	6.002	$S_L^{pre}$	1.488	5.974

Only the total feeder loads can be compared directly, as the modelling of the load is different in the analytical and the simulation model. However, little difference is seen between the total estimated load and the total load read from simulations. Estimating the pre-fault load using the simple lumped feeder model thus works with satisfactory accuracy also for a feeder with three DG-units.

### 6.3.2 Fault cases for feeder with three DG-units

Four different fault cases are considered, according to the assumed location of the fault.

The fault is assumed to be located:

- Fault located before the  $G1$ -node
- Fault located between the  $G1$ -node and  $B$ -node
- Fault located between the  $B$ -node and  $G3$ -node (alternatively  $G5$ -node)
- Fault located after the  $G3$ -node (alternatively after the  $G5$ -node)

The two first cases for this type of feeder are similar to the two first cases for the feeder with one DG-unit, so these cases are not treated here. The two last cases are not handled as separate cases for faults on branch 1 and 2, since these are in principle equal cases with equal equations.

The voltage in the branching node is estimated by (6.30), and the current floating into the node by (6.31).

$$U_B = U_{G1} - Z_{12} (I_S - I_{L1,a} - I_{L1,b} - I_{L2,a} + I_{G1}) \quad (6.30)$$

$$I_B = I_S - I_{L1,a} - I_{L1,b} + I_{G1} - I_{L2,a} - I_{L2,b} = I_{B1} + I_{B2} \quad (6.31)$$

When the fault is assumed to be on branch 2, the current on branch 1 has to be estimated first, and the current  $I_{B1}$  is calculated from (6.32). The current on branch 2 is then given by (6.33).

$$I_{B1} = I_{G3} - I_{L3,a} - I_{L3,b} - I_{L4,a} - I_{L4,b} \quad (6.32)$$

$$I_{B2} = I_B - I_{B1} \quad (6.33)$$

The currents are functions on the voltages on branch 1. If no measurements are available from the DG-unit during fault (method 1), all loads and the DG-unit are assumed to be connected in the branching point. If the DG-node voltage magnitude is measured during fault (method 2) the voltage phasor can be estimated:

$$\begin{aligned} U_B &= U_{G3} - Z_{13} (I_{G3} - I_{L3,b} - I_{L4,a} - I_{L4,b}) \\ &= U_{G3} - Z_{13} \left( \left( \frac{S_{G3}}{U_{G3}} \right)^* - \left( \frac{S_{L3,b}}{U_{G3}} \right)^* - 2 \left( \frac{S_{L4,a}}{U_{G3}} \right)^* \right) \\ \Rightarrow U_{G3} &= \frac{|U_{G3}|^2 - (Z_{13})^* (S_{G3} - S_{L3,b} - 2 \cdot S_{L4,a})}{(U_B)^*} \end{aligned} \quad (6.34)$$

As a simplification it has been assumed that the voltage at the end of branch 1 is equal to the voltage in the  $G3$ -node:  $U_{E1} \approx U_{G3}$ . This means that losses of section 4 are neglected.

Loads during fault are estimated using (5.30) and (5.31). The same voltage dependency characteristics have been used for loads in all sections.

### 6.3.3 Fault located after branching node, and before the $G5$ -node

If the fault can be assumed to be located after the branching node, and before the  $G5$  node, both DG1 and DG2 contribute to the error in the distance estimate. The equivalent circuit for this case is shown in Figure 6.11.

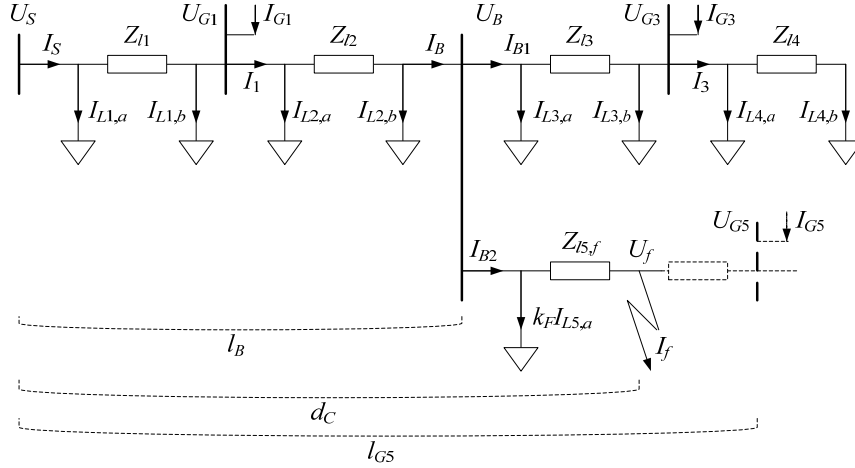


**Figure 6.11: Equivalent circuit when the fault can be assumed to be located between the branching node and the G5-node**

The fractional constant  $k_F$  is equal to the distance from the branching node to the assumed fault location divided by the distance from the branching node to the G5-node:

$$k_F = \frac{d_s - l_B}{l_{G5} - l_B} \quad (6.35)$$

The impedance of the line section between the branching node and the assumed fault location is:

$$Z_{I5,f} = Z_C - (Z_{I1} + Z_{I2}) \quad (6.36)$$

The estimation of load currents is shown in Ch. 5.4, and the estimation of DG-currents is shown in Ch. 5.5. The compensated distance estimate is calculated from:

$$Z_C = Z_{I1} + Z_{I2} + \frac{\Delta(U_B)}{\Delta(I_{B2} - k_F I_{L5,a})} \quad (6.37)$$

The calculations will be similar if the fault is on the other branch, between the branching node and the G3-node.

### 6.3.4 Fault located after the G5-node

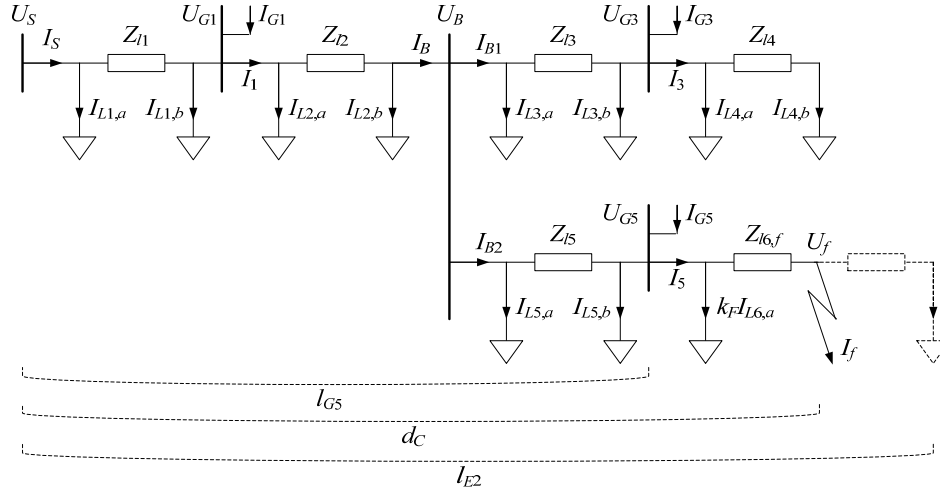


Figure 6.12: Equivalent circuit when the fault can be assumed to be located after the G5-node

The fractional constant of the faulted section is equal to:

$$k_F = \frac{d_s - l_{G5}}{l_{E2} - l_{G5}} \quad (6.38)$$

The impedance of the line section between the G5-node and the assumed fault location is:

$$Z_{l6,f} = Z_C - (Z_{l1} + Z_{l2} + Z_{l5}) \quad (6.39)$$

Estimation of G3-node voltage

$$U_{G3} = U_B - Z_{l3} I_{B2} \quad (6.40)$$

The current floating out of node G5,  $I_5$ , is equal to:

$$I_5 = I_{B2} - I_{L5,a} - I_{L5,b} + I_{G5} \quad (6.41)$$

The estimation of load currents is performed as shown in Ch. 5.4, and the estimation of DG-currents is shown in Ch. 5.5. The compensated impedance estimate is calculated from:

$$Z_C = Z_{l1} + Z_{l2} + Z_{l5} + \frac{\Delta(U_{G5})}{\Delta(I_5 - k_F I_{L6,a})} \quad (6.42)$$

The calculations will be similar if the fault is on the other side-branch, located after the G3-node.

## 7 COMPENSATED DISTANCE ESTIMATE RESULTS

In Chapter 4 the conventional distance fault localization using distance relays were presented. The impacts of various parameters on the results obtained from the conventional method were investigated, and resulting distance estimate errors were shown for each case. Chapter 5 presented methods for compensation of the impact from load and DG-units on the distance estimation for a general MV-feeder. Chapter 6 described the application of the compensation method for three specific MV-feeders:

- feeder without DG,
- feeder with one DG-unit
- feeder with three DG-units

This chapter presents the distance estimate errors results with compensation for fault cases on the three feeders. For clarity, the results without compensation are repeated from Chapter 4, and presented together with the results with compensation.

### 7.1 Overview of compensation results cases

The cases that are presented in this chapter are summarized in Table 7.1. The fault- and DG-locations are given as the point where they are connected on the feeder, referring to Figure 7.1, which is the same feeder as presented in Figure 3.1.

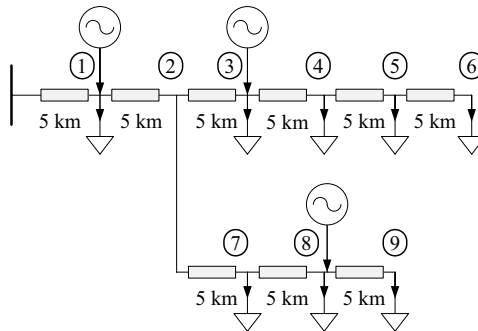


Figure 7.1: Feeder simulated in PSCAD, without DG, with one DG-unit or with three DG-units

Some general abbreviations used in the figure legends were given in Table 4.1, and the same abbreviations are used in Table 7.1. Results with a DG connected at 0 km are not included. As stated in Ch. 4, a DG located very close to the substation is not assumed to be connected to the feeder, but instead directly to the substation.

Distance estimate error is defined as the estimated minus the correct distance to the fault location. A positive error means that the estimated distance is longer than the real distance, while a negative error means that the estimated distance is shorter than the real distance to the fault location.

Table 7.1: Summary of cases with compensation

Load level	Fault type	Fault location	DG location	Case
<b>Feeder without DG</b>				
LL HL	2 $\phi$ /3 $\phi$	1, 2, 3, 4, 5, 6, 7, 8, 9	-	Impact of fault location, load level and fault type
LL HL	3 $\phi$	1, 2, 3, 4, 5, 6	-	Impact of load distribution: L-N, L-1, L6
LL HL	3 $\phi$	1, 2, 3, 4, 5, 6	-	Impact of voltage dependency factor: NP = 0, NP = 1, NP = 2
LL HL	3 $\phi$	1, 2, 3, 4, 5, 6	-	Impact of using wrong voltage dependency factor in compensation
<b>Feeder with one DG-unit</b>				
LL HL	2 $\phi$ /3 $\phi$	6	1, 2, 3, 4, 5, 6	Impact of DG location for fixed fault location
LL HL	2 $\phi$ /3 $\phi$	1, 2, 3, 4, 5, 6,	1	Impact of fault location for a fixed DG location
LL	2 $\phi$ /3 $\phi$	7, 8, 9	6	Impact of fault location for a fixed DG location
LL	3 $\phi$	1, 2, 3, 4, 5, 6	3	Impact of DG-rating: $S_{DG} = 3$ MW, $S_{DG} = 6$ MW, $S_{DG} = 7.5$ MW
LL	3 $\phi$	1, 2, 3, 4, 5, 6	3	Impact of d-axis transient reactance: $x'_d = 0.15$ [pu], $x''_d = 0.5$ [pu]
LL	3 $\phi$	1, 2, 3, 4, 5, 6	3	Impact of substation transformer rating: $S_T = 12$ MVA, $S_T = 25$ MVA
LL HL	3 $\phi$	1, 2, 3, 4, 5, 6	1, 3	Impact of feeder length: 30 km, 60 km
<b>Feeder with three DG-units</b>				
LL HL	3 $\phi$	1, 2, 3, 4, 5, 6	1, 3, 8	Comparison between three 1 MW DG units and one 3 MW DG unit in point 1 or 3.

## 7.2 Results with compensation in network without DG

In Ch. 4.3 the impact of load on the distance estimate error were explored. In Ch. 6.1 it is shown how impact from the load can be compensated for in a network without DG, using the simplified lumped feeder model. In this chapter the results with compensation for the load impact are shown together with the result without compensation.

### 7.2.1 Load level on feeder without DG

Distance estimate errors for three-phase and two-phase short circuits at the main branch are shown in Figure 7.2, and at the side branch are shown in Figure 7.3. Results are shown for both low load and high load cases. Figure (a) shows distance estimate errors after load compensation and figure (b) shows errors without compensation. The plots without compensation are the same as shown earlier in Figure 4.5. It is obvious that without any compensation the errors are largest for the high load level and for faults located at the feeder end, since these are the case with most load connected between the substation and the fault location.

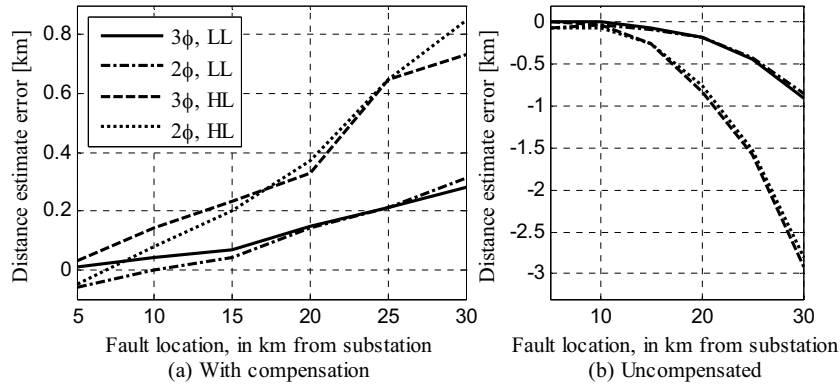


**Figure 7.2: Distance estimate errors (a) with load compensation and (b) uncompensated for low load and high load. 3-phase and 2-phase short circuits at varying locations at the main branch**

For faults on the main feeder branch, worst case after compensation is a two-phase short circuit at the end of the branch at high load. The distance estimate error after compensation for this case is 0.85 km. The error without compensation was -2.8 km, so the accuracy is still improved by 70 % for this case.

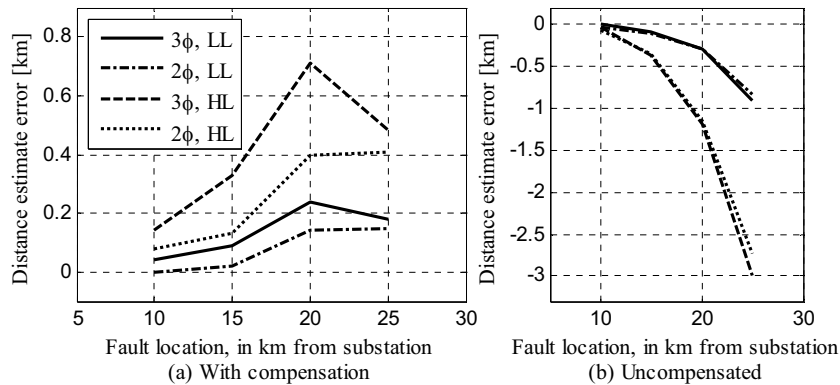


**Figure 7.3: Distance estimate errors (a) with load compensation and (b) uncompensated for low load and high load. 3-phase and 2-phase short circuits at varying locations at the side branch**

For faults at the side-branch, a three-phase short circuit 20 km from the substation at high load represents worst case after compensation, with an error of 0.71 km. Without compensation the error was -1.2 km, and the improvement of the accuracy as compared to without compensation for this case is 40 %.

The distance estimate errors are reduced when compensation is applied for almost all cases. However, for faults located 5-10 km from the substation there is very little or no improvement of the accuracy. In most cases there is some overcompensation of the impact from the load, resulting in positive errors after compensation.

### 7.2.2 Load distribution

The impact of the load distribution on the distance estimate error was shown in Ch. 4.3.2. In this chapter it is attempted to compensate for the errors in the same three load distributions given in Table 7.2.

**Table 7.2: Abbreviations used for load distributions in Figure legends**

L-N	normal distribution of load, loads are evenly distributed between the 6 load points
L-1	all loads are connected in the first load point, 5 km from the substation
L-6	all loads are connected in the last load point, 30 km from the substation

The impact of the distribution of loads on the distance estimate error is shown in Figure 7.4 (a) for low load and Figure 7.5 (b) for high load. The plots are based on PSCAD simulations with the three load distributions described above. The distance estimate errors after compensation of load are shown in Figure 7.4 (b) for low load and Figure 7.5 (b) for high load.

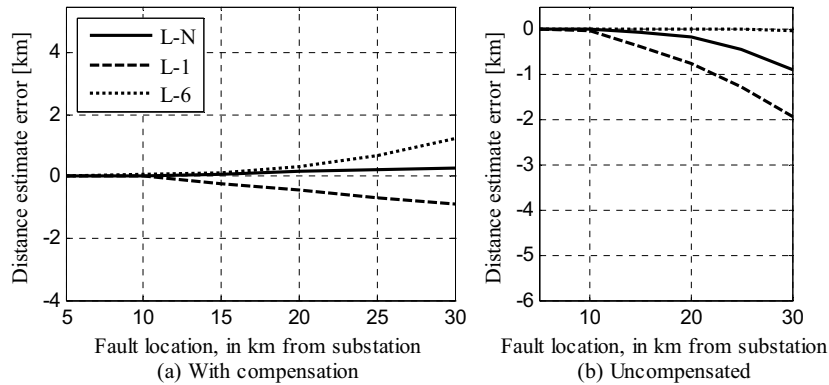


**Figure 7.4: Distance estimate errors (a) with load compensation and (b) uncompensated using pi-equivalent load model at low load for a 3-phase short circuit**

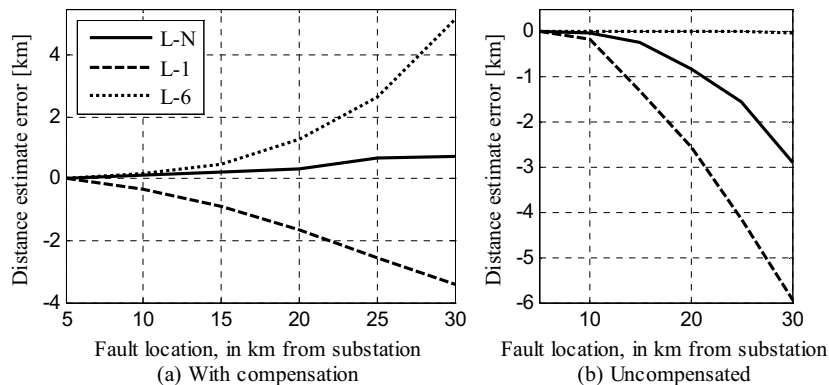


**Figure 7.5: Distance estimate errors (a) with load compensation and (b) uncompensated using pi-equivalent load model at high load for a 3-phase short circuit**

As expected the results with load compensation are best for the feeder with evenly distributed loads (L-N). For the worst-case with distribution L-1, fault at the feeder end at high load, the error after compensation is -3.4 km. Without compensation the error was -6.0 km, which means an improvement of the accuracy by 43 %.

With load distribution L-6 there was negligible error without compensation, since the load had no impact on the distance estimate. Worst case after compensation is when the fault is located at the feeder end. For the low load case the error becomes 1.3 km with compensation, and 5.2 km for the high load case. Still, this is a smaller error than worst-case without compensation with load distribution L-1, so the overall errors are reduced with compensation.

### 7.2.3 Voltage dependency factor

The distance estimate errors for three different voltage dependency factors for the active power was shown in Figure 4.8, and are repeated in Figure 7.6 (b) for low load and Figure 7.7 (b) for high load. The tree voltage dependency factors and the corresponding load characteristics were given in Table 4.3, and are repeated in Table 7.3.

**Table 7.3: Three voltage dependency factors and corresponding active power load characteristics**

NP = 0	constant active power load
NP = 1	active power is a constant current load (default)
NP = 2	active power is a constant impedance load

The errors after compensation of load are shown in Figure 7.6 (b) for low load and Figure 7.7 (b) for high load. The same active power characteristics (same NP-value) were used in the compensation as in the simulation in each case. Largest distance estimate errors appear when the fault is located at the feeder end both with and without compensation.

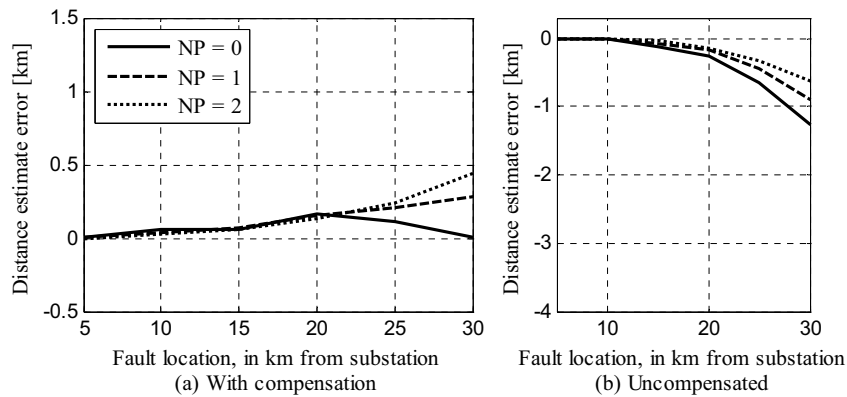


**Figure 7.6: Distance estimate errors (a) with load compensation and (b) uncompensated. The correct NP is used in the compensation for all cases. 3-phase short circuit on the main branch at low load**

Worst case after compensation at low load is with NP = 2, with an error of 0.44 km. Still, this is an improvement of 29 % as compared to the case without compensation with an error of -0.62 km, so there is overcompensation of the impact from the load.

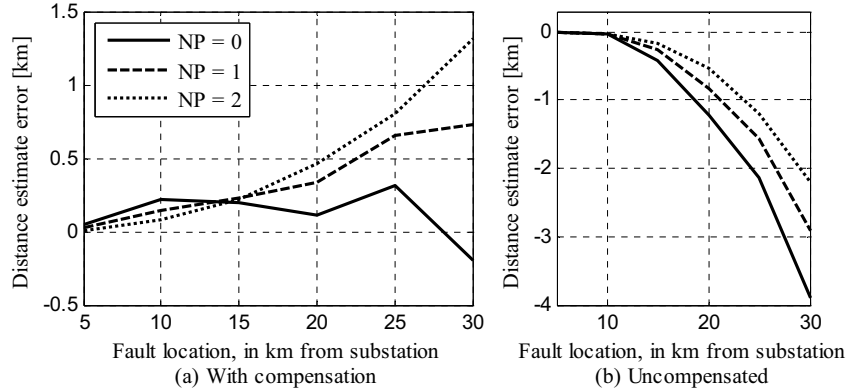


**Figure 7.7: Distance estimate errors (a) with load compensation and (b) uncompensated. The correct NP is used in the compensation for all cases. 3-phase short circuit on the main branch at high load**

Worst case after compensation at high load is with constant impedance characteristics (NP = 2), with an error of 1.3 km. This is an improvement of 41 % as compared to the case without compensation with an error of -2.2 km. In this case the impact from the load has been overcompensated. It can be seen from the two figures with compensation that the distance estimate errors generally are smallest with constant power characteristics (NP = 0), even if there is some overcompensation. With constant current (NP=1) and constant impedance (NP = 2) characteristics there is even more overcompensation, and for the low load cases there are only very small reductions in the errors with compensation. The compensation works best with the constant power load characteristics.

To see the importance of using the correct voltage dependency factor when compensating for the load, a NP-factor different from that in the simulation were used in the compensation. The distance estimate errors for these cases are shown in Figure 7.8. The active power voltage dependency factors used in the simulation and the assumed factors for the compensation are given in Table 7.4.

**Table 7.4: Voltage dependency characteristics used in simulation and compensation, explanation of legends used in Figure 7.8**

NP = 0,0	Constant active power assumed both in simulation and compensation
NP = 0,1	Constant active power in simulation, constant current assumed in compensation
NP = 2,1	Constant impedance in simulation, constant current assumed in compensation
NP = 2,2	Constant impedance assumed in both simulation and compensation

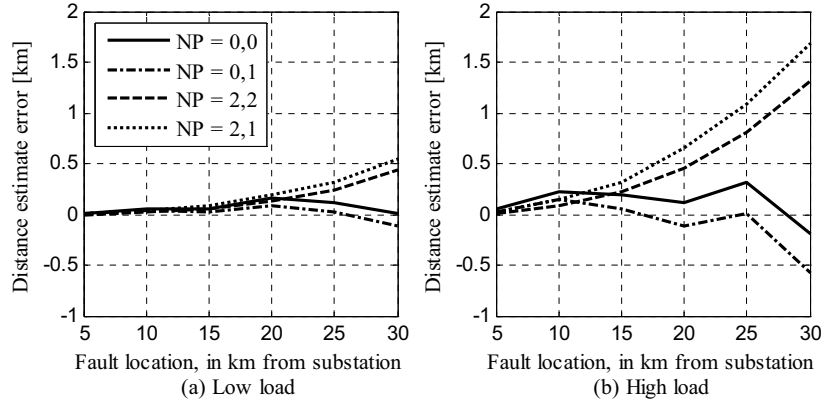


Figure 7.8: Distance estimate errors after load compensation. NP = 1 in used in the compensation for both cases. 3-phase short circuit on the main branch at (a) low load and (b) high load.

The errors after compensation are smallest when the loads have voltage dependency factor NP=0, both when a correct (=0) and a wrong (=1) NP-value is assumed in the compensation. The errors are also reduced with compensation when the loads have voltage dependency factor NP=2, both with correct and incorrect NP-value assumed. It can be concluded that the improvement with using the correct versus an incorrect NP-value in the compensation is not very large, and to use the correct voltage dependency factor in the compensation is not very critical.

### 7.3 Compensation results in network with 1 DG-unit

In Ch. 4.4 the impact of one DG-unit on the distance estimate error were explored. In this chapter it is attempted to compensate for the impact from the load and the DG-unit using the lumped feeder model. The DG in-feed generally causes a positive distance estimate error, which is opposite to that of the load. To some degree the impact from the DG is neutralized by that from the load. As expected the estimates obtained using method 2 are generally more accurate than those obtained using method 1, since in method 2 measurement from the DG-unit during fault are utilized.

#### 7.3.1 Impact of the location of the DG-unit

The distance estimate error as a function the DG-location for faults at the end of the main feeder branch was shown in Figure 4.10. The distance estimates were then obtained from simulated substation voltages and currents. Figure 7.9 (a) shows the distance estimate errors for the same cases with compensation 1 and 2 for low load and Figure 7.10 (a) for high load. Figure 7.9 (b) and Figure 7.10 (b) shows the results without compensation, and are the same results as shown in Figure 4.10.

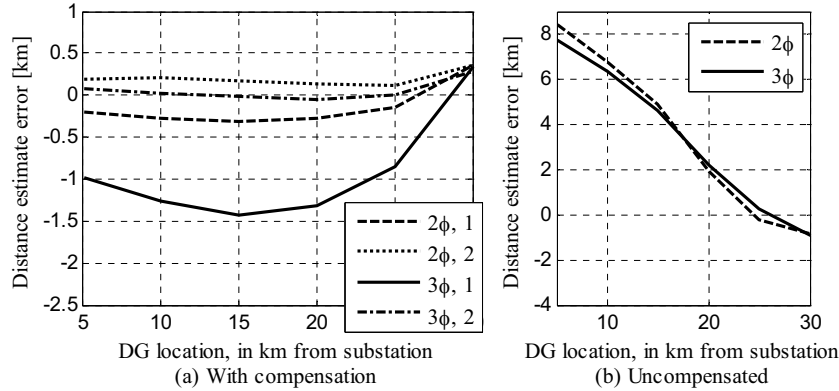


**Figure 7.9: Distance estimate errors (a) without compensation and (b) with compensation at low load. 2-phase and 3-phase short circuits at the feeder end (30 km), with a 3 MW DG at varying locations**

Worst case at low load is with compensation 1 for a three-phase short circuit and the DG connected at 15 km. The error is then -1.4 km. Without compensation the error was 4.6 km, so despite of the overcompensation there is an improvement of the accuracy of 70 %. When the DG is connected at 25 km there is no improvement of the accuracy, since the error is very small without compensation. With compensation 1 and a three-phase short circuit the error is -0.9 km, while it is 0.3 km without compensation.

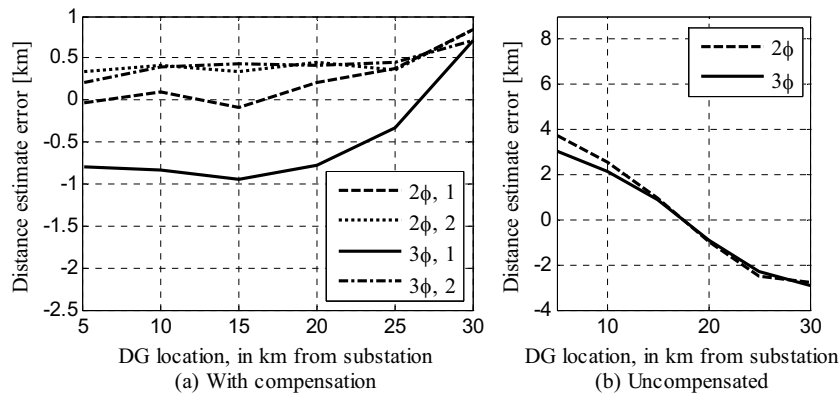


**Figure 7.10: Distance estimate errors (a) without compensation and (b) with compensation at high load. 2-phase and 3-phase short circuits at the feeder end (30 km), with a 3 MW DG at varying locations.**

The results with compensation for high load are quite similar to those for low load, and worst case is the same. The error in the worst case at high load is -0.9 km. Without compensation the error was 0.9 km, so the size of the error is the same but with opposite sign after compensation. As shown in Ch. 6.2.5, the estimated DG-currents are larger than the simulated in almost all cases. Consequently, in cases where the error is close to zero without compensation, the overcompensation of the DG-current may result in an increase of the error when the compensation is applied. With compensation 2 however, the error is reduced to 0.4 km.

### 7.3.2 Impact of the location of the fault

In the previous subchapter the fault was always located at the end of the main branch, while the location of the DG-units was varied. In this subchapter the DG-unit is always located 5 km from the substation (point 1) while the fault location is varied along the main branch. Figure 7.11 (a) and Figure 7.12 (a) show distance estimate errors with compensation 1 and 2 for low load and high load respectively. Errors without compensation are shown in Figure 7.11 (b) and Figure 7.12 (b).

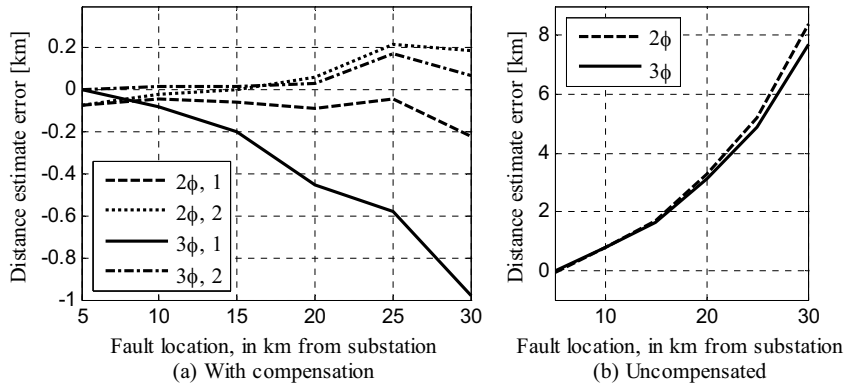


Figure 7.11: Distance estimate errors at low load (a) with compensation and (b) uncompensated. 2-phase and 3-phase short circuits at varying locations, and a 3 MW DG located 5 km from the substation

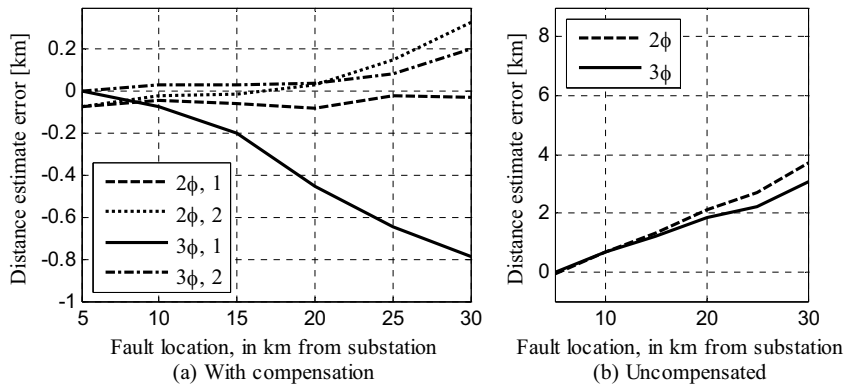
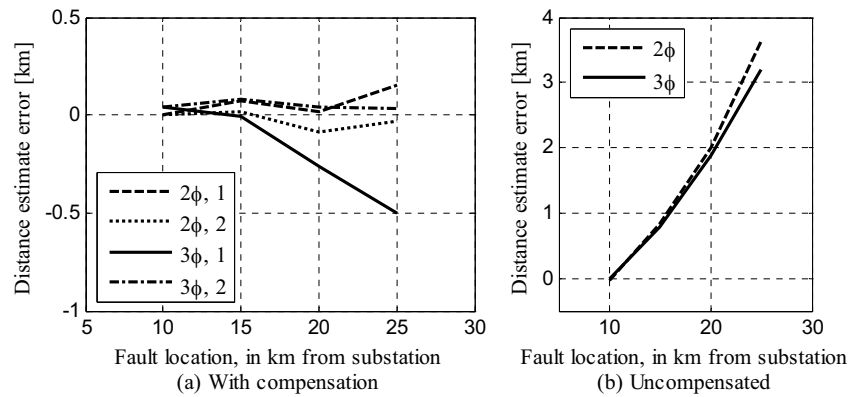


Figure 7.12: Distance estimate errors at high load (a) with compensation and (b) uncompensated. 2-phase and 3-phase short circuits at varying locations, and a 3 MW DG located 5 km from the substation

The errors with compensation are increasing as the fault location is moved towards the feeder end. There is little difference between the results for low load and high load, despite the difference seen without any compensation. With compensation 1 there is overcompensation of the impact from the DG in all cases, but 3-phase short circuit at 30 km is worst case with an error of -1.0 km for low load and -0.8 km for high load. This represents an improvement of 87 % and 74 % for low and high load respectively, as compared to the uncompensated results.

Results with compensation 1 and 2 for two-phase and three-phase short circuits at varying locations on the side branch are shown in Figure 7.13. The DG-unit connected at the end of the main branch (30 km), and the uncompensated results have previously been shown in Figure 4.12.



**Figure 7.13: Distance estimate errors at low load (a) with compensation and (b) without compensation. 2-phase and 3-phase short circuits at varying locations on the side branch. A 3 MW DG-unit located at the end of the main branch**

As in previous cases there is overcompensation of the impact from the DG with method 1 for three-phase short circuits. This results in an increasing negative error as the fault location is moved towards the end of the side branch. Worst case is a short circuit at 25 km, with an error of -0.5 km. This is an improvement of 72 % compared to the uncompensated result. Results with compensation 1 for two-phase faults are much more accurate. The results seen with method 1 are in principle the same as for faults located after the DG-unit on the main branch. With compensation 2 the errors become negligible for both fault types and all fault locations.

### 7.3.3 Generator rating

In Ch. 7.3.1 the worst case after compensation was found to be a three-phase short circuit at the feeder-end and the DG located 15 km from the substation, using compensation method 1. Highest accuracy were generally achieved when applying the compensation on two-phase short circuits. Only three-phase short circuits are treated in this subchapter. To see how the compensation works with larger generating units, it is applied for a network with a 6 MW and a 7.5 MW DG-unit, respectively. Results with compensation 1 are shown in Figure 7.14 (a) for with compensation 2 in Figure 7.15 (a). Results without compensation were shown in Ch. 4.4.3, and are repeated in Figure 7.14 (b) and Figure 7.15 (b). Only results for low load are shown, since the results after compensation have been shown to be very similar for low load and high load.

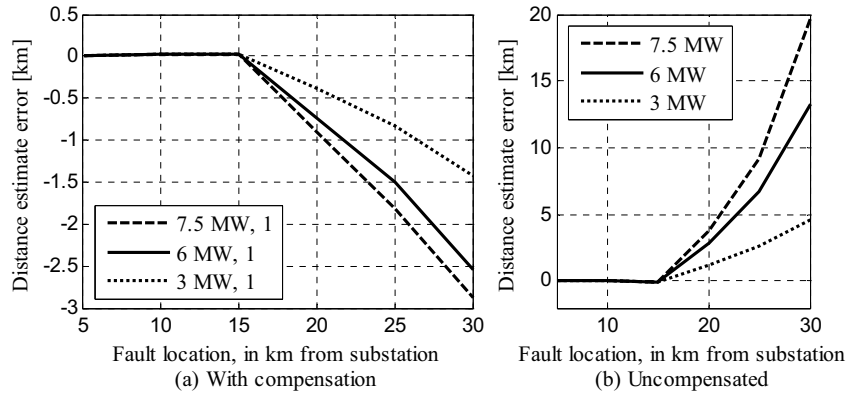


Figure 7.14: Distance estimate errors at low load (a) with compensation 1 and (b) without compensation. 7.5 MW, 6 MW or 3 MW DG-unit 15 km from the substation. 3-phase short circuit at varying locations

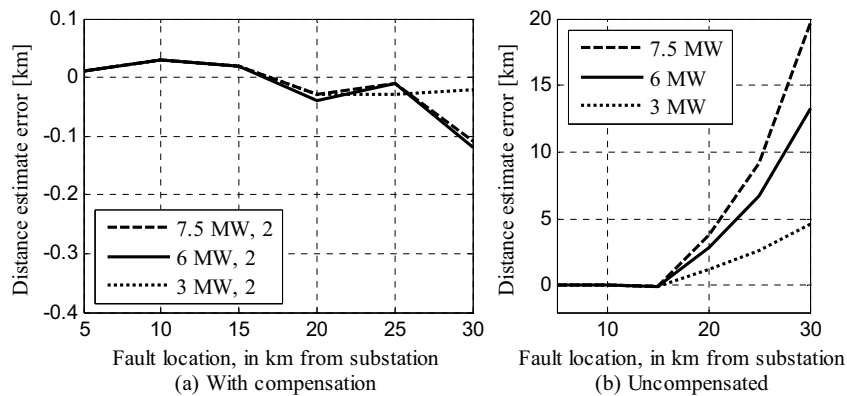


Figure 7.15: Distance estimate errors at low load (a) with compensation 2 and (b) without compensation. 7.5 MW, 6 MW or 3 MW DG-unit 15 km from the substation. 3-phase short circuit at varying locations

Table 7.5 summarizes the results with compensation methods 1 and 2 for the worst case, which is a fault at the feeder end. The DG is located at 15 km and generating 3, 6 or 7.5 MW.

Table 7.5: Summary of compensation results for a 3-phase short circuit at the feeder end with 3, 6 and 7.5 MW DG

DG power [MW]	Distance estimate error without compensation [km]	Compensation 1		Compensation 2	
		Error [km]	Reduction of error [%]	Error [km]	Reduction of error [%]
3	4.63	-1.43	69	-0.02	99.6
6	13.28	-2.55	81	-0.12	99.1
7.5	19.75	-2.87	85	-0.11	99.4

Both methods 1 and 2 results in improvement of the accuracy of the distance estimate. The overcompensation of the impact from the DG in method 1 is increasing with the DG-rating. Despite the overcompensation effect, the accuracy is substantially improved. Using

compensation 2, very accurate distance to fault estimates can be obtained, independent of the DG-rating and generation level.

### 7.3.4 Generator transient reactance

Two generators with equal ratings may have different parameters, and Figure 7.16 (a) shows the distance estimate errors with compensation 1 and 2 for two generators with different transient reactance. Figure (b) shows errors without compensation, which was also shown in Figure 4.14 (a). The reactances are larger than the value used in all other cases in this thesis ( $x'_d \approx 0.22$  pu); 0.3 pu and 0.4 pu. It has been observed that some generators used in small hydro power plants have higher reactance values than the “typical” synchronous machine. The DG-unit is connected 15 km from the substation on the main feeder branch, and is generating 3 MW. The fault is a three-phase short circuit, and the fault location is varied along the main branch. All cases are at low load.

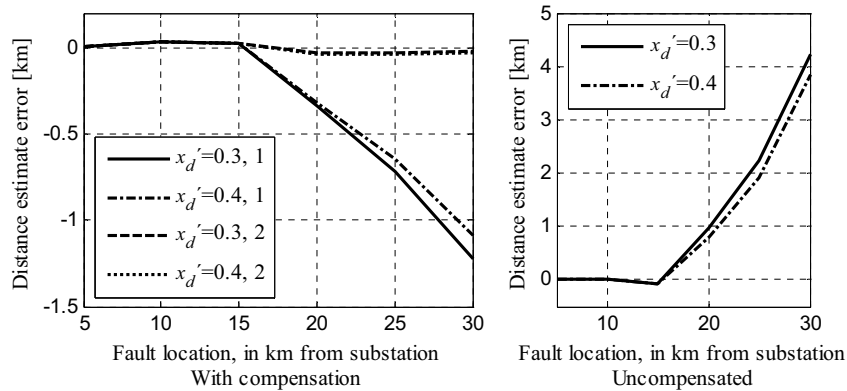


**Figure 7.16: Distance estimate errors for low load (a) with compensation methods 1 and 2 and (b) without compensation. 3-phase short circuit at varying locations and 3 MW DG-unit connected 15 km from the substation**

It is seen that the distance estimate error is always largest when the fault is located at the feeder-end, both with and without compensation. The errors are a bit larger for the generator with  $x'_d \approx 0.3$  pu than with 0.4 pu without compensation and with compensation method 1. The largest error without compensation is 4.2 km. With compensation 1 the error is reduced to -1.2 km, which is a 71 % reduction of the error. Correspondingly the error is reduced to -0.02 km with compensation 2, a reduction of 99.5 %. For compensation method 2 the transient reactance has negligible impact.

A smaller transient reactance means larger distance estimate error without compensation if the generator rating is unchanged (Ch. 5). The effect of decreasing the transient reactance is to increase the transient short circuit capacity of the DG-unit. This will have the same impact as increasing the DG-rating, which means an increased positive error with the conventional distance estimation and an increased negative error after compensation 1 is applied. The distance estimate errors are reduced in all cases with both compensation methods. The reduction of the error with compensation 1 is a bit dependent on the transient reactance, and the results are best for the generator with the largest reactance. The performance of compensation method 2 is not dependent on the transient reactance value.

### 7.3.5 Substation short circuit capacity

Figure 7.17 (a) shows a comparison between results with compensation 1 and 2 for two different substation transformer ratings, 25 MVA (normal value) and 12 MVA. Reducing the transformer rating corresponds to decreasing the short circuit capacity at the 22 kV side of the transformer. The distance errors without compensation were shown in Figure 5.15 and are repeated in (b) for low load.

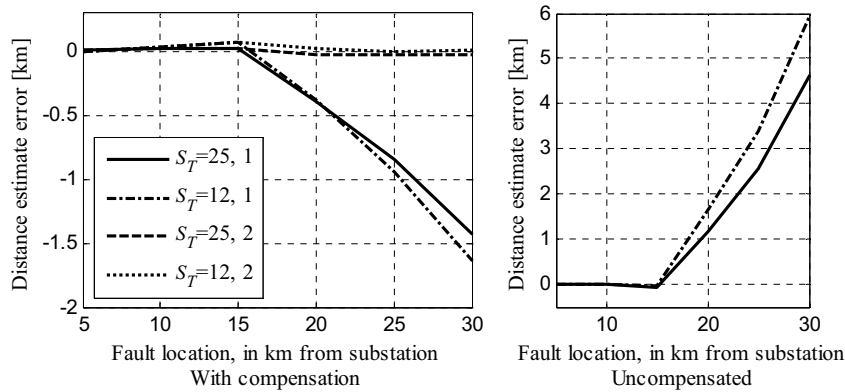


**Figure 7.17: Distance estimate errors for low load (a) with compensation and (b) without compensation. Two different substation ratings, 25 and 12 MVA, and 3 MW DG at 15 km. 3-phase short circuits at varying locations along the main branch**

In the uncompensated case the errors were increased when the transformer rating was reduced. With compensation 1 the errors are also a bit larger with the smallest transformer rating, but the differences are not large. A decrease of the substation transformer rating means that the relative short circuit capacity of the DG versus the substation capacity becomes larger. Again the effect will be the same as increasing the DG-unit rating. With compensation 2 the difference between the results for the two ratings are negligible. It can be concluded that the compensation methods are little dependent on the substation transformer rating.

### 7.3.6 Feeder length

The base feeder model has a length of 30 km for the main branch. To see how the compensation works for a different feeder length it has been tested on the feeder with double length, 60 km. Results without compensation were shown in Figure 4.17. Results with compensation 1 and 2 are shown in Figure 7.18 (a) for low load and Figure 7.19 (a) for high load. DG in 1 means that the DG is located at 10 km and DG in 3 means that the DG is located 30 km from the substation.

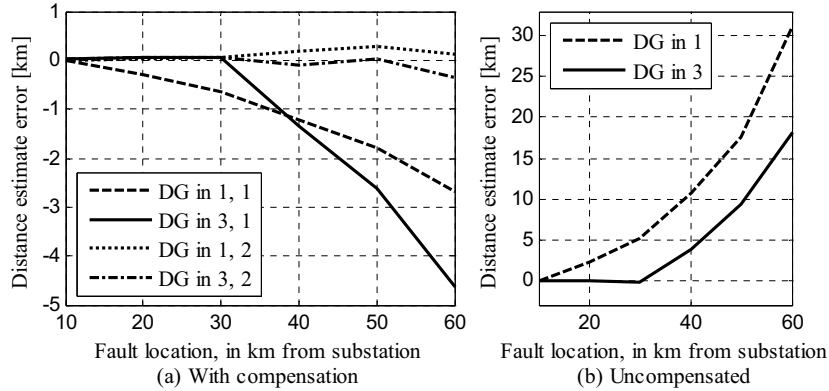


Figure 7.18: Distance estimate errors at low load (a) with compensation and (b) without compensation. 3 MW DG-unit located 10 km or 30 km from the substation and 3-phase short circuit at varying locations

Largest error after compensation for low load is when the DG is located 30 km from the substation for both compensation 1 and 2. With compensation 1 the largest error is -4.6 km, which is an improvement of the accuracy of 74 %. With compensation 2 the largest error is -0.4 km, and the accuracy is improved 98 %.

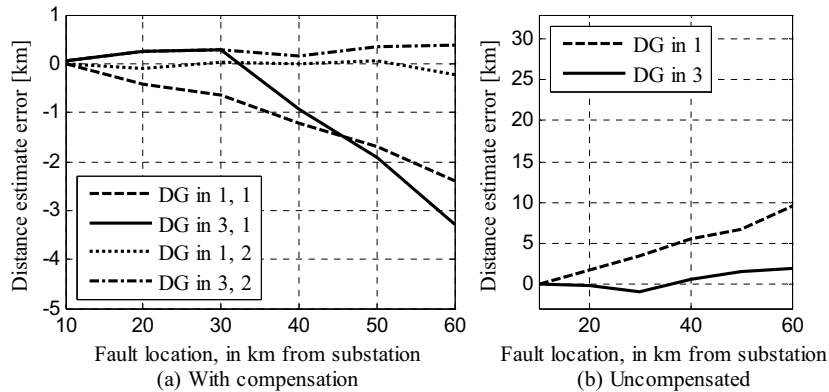


Figure 7.19: Distance estimate errors at high load (a) with compensation and (b) without compensation. 3 MW DG-unit located 10 km or 30 km from the substation and 3-phase short circuit at varying locations

Largest error with compensation 1 is when the DG is located 30 km from the substation, with an error of -3.3 km. Without compensation the error was only 2.0 km, and thus the accuracy becomes less with compensation in this case. Thus the largest error with compensation 1 occurs when the DG is located at the middle of the feeder also for the longer feeder. Largest error with compensation 2 is when the DG is located 10 km from the substation, with an error of 0.4 km. In this case the accuracy is improved by 81 %.

#### 7.4 Compensated distance estimate in network with 3 DG-units

In Figure 4.1 the feeder modeled in PSCAD were shown with three DG-units connected in point 1 and point 3 on the main branch and point 8 on the side branch. Figure 7.20 (a) and Figure 7.21 (a) shows distance estimate errors for a feeder with three 1 MW DG-units and a

feeder with one 3 MW DG-unit with compensation methods 1 and 2. (b) shows results without compensation. Legend 3xDG means feeder with three DG-units and 1xDG means feeder with one DG-unit after 5 km, see also Table 4.6. The faults are three-phase short circuits at varying locations along the main branch.

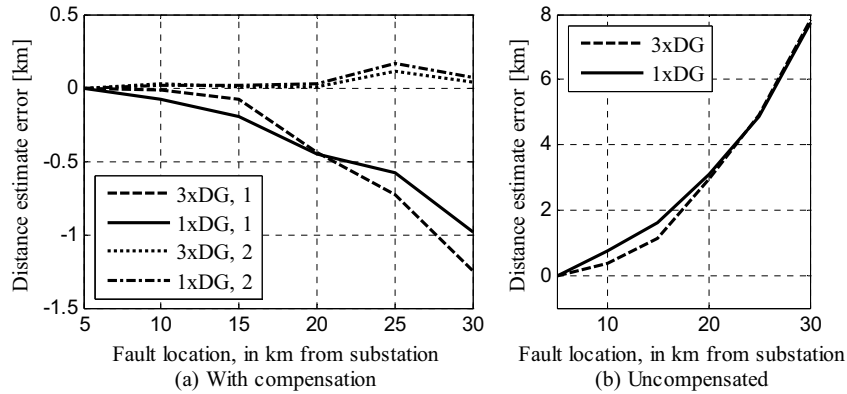


Figure 7.20: Distance estimate errors at low load (a) with compensation 1 and 2 and (b) without compensation. Comparison between a feeder with three DG-units and a feeder with one DG-unit

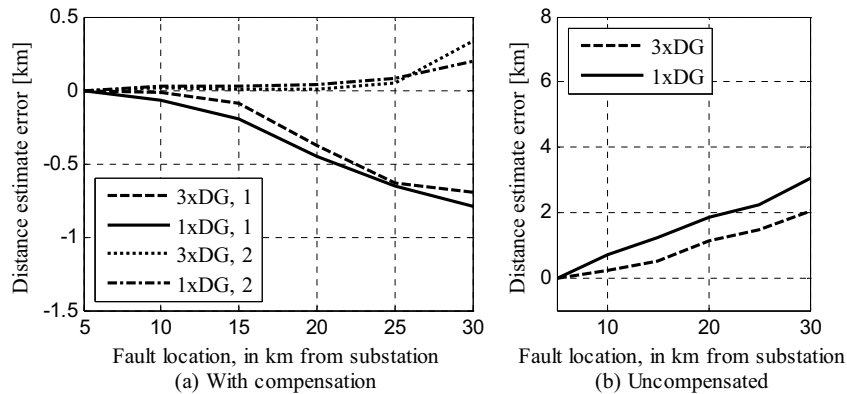


Figure 7.21: Distance estimate errors at high load (a) with compensation 1 and 2 and (b) without compensation. Comparison between a feeder with three DG-units and a feeder with one DG-unit

After compensation, errors are a bit larger for the low load cases than the high load cases. The results are not very different for the feeder with three DG-units than the feeder with one DG-unit. With three DG-units the feeder is divided into more sections, and the load estimation could be expected to become more accurate, but this is not seen from the plots. Worst case for the feeder with 3 DG-units with compensation 1 is -1.3 km. Without compensation the error was 7.8 km, so this is an improvement of 84 %. It can be concluded that both compensation methods work to reduce the distance estimate errors on a feeder with three DG-units. The largest error reductions are seen for the faults at low load, since at high load the errors are small also without any compensation applied.

## 8 IDENTIFICATION OF THE CORRECT FAULTED BRANCH

Distribution feeders generally have a tree structure, and one estimated distance might correspond to several possible fault locations on different branches. Thus there is a need for methods to help deciding the correct fault location among several possible candidates, [92]. Different approaches can be used. One is to install fault indicators in each branching node, and in this way obtain an indication on the faulted branch. The indicators should have communication to the network control centre. The use of fault indicators for fault management in distribution networks have been described in e.g. [93], [94], [2]. Fault statistics can give information about where in the network faults occur most commonly. Phone calls from customers can also give information about the fault location. [92] suggests an approach where the distance to the fault is calculated in two ways; neglecting the load and including the load. The difference between the two calculated distances is assumed to be smallest on the faulted lateral, and in this way the faulted lateral can be decided using only single-end measurements. All this information can be combined with the distance estimation described in this work to obtain the correct fault location. This chapter describes two methods for utilizing measurements in the DG-location during fault in order to decide the right faulted branch. Both methods thus require measurements from the DG during fault, like compensation method 2, and could be used in combination with this. Figure 8.1 shows an example of two locations with an equal distance of 25 km from the substation on the feeder with one DG-unit.

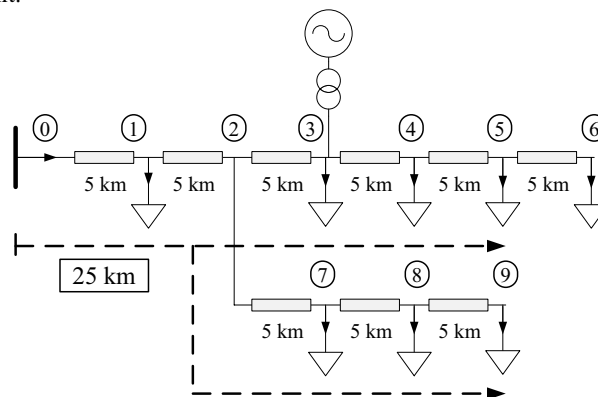


Figure 8.1: Two possible fault locations 25 km from the substation

In the example cases shown in the following subchapters the DG is generating nominal power of 3 MW, and is either connected in point 1 or point 6 on the feeder in Figure 8.1.

### 8.1 Comparison between measured and estimated DG voltage

One way to decide the correct faulted branch is to compare the estimated DG voltage with the measured (simulated) voltage. When the distance to the fault location is estimated, the fault is first assumed to be located on the main branch and next on the side branch in Figure 8.1. For each of the two assumed fault locations the corresponding  $G$ -node voltage is estimated from the lumped feeder model. Then the estimated values are compared to the corresponding simulated value (in a real network they would be compared to measured values). The assumed location which results in the smallest difference between the estimated and the simulated voltages is assumed to be the most probable fault location. The DG voltage is estimated from (6.19) if the fault is assumed to be located on the main branch before the  $G$ -node, from (6.21)

if the fault is assumed to be located after the  $G$ -node on the main branch, and from (6.29) if the fault is assumed to be located on the side-branch.

### 8.1.1 Results with three-phase short circuits

Figure 8.2 shows the difference between the estimated and the simulated voltage magnitudes for faults located 15, 20 and 25 km from the substation. All faults are three-phase short circuits. The DG is connected in point 3, 15 km from the substation on the main branch. Legend “Main” means that the fault was assumed to be located on the main branch when estimating the  $G$ -node voltage. Legend “Side” means that the fault was assumed to be located on the side branch when estimating the  $G$ -node voltage. Results when the faults are located on the main branch are shown in the (a) figures and results when the faults are located on the side branch are shown in the (b) figures.

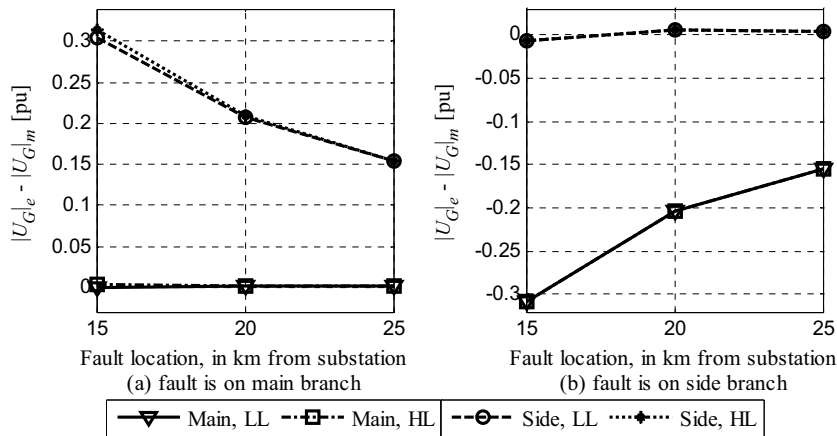


Figure 8.2: Difference between estimated and measured voltage magnitudes when the faults are assumed to be located on the main branch and on the side branch. 3-phase short circuits (a) on the main branch and (b) on the side branch. Low load (LL) and high load (HL), DG located in point 3

In Figure 8.2 (a) the faults are actually located on the main branch. When the faults are also assumed to be located on the main branch the differences between the estimated and simulated DG voltage magnitudes are approximately zero for all three fault locations, at both load levels. If the faults are assumed to be located on the side branch the difference varies from 0.31 to 0.15 pu. In Figure 8.2 (b) the faults are located on the side branch. In the cases where the fault is assumed to be located on the main branch the differences between the estimated and simulated DG voltage magnitudes varies from -0.31 to -0.15 pu. When the faults are assumed to be located on the side branch the differences close to zero. There is little difference between the results for low load and high load.

Figure 8.3 shows the difference between the estimated and the simulated voltage magnitudes for faults located 15, 20 and 25 km from the substation. All faults are three-phase short circuits. The DG is connected in point 6, 30 km from the substation at the end of the main branch.

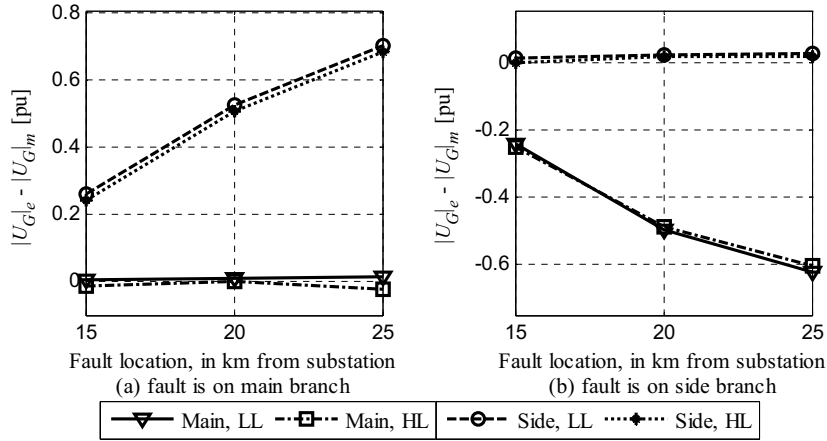


Figure 8.3: Difference between estimated and measured voltage magnitudes when the faults are assumed to be located on the main branch and on the side branch. 3-phase short circuits (a) on the main branch and (b) on the side branch. Low load (LL) and high load (HL), DG located in point 6

In Figure 8.3 (a) the faults are actually located on the main branch. When the faults are also assumed to be located on the main branch, the differences between the estimated and simulated DG voltage magnitudes are small for all three fault locations, varying from 0.01 to -0.02 pu. If the faults are assumed to be located on the side branch the differences are significantly larger, and vary from 0.24 to 0.70 pu. In Figure 8.3 (b) the faults are located on the side branch. In the cases where the fault are assumed to be located on the main branch the differences between the estimated and simulated DG voltage magnitudes varies from -0.24 to -0.62 pu. When the faults are assumed to be located on the side branch the difference is maximum 0.03 pu. The results for low load and high load cases are quite similar.

### 8.1.2 Results with two-phase short circuits

The two previous figures presented results for three-phase short circuits. Figure 8.4 shows the difference between the estimated and the simulated voltage magnitudes when the faults are two phase short circuits and the DG is connected in point 3. Figure 8.5 shows corresponding results for two-phase short circuits when the DG is connected in point 6. Results are only shown for high load, since this represents worst case in this context.

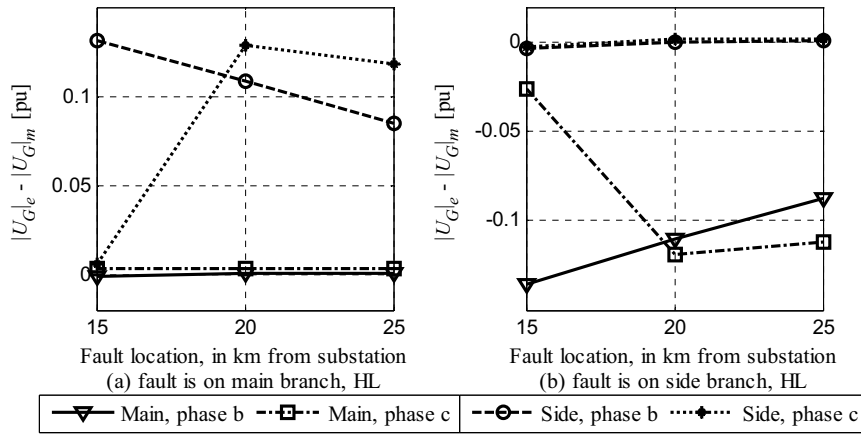


Figure 8.4: Difference between estimated and simulated voltage magnitudes when the faults are assumed to be located on the main branch and on the side branch. 2-phase short circuits (a) on the main branch and (b) on the side branch. High load and DG connected in point 3

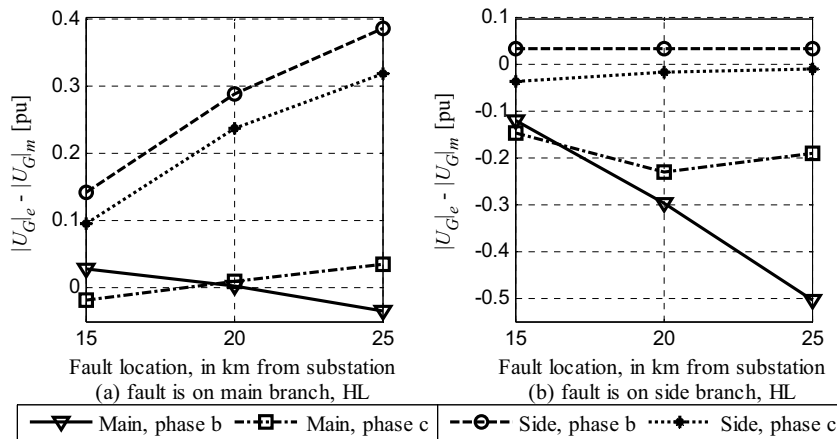


Figure 8.5: Difference between estimated and simulated voltage magnitudes when the faults are assumed to be located on the main branch and on the side branch. 2-phase short circuits (a) on the main branch and (b) on the side branch. High load and DG connected in point 6

In Figure 8.4 (a) and Figure 8.5 (a) the faults are located on the main branch. When the faults are assumed to be located on the main branch the differences between the estimated and simulated DG voltage magnitudes are larger than for the tree-phase short circuit cases, but still close to zero, varying from -0.03 to -0.04 pu. In Figure 8.4 (b) and Figure 8.5 (b) the faults are located on the side branch, and when the faults are assumed to be located at the side branch when estimating the DG voltage, the differences between estimated and simulated values vary from -0.04 pu to 0.04 pu. When DG voltage is estimated assuming the wrong fault location the differences between the estimated and simulated voltage magnitudes are in most cases significantly larger than when the correct fault location is assumed, except for the cases when the fault is 15 km from the substation. In these cases the differences are only slightly larger in one of the phases. Still, by looking at the voltage differences in both phase B and C,

the method can be used to find the correct faulted branch also when the fault is located 15 km from the substation.

## 8.2 Distance calculation from DG-measurements

With measurements from the DG during fault available, a distance from the DG-node to the fault location can be estimated the same way as was done using the substation measurements. The idea is then to compare the distance estimates from the two different locations, and then find the correct fault location. For instance if the estimated distance from the substation to the fault location is 20 km, the fault can be located in point 4 or point 8. If the DG unit is connected in point 3 and the estimated distance from the DG to the fault location is 5 km, point 4 is the correct fault location. Likewise, if the estimated distance from the DG is 15 km, point 8 is the correct fault location.

Since only magnitude values from the DG are available, the phasor angles are estimated as described in chapter 6. The distance estimate is obtained from the following equation:

$$Z_{G-f} = \frac{\Delta\left(\left(U_G\right)_{m-e}\right)}{\Delta\left(\left(I_G\right)_{m-e}\right)} \quad (8.1)$$

As shown in (5.1) and (5.3), subscript *m-e* means measured (simulated) magnitude value and estimated phasor angle.

The distance from the *G*-node to the fault location is calculated from (8.2). This corresponds to calculating the distance from the substation to the fault location in (5.2).

$$d_{G-f} = \frac{\text{Im}\left(Z_{G-f}\right)}{x_l} \quad (8.2)$$

As a simplification the line reactance per unit of length,  $x_l$ , is set to a constant value, equal to the reactance of the FeAl 1X50 line.

The distance from the *G*-node to the fault location is estimated for different fault locations along the main- and side- branch, and the difference between the estimated and real distance are plotted with distance from the substation to the fault location on the horizontal axis. Results for three-phase short circuits are shown in Figure 8.6 and results for two-phase short circuits are shown in Figure 8.7. In (a) the DG is connected in point 3 and in (b) the DG is connected in point 6.

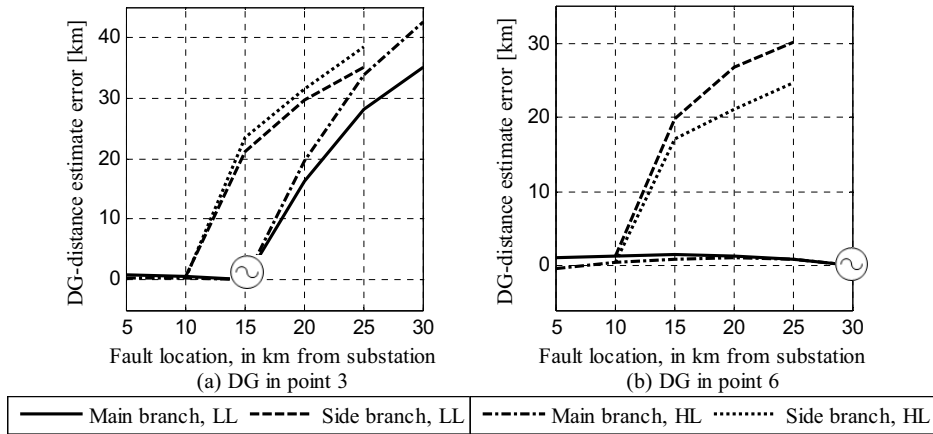


Figure 8.6: Error in estimated distance from DG when the DG is located in (a) point 3 and (b) point 6. 3-phase short circuits at varying locations and feeder at low load (LL) and high load (HL)

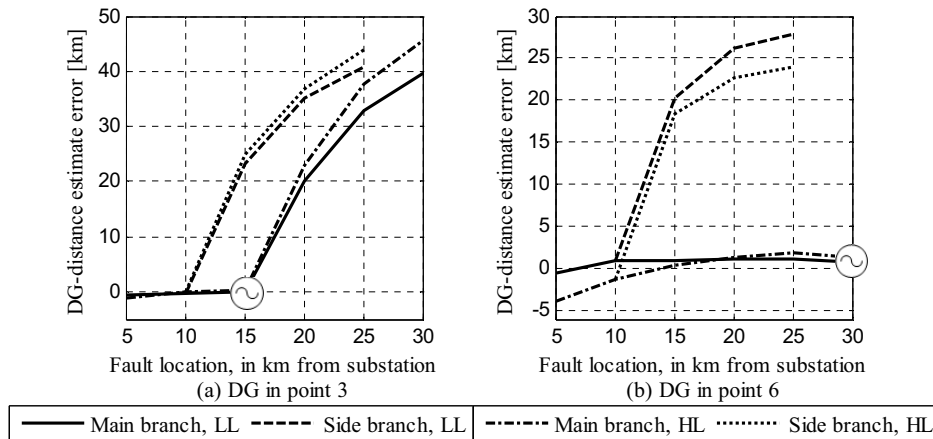


Figure 8.7: Error in estimated distance from DG when the DG is located in (a) point 3 and (b) point 6. 2-phase short circuits at varying locations and feeder at low load (LL) and high load (HL).

It can be seen that if the fault is located on the main branch between the substation and the  $G$ -node, the estimated distance from the DG to the fault location is approximately correct. The errors seen in these cases are mostly due to load, and are negative and highest at high load. If the fault is located on the side branch before the  $G$ -node or on the main branch after the DG-node, the estimated distance is much larger than the real distance. When the DG is located in point 3 the estimated distance is approximately correct only if the fault is located 5-15 km from the substation, on the main branch. In case the DG is located in point 6 the estimated distance is approximately correct if the fault is located on the main branch, 5-30 km from the substation.

## 9 OVERCURRENT PROTECTION IN DISTRIBUTION NETWORK WITH DG

Radial distribution lines are commonly protected by overcurrent relays [95], [96], [2]. The goal of the analysis presented in this chapter is to find out how a DG-unit impacts on the fault current seen by the overcurrent relay in the substation. This can be used to decide if the relay settings need to be adjusted when a new DG-unit is connected to a distribution feeder. Two phenomenons which may occur in networks with DG protected by overcurrent relays are discussed here; blinding and sympathetic tripping. An overcurrent relay has to be set to pickup for a current larger than the maximum load current and smaller than the smallest possible short circuit current. The following margins for setting of pickup current for overcurrent relays are given in [77]:

$$1.5 \cdot I_{load,max} \leq I_{relay,pickup} \leq 0.8 \cdot I_{short\ circuit,min} \quad (9.1)$$

Other sources suggest some different margins for the relay settings. In [86] a current pick-up setting of approximately 1.3 times the maximum load current is suggested. In addition it is recommended that the smallest short circuit current should not be less than twice the maximum load current if overcurrent protection is to be used. [95] recommend a setting of 1.25 to 1.5 times the maximum load current, or even as high as 2 for distribution lines where additional overload is permitted during emergency conditions. In [11] a pickup setting between 2 times the maximum load current and 1/3 of the minimum fault current is suggested, which imply larger margins than the settings in (9.1). Generally solid-state and digital relays can be set with lower margins than the old-type electromechanical relays due to a more accurate response.

A simple method for blinding estimation was introduced by [97], neglecting loads and only valid for three-phase faults. Here a new method is presented, utilizing the lumped feeder model introduced in Ch. 3.2 for estimation of loads and voltages in the pre-fault state in the same way as for the compensated distance estimation. The method can also be used for two-phase short circuits. The intention is to have a method for simple and rough estimation of the blinding probability. Simplifications are made in the analysis; the side-branch is neglected, and loads are neglected in the faulted state. Since the short circuit current through the substation contains a load current component, low load represents a worst case in finding the lowest short circuit current detected by the feeder relay. If an analysis without load shows that the blinding probability is low, the probability will be even lower if loads are included. Neglecting the load impact during fault thus results in conservative blinding estimates, and exclusion of loads can therefore be justified. Also, a static, voltage dependent load will have less significance during fault than in steady-state due to the reduction of the voltage across the load. If the conclusions from the simplified analysis are uncertain, a more detailed model including loads can be studied, but it has not been included in this work. Such a study including the load impact during fault in a similar way as was done for the fault location requires measurements in the substation during fault. The blinding analysis presented here is however only based on pre-fault, steady-state measurements.

An explanation of sympathetic tripping with general conclusions and references are given at the end of the chapter.

### 9.1 Blinding

Blinding occurs when, for a short circuit on the line, the current measured in the substation is not large enough to trip the relay. This can happen when there is DG-units connected to the

line, [6], [98], [19], [8]. DG generally increase the fault current levels since they contribute to the fault current [99], [26], [16], [100]. However, depending on the location of the fault relative to the DG location, the fault current fed through the substation might decrease. As a result the substation relay can be blinded due to the fault current infeed from the DG. The phenomenon is also referred to as protection underreach by some authors, [17], [3]. [97] introduces a common feeding point, CFP, which is the point closest to the fault that is fed in parallel by the DG unit and the feeding network. CFP varies with the fault location, and is used for calculation of a blinding ratio. This ratio is an approximate measure on how strong the blinding problem will be, and a higher ratio means a more severe blinding problem. It is stated that the easiest way to avoid blinding is adjusting the overcurrent relay settings on the feeder with DG so that it picks up for a lower current value.

An analytical analysis on blinding of the line protection in the substation can be done based on the simplified equivalent scheme shown in Figure 9.1, for the pre-fault state. The line is represented by the lumped impedances  $Z_{l1}$ , for the line between the substation and the G-node, and  $Z_{l2}$ , for the line between the G-node and the feeder end. The not-constant cross section area of the feeder is taken into account.  $Z_{Fn}$  is the impedance of the high voltage feeding network and the substation transformer.  $Z_G$  includes the impedance of the generator and the generator transformer. The pre-fault load is estimated as described in Ch. 5.3.1.

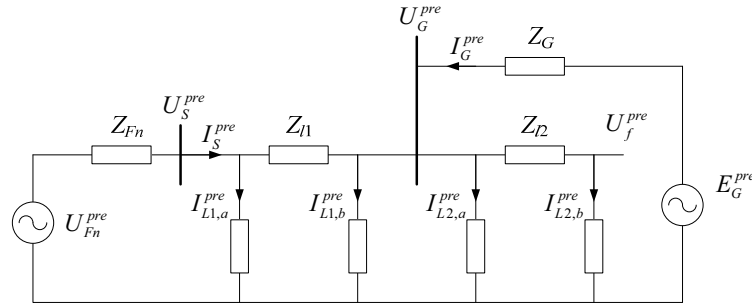


Figure 9.1: Simplified representation of the network in the pre-fault state, used for analytical analysis.

The voltage of the high voltage feeding network,  $U_{Fn}$ , is assumed to be a stiff voltage equal to 1.0 pu with angle  $0^\circ$  both in the pre-fault and faulted states ( $U_{Fn} = U_{Fn}^{pre}$ ).  $I_S^{pre}$  and  $U_S^{pre}$  are substation current and voltage in the pre-fault state, and are assumed known from measurements. The magnitude values of the pre-fault current fed from the DG-unit ( $I_G^{pre}$ ) and the voltage in the DG connection point ( $U_G^{pre}$ ) are assumed known from measurements, together with the phase angle between current and voltage. These are the same measurements that were available for both compensated distance estimate methods.  $U_f^{pre}$  is the pre-fault voltage in the fault location, and can be calculated from:

$$\begin{aligned} U_f^{pre} &= U_G^{pre} - Z_{l2} (I_S^{pre} - I_{L1,a}^{pre} - I_{L1,b}^{pre} + I_G^{pre} - I_{L2,a}^{pre}) \\ &= U_S^{pre} - Z_{l1} (I_S^{pre} - I_{L1,a}^{pre}) - Z_{l2} (I_S^{pre} - I_{L1,a}^{pre} - I_{L1,b}^{pre} + I_G^{pre} - I_{L2,a}^{pre}) \end{aligned} \quad (9.2)$$

The pre-fault voltage is included in the expression for the fault current, as seen in Ch. 9.1.1 and Ch. 9.1.2.

### 9.1.1 Analytical analysis of three-phase short circuit

With a three phase short circuit fault, there will not be any connection between the three sequence networks (positive, negative, zero), and the fault current can be found by studying

the positive sequence network alone. The positive sequence network for the feeder with a three-phase short circuit located after the DG connection point is shown in Figure 9.2. The feeding source and the DG-unit are both represented by a voltage source behind an impedance. According to [80], the machine can be represented by the transient internal emf behind the transient impedance during the transient period. The internal transient emf of the generator is unknown, and needs to be estimated. Loads are neglected, as explained initially in this chapter.

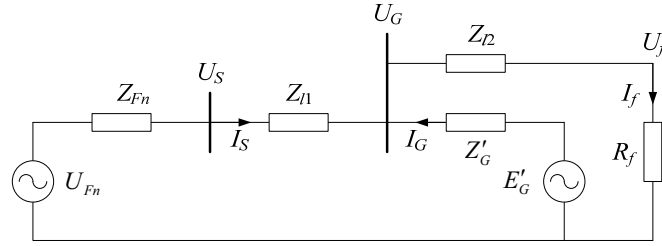


**Figure 9.2: Positive sequence network for analytical analysis of 3-phase short circuit**

The fault current can be expressed as a function of the equivalent impedance seen from the fault location,  $Z_{thf}$  and the pre-fault voltage at the fault location  $U_f^{pre}$  [77].

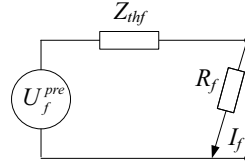


**Figure 9.3: Thevenin-equivalent seen from the fault location**

The fault current as shown in Figure 9.3 is given by (9.3). The thevenin impedance seen from the fault location is given by (9.4), and the pre-fault voltage is calculated from (9.2).

$$I_f = \frac{U_f^{pre}}{Z_{thf} + R_f} \quad (9.3)$$

$$Z_{thf} = Z_{l2} + \frac{Z'_G (Z_{Fn} + Z_{l1})}{Z'_G + Z_{Fn} + Z_{l1}} \quad (9.4)$$

The fault is fed by two sources; the feeding network through the substation and the DG-unit. Since the impact of loads during fault is neglected, the substation current equals the DG current in magnitude, but with opposite signs. Thus the fault current equals:

$$I_f = I_S + I_G \quad (9.5)$$

The relative size of the two currents depends on the sizes of the impedances  $Z_G$  and  $Z_{Fn} + Z_{l1}$ , and the difference between the feeding network voltage and the internal voltage of the generator. Starting from (9.5) and considering the positive sequence equivalent in Figure 9.2, the following expression is found for the fault current through the substation:

$$I_S = I_f - I_G = I_f - \frac{E'_G - U_G}{Z'_G} = I_f - \frac{E'_G - U_{Fn} + (Z_{Fn} + Z_{l1}) I_S}{Z'_G} \quad (9.6)$$

$$\Rightarrow I_S = \frac{U_{Fn} - E'_G}{Z'_G + Z_{Fn} + Z_{l1}} + \frac{Z'_G}{Z'_G + Z_{Fn} + Z_{l1}} \cdot I_f$$

The simple generator model assumes constant rotor flux linkages. The transient internal emf can be assumed to remain constant and equal to the pre-fault value in the transient state following a short circuit, and can be calculated from pre-fault DG-unit voltage and current. From this an expression for the first term in (9.6) can be obtained:

$$\begin{aligned}
 E'_G &= E'_G{}^{pre} = U_G{}^{pre} + Z'_G \cdot I_G{}^{pre} \\
 &= U_{Fn} - (Z_{Fn} + Z_{l1}) I_S{}^{pre} + Z_{l1} I_{L1,a}{}^{pre} + Z'_G \cdot I_G{}^{pre} \\
 &= U_{Fn} - (Z_{Fn} + Z_{l1} + Z'_G) I_S{}^{pre} + Z_{l1} I_{L1,a}{}^{pre} + Z'_G \cdot (I_{L1,a}{}^{pre} + I_{L1,b}{}^{pre} + I_{L2,a}{}^{pre} + I_{L2,b}{}^{pre}) \\
 \Rightarrow \frac{U_{Fn} - E'_G}{Z_{Fn} + Z_{l1} + Z'_G} &= I_S{}^{pre} - \frac{Z_{l1} I_{L1,a}{}^{pre} + Z'_G \cdot (I_{L1,a}{}^{pre} + I_{L1,b}{}^{pre} + I_{L2,a}{}^{pre} + I_{L2,b}{}^{pre})}{Z_{Fn} + Z_{l1} + Z'_G}
 \end{aligned} \quad (9.7)$$

Inserting the result from (9.7) into (9.6) gives the following expression for the substation current during fault:

$$I_S = I_S{}^{pre} - \frac{Z_{l1} I_{L1,a}{}^{pre} + Z'_G \cdot (I_{L1,a}{}^{pre} + I_{L1,b}{}^{pre} + I_{L2,a}{}^{pre} + I_{L2,b}{}^{pre})}{Z_{Fn} + Z_{l1} + Z'_G} + \frac{Z'_G}{Z'_G + Z_{Fn} + Z_{l1}} \cdot I_f \quad (9.8)$$

Plotting  $I_S$  as a function of  $Z_{l1}$  corresponds to moving the connection point of the DG unit when the fault location is unchanged. Figure 9.4 shows the substation short circuit current as a function of the connection point of the DG for two DG-ratings: 3 MW and 6 MW, both generating nominal power with zero reactive power. For comparison the simulated substation current without any DG-unit connected to the feeder is shown. In the simulations, the DG-unit can be connected 5, 10, 15, 20, 25 or 30 km from the substation. The point 0 km corresponds to the substation, and is not considered. The simulations are performed with the feeder at low load, since this is the case which results in the lowest current levels, and therefore represent worst case for blinding probability. The meaning of the plot legends are explained in Table 9.1. Simulated values are read 50 ms after fault inception. 1 pu current corresponds to high load for the feeder (6 MVA).

**Table 9.1: Explanation of plot legends**

Legend	Description
E	Estimated current using (9.8), with input $I_S{}^{pre}$ taken from simulation at low load
S	Simulated current with feeder at low load

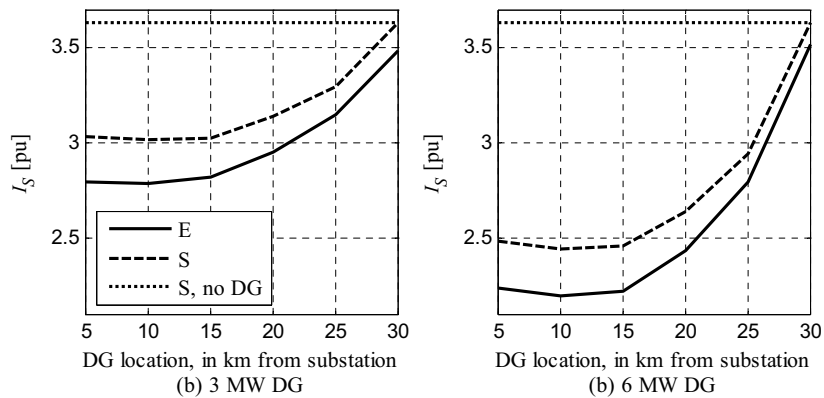


**Figure 9.4: The substation fault current  $I_S$  as a function of the DG connection point when the DG is generating (a) 3 MW and (b) 6 MW. With a 3-phase short circuit at the feeder end at low load**

There is good agreement between shapes of the curves with simulated and estimated substation fault currents, but the estimated currents are smaller than the simulated, as expected. This confirms that the estimated currents without load represent conservative estimates, since when studying blinding finding the smallest possible substation fault current is of interest. Figure 9.5 shows a comparison between the simulated short circuit current in the substation for low load (LL) and high load (HL). As before the current is plotted as a function of the DG-connection point. The DG is generating 3 MW, and the faults are three-phase short circuits at the feeder end.

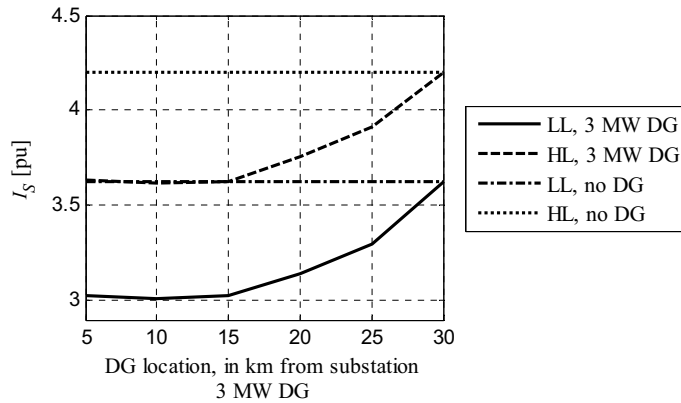


Figure 9.5: The substation fault current  $I_S$  as a function of the DG connection point when the DG is generating 3 MW. 3-phase short circuit at the feeder end at low load and high load.

It is seen that the short circuit currents are generally lowest at low load, and low load thus represents the worst case related to blinding. When the load level is increased the current curves are lifted and the overall current level is increased. An approximate way to include the load current can therefore be to add a constant current value to the estimated current at no-load.

The above plots show that the reduction in the short circuit current is largest when the DG is connected 5 to 15 km from the substation, and thus the probability of blinding is largest for these locations of the DG-unit. When the DG is connected at the end of the feeder there is no reduction of the short circuit current in the substation, which means that a DG-unit connected at the feeder end do not cause any blinding. It can be concluded that the location of the DG-unit is important for the probability of blinding of the overcurrent protection. The rating of a DG-unit and the level of generated power are also very important parameters. From the simulated results shown in Figure 9.4 it can be seen that the reduction of  $I_S$  due to the DG in the worst case are 16.9 % with a 3 MW DG and 32.7 % with a 6 MW DG. If the generator is generating less than nominal power in the pre-fault state, the contribution to the fault current and blinding becomes less. When analysing the blinding probability is should also be taken into consideration that generators with the same rating can have different short circuit capacities due to different reactance parameters.

An important parameter when studying the short circuit current is the feeder length. Figure 9.6 shows a comparison between the estimated and simulated substation current for a 60 km long feeder. The length of each line section is doubled as compared to the previous case, while other data are unchanged. The simulations are carried out at low load, and the DG-unit

can be located 10, 20, 30, 40, 50 or 60 km from the substation, generating nominal power of 3 MW.

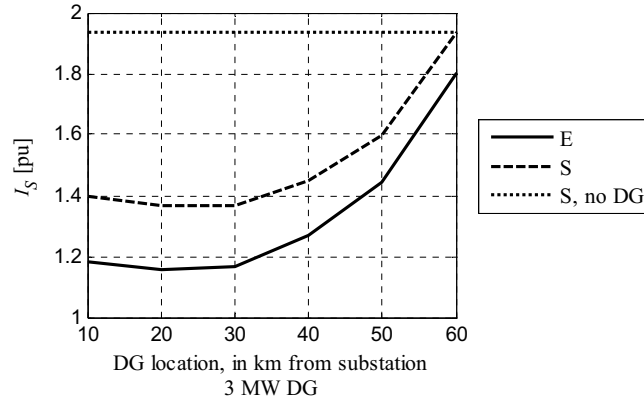


**Figure 9.6:** The substation fault current  $I_S$  as a function of the DG connection point when the DG is generating 3 MW. The feeder is 60 km long, and the fault is a 3-phase short circuit at the feeder end.

The short circuit current is generally reduced as the feeder length is increased. Without DG it is 3.6 pu for the 30 km feeder, and 1.9 pu for the 60 km feeder. The reduction of  $I_S$  due to the DG in the worst case is 29.5 %. The probability of blinding is increased for a longer feeder since the margin between short circuit and load current is decreased. Connecting DG to the network worsens this problem. For very long lines it might not be possible to use overcurrent protection even without DG.

Another parameter influencing the size of the short circuit current is the short circuit capacity available through the feeding substation transformer. If this short circuit capacity is decreased the relative impact from the DG is increased. This short circuit capacity is determined by the short circuit capacity of both the high voltage feeding network and the substation transformer. For the example network the transformer was found to be the most limiting factor.

### 9.1.2 Analytical analysis of two-phase short circuit

Two-phase short circuits cause smaller fault currents than three-phase short circuits. The smallest possible short circuit current occurs when there is a two-phase short circuit at the end of the feeder, and this case should be studied in relation to blinding. Figure 9.7 shows a three-phase representation of the feeder when there is a short circuit between phase *B* and *C*, at the feeder-end. As for three-phase short circuits, impact from loads during fault is neglected.

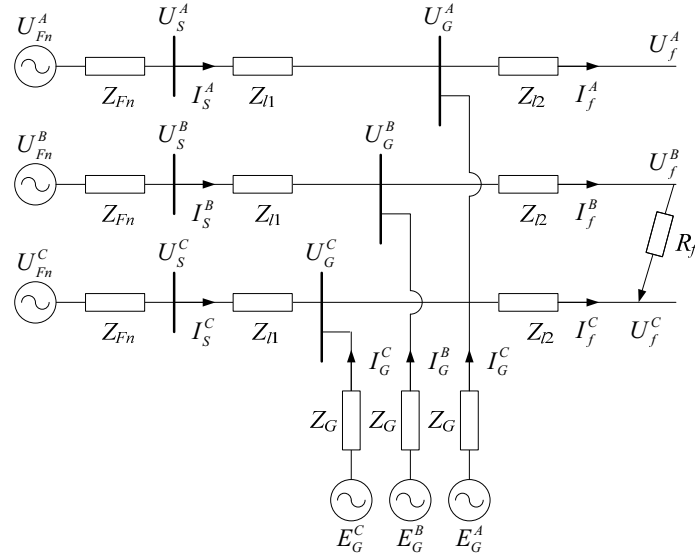


Figure 9.7: 3-phase representation of the feeder with a short circuit between phase B and C, at the feeder-end

The two-phase short circuit is an unsymmetrical fault, and when analysing such a fault it is useful to introduce the positive, negative and zero sequence transform.

$$\begin{bmatrix} I^A \\ I^B \\ I^C \end{bmatrix} = \begin{bmatrix} 1 & 1 & 1 \\ h^2 & h & 1 \\ h & h^2 & 1 \end{bmatrix} \cdot \begin{bmatrix} I^+ \\ I^- \\ I^0 \end{bmatrix}, \quad \begin{bmatrix} U^A \\ U^B \\ U^C \end{bmatrix} = \begin{bmatrix} 1 & 1 & 1 \\ h^2 & h & 1 \\ h & h^2 & 1 \end{bmatrix} \cdot \begin{bmatrix} U^+ \\ U^- \\ U^0 \end{bmatrix} \quad (9.9)$$

Where  $h = e^{j2\pi/3}$

Fault currents in phases B and C are equal, but opposite in direction, while the fault current in phase a is zero, as expressed in (9.10). The resulting positive, negative and zero sequence currents are given by (9.11)

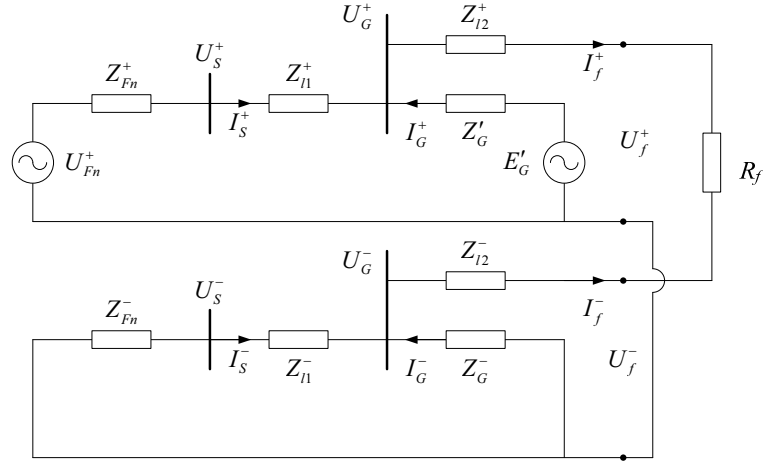
$$I_f^B = -I_f^C \quad (9.10)$$

$$I_f^A = 0$$

$$I_f^- = -I_f^+ \quad (9.11)$$

$$I_f^0 = 0$$

For a two-phase short circuit, fault currents flows in the positive and negative sequence systems, while the zero sequence system is not energized. The sequence network for the phase-to-phase fault is shown in Figure 9.8.


 Figure 9.8: Sequence network for short circuit between phase *B* and *C*

The fault location voltages in phase *B* and *C* are related as stated in (9.12). Expressing the fault current by the pre-fault voltage and thevenin equivalent impedance in the fault location, similar to (9.3), result in the expression given in (9.13) for the positive sequence fault current for a two-phase short circuit. The equivalent impedances are given in (9.14)

$$U_f^B - R_f I_f^B = U_f^C \quad (9.12)$$

$$I_f^+ = \frac{U_f^{pre}}{Z_{thf}^+ + Z_{thf}^- + R_f} \quad (9.13)$$

$$Z_{thf}^+ = Z_{l2} + \frac{Z_G' (Z_{Fn} + Z_{l1})}{Z_G' + Z_{Fn} + Z_{l1}}, \quad Z_{thf}^- = Z_{l2} + \frac{Z_G^- (Z_{Fn} + Z_{l1})}{Z_G^- + Z_{Fn} + Z_{l1}} \quad (9.14)$$

For non-rotating components the impedance values are equal in the positive and negative sequence systems.

The pre-fault voltage in the fault location is calculated the same way as for three-phase short circuits, expressed by (9.2). The overcurrent protection operates based on the substation current, and not the fault current. Thus expressions for the substation fault currents are required. Based on the sequence network in Figure 9.8 the expressions in (9.15) and (9.16) are found.

$$I_s^+ = I_f^+ - I_G^+ \quad (9.15)$$

$$\Rightarrow I_s^+ = I_s^{pre} - \frac{Z_{l1} I_{L1,a}^{pre} + Z_G' \cdot (I_{L1,a}^{pre} + I_{L1,b}^{pre} + I_{L2,a}^{pre} + I_{L2,b}^{pre})}{Z_{Fn} + Z_{l1} + Z_G'} + \frac{Z_G'}{Z_G' + Z_{Fn} + Z_{l1}} \cdot I_f^+$$

$$I_s^- = I_f^- - I_G^- \quad (9.16)$$

$$\Rightarrow I_s^- = \frac{Z_G^-}{Z_G^- + Z_{Fn} + Z_{l1}} \cdot I_f^- = -\frac{Z_G^-}{Z_G^- + Z_{Fn} + Z_{l1}} \cdot I_f^+$$

The currents are converted back to phase quantities using (9.17), inserting the expressions from (9.15) and (9.16).

$$I_s^B = h^2 I_s^+ + h I_s^- \quad (9.17)$$

$$I_s^C = h I_s^+ + h^2 I_s^-$$

As previously presented for the three-phase short circuit cases, the substation fault current is plotted as a function of the DG connection point for two-phase short circuits in Figure 9.9. The substation currents in (a) phase *B* and (b) phase *C* are shown. The DG is generating nominal power, 3 MW. Simulated (S) values obtained with the feeder at low load are compared with estimated (E) values using (9.17). The simulated substation currents without any DG-unit are also shown.

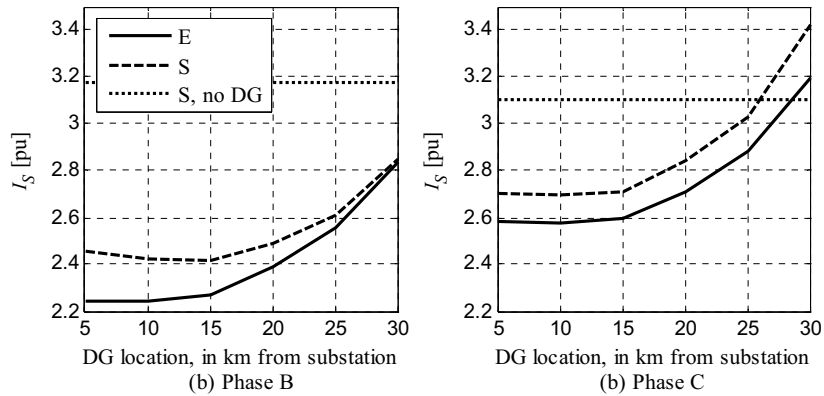


**Figure 9.9: The substation fault current  $I_S$  as a function of the DG connection point in (a) phase *B* and (b) phase *C*. The DG is generating 3 MW and low load. 2-phase short circuit between phase *B* and *C* at the feeder-end.**

The substation short circuit current is smaller in phase *B* than in phase *C* when there is DG connected to the feeder. The DG-unit has different parameters in the positive and negative sequence systems, and as seen from (9.15) and (9.16), the positive and negative sequence components of the substation currents are not equal. From this it follows that the phase currents also become unequal. The smallest substation fault current is seen in phase *B* when the DG is located 15 km from the substation. The current is then 2.4 pu, which is a reduction of 25.1 % compared to the case without any DG. The smallest current in phase *C* is 2.7 pu. Due to the difference between the currents there is a risk that a fault is only detected in one phase, and this should then be sufficient to trip the relay.

Figure 9.10 shows a comparison between estimated and simulated substation currents in (a) phase *B* and (b) phase *C* for with one DG-unit generating nominal power of 6 MW.

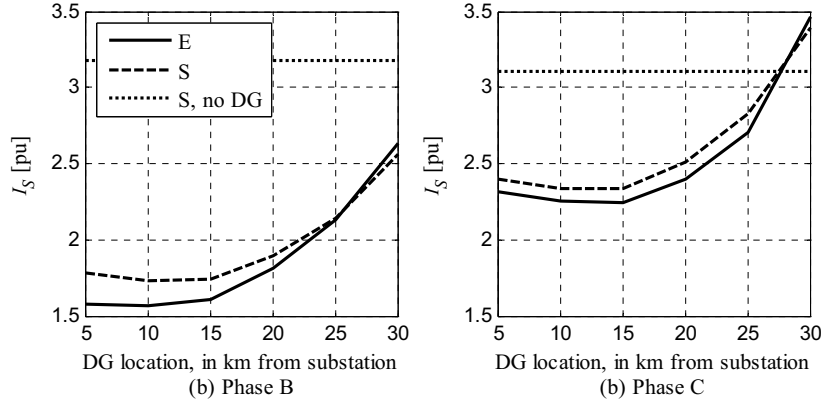


**Figure 9.10: The substation fault current  $I_S$  as a function of the DG connection point in (a) phase B and (b) phase C. The DG is generating 6 MW and low load. 2-phase short circuit between phase B and C at the feeder end.**

If the DG-rating is increased to 6 MW, the lowest substation current is 1.7 pu in phase B and 2.3 pu in phase C when the DG is connected 10-15 km from the substation.

Like for three-phase short circuits, the currents obtained from simulations on the feeder at low load are slightly higher than the currents obtained from estimation with loads neglected. Exceptions are the phase B current with a 3 MW DG-unit at the feeder-end, and for both phase B and C with a 6 MW DG-unit at the feeder-end. Still, conservative estimates of the substation fault current are obtained for most cases, and it can be concluded that the simple analytical model can be used for studying the blinding probability also for two-phase short circuits.

A general conclusion is that a DG-unit causes a reduction of the fault current seen by the substation overcurrent relay. It might be necessary to adjust the relay settings so that it trips for a lower current when a DG is connected to the network, depending of the rating of the DG. Small units have negligible impact, and new acceptable settings can be found for moderate DG-levels. The margins between highest load current and lowest short circuit current decrease as the DG-level increase. Blinding problems arise first on longer feeders with relatively small short circuit currents, as the minimum short circuit current might be small already before the connection of the DG. A further discussion is provided in Ch. 10.6.

## 9.2 Sympathetic tripping

The other phenomenon which may occur when using overcurrent relays for protection of distribution feeders is sympathetic tripping. Sympathetic tripping occurs when the overcurrent relay trips because of a fault on a neighbouring feeder connected to the same substation transformer [99], [6], [17], [19], [25]. The DG-unit feeds current to the fault on the neighboring feeder, and this current may become large enough to trip the relay on the feeder with DG. Hence the relay trips “in sympathy with” the faulted neighbour feeder. This is not a desired operation of the relay, since it should only trip for faults on its own feeder. An easy solution to the problem would be to use directional overcurrent protection. This is not standard today, as it is more expensive than the non-directional relays. [101] states that the sympathetic tripping problem in many cases can be avoided by using inverse-time characteristics in the non-directional overcurrent relays instead of the commonly used

definite-time characteristics, [2]. Figure 9.11 shows a case with a fault on a neighbouring feeder.

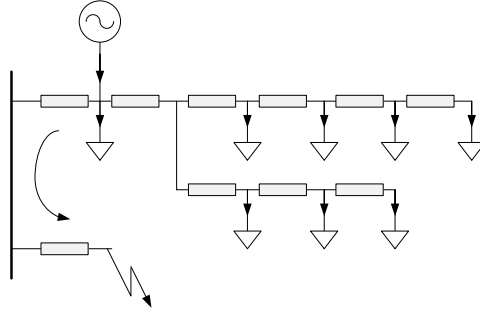


Figure 9.11: Illustration of fault on a neighbouring feeder. The DG is feeding current to the fault via the substation.

Figure 9.12 show simulated substation currents on the feeder with DG, when there is a three phase short circuit at the neighbour feeder, 5 km from the substation. The DG-unit is also located 5 km from the substation, on the non-faulted feeder. Results are shown with three DG-ratings, 3 MW, 6 MW and 7.5 MW.

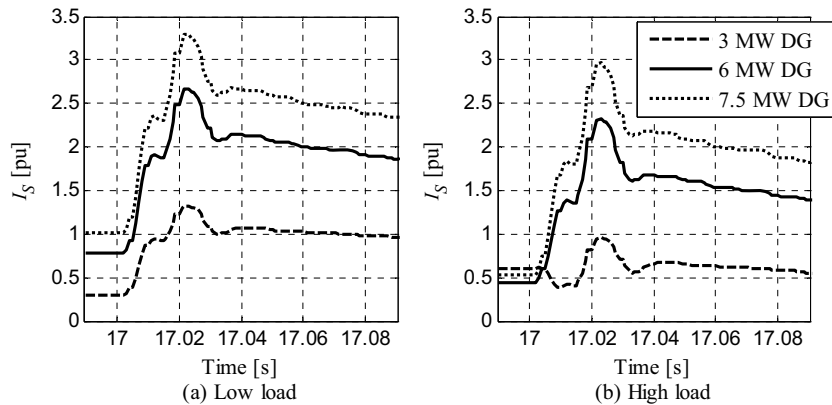


Figure 9.12: Simulated substation current ( $I_s$ ) with three-phase short circuit on a neighbouring feeder for (a) low load and (b) high-load. DG-ratings are 3 MW, 6 MW or 7.5 MW.

The highest currents due to fault on a neighbour feeder occur at low load, and thus the probability for sympathetic tripping is largest during low load. The probability is increased when the DG-rating is increased. Current values read 50 ms after the three-phase short circuit occurred on the neighbour feeder are shown in Table 9.2.

Table 9.2 Simulated substation current read 50 ms after three-phase short circuit on neighbour feeder.

DG rating [MW]	Substation current $I_s$ [pu], 50 ms after fault inception	
	Low load	High load
3	2.59	2.10
6	2.07	1.62
7.5	1.05	0.66

If a non-directional overcurrent relay is used, the setting may need to be adjusted so that the relay trips for a higher current than without DG to avoid sympathetic tripping. This means that opposite actions are required in order to prevent blinding and sympathetic tripping, and a compromise solution has to be found, [8].

## 10 DISCUSSION

This chapter discusses some of the results presented in previous chapters.

### 10.1 Conventional distance-to-fault estimation

In Ch. 4 the impact of various parameters on the distance estimate obtained by use of conventional distance relays have been investigated. Emphasis was on finding which parameters impacts most on the accuracy and on quantifying the errors in the estimates. The results found are discussed here.

For short circuit faults the fault impedance generally corresponds to the resistance of an arc. To avoid impact from this resistance, the distance to the fault is estimated from the reactance rather than the total impedance seen by the relay. With remote infeed to the fault from a DG, the fault impedance may appear to have a reactive component, as seen from the substation relay. This can be explained by considering the simplified feeder shown in Figure 10.1.

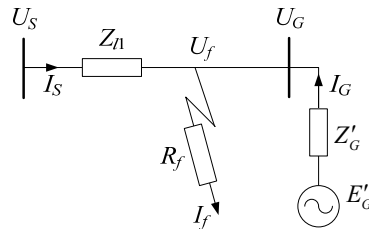


**Figure 10.1: Simplified feeder with remote infeed from DG-unit and fault through a resistance, with a 3-phase short circuit.**

The impedance seen by the substation relay is:

$$\frac{U_s}{I_s} = \frac{Z_n I_s + (I_s + I_G) R_f}{I_s} = Z_n + R_f + \frac{I_G}{I_s} R_f \quad (10.1)$$

If  $I_G$  is in phase with  $I_s$ , the last term in (10.1) will be purely resistive (a constant times  $R_f$ ). If they are not in phase the last term will have a reactive component. Due to this the fault resistance may have an impact on the distance estimated from the reactance, but it will anyway be less than if the distance was estimated from the impedance. This is confirmed by Figure 4.4.

The impact of load on the distance estimate accuracy on a feeder without DG was studied using the feeder model in Figure 10.2.

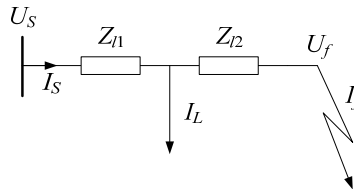


**Figure 10.2: Simplified feeder with a load tapping, with a 3-phase short circuit.**

The impedance seen by the substation relay can be expressed by:

$$\frac{U_s}{I_s} = \frac{Z_{l1}I_s + Z_{l2}(I_s - I_L)}{I_s} = (Z_{l1} + Z_{l2}) - Z_{l2} \frac{I_L}{I_s} \quad (10.2)$$

The last term represents the distance estimate error, and the negative sign shows that the error due to the load current is negative. A larger  $I_L$  gives a larger error, and Figure 4.5 showed that errors were largest in the high load cases. Three different distributions of loads along the feeder were tested, with results shown in Ch. 4.3.2. It was found that concentrating the loads close to the substation lead to the largest errors. Moving the load closer to the substation corresponds to increasing  $Z_{l2}$  in Figure 10.2, and thus increasing the last term of (10.2). This is in accordance with the simulation results.

Most of the presented cases were for a feeder with one DG-unit. It was found that the DG-unit only impacts on the distance estimate if the fault is located either after the DG connection point or if the fault is located on a side branch before the DG connection point. The DG only impacts if the substation current and DG-current have a common path to the fault location. A simplified feeder model with one DG-unit and a fault located after the DG connection point is shown in Figure 10.3.

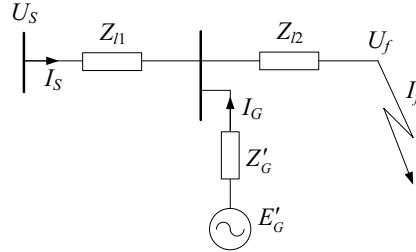


**Figure 10.3: Simplified feeder with fault located after DG connection point, with a 3-phase short circuit.**

The impedance seen by the substation relay can in this case be expressed by:

$$\frac{U_s}{I_s} = \frac{Z_{l1}I_s + Z_{l2}(I_s + I_G)}{I_s} = (Z_{l1} + Z_{l2}) + Z_{l2} \frac{I_G}{I_s} \quad (10.3)$$

The equation is quite similar to the equation for the load impact, (10.2). The last term is the error, and has a positive sign. Thus the DG current has opposite impact than the load current. It will generally impact more on the distance estimate than a load of equal rating. The DG responds to a short circuit with a current higher than the normal operating current, while for a static load the current may be held constant or is reduced during a disturbance, depending on the severity. The result is that the impact from the DG is reduced by the impact from the load. The largest errors therefore occur when the feeder is at low load, and becomes even larger if the loads are concentrated close to the feeder end. This is opposite to the case for a feeder without DG. The error due to the DG increases with the distance from the DG to the fault location (corresponds to an increase of  $Z_{l2}$ ). The largest error occurs when the DG is connected close to the substation and the fault is at the end of the feeder. It is also obvious that increasing the DG-rating leads to an increase of the error (corresponds to an increase of  $I_G$ ).

Decreasing the short circuit capacity of the feeding source by decreasing the substation transformer rating leads to larger estimate errors, because the short circuit capacity of the DG relative to the feeding source become larger. Increasing the feeder length also leads to increased distance estimate errors (corresponds to increasing  $Z_{l2}$ ). Two-phase short circuits were found to generally cause a bit larger errors than three-phase short circuits. This can be

explained by looking at simplified expressions for the generator fault currents. Referring to Appendix B, the following equations are valid for three-phase and two-phase short circuits at the generator terminals, for three-phase short circuits:

$$I'_{G,3-ph} \approx \frac{E'_{G,q}}{X'_{G,d}} \quad (10.4)$$

For two-phase short circuits:

$$I'_{G,2-ph} \approx \frac{\sqrt{3} \cdot E'_{G,q}}{X'_{G,d} + \sqrt{X''_{G,d} X''_{G,q}}} \quad (10.5)$$

The fault resistance is here assumed to be zero. The positive sequence impedance of the generator is equal to the transient d-axis reactance, and the negative sequence impedance is as given by (5.54). The two-phase short circuit current becomes larger than the three-phase current because of the  $\sqrt{3}$  in the numerator and  $\sqrt{X''_{G,d} X''_{G,q}}$  is one tenth of  $X'_{G,d}$ , with the generator data used in this thesis. The result is that the short circuit current from the DG is larger for two-phase than for three-phase short circuits, and thus the distance estimate errors due to the DG becomes largest for two-phase short circuits.

Summarized, the worst case is a two-phase short circuit at the feeder end when there is a DG-unit connected close to the substation and the feeder is at low load.

In addition to the factors discussed here, there might be errors due to inaccuracies in measurements and line parameters. This has not been treated in this work.

## **10.2 Short circuit representation of the synchronous generator**

A very simple model has been chosen for representing the DG-unit during fault in the analytical calculations. The model is only taking the transient short circuit current into account, which is somewhere in between the maximum short circuit current and the steady-state current. In reality the short circuit response of a synchronous machine consists of a subtransient, a transient and a synchronous current component. There is a sliding transition between the three stages, and the duration of each stage is described by a set of time constants. One set of time-constants is used for describing the open circuit behaviour and another set for describing the short circuit behaviour. The short circuit time constants are generally smaller than the open circuit time constants. In addition there is a time constant describing the decrease of the dc-current component. The short circuit response with the short circuit currents of the three stages and the corresponding time constants are shown in Figure 10.4.

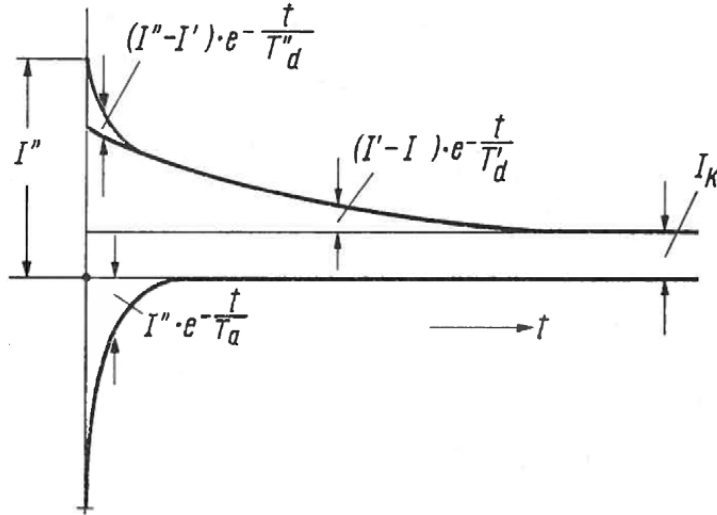


Figure 10.4: Components of the decaying short circuit current of a synchronous machine, [102].

$I'', I', I$  in Figure 10.4 are the subtransient, transient and synchronous short circuit current components

The short circuit time constants of the different stages depend on the impedance from the generator terminal to the fault location. As the fault is moved away from the terminals, the short circuit time constants increase towards the value of the open circuit time-constant. For a short circuit far away from the generator the two sets of time constants become equal, and it can be observed that the short circuit current curve flattens out. The short circuit transient d-axis time constants are given for two-phase short circuits in (10.6) and three-phase short circuits in (10.7), [102].

$$T'_{d,2\phi} \approx \frac{X'_{G,d} + X_{G,-} + 2 \cdot Z_{net}}{X_{G,d} + X_{G,-} + 2 \cdot Z_{net}} \cdot T'_{do} \quad (10.6)$$

$$T'_{d,3\phi} \approx \frac{X'_{Gd} + Z_{net}}{X_{Gd} + Z_{net}} \cdot T'_{do} \quad (10.7)$$

$Z_{net}$  is the equivalent network impedance between the DG connection point and the fault location

In the simple model used in this work this is not taken into account, since the same model is used in all cases, independently of the distance from the generator to the fault location.

When the fault is not at the generator terminal, the impedance of the network between the terminal and the fault location has to be taken into account when calculating the short circuit current. Since the network impedance from the terminal to the fault location in principle is unknown, it is not convenient to use this impedance when calculating the short circuit current. As a solution to take into account that the fault is not at the terminals, the voltage in the DG-connection point is subtracted from the internal emf, as shown in (5.48) and (5.52). The voltage in the DG-connection point during fault is not measured, so it has to be estimated

using the simple analytical feeder model. The changes in the time-constants as a function of the fault location have not been considered.

It is common in many text books to consider only the case with a short circuit at the generator terminals, and to assume that the generator was unloaded prior to the fault. This simplifies the expression for the short circuit current, since only d-axis components are present, and all internal emfs (subtransient, transient and synchronous) are equal to the pre-fault terminal voltage. One common expression for the DG-current is (for a round-rotor machine) [28].

$$i_G = i_{G,d} = U_G^{pre} \left( \frac{1}{X_{G,d}} + \left( \frac{1}{X'_{G,d}} - \frac{1}{X_{G,d}} \right) e^{-\frac{t}{T'_d}} + \left( \frac{1}{X''_{G,d}} - \frac{1}{X'_{G,d}} \right) e^{-\frac{t}{T''_d}} \right) \cos(\omega t + \lambda) - U_G^{pre} \left( \frac{1}{X''_{G,d}} \right) e^{-\frac{t}{T''_d}} \cos(\lambda) \quad (10.8)$$

When the machine is loaded, the short circuit current also has a q-axis component. The internal emf has a d-axis component, and the internal emfs of the three stages are not equal to each other. The short circuit current of a loaded machine may be larger or smaller than for a unloaded machine, depending on the power factor the generator was operating at prior to the fault. The model used in this work takes the pre-fault loading of the machine into account, by considering both d- and q- axis transient current components.

### 10.3 Distance estimates with compensation

The results found in Ch. 7 are discussed further here.

#### 10.3.1 Feeder without DG

Distance estimate results after compensation of errors due to DG and loads were shown in Ch. 7. Initially, results for a feeder without DG were shown. There is generally overcompensation of the impact from the load, resulting in positive errors.

Comparisons between three different distributions of the load along the feeder were shown in Ch. 7.2.2. The load was either evenly distributed (L-N), or all load were either connected 5 km from the substation (L-1) or at the feeder-end (L-6). The purpose was to investigate how sensitive the compensation is to knowing the actual load distribution. The results were most accurate for distribution L-N, which is the case where the lumped feeder model is closest to the simulation model. There is a small positive error after compensation for this case, and this means that the assumed load between the substation and the fault location is larger than the real load, resulting in a small overcompensation of the impact from the load in this case. For load distribution L-1 the assumed load before the fault location is smaller than the real load, and the impact from load is under-compensated. Still, the error is reduced as compared to the uncompensated case. With load distribution L-6 the compensation causes an increase of the distance estimate error. In this case the assumed load before the fault location is larger than the real load, and the impact from the load is overcompensated.

Distribution L-6 represents an extreme case, and the compensation is done without any knowledge about the load distribution. In a real case some information about the typical load distribution is expected to be known, and thus the result with compensation could be improved. One solution could be not to have two equal loads on each side of the line impedance, but instead divide the load closer to the real known distribution. If it for instance is known that most of the load is normally connected close to the substation, a larger amount of the total load should be allocated to the shunt load connected in the substation than to the

load at the feeder end. The influence of the load distribution is discussed in [12] for a network without DG. Here it is stated that the load distribution has little impact on the accuracy of the fault location. In the paper, loads are calculated in all nodes of the network, so it is a more complex model than the lumped model proposed here.

The compensation has also been applied with three different voltage dependency factors for the active power load, and results were shown in Ch. 7.2.3. The errors after compensation are smallest when the load is independent of the voltage (NP=0), and highest with the largest voltage dependency factor (NP=2). The compensation is based on assuming half of the load connected in the substation and the second half connected at the feeder-end. The load at the feeder-end becomes short circuited, and has therefore no influence on the compensation result. The change of the load during fault depends on the voltage across the load, as described by (3.1) for a static load characteristic. The voltage in the substation is higher than in the real load points along the feeder, and the estimated load during fault becomes too large. This results in overcompensation of the load impact and positive errors after compensation. This effect becomes larger for a higher voltage dependency factor. If the load is independent of voltage the result of the compensation is less sensitive to the voltage in the point where the load is located.

### 10.3.2 Feeder with one DG-unit

Distance estimate errors after compensation with faults at the feeder-end and varying locations of the DG-unit were shown in Ch. 7.3.1. Compensation method 1 with estimation of the DG-current give more accurate results for two-phase than three-phase short circuits. The reason for this is not obvious, but is related to the simple representation of the synchronous generator chosen for the analytical model. For a two-phase short circuit both positive and negative sequence voltages and currents are present. The negative sequence short circuit current is constant throughout the subtransient, transient and steady state stages. Due to this the estimation of the negative sequence current is expected to give more correct results independent of the fault location and the time for sampling than the positive sequence current.

Compensation method 2 generally give more accurate distance estimates than method 1, which is as expected since DG current magnitudes are obtained from the simulation instead of being estimated. It is a great advantage if measurements from the DG-unit during fault are available for use in the fault localization.

To explain the results, the expression for the compensated impedance to the fault location is studied. The expression valid for a fault located after the  $G$ -node on the main branch is given by (6.22) in Ch. 6.2.3. The reactance part of the compensated impedance is given in (10.9), and the delta symbol is removed since the fault is assumed to be a three-phase short circuit.

$$X_C = \text{Im}(Z_C) = X_{l1} + \text{Im}\left(\frac{U_G}{I_S - I_{L1,a} - I_{L1,b} + I_G - k_F I_{L2,a}}\right) = X_{l1} + X_{l2-f} \quad (10.9)$$

Where  $X_{l2-f}$  is the estimated reactance from the  $G$ -node to the fault location

Figure 10.5 (a) shows separate plots of the first and second term in (10.9) and (b) shows the sum of the reactance as functions of the DG location. Numbers 1 and 2 means results with compensation method 1 and 2, respectively.

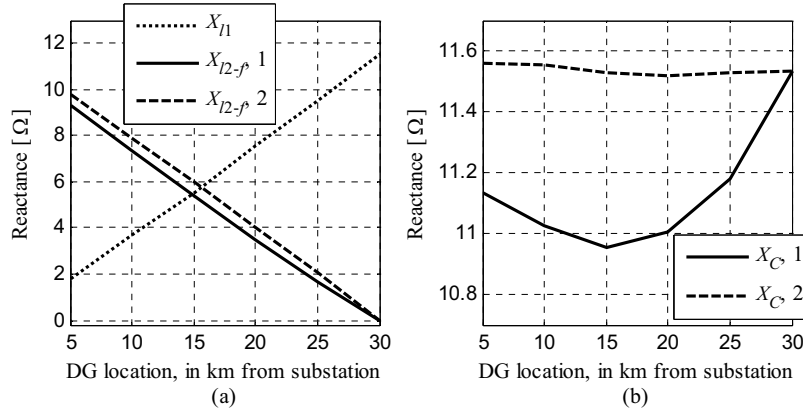


**Figure 10.5:** Plot of the reactance part of the compensated impedance to the fault location at low load. 3-phase short circuits at the feeder end while the DG connection point is varied

The first term ( $X_{l1}$ ) is the line reactance between the substation and the DG location, and is common for the two methods. This reactance has an approximately linear increase as the DG connection point is moved from 5 to 30 km. The second term ( $X_{l2-f}$ ) is the estimated reactance seen from the  $G$ -node to the fault location. This term depends on the DG voltage and current, and is different for the two methods. The reactance is decreasing approximately linearly as the DG is moved from 5 to 30 km, and this is due to a decrease of the DG voltage and increase of the DG current as the distance from the DG to the fault location becomes shorter. The reactance becomes zero when the DG is connected at 30 km, since the DG voltage becomes equal to the fault location voltage which is approximately zero. Method 2 result in a bit larger estimated reactance values for all DG-locations, except 30 km. The reason for this is that the estimated DG currents in method 1 are larger than the simulated currents, as was shown in Ch. 6.2.5.

The difference between the curves for method 1 and 2 is not very large, but still large enough to result in different shapes for the two curves showing the sum of the reactances ( $Z_C$ ). The curve obtained using method 1 has a minimum when the DG is connected at 15 km, while the curve obtained using method 2 is almost a constant value independent of the location of the DG. Figure 10.5 (b) shows that the maximum difference between the methods is 0.57  $\Omega$ , occurring with the DG at 15 km. With a line reactance of 0.40  $\Omega/\text{km}$ , the difference in reactance corresponds to a difference of 1.43 km. This same difference can be found between the results for method 1 and 2 in Figure 7.9 (a) when the DG is located 15 km from the substation. It can be concluded that the distance estimation is sensitive to the accuracy of the DG current estimation. Even though the error in the estimated reactance to the fault location is small, the distance estimate error becomes considerable in km because the line reactance per unit of length is very small.

Results after compensation with the DG-unit located 5 km from the substation and with varying locations were shown in Ch. 4.4.2. Plots of (10.9) as a function of the fault location are shown in Figure 10.6. The plots correspond to those shown in Figure 10.5. Figure (a) shows separate plots of the first term ( $X_{l1}$ ) and the second term ( $X_{l2-f}$ ) obtained using method 1 and 2, respectively. Plot (b) shows the resulting estimated reactance to the fault location.

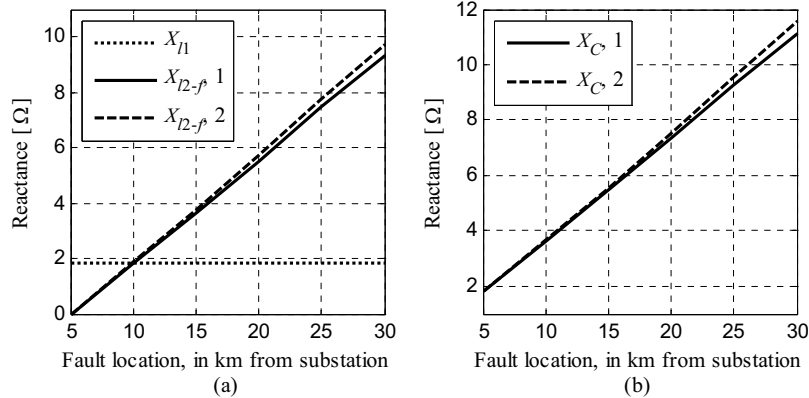


**Figure 10.6:** Plot of the reactance part of the compensated impedance to the fault location at low load. 3-phase short circuits at varying locations while the DG is connected at 5 km

Since the DG location is set, the reactance between the substation and the  $G$ -node is constant. The line reactance between the  $G$ -node and the fault location is increasing approximately linearly as the fault location is moved towards the feeder end. The  $G$ -node voltage is increased, while both the substation current and DG current are decreased, as the fault location is moved away from the  $G$ -node, and this cause the increase of the reactance  $X_{I2-f}$ . The estimated reactance using method 1 is a bit smaller than the one obtained using method 2, because the estimated DG current is a bit larger than the simulated, as shown in Ch. 6.2.5. The difference between the estimated and simulated DG currents is not increasing as the fault is moved towards the feeder, but since the total current is decreased the inaccuracy in the current estimation has a larger effect on the resultant reactance. The smaller reactance value corresponds to a shorter estimated distance to the fault location, as seen in Figure 7.11 and Figure 7.12. Relatively small inaccuracies in the estimated reactance result in significant errors in the estimated distance to the fault. The non-linearity of the distance estimate error curves are due to the varying cross sections of the lines.

#### 10.4 Finding the correct faulted branch

The results found in Ch. 8 for decision of the correct faulted branch are discussed in this subchapter.

##### 10.4.1 Comparison between measured and estimated DG-voltage

A method of comparing the measured DG-node voltage amplitude with the estimated in order to decide the correct faulted branch was introduced in Ch. 8.1. When the correct fault location is assumed, the differences between estimated and simulated voltages are generally a bit larger in the cases when the DG is connected in point 6 than when it is connected in point 3. In order to estimate the DG voltage when the fault is between the substation and the DG or on the side branch, some simplifications are necessary. For instance is the load of the section after the fault location assumed to be connected in the fault location or in the branching node, respectively. Only the reactance part of the line impedance from the fault location or the branching node to the DG is taken into account when estimating the DG current during fault. The estimation errors caused by these simplifications increase as the distance from the fault location or from the branching node to the DG connection point are increased. For three-phase short circuits there is negligible difference between the results for low load and high load. For

two-phase short circuits only results for high load are shown. Generally the results are quite similar for the two load levels, but the differences between estimated and simulated voltages have been found to be slightly smaller when the correct faulted branch is assumed at low load.

For all of the tested cases the difference between the estimated and simulated voltage magnitude values is close to zero when the correct fault location has been assumed. When the wrong fault location is assumed, the difference is significantly larger for all of the tested cases with three-phase short circuits, and for most of the two-phase short circuit cases. However, for two-phase short circuits 15 km from the substation the voltage differences in one of the phases are seen to be only slightly larger when the wrong fault location was assumed. Still, by considering the voltage difference in both of the involved phases the correct faulted branch can be found also for these faults.

It can be concluded that the difference between estimated and simulated DG voltage magnitudes can be utilized to determine the correct faulted branch for all of the tested cases. With more laterals it becomes more difficult to distinguish between possible locations. The method will not be useful when the fault is on a lateral branch after the DG-node, e.g if the DG is located in point 1 in Figure 8.1.

The possibility for utilizing the difference between the estimated and simulated DG current magnitudes in order to find the faulted branch was also investigated. It was found that in most cases the smallest difference corresponded to the correct faulted branch, but not in all cases. Therefore it was concluded that the difference in voltage is a more reliable parameter than the difference in current for this purpose.

### 10.5 Distance calculation from DG measurements

In Ch. 8.2 a method of estimating the distance from the DG-unit to the fault for comparing with the estimated distance from the substation was described. The distance estimate errors in these cases are in principle due to the same side infeed effect as previously seen in the distance estimates obtained from the substation. In those cases the DG-unit was the source of the side infeed. When estimating the distance from the DG connection point, the substation instead acts as the source of side infeed. Since the substation has a much larger short circuit capacity than the DG, the distance estimate errors become much larger than the case was for the estimates obtained from the substation. The side infeed from the substation can be explained by looking at the simplified feeder equivalent in Figure 10.7, where loads are neglected and the DG is assumed to be connected in point 3.

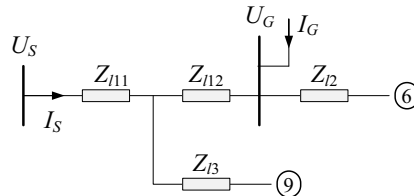


Figure 10.7: Simplified feeder equivalent where impedance is measured from the DG connection point, with the substation as a source of side infeed.

- $Z_{l11}$  is the impedance between the substation and the branching node
- $Z_{l12}$  is the impedance between the branching node and the G-node
- $Z_{l2}$  is the impedance between the G-node and the end of the main branch
- $Z_{l3}$  is the impedance between the branching node and the end of the side branch

The estimated impedance from the DG to the fault location if the fault is located in point 6 is given by (10.10), and by (10.11) if the fault is located in point 9 on the side branch.

$$Z_{G-f} \approx Z_{l2} + \frac{I_S}{I_G} Z_{l2} \quad (10.10)$$

$$Z_{G-f} \approx Z_{l12} + Z_{l3} + \frac{I_S}{I_G} Z_{l3} \quad (10.11)$$

The error in the distance estimate is proportional to the  $I_S$  divided by  $I_G$ , which is expected to be a number greater than one due to the larger available short circuit capacity from the substation. An increase of the DG rating is expected to lead to a reduction of the error. The error is also proportional to the line impedance of the common path of the two currents to the fault location, and this means that the error is increasing as the fault is moved towards the end of one of the branches.

A similar solution has been suggested in [66]. In that paper an example network with four DG units is presented, and faults are applied at various locations. Each DG have a relay measuring the distance to the fault, but the correct distances are only measured in the units who have an own particular path to the fault. If the DG has a path parallel to the main source or other DG units, the measured distances become too large. For the example network there is always one of the units who sees the correct distance to the fault, and it is suggested by the authors to use the measured distances from the DG together with information about the network topology to find the correct fault location. However, the paper contains little details regarding necessary measurements and communication.

It can be concluded that the method investigated in this chapter is not a very suitable method for deciding the correct faulted branch, since it only works for some specific cases.

### 10.6 Overcurrent protection and blinding

This subchapter provides some further discussion and quantification of the blinding probability treated in Ch. 9. As stated, an overcurrent relay protecting a MV-feeder should be set to operate for a current larger than the maximum load current and smaller than the smallest short circuit current, with some additional margins. Referring to (9.1),  $I_{load,max}$  equals 1 pu with the chosen per unit system.  $I_{short\ circuit,min}$  is the smallest possible short circuit current, and corresponds to a two-phase short circuit at the feeder-end at low load. For a feeder without DG this fault current is equal to 3.1 pu. Inserting these numbers into the equation, the following limits are obtained for possible setting of the substation overcurrent relay

$$1.5\ pu \leq I_{relay,pick-up} \leq 2.5\ pu \quad (10.12)$$

For this discussion a setting of  $I_{relay,pick-up} = 2.0$  pu is chosen.

The smallest short circuit current with a three-phase short circuit at the feeder end occurred when the DG was located 10 km from the substation. With a 3 MW DG the current was 3.01 pu, while with a 6 MW DG the current was 2.44. Thus with the chosen relay setting the faults would be detected in both cases.

Two-phase short circuits give lower short circuit currents. The lowest currents with DG rating and location are shown in Table 10.1.

**Table 10.1 Smallest occurring 2-phase short circuit currents in the substation with corresponding rating and location of the DG-unit**

DG rating [MW]	DG location [km]	Phase B current [pu]	Phase C current [pu]
3	15, 10	2.42	2.69
6	10, 15	1.73	2.34

The only case where the relay will fail to detect the short circuit is in phase B with a 6 MW DG connected 10 km from the substation. However, the fault will still be detected in phase C for this case.

For the feeder with double length results were only shown for three-phase faults. The smallest short circuit current without DG was 1.93 pu. The setting  $I_{relay,pickup} = 1.5$  pu can be chosen in this case. The short circuit current with a 3 MW DG connected 10 km from the substation and fault at the feeder-end was only 1.36 pu. This is smaller than the pick-up current, and the fault will not be detected by the relay. The result would be even worse with a two-phase short circuit.

Summarised, a DG connected to a distribution feeder causes a reduction of the fault current seen by the substation overcurrent relay if the current from the DG and from the substation has a common path to the fault location. For the example feeder problems with detecting two-phase short circuits may occur when the DG-rating is equal to or higher than the high load level of the feeder, 6 MVA. Thus blinding will occur only with relatively high DG-ratings, because the initial margin between highest load current and lowest short circuit current is large. For the feeder with double length and same load level the situation is very different. The margin between highest load current and lowest short circuit current without DG is much smaller for this feeder. With a 3 MW DG-unit connected 10 km from the substation, even a three-phase short circuit will remain undetected. Protection blinding is thus more probable on a feeder where the margin for the relay setting is small already before any DG is connected. Adjustments of the relay settings may be necessary when connecting a DG to a distribution feeder, depending on the network characteristics, DG-rating and location. For a long feeder it might be necessary to split the feeder into parts and install more relays in series along the radial.

Sympathetic tripping due to fault on a neighbour feeder was discussed briefly in Ch. 9.2. With the pickup setting of 2 pu for the relay, sympathetic tripping will occur with 6 MW and 7.5 MW DG at low load and with 7.5 MW DG at high load. With a 3 MW DG sympathetic tripping will not occur. To avoid tripping with a 6 MW DG the pickup setting can be adjusted up, but that will increase the probability for blinding.

An alternative approach for restoring the original relay coordination after connection of DG to the network has been introduced by [103]. This is achieved through implementation of a fault current limiter to locally limit the DG fault current.

## 11 CONCLUSION

The amount of DG is growing, changing the network conditions both in normal operation and during fault occurrences. The topic of this work has been short circuit fault conditions. An increased focus on reducing the durations of outages is seen among the DSOs, motivated by raised penalty costs for non-delivered energy. A more automated fault handling at distribution level is considered to reduce outage times, and one step in this direction is to have general fault localization methods. Two methods for locating three-phase and two-phase short circuit faults in networks with DG are presented in this thesis, intended for use in a general distribution network.

The possibilities of being allowed to carry out short circuit tests in a real distribution network are very small. An alternative is to install equipment in a network and measure on a long term basis, and wait for a fault to occur. This has been done in the project this work is a part of, but unfortunately no short circuit data were gathered. In any case real data would be obtained for only a few fault cases in a specific network. Performing simulations allows for varying of network parameters and for gathering fault data from a large variety of cases. In this work emphasis has been put on modelling of DG and load, and all fault data were gathered through PSCAD simulations. In addition to the simulation model, a simplified model with lumped parameters has been introduced. A lumped model is used for analytical calculations of voltages and currents on the feeder, with simulated values from the measuring points as inputs. Having fault data from both a real network and simulations for a few of the cases would have been desirable.

Overcurrent relays is the most common short circuit protection for distribution network feeders. When a short circuit occurs, the DG-unit will feed current to the fault so that the total fault current is increased, but the fault current through the substation is reduced compared to the case without DG. If the reduction is large, there is a risk that the short circuit is not detected by the substation relay. This is commonly referred to as protection blinding. The reduction of the substation current during fault is highly dependent on the location of the DG-unit. Simulations show that for faults at the end of the example feeder, the current is smallest when the DG is located between the substation and the middle of the feeder. A DG connected at the end of the feeder has no impact on the substation fault current. The substation current has also been calculated analytically using the lumped feeder model and neglecting loads, and the agreement with the simulated current at low load was good. The lumped model can thus be a useful tool for making rough estimations of the minimum short circuit current when a new DG-unit is connected to a network, and for checking if the relay settings need to be adjusted. Another possible problem may occur if the DG feeds current to a fault on a neighbouring feeder. If the current from the DG is large enough to trip the relay on its "own" feeder this is referred to as sympathetic tripping. This is undesirable, since only the relay on the faulted feeder should trip. While the probability for blinding may require that the relay is set to trip for a lower current, the probability for sympathetic tripping may require that the relay is set to trip for a higher current. Compromise solutions between the two can be found for moderate DG-levels. Else, it may be necessary to use directional overcurrent or distance protection.

Conventional distance-to-fault estimation in a distribution network means utilizing measurements from one terminal, the substation, and converting the "measured" impedance to a corresponding distance to the fault location. The impacts of various parameters on the estimated distance have been investigated. A DG feeds current to the fault and causes a

positive error in the estimate, while loads draw current and cause a negative error. Usually the impact from the DG is larger than that from the load since the load currents remain constant or decrease during fault due to the voltage drop. Because of the opposite impacts from DG and load, the maximum distance estimate error is found at low load. For a feeder without DG the errors are largest at high load and if the loads are concentrated close to the substation.

Most cases have been presented for a feeder with one DG-unit. It is found that the DG-unit only impacts on the distance estimate if the fault is located either after the DG connection point or on a side branch before the DG connection point. The error due to the DG increase with the distance from the DG to the fault location, and the largest errors are therefore found when the DG is connected close to the substation and the fault is at the feeder-end. For the same reason a longer feeder means larger maximum error. It is also obvious that increasing the DG-rating leads to an increase of the error. A decrease of the available short circuit capacity from the substation also leads to larger errors, since the relative fault current contribution from the DG is increased. Two-phase short circuits are found to generally cause a bit larger errors than the corresponding three-phase short circuits. Some results for a feeder with three DG-units have also been presented. Having three units connected in different points result in errors almost as large as the worst case with one unit connected in the point closest to the substation. When studying a feeder with more than one DG, the impact from the unit closest to the substation should be emphasized. This is important to take into consideration if for instance DG-units are to be merged together in an aggregated model. The results from the conventional distance estimation prove that there is a need for methods to improve the accuracy of the estimates in a network with intermediate loads and DG. For a real feeder, measurement errors and inaccurate line data may contribute to errors additional to those included in the investigation.

As given in (4.2), the distance to a fault location is calculated by dividing the impedance seen from the substation by the line impedance per unit of length. To avoid impact from fault resistance, distance is estimated from the reactance part of the impedance. A possible difficulty can be to handle the varying cross-sections of a typical distribution feeder. The line impedance per length is then not linear, as it generally is for transmission lines. The varying cross-sections have been handled using the algorithm shown in Appendix C, Figure C.3. However, when decreasing the line cross-section the reactance is fairly constant while the resistance is increasing. Thus, when calculating distance from reactance the line reactance per length unit could be assumed constant for simplification. Figure 4.3 showed that the relation between line length and reactance is approximately linear for the example feeder.

The lumped feeder model can be used for compensation of the impact from loads on a feeder without DG. It was found that this compensation works best if the loads are evenly distributed along the feeder, and also if the load have a current characteristics that is little dependent on the voltage. The results for other characteristics or distributions of the loads can be improved by splitting the line into more sections.

The two presented methods for compensation of errors due to both load and DG are advancements of the conventional distance estimation based on impedance. In method 1 DG-quantities are estimated during fault, while in method 2 measured DG-quantities are instead utilized. Both methods utilize pre-fault measurements from the DG and substation for estimation of the distribution of loads between the section(s) before and after the DG-unit(s) in the lumped feeder model. The measured DG-quantities are voltage and current magnitudes, and the phase angle (power factor). The phasor angle of the DG voltage relative to the

substation voltage is estimated analytically from the lumped feeder model. Voltage and current are measured in the substation.

The methods are not meant for protection, only for fault localization, and the calculation of the compensated distance estimate can be performed after the circuit breaker has been opened. To have a high communication speed is therefore not critical. The fact that only magnitude values are required to be communicated from the DG-unit(s) allows for a simpler communication solution and less accurate time-synchronization with the substation measurement than if phasors were required.

For estimation of the DG current during fault in method 1, a very simple representation consisting of the transient internal emf behind the transient reactance is chosen. For two-phase faults the negative sequence equivalent consisting of only a reactance is included. For three-phase short circuits the estimated DG currents are generally larger than the simulated. This results in overcompensation of the impact from the DG, resulting in negative errors in the distance estimates after compensation. The differences between estimated and simulated DG currents are generally much smaller for two-phase than for three-phase faults. Therefore the largest distance estimate errors with compensation are always found for three-phase faults. The accuracy of the compensated distance estimate is dependent on the DG location. With a three-phase short circuit at the feeder end, the lowest accuracy is obtained when the DG is located at the middle of the feeder. The error is then -1.9 km, which still is an improvement compared to worst case without compensation. The estimates obtained at high load are only slightly more accurate than for low load, despite of the larger difference without compensation. If the DG location is fixed and the fault location is varied, the accuracy of the compensated estimate is decreasing as the fault is moved away from the substation, and the lowest accuracy is obtained when the fault is at the feeder-end. The model used for calculating the DG current is not taking the subtransient and synchronous short circuit current components and corresponding time constants into consideration. More accurate results could be obtained by using a more complex model, but the choice of model should be based on a compromise between obtaining high accuracy and having a simple model requiring few input parameters.

In method 2, measurements of the DG-current and voltage magnitudes and the phase angle during fault are utilized. The DG-voltage phasor angle relative to the substation voltage is estimated from the lumped feeder model, like in the pre-fault state. The distance estimates are very accurate for all fault cases, so to have measurements from the DG during fault is very advantageous.

Since distribution feeders generally have tree structure, one estimated distance to a fault location may correspond to locations on several different branches. Methods to distinguish between the possible locations are therefore required. If measurements are available from the DG-unit during fault, like in method 2, they can be utilized for finding the faulted branch. A method of comparing the measured (simulated) DG voltage with the one estimated using the lumped feeder model is presented. The procedure is to assume a fault location and estimate the DG voltage from the corresponding lumped feeder model. This is repeated for all possible fault locations, and the location with the smallest difference between the estimated and measured voltage is assumed to be the correct fault location. For the example feeder with only one side branch the correct fault location could be found for all fault cases. With more laterals or several DG-units connected to the feeder, it might be more difficult to distinguish between possible locations, and this should be further investigated.

### **11.1 Further work**

- A limitation of this work is the simple feeder model used for simulation of fault cases. In reality, distribution feeders generally have more complex and extended structures. The next step for further development of the fault location algorithm would be to test them with fault data from real distribution networks.
- Fault location method 1 with estimation of the DG-current during fault can possibly be improved. More details can be included in the modelling of the synchronous generator, and this could be further investigated.
- Tests of the compensation methods through simulation of fault cases with higher fault resistances would be very valuable. The assumption that the fault resistance has negligible impact on the distance estimated from reactance should be investigated for more cases. The last term of (5.6) could be included in the compensation methods to account for possible impact from fault resistance.
- Single-phase faults (earth faults) are much more common than two-phase and three-phase short circuits. Corresponding methods for location of earth faults would be very useful, and development of such methods would be a natural next step for further work.

## 12 REFERENCES

1. Gjerde, O. and A. Petterteig, *Det norske distribusjonsnettet*. 2006, SINTEF Energiforskning AS: Trondheim, Norway. p. 45.
2. CIRED, *Final report of CIRED Working Group WG03 Fault management. Fault management in electrical distribution systems*, M. Lethonen and D. Cortinas, Editors. 1999, International Conference on Electricity Distribution: France. p. 41.
3. Dugan, R.C. and T.E. McDermott, *Distributed Generation*. IEEE Industry Applications Magazine, 2002. **8**(2): p. 19-25.
4. Jensen, T., (red.), *Beregning av potensial for små kraftverk i Norge*. 2004, NVE: Oslo, Norway.
5. Petterteig, A., et al., *Tekniske retningslinjer for tilknytning av produksjonsheter, med maksimum aktiv effektproduksjon mindre enn 10 MW, til distribusjonsnettet*. 2006, SINTEF Energy Research: Trondheim, Norway. p. 56.
6. Häger, M., F. Sollerkvist, and M.H.J. Bollen. *The impact of distributed energy resources on distribution-system protection*. in *NORDAC*. 2006. Stockholm, Sweden.
7. Bjerkan, E. and G. Svendsen. *Efficiency Improvement by systematic investments in remote control systems*. in *Nordic Distribution and Asset Management Conference, NORDAC*. 2006. Stockholm, Sweden.
8. Mäki, K., *Novel Methods for Assessing the Protection Impacts of Distributed Generation in Distribution Network Planning*. 2007, Tampere University of Technology: Tampere. p. 69.
9. IEEE, *Guide for Determining Fault Location on AC Transmission and Distribution Lines*. 2005, IEEE Power System Relaying Committee. p. 36.
10. Saha, M.M., J. Izykowski, and E. Rosolowski, *Fault Location on Power Networks*. 2010, London: Springer.
11. Horowitz, S.H. and A.G. Phadke, *Power System Relaying*. Second ed. 1995, New York, Chichester: John Wiley & Sons, Ltd.
12. Senger, E.C., et al., *Automated Fault Location System for Primary Distribution Networks*. IEEE Transactions on Power Delivery, 2005. **20**(2): p. 1332-1340.
13. Lethonen, M., S. Pettisalo, and J.-H. Etula. *Calculational fault location for electrical distribution networks*. in *Third International Conference on Power System Monitoring and Control*. 1991. London.
14. Tenschert, W. *Fault location using fault distance measurement of digital relays*. in *CIRED*. 1993. Birmingham.
15. Andrieu, C., et al., *Fault detection, analysis and diagnostics in high-DG distribution systems, CRISP report D.1.4*. 2004. p. 38.
16. Geidl, M., *Protection of Power Systems with Distributed. Generation: State of the Art*. 2005, Swiss Federal Institute of Technology. p. 35.
17. Kauhaniemi, K. and L. Kumpulainen, *Impact of distributed generation on the protection of distribution networks*, in *Electric Energy T&D Magazine*. 2005, Jaguar Media Inc.: Terrebonne, Canada. p. 161-163.
18. IEEE, *Impact of Distributed Resources on Distribution Relay Protection*. 2004, IEEE, Power System Relay Committee. p. 24.
19. Jäntti, S., *Connection of Distributed Energy Generation Units in the Distribution Network and Grid*, in *CODGUNet Final Report*. 2003, CODGUNet project group. p. 62.
20. Barker, P.P. and R.W. De Mello. *Determining the impact of distributed generation on power systems. I. Radial distribution systems*. in *IEEE Power Engineering Society Summer Meeting*. 2000. Seattle.

21. Penkov, D., et al., *Simulation Study of DG Effect on Fault location Methods in Distribution Networks*, in *ELMA*. 2005: Sofia, Bulgaria. p. 6.
22. Freitas, W., et al., *Comparative analysis between synchronous and induction machines for distributed generation applications*. IEEE Transactions on Power Systems, 2006. **21**(1): p. 301-311.
23. IEEE, *IEEE Application Guide for IEEE Std 1547, IEEE Standard for Interconnecting Distributed Resources with Electric Power Systems*. 2009. p. 1-207.
24. Kumpulainen, L., et al. *New requirements for system protection caused by distributed generation*. in *International Conference on Electricity Distribution, CIRED*. 2005. Turin, Italy.
25. Walling, R.A., et al., *Summary of Distributed Resources Impact on Power Delivery Systems*. IEEE Transactions on Power Delivery, 2008. **23**(3): p. 1636-1644.
26. Kaur, G. and M.Y. Vaziri. *Effects of distributed generation (DG) interconnections on protection of distribution feeders*. in *IEEE Power Engineering Society General Meeting*. 2006. Montreal, Canada.
27. Guillot, M., et al. *Protection of embedded generation connected to a distribution network and loss of mains detection*. in *International Conference and Exhibition on Electricity Distribution, CIRED*. 2001. Amsterdam, The Netherlands.
28. Jenkins, N., et al., *Embedded Generation*. 2000, London: The institution of Electrical Engineers.
29. Mugggerud, H.K., *Detektering av Øydrift i Distribusjonsnett*, in *Electric Power Engineering*. 2007, NTNU: Trondheim. p. 169.
30. Girgis, A. and S. Brahma. *Effect of distributed generation on protective device coordination in distribution system*. in *Large Engineering Systems Conference on Power Engineering, LESCOPE*. 2001. Halifax.
31. Chilvers, I., N. Jenkins, and P. Crossley, *Distance relaying of 11 kV circuits to increase the installed capacity of distributed generation*. IEE Proceedings - Generation, Transmission and Distribution, 2005. **152**(1): p. 40-46.
32. Li, H.Y., P.A. Crossley, and N. Jenkins. *Transient Directional Protection for Distribution Feeders with Embedded Generations*. in *Power Systems Computation Conference (PSCC)*. 2002. Sevilla, Spain.
33. Diaz, H., R. and M. Lopez, T. *Fault location techniques for electrical distribution networks: A literature survey*. in *Fifth IASTED International Conference on Power and Energy Systems*. 2005. Benalmeda, Spain.
34. Saha, M.M., et al., *Review of fault location techniques for distribution systems*, in *Power Systems and Communications Infrastructures for the future*. 2002: Beijing. p. 6.
35. Short, T., K. Jinsang, and C. Melhorn. *Update on distribution system fault location technologies and effectiveness*. in *CIRED*. 2009. Prague.
36. Lethonen, M., *Novel techniques for fault location in distribution networks*, in *Power Quality and Supply Reliability Conference*. 2008: Pärnu, Estonia. p. 6.
37. Vähämäki, O., et al. *A new technique for short-circuit fault location in distribution networks*. in *NORDAC*. 2006. Stockholm, Sweden.
38. Balcerek, P., M. Fulczyk, and J. Izykowski. *ATP-EMTP investigation of digital algorithms for synchronisation of two-end measurements in transmission line fault location*. in *European EMTP-ATP Conference*. 2007. Leon, Spain.
39. Girgis, A.A. and C.M. Fallon, *Fault location techniques for radial and loop transmission systems using digital fault recorded data*. IEEE Transactions on Power Delivery, 1992. **7**(4): p. 1936-1945.

40. Takagi, T., et al., *Development of a new type fault locator using the one-terminal voltage and current data*. IEEE Transactions on Power Apparatus and Systems, 1982(8): p. 2892-2898.
41. Girgis, A.A., C.M. Fallon, and D.L. Lubkeman, *A fault location technique for rural distribution feeders*. IEEE Transactions on Industry Applications, 1993. **29**(6): p. 1170-1175.
42. Eriksson, L., M.M. Saha, and G.D. Rockefeller, *An Accurate Fault Locator with Compensation for Apparent Reactance in the Fault Resistance Resulting from Remote-end Infeed*. IEEE Transactions on Power Apparatus and Systems, 1985. **104**(2): p. 423-436.
43. Lethonen, M., et al. *An automated fault management model for distribution networks*. in *International Conference on Energy Management and Power Delivery*. 1998. Singapore.
44. Lampley, G.C., *Fault Detection and Location on Electrical Distribution System*, in *IEEE Rural Electric Power Conference*. 2002: Colorado Springs. p. 5.
45. Lethonen, M., et al., *An Advanced Model for Automatic Fault Management in Distribution Networks*, in *IEEE Power Engineering Society Winter Meeting*. 2000. p. 1900-1904.
46. Pettisalo, S., et al., *A new application for fault location in distribution networks*, in *TESLA-report*. 2000, VTT: Vaasa, Finland. p. 13.
47. Lehtonen, M., et al. *New techniques for fault location in distribution networks*. in *NORDAC*. 2006. Stockholm, Sweden.
48. Saha, M.M., E. Rosolowski, and J. Izykowski. *ATP-EMTP Investigation for Fault Location in Medium Voltage Networks*. in *International Conference on Power Systems Transients, IPST*. 2005. Montreal, Canada.
49. Das, R., *Determining the Location of Faults in Distribution Systems*. 1998, University of Saskatchewan: Saskatchewan, Canada. p. 206.
50. Resener, M., et al. *Optimized Fault Location Formulation for Unbalanced Distribution Feeders Considering Load Variation*. in *16 th Power Systems Computation Conference, PSCC*. 2008. Glasgow, Scotland.
51. Kim, J., M.E. Baran, and G.C. Lampley, *Estimation of Fault Location on Distribution Feeders using PQ Monitoring Data*, in *IEEE Power Engineering Society General Meeting*. 2007: Tampa, USA. p. 1-4.
52. Pereira, R.A.F., et al., *Improved Fault Location on Distribution Feeders Based on Matching During-Fault Voltage Sags*. IEEE Transactions on Power Delivery, 2009. **24**(2): p. 852-862.
53. Choi, M.-S., et al., *A Direct Three-Phase Circuit Analysis-Based Fault Location for Line-to-Line Fault*. IEEE Transactions on Power Delivery, 2007. **22**(4): p. 2541-2547.
54. Hizam, H., et al. *Fault Section Identification and Location On A Distribution Feeder Using Travelling Waves*. in *IEEE Power Engineering Society Summer Meeting*. 2002. Chicago, USA.
55. Elhaffar, A. and M. Lethonen. *Multi-End Travelling Wave Fault Location based on Current Travelling Waves*. in *Power Systems Computation Conference*. 2008. Glasgow, Scotland.
56. Redfern, M.A., S.C. Terry, and F.V.P. Robinson. *The Application of Distribution System Current Transformers for High Frequency Transient Based Protection*. in *8th IEE International Conference on Developments in Power System Protection*. 2004.
57. Borghetti, A., et al., *Continuous-Wavelet Transform for Fault Location in Distribution Power Networks: Definition of Mother Wavelets Inferred from Fault Originated Transients*. IEEE Transactions on Power Systems, 2008. **23**(2): p. 9.

58. Bo, Z.Q., G. Weller, and M.A. Redfern, *Accurate fault location technique for distribution system using fault-generated high-frequency transient voltage signals*. IEE Proceedings - Generation, Transmission and Distribution, 1999. **146**(1): p. 73-79.
59. Magnago, F.H. and A. Abur, *Fault location using wavelets*. IEEE Transactions on Power Delivery, 1998. **13**(4): p. 6.
60. Davidson, E.M., et al., *Applying multi-agent system technology in practice: automated management and analysis of SCADA and digital fault recorder data*. IEEE Transactions on Power Systems, 2006. **21**(2): p. 559-567.
61. Mora-Florez, J., V. Barra-Nuez, and G. Carillo-Cacedo, *Fault Location in Power Distribution Systems Using a Learning Algorithm for Multivariable Data Analysis*. IEEE Transactions on Power Delivery, 2007. **22**(3): p. 7.
62. Thukaram, D., H.P. Khincha, and H.P. Vijaynarasimha, *Artificial neural network and support vector machine approach for locating faults in radial distribution systems*. IEEE Transactions on Power Delivery, 2005. **20**(2): p. 710-721.
63. Martins, L.S., et al. *A Network Distribution Power System Fault Location Based on Neural Eigenvalue Algorithm*. in *IEEE Power Tech Conference*. 2003. Bologna, Italy.
64. Järventausta, P., P. Verho, and J. Partanen, *Using fuzzy sets to model the uncertainty in the fault location process of distribution networks*. IEEE Transactions on Power Delivery, 1994. **9**(2).
65. Zhang, X., et al., *A Distribution Short Circuit Analysis Approach using Hybrid Compensation Method*. IEEE Transactions on Power Systems, 1995. **10**(4): p. 2053-2059.
66. Penkov, D., et al. *DG impact on three phase fault location. DG use for fault location purposes?* in *International Conference on Future Power Systems*. 2005. Netherlands.
67. Aggarwal, R.K., Y. Aslan, and A.T. Johns, *An interactive approach to fault location on overhead distribution lines with load taps*, in *Sixth International Conference on Developments in Power System Protection*. 1997: Nottingham. p. 184-187.
68. Perera, N., A.D. Rajapakse, and A.M. Gole. *Wavelet-based relay agent for isolating fault sections in distribution grids with distributed generators*. in *IEE International Conference on AC and DC Power Transmission*. 2006. London, UK.
69. Brahma, S.M. and A.A. Girgis, *Development of adaptive protection scheme for distribution systems with high penetration of distributed generation*. IEEE Transactions on Power Delivery, 2004. **19**(1): p. 56-63.
70. X., Z., et al. *Multi-agents based protection for distributed generation systems*. in *IEEE International Conference on Electric Utility Deregulation, Restructuring and Power Technologies*. 2004.
71. Zhu, J., D.L. Lubkeman, and A.A. Girgis, *Automated Fault Location and Diagnosis on Electric Power Distribution Feeders*. IEEE Transactions on Power Delivery, 1997. **12**(2): p. 801-809.
72. Xyngi, I., M. Popov, and L. van der Sluis. *Hybrid Transient Based Protection Scheme for Distribution Grids Supplied with Distributed Generation*. in *EEUG Meeting, European EMTP-ATP Conference*. 2009. Delft, Netherlands.
73. Javadian, S.A.M., M.R. Haghifam, and N. Rezaei. *A Fault Location and Protection Scheme for Distribution Systems in presence of DG Using MLP Neural Networks*. in *IEEE Power & Energy Society General Meeting*. 2009. Calgary, Canada.
74. PSCAD, *PSCAD Manual*. 2006, Manitoba HVDC Research Centre Inc.: Manitoba, Canada.
75. Øksnes, T., *E-mail regarding short circuit capacities in substations in the network of the utility NTE*, J. Marvik and A. Petterteig, Editors. 2006.
76. NVE, *Forskrift om leveringskvalitet*, OED, Editor. 2004: Oslo, Norway.

77. Faanes, H.H. and K.J. Olsen, *TET 4115 Elektriske kraftsystemer*. 2005, Trondheim, Norway: Department of Electric Power Engineering, NTNU. 279.
78. Srinivasan, K. and A. St-Jaques, *A new fault location algorithm for radial transmission lines with loads*. IEEE Transactions on Power Delivery, 1989. **4**(3).
79. IEEE, *Load representation for dynamic performance analysis (of power systems). Task Force on Load Representation for Dynamic Performance*. IEEE Transactions on Power Systems, 1993. **8**(2): p. 472-482.
80. Kundur, P., *Power System Stability and Control*. 1994, New York, USA: McGraw-Hill.
81. IEEE, *Computer Models for Representation of Digital-Based Excitation Systems. A paper prepared by the Digital Excitation Task Force of the Equipment Working Group*. IEEE Transactions on Energy Conversion, 1996. **11**(3): p. 9.
82. IEEE, *IEEE Std 421.5 Recommended Practice for Excitation System Models for Power System Stability Studies*. 2005, IEEE: New York, USA.
83. Statnett, *FIKS, Funksjonskrav i kraftsystemet*, S. SF, Editor. 2008. p. 77.
84. Elmore, W.A., *Protective relaying Theory and Application*. 2 ed. 2004, New York: Markel Dekker. 410.
85. Phadke, A.G., M. Ibrahim, and T. Hlibka, *Fundamental Basis for Distance Relaying with Symmetrical Components*. IEEE Transactions on Power Apparatus and Systems, 1977. **96**(2): p. 635.
86. Ziegler, G., *Numerical Distance Protection, Principles and Applications*. Second ed. 2006, Erlangen: Publicis Corporate Publishing. 378.
87. Warrington, A.R.V.C., *Reactance Relays Negligibly Affected by Arc Impedance*. Electrical World, 1931. **98**(No. 12): p. 502-505.
88. Terzija, V.V., R.M. Ciric, and H. Nouri, *Fault currents calculation using hybrid compensation method and new arc resistance formula*, in *39 th International Universities Power Engineering Conference, UPEC*. 2004: Bristol, UK. p. 49-54.
89. Salim, R.H., et al., *Extended Fault-Location Formulation for Power Distribution Systems*. IEEE Transactions on Power Delivery, 2009. **24**(2): p. 9.
90. Machowski, J., J.W. Bialek, and J.R. Bumby, *Power System Dynamics and Stability*. 1997, Chichester, England: John Wiley & Sons Ltd.
91. Grainger, J.J. and W.D. Stevenson, *Power System Analysis*. 1994: McGraw-Hill, Inc. 784.
92. Morales-Espana, G., J. Mora-Florez, and H. Vargas-Torres, *Elimination of Multiple Estimation for Fault Location in Radial Power Systems by Using Fundamental Single-End Measurements*. IEEE Transactions on Power Delivery, 2009. **24**(3): p. 1382-1389.
93. Bjerkan, E. *Efficient fault management using remote fault indicators*. in *20th International Conference and Exhibition on Electricity Distribution, CIRED*. 2009. Prague, Czech Republic.
94. Cong, D.-p., et al., *Optimization of fault indicators placement with dispersed generation insertion*, in *IEEE Power Engineering Society General Meeting, 2005*. 2005: San Francisco. p. 8.
95. Gers, J.M. and E.J. Holmes, *Protection of electricity distribution networks*. 2 ed. 2004, London, UK: The Institution of Electrical Engineers. 342.
96. IEEE, *Distribution Line Protection Practices. Industry Survey Results*. 2002, IEEE, Power System Relaying Committee. p. 29.
97. Mäki, K., S. Repo, and P. Järventausta, *Protection Coordination to meet the Requirements of Blinding Problems caused by Distributed Generation*. WSEAS Transactions on Circuits and Systems, 2005. **4**(7): p. 674-683.

98. Baran, M. and I. El-Markabi, *Adaptive over current protection for distribution feeders with distributed generators*. in *IEEE PES Power Systems Conference and Exposition*. 2004. New York, USA.
99. Hadjsaid, N., J.-F. Canard, and F. Dumas, *Dispersed generation impact on distribution networks*. *IEEE Computer Applications in Power*, 1999. **12**(2): p. 22-28.
100. Nuroglu, F.M. and A.B. Arsoy, *Voltage profile and short circuit analysis in distribution systems with DG*, in *IEEE Canada Electric Power Conference*. 2008: Vancouver. p. 1-5.
101. Mäki, K., S. Repo, and P. Järventausta, *Protection requirement graph for interconnection of distributed generation on distribution level*. *International Journal of Global Energy Issues (IJGEI)*, 2007. **28**(1): p. 47-64.
102. Roeper, R., *Short-Circuit Currents in Three-phase networks*. 1972, Berlin, Munich: Siemens Aktiengesellschaft, Pitman Publishing. 98.
103. El-Khattam, W. and T.S. Sidhu, *Restoration of Directional Overcurrent Relay Coordination in Distributed Generation Systems Utilizing Fault Current Limiter*. *IEEE Transactions on Power Delivery*, 2008. **23**(2): p. 576-585.
104. Henriksen, T. and A. Petterteig, *Detection of earth fault in a medium voltage distribution network*, in *International Conference on Power System Transients (IPST)*. 2007: Lyon, France. p. 6.

## A Appendix A – Feeder modelling

This appendix provides additional details to the main chapters of the thesis.

### A.1 Voltage profile on feeder with DG

As described in Ch. 3.1.2, the position of the substation tap changer is 0.98 for low load, and 0.922 for high load. Figure A.1 shows the simulated steady-state voltages on the on the main branch as a function of distance from the substation with the chosen tap positions. The voltage profile without any DG-unit connected is plotted together with the profile when a 3 MW DG-unit is connected 15 km from the substation.

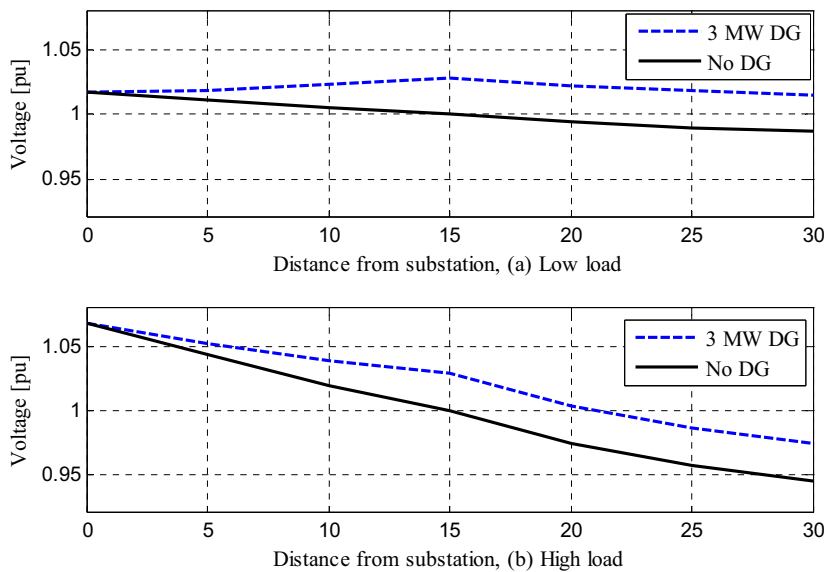


Figure A.1: Stationary voltage distribution on MV-feeder for low load and high load.

Without DG connected to the feeder the voltage is decreasing gradually from the substation towards the feeder-end. At high load it may be necessary to adjust the voltage in the substation up to avoid too low voltage at the feeder-end. With DG on the feeder the voltage profile is changed, and the overall voltage level are increased. At low load the voltage is increasing from the substation towards the DG connection point, and it is important to be aware of this and to avoid too high voltages on the feeder [22], [100], [25].

### A.2 Line modeling

The PSCAD coupled pi-equivalent line model is shown in Figure A.2. A pi-section is suited for representing a very short overhead transmission line or underground cable. The R and L elements are represented in matrix format and thereby provide coupling between the three phases. There is also both a mutual capacitance C and a capacitance to ground  $C_m$  at each end [74]. Parameters used in the line modelling are explained in Table A.1.

**Table A.1: Explanation of line modelling parameters**

Line	
$X_{aa}, X_{bb}, X_{cc}$	self inductance
$X_{ab}, X_{bc}, X_{ca}$	mutual inductance
$R_a$	conductor ac-resistance, positive sequence resistance
$R_e$	equivalent resistance in earth
$D_g$	equivalent distance to earth
$\rho$	specific resistivity in earth
$f$	frequency
$D$	distance between conductors
$D_m$	geometric mean distance between conductors
$g$	geometric mean radius of conductor
$r$	conductor radius
$h$	conductor height above earth
$R^+$	positive sequence resistance
$X^+$	positive sequence inductive reactance
$X_C^+$	Positive sequence capacitive reactance
$R^0$	zero sequence resistance
$X^0$	zero sequence inductive reactance
$X_C^0$	Zero sequence capacitive reactance
$\mu_0$	permeability ( $\mu_0 = 4\pi \cdot 10^{-7}$ )
$C_d$	Operating capacitance, $C_d = C_g + 3C_{ab}$
$C_g$	Capacitance between phase and ground
$C_{ab}$	Capacitance between two phases

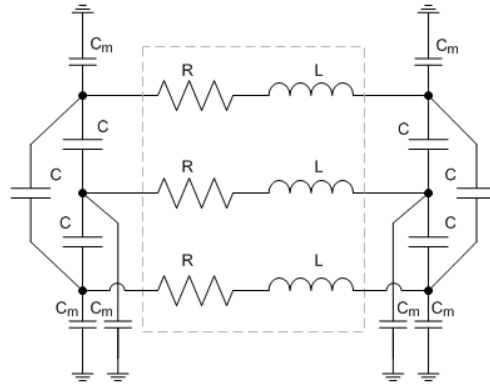


**Figure A.2: Coupled pi-equivalent model from PSCAD library.**

A 3-phase transmission line with possible return path through earth can be described by the following set of equations:

$$\begin{bmatrix} U^A \\ U^B \\ U^C \end{bmatrix} = \begin{bmatrix} R_a + R_e & R_e & R_e \\ R_e & R_a + R_e & R_e \\ R_e & R_e & R_a + R_e \end{bmatrix} \begin{bmatrix} I^A \\ I^B \\ I^C \end{bmatrix} + j \begin{bmatrix} X_{aa} & X_{ab} & X_{ac} \\ X_{ab} & X_{bb} & X_{bc} \\ X_{ac} & X_{bc} & X_{cc} \end{bmatrix} \begin{bmatrix} I^A \\ I^B \\ I^C \end{bmatrix} \quad (\text{A.1})$$

## Appendix A

The parameters can be calculated based on geometry shown in Figure A.3.

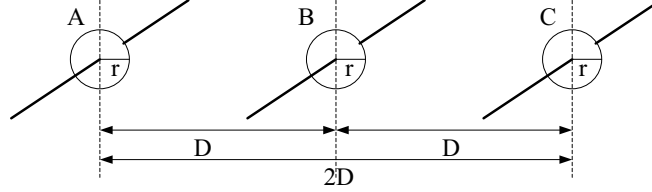


**Figure A.3: 3-phase plane suspension line.**

The mean distance between the three conductors shown in Figure A.3 is calculated in (A.2).  $D_g$  is “equivalent distance” to earth, and is calculated in (A.3). It represents the fact that the magnetic field created by the current also penetrates and distributes in the earth because of the non-ideal surface.

$$D_m = \sqrt[3]{D \cdot D \cdot 2D} = D \cdot \sqrt[3]{2} \quad (\text{A.2})$$

$$D_g = 1.31 \sqrt{\frac{2\rho}{\mu \cdot \omega}} = 660 \sqrt{\frac{\rho}{f}} \quad (\text{A.3})$$

The equations for calculating the parameters in (A.1) (except  $R_a$ ) are shown below:

$$R_e = \frac{1}{4} \mu f \pi \cdot 1000 = 0.049 \mu_0 \left( \frac{f}{50} \right) [\Omega/\text{km}] \quad (\text{A.4})$$

$$g = e^{-1/4} \cdot r = 0.7788 \cdot r \quad (\text{A.5})$$

$$X_{aa} = X_{bb} = X_{cc} = \mu_0 f \cdot \ln \left( \frac{D_g}{g} \right) = 0.063 \left( \frac{f}{50} \right) \ln \left( \frac{D_g}{g} \right) [\Omega/\text{km}] \quad (\text{A.6})$$

$$X_{ab} = X_{bc} = X_{ac} = \mu_0 f \cdot \ln \left( \frac{D_g}{D_m} \right) = 0.063 \left( \frac{f}{50} \right) \ln \left( \frac{D_g}{D_m} \right) [\Omega/\text{km}] \quad (\text{A.7})$$

### A.2.1 Positive sequence impedance

In the positive sequence system the three phases are  $120^\circ$  apart, as expressed by (A.8). By inserting this relation into (A.1), the expression for the positive sequence voltage becomes as shown in (A.9)

$$I^{B+} = h^2 I^{A+} \quad (\text{A.8})$$

$$I^{C+} = h I^{A+}$$

$$\begin{aligned} U^{A+} &= (R_a + R_e + jX_{aa}) I^{A+} + (R_e + jX_{ab}) I^{B+} + (R_e + jX_{ab}) I^{C+} \\ &= (R_a + (1+h^2+h)R_e + j(X_{aa} + (h^2+h)X_{ab})) I^{A+} \\ &= (R_a + j(X_{aa} - X_{ab})) I^{A+} \end{aligned} \quad (\text{A.9})$$

$$\text{Where } h = e^{j120^\circ} \text{ and } h^2 + h + 1 = 0$$

From (A.9), the positive sequence resistance and reactance are:

$$R^+ = R_a$$

$$X^+ = X_{aa} - X_{bc} = 0.063 \left( \frac{f}{50} \right) \ln \left( \frac{D_m}{g} \right) \quad (\text{A.10})$$

The positive sequence capacitance is equal to the operating capacitance ( $C_d$ ), and the positive sequence capacitive reactance is calculated from:

$$X_C^+ = \frac{1}{2\pi \cdot f \cdot C_d} \quad (\text{A.11})$$

For non-rotating components the negative sequence impedances are equal to the positive sequence impedances, and this applies to the line.

### A.2.2 Zero sequence impedance

In the zero sequence there is no phase displacement between the three phases (A.12). By inserting this relation into (A.1), the expression for the positive sequence voltage becomes as shown in (A.13).

$$I^A = I^B = I^C \quad (\text{A.12})$$

$$U^{A0} = (R_a + R_e + jX_{aa})I^{A0} + (R_e + jX_{ab})I^{B0} + (R_e + jX_{ab})I^{C0} \\ = (R_a + 3R_e + j(X_{aa} + 2X_{ab}))I^{A0} \quad (\text{A.13})$$

From (A.13), the zero sequence resistance and reactance are:

$$R^0 = R_a + 3R_e = R_a + 3 \cdot 0.049 \mu_r \left( \frac{f}{50} \right) \\ X^0 = X_{aa} + 2 \cdot X_{ab} = 0.063 \left( \frac{f}{50} \right) \ln \left( \frac{D_g^3}{g \cdot D_m^2} \right) \quad (\text{A.14})$$

The zero sequence capacitance is equal to the capacitance from phase to ground ( $C_g$ ), and the zero sequence capacitive reactance is calculated from:

$$X_C^0 = \frac{1}{2\pi \cdot f \cdot C_g} \quad (\text{A.15})$$

### A.2.3 Line data

Data for the conductor types used in the PSCAD line model are given in Table A.2, and general data for the line are given in Table A.3.

**Table A.2: Overhead line conductor data [1].**

Conductor type			R [Ω/km]	X [Ω/km]	C <sub>j</sub> [nF/km]	C <sub>d</sub> [nF/km]	I <sub>th</sub> [A]
FeAl	1X70	26/7	0.257	0.362	4.93	10.09	454
FeAl	1X50	6/1	0.359	0.373	4.85	9.79	362
FeAl	1X25	6/1	0.721	0.395	4.71	9.22	235
FeAl	1X16	6/1	1.126	0.409	4.62	8.89	171

**Table A.3: General data for plane suspension line without earth wire.**

D [m]	h [m]	ρ [Ω·m]
1.5	7	200

The earth resistivity is an assumed (guessed) value.

## A.3 Load modelling

The PSCAD master library has a fixed load component based on the static load model which was initially used in the simulation model:

$$S_L = P_L + jQ_L = P_L^{pre} \left( \frac{|U_L|}{|U_L^{pre}|} \right)^{NP} \cdot (1 + K_{PF} dF) + jQ_L^{pre} \left( \frac{|U_L|}{|U_L^{pre}|} \right)^{NQ} \cdot (1 + K_{QF} dF) \quad (\text{A.16})$$

It was observed from the simulations that when the coefficients NP and NQ were set to other values than 2, the voltages become distorted. It was assumed that the distortion of the voltage waves was caused by the fixed load component. Because of this, a new load module has been made. Typical values for the frequency dependency factors are  $K_{PF} = 0-3$  and  $K_{QF} = -2-0$  [80]. In the new load module loads are assumed to be independent of frequency variations ( $K_{PF}, K_{QF} = 0$ ). Voltage dependency factors for different load classes are shown in Table A.4 [80].

**Table A.4: Sample characteristics of different load classes.**

Load class	Power factor	NP	NQ
<b>Residential</b>			
<b>Summer</b>	0.9	1.2	2.9
<b>Winter</b>	0.99	1.5	3.2
<b>Commercial</b>			
<b>Summer</b>	0.85	0.99	3.5
<b>Winter</b>	0.9	1.3	3.1
<b>Industrial</b>	0.85	0.18	6.0

Some possible values for the voltage dependency factors for active power, NP, and reactive power, NQ, are shown in Table A.5 together with the corresponding load characteristics.

**Table A.5: Voltage dependency factors and load characteristics.**

NP, NQ	Load characteristics
0	Constant power
1	Constant current
2	Constant impedance

Constant current characteristic is used for the active power, and constant impedance characteristic is used for the reactive power.

### A.3.1 Load resistance and reactance

The load is modeled as star-coupled in the PSCAD-model. The load in each phase consists of a resistance and an inductance in parallel, and the size of the resistance and inductance can be controlled externally. Three-phase delta-coupled loads were shown in Figure 3.2. If it is assumed that the three phases are symmetric, as in (A.17), the expression given in (A.18) is found for the three-phase power of the load.

$$U_L^{AB} = U_L^{BC} = U_L^{CA} = U_{L,\Delta}$$

$$R_L^{AB} = R_L^{BC} = R_L^{CA} = R_{L,\Delta} \quad (\text{A.17})$$

$$X_L^{AB} = X_L^{BC} = X_L^{CA} = X_{L,\Delta}$$

$$S_L = P_L + jQ_L = 3 \cdot \frac{|U_{L,\Delta}|^2}{(Z_{L,\Delta})^*} = 3 \cdot \frac{|U_{L,\Delta}|^2}{\left( \frac{jR_{L,\Delta}X_{L,\Delta}}{R_{L,\Delta} + jX_{L,\Delta}} \right)^*} = 3 \cdot \left( \frac{|U_{L,\Delta}|^2}{R_{L,\Delta}} + j \frac{|U_{L,\Delta}|^2}{X_{L,\Delta}} \right) \quad (\text{A.18})$$

This means that for a given active and reactive 3-phase power, the corresponding resistance and reactance can be calculated. An example is shown in (A.19), with the apparent power

equal to 1 MVA, and the load power factor is 0.9.  $U_{L,\Delta}$  is the phase-to-phase voltage and is equal to 22 kV.

$$\begin{aligned} R_{L,\Delta} &= 3 \cdot \frac{|U_{L,\Delta}|^2}{P_L} = 3 \cdot \frac{(22 \text{ kV})^2}{0.9 \text{ MW}} = 1613.34 \ \Omega \\ X_{L,\Delta} &= 3 \cdot \frac{|U_{L,\Delta}|^2}{Q_L} = 3 \cdot \frac{(22 \text{ kV})^2}{\sqrt{1^2 - 0.9^2} \text{ MW}} = 3331.12 \ \Omega \end{aligned} \quad (\text{A.19})$$

### A.3.2 Some example characteristics

Constant current characteristics for the active power, NP = 1.

$$P_L = P_L^{nom} \left( \frac{|U_L|}{|U_L^{nom}|} \right)^1 \Rightarrow \frac{|U_L|^2}{R_L} = \frac{|U_L^{nom}|^2}{R_L^{nom}} \cdot \left( \frac{|U_L|}{|U_L^{nom}|} \right) \Rightarrow R_L = \frac{R_L^{nom}}{|U_L^{nom}|} \cdot |U_L| \quad (\text{A.20})$$

The active power of the load is modelled by a resistance that is varying proportional to the magnitude line-to-line voltage.

Constant impedance characteristics for the reactive power, NQ = 2.

$$Q_L = Q_L^{nom} \left( \frac{|U_L|}{|U_L^{nom}|} \right)^2 \Rightarrow \frac{|U_L|^2}{X_L} = \frac{|U_L^{nom}|^2}{X_L^{nom}} \cdot \left( \frac{|U_L|}{|U_L^{nom}|} \right)^2 \Rightarrow X_L = X_L^{nom} \quad (\text{A.21})$$

The reactive power of the load is modelled by a constant inductive reactance.

Constant active power characteristics, NP = 0.

$$P_L = P_L^{nom} \left( \frac{|U_L|}{|U_L^{nom}|} \right)^0 \Rightarrow \frac{|U_L|^2}{R_L} = \frac{|U_L^{nom}|^2}{R_L^{nom}} \Rightarrow R_L = \frac{|U_L|^2}{|U_L^{nom}|^2} R_L^{nom} \quad (\text{A.22})$$

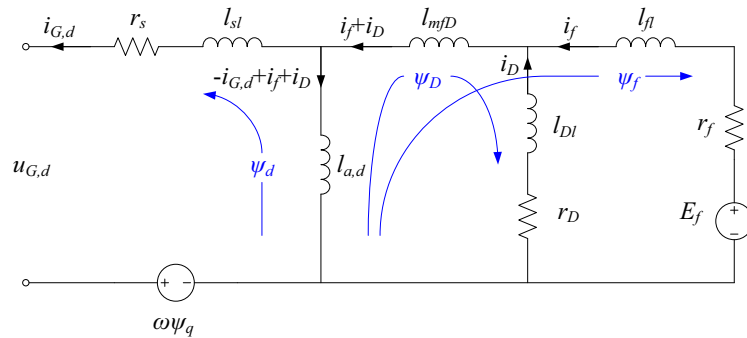
The active power of the load is modelled by a resistance proportional to the magnitude of the voltage across the load squared.

## B Appendix B - Synchronous generator equivalent circuits

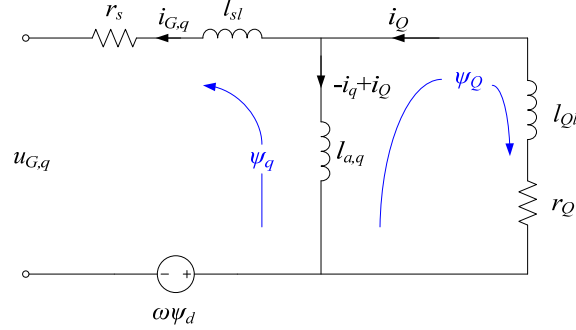
Generator modelling is based on equivalent circuits in the fictitious  $d$ - and  $q$ -axes. Equivalent circuits for the  $d$ - and  $q$ -axis circuits are shown in Figure B.1 and Figure B.2. Symbols are explained in Table B.1.

**Table B.1: Explanation of synchronous generator equivalent scheme parameters**

$u_{Gd}, u_{Gq}$	voltages across the fictitious $d$ - and $q$ -axis armature coils
$e_f$	field voltage referred to the fictitious $q$ -axis armature coil
$i_{Gd}, i_{Gq}$	currents flowing in the fictitious $d$ - and $q$ -axis armature coils
$i_f$	field current
$i_D, i_Q$	instantaneous $d$ - and $q$ -axis damper winding current
$\psi_d, \psi_q$	total $d$ - and $q$ -axis flux linkages
$\psi_D, \psi_Q$	total flux linkage of damper windings in the $d$ - and $q$ -axes
$\psi_f$	total flux linkage of the field winding
$l_{sl}$	stator leakage inductance
$r_s$	stator resistance
$l_{ad}, l_{aq}$	$d$ - and $q$ -axis common air-gap inductance
$l_{m/D}$	inductance between field winding and $d$ -axis damper winding
$l_{Dl}, l_{Ql}$	$d$ - and $q$ -axis damper winding leakage inductance
$r_D, r_Q$	$d$ - and $q$ -axis damper winding resistance
$l_{fl}$	field winding leakage inductance
$r_f$	field winding resistance
$x_0$	Zero sequence reactance
$T_d''$	Short circuit $d$ -axis subtransient time constant
$T_q''$	Short circuit $q$ -axis subtransient time constant



**Figure B.1: d-axis equivalent circuit.**


**Figure B.2: q-axis equivalent circuit.**

Referring to Figure B.1, expressions for the flux linkages in the  $d$ -axis are given in (B.1), and voltages in (B.2).

$$\begin{aligned}\psi_d &= -(l_{sl} + l_{a,d})i_{G,d} + l_{a,d}i_D + l_{a,d}i_f = -l_d i_{G,d} + l_{a,d}i_D + l_{a,d}i_f \\ \psi_D &= -l_{ad}i_{G,d} + (l_{Dl} + l_{mD} + l_{a,d})i_D + (l_{mD} + l_{a,d})i_f = -l_{a,d}i_{G,d} + l_D i_D + (l_{mD} + l_{a,d})i_f \\ \psi_f &= -l_{a,d}i_{G,d} + (l_{mD} + l_{a,d})i_D + (l_{fl} + l_{mD} + l_{a,d})i_f = -l_{a,d}i_{G,d} + (l_{mD} + l_{a,d})i_D + l_f i_f \\ u_{G,d} &= -r_s i_{G,d} + \frac{1}{\omega_b} \frac{d\psi_d}{dt} - \omega \psi_q \\ 0 &= r_D i_D + \frac{1}{\omega_b} \frac{d\psi_D}{dt} \\ e_f &= r_f i_f + \frac{1}{\omega_b} \frac{d\psi_f}{dt}\end{aligned}\quad (\text{B.2})$$

Referring to Figure B.2, expressions for the flux linkages in the  $q$ -axis are given in (B.3), voltages in (B.4).

$$\begin{aligned}\psi_q &= -(l_{sl} + l_{a,q})i_{G,q} + l_{a,q}i_Q = -l_q i_{G,q} + l_{a,q}i_Q \\ \psi_Q &= -l_{a,q}i_{G,q} + (l_{Ql} + l_{a,q})i_Q = -l_{a,q}i_{G,q} + l_Q i_Q \\ u_q &= -r_s i_q + \frac{1}{\omega_b} \frac{d\psi_q}{dt} + \omega \psi_d \\ 0 &= r_Q i_Q + \frac{1}{\omega_b} \frac{d\psi_Q}{dt}\end{aligned}\quad (\text{B.4})$$

In per unit  $\psi$  equals 1, and the reactance values are equal to the inductance values.

### B.1 Conversion between generator- and equivalent- format

Machine parameters are usually given as generator format data. This way of giving machine parameters is based on the partition into the stationary, transient and sub-transient time frames. The dynamics of the damper winding is assumed to be much faster than the transient dynamics of the field winding, due to their higher resistance. It is assumed that the field winding resistance can be neglected during the sub-transient period. No current is assumed to flow in the damper winding during the transient period.

The armature leakage reactance can be assumed to equal the zero sequence reactance, (B.5).  
 The armature resistance can be calculated from the negative sequence reactance and the armature winding time constant, (B.6).

$$x_{a,d} = x_d - x_{sl} \approx x_d - x_0 \quad (\text{B.5})$$

$$x_{a,q} = x_q - x_{sl} \approx x_q - x_0 \quad (\text{B.5})$$

$$r_s = \frac{1}{\omega_b T_a} \left( \frac{x_d'' + x_q''}{2} \right) = \frac{x_2}{\omega_b T_a} \quad (\text{B.6})$$

The transient  $d$ -axis open-circuit (a) and short circuit (b) equivalent circuits are shown in Figure B.3.

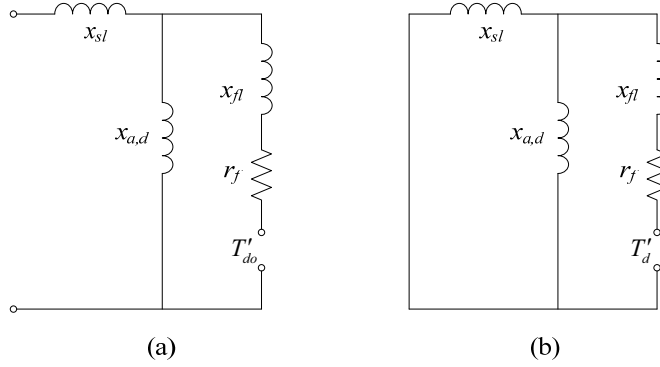


Figure B.3:  $d$ -axis open-circuit (a) and short circuit (b) equivalent circuits for the transient time.

From Figure B.3 (a) expressions for calculation of the field resistance and the field leakage reactance can be found:

$$T'_{do} = \frac{1}{\omega r_f} (x_{fl} + x_{a,d}) \Rightarrow r_f = \frac{1}{\omega T'_{do}} (x_{fl} + x_{a,d}) \quad (\text{B.7})$$

$$x'_d = x_{sl} + \frac{x_{a,d} x_{fl}}{x_{a,d} + x_{fl}} \Rightarrow x_{fl} = \frac{x_{a,d} (x'_d - x_{sl})}{x_{a,d} - (x'_d - x_{sl})} \quad (\text{B.8})$$

The following expression for the transient short circuit time constant is found from Figure B.3 (b):

$$T'_d = \frac{1}{\omega r_f} \left( x_{fl} + \frac{x_{a,d} x_{sl}}{x_{a,d} + x_{sl}} \right) \quad (\text{B.9})$$

The sub-transient  $d$ -axis open-circuit (a) and short circuit (b) equivalent circuits are shown in Figure B.4.

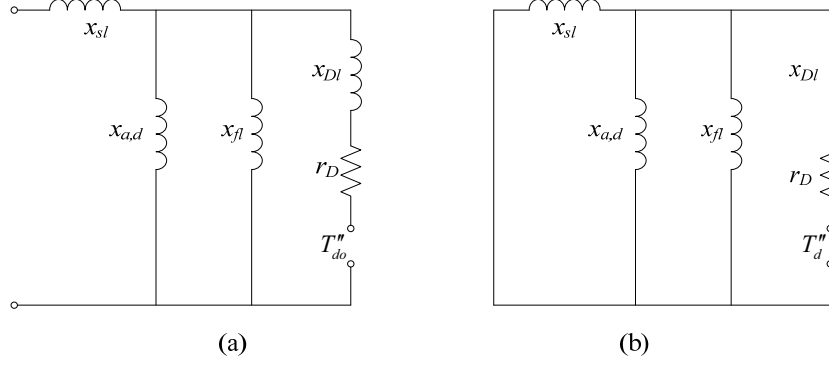


**Figure B.4: d-axis open-circuit (a) and short circuit (b) equivalent for the subtransient time.**

From Figure B.4 (a) expressions for calculating the  $d$ -axis damper winding resistance and leakage reactance are found:

$$T''_{do} = \frac{1}{\omega r_D} \left( x_{Dl} + \frac{x_{a,d} x_{fl}}{x_{a,d} + x_{fl}} \right) \quad (B.10)$$

$$\Rightarrow r_D = \frac{1}{\omega T''_{do}} \left( x_{Dl} + \frac{x_{a,d} x_{fl}}{x_{a,d} + x_{fl}} \right) = \frac{1}{\omega T''_{do}} (x_{Dl} + x'_d - x_{sl})$$

$$x''_d = x_{sl} + \frac{x_{a,d} x_{fl} x_{Dl}}{x_{a,d} x_{fl} + x_{a,d} x_{Dl} + x_{fl} x_{Dl}} \Rightarrow x_{Dl} = \frac{x_{a,d} x_{fl} (x''_d - x_{sl})}{x_{fl} x_{a,d} - (x''_d - x_{sl})(x_{a,d} + x_{fl})} \quad (B.11)$$

An expression for the subtransient short circuit time constant can be found from Figure B.4 (b):

$$T''_d = \frac{1}{\omega r_D} \left( x_{Dl} + \frac{x_{a,d} x_{sl} x_{fl}}{x_{a,d} x_{sl} + x_{a,d} x_{fl} + x_{sl} x_{fl}} \right) \quad (B.12)$$

The sub-transient  $q$ -axis open-circuit and short circuit equivalent circuits are shown in Figure B.5.

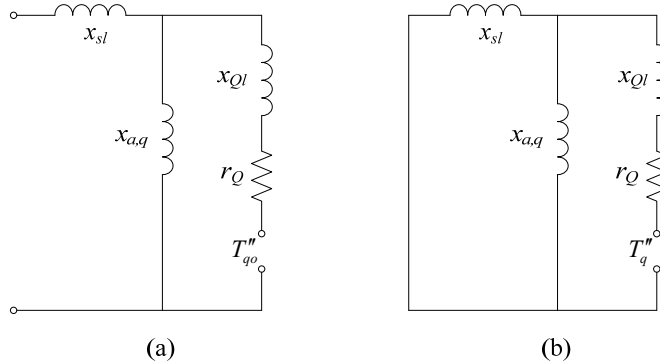


**Figure B.5: q-axis open-circuit (a) and short circuit (b) equivalent for the subtransient time.**

Expressions for calculating the  $q$ -axis damper winding resistance and leakage reactance are found from Figure B.5 (a):

$$T_{qo}'' = \frac{1}{\omega r_Q} (x_{a,q} + x_{Ql}) \Rightarrow r_Q = \frac{1}{\omega T_{qo}''} (x_{a,q} + x_{Ql}) \quad (\text{B.13})$$

$$x_q'' = x_{sl} + \frac{x_{a,q} x_{Ql}}{x_{a,q} + x_{Ql}} \Rightarrow x_{Ql} = \frac{x_{a,q} (x_q'' - x_{sl})}{x_{a,q} - (x_q'' - x_{sl})} \quad (\text{B.14})$$

An expression for the sub-transient short circuit time-constant is found from Figure B.5 (b):

$$T_q'' = \frac{1}{\omega r_Q} \left( x_{Ql} + \frac{x_{a,q} x_{sl}}{x_{a,q} + x_{sl}} \right) \quad (\text{B.15})$$

## B.2 Calculation of steady-state emf

$$I_G^{pre} = \left( \frac{S_G^{pre}}{U_G^{pre}} \right)^* = \frac{3 \angle 0^\circ}{1} = 0.84 \angle 0^\circ \text{ [pu]} \quad (\text{B.16})$$

$$E_{GQ}^{pre} = U_G^{pre} + jx_q I_G^{pre} = 1 + j1.4 \cdot 0.84 = 1 + j1.176 = 1.5437 \angle 49.6 \quad (\text{B.17})$$

$$U_{G,d}^{pre} = -U_G^{pre} \sin \delta_G^{pre} = -1 \cdot \sin(49.6) = -0.7615 \quad (\text{B.18})$$

$$U_{G,q}^{pre} = U_G^{pre} \cos \delta_G^{pre} = 1 \cdot \cos(49.6) = 0.6481$$

$$I_{G,d}^{pre} = -I_G^{pre} \sin(\delta_G^{pre} + \varphi_G^{pre}) = -0.84 \cdot \sin(49.6) = -0.6397 \quad (\text{B.19})$$

$$I_{G,q}^{pre} = I_G^{pre} \cos(\delta_G^{pre} + \varphi_G^{pre}) = 0.84 \cdot \cos(49.6) = 0.5444$$

$$\begin{aligned} E_f &= E_{G,q}^{pre} = U_{G,q}^{pre} + r_s I_{G,q}^{pre} + x_d I_{G,d}^{pre} \\ &= 0.6481 + (0.0064 \cdot 0.5444) + (2 \cdot 0.6397) = 1.931 \end{aligned} \quad (\text{B.20})$$

PSCAD simulations confirm that the steady-state emf with nominal active power and zero reactive power is approximately 1.93 pu.

## B.3 Calculation of transient short circuit capacity

$$I_G^{nom} = \left( \frac{S_G^{nom}}{U_G^{nom}} \right)^* = 1 \angle \cos(0.84) = 1 \angle -32.9^\circ \text{ [pu]} \quad (\text{B.21})$$

$$E_{GQ}^{nom} = U_G^{nom} + jx_q I_G^{nom} = 1 + (1.4 \angle 90^\circ \cdot 1 \angle -32.86^\circ) = 2.116 \angle 33.8^\circ \quad (\text{B.22})$$

$$U_{G,d}^{nom} = -U_G^{nom} \sin \delta_G^{nom} = -1 \cdot \sin(33.8) = -0.5563 \quad (\text{B.23})$$

$$U_{G,q}^{nom} = U_G^{nom} \cos \delta_G^{nom} = 1 \cdot \cos(33.8) = 0.8310$$

$$I_{G,d}^{nom} = -1 \cdot \sin(66.7) = -0.9184 \quad (\text{B.24})$$

$$I_{G,q}^{nom} = 1 \cdot \cos(66.7) = 0.3955$$

Then the transient internal emfs can be calculated as follows

$$\begin{aligned} E_d^{nom} &= U_{G,d}^{nom} + x'_q I_{G,q}^{nom} = -0.5563 + (1.4 \cdot 0.3955) = -0.0026 \\ E_q^{nom} &= U_{G,q}^{nom} - x'_d I_{G,d}^{nom} = 0.8310 - (0.22 \cdot (-0.9184)) = 1.0330 \end{aligned} \quad (B.25)$$

The d-axis transient emf is negligible, and the transient short circuit capacity of the generator can be expressed as a function of the q-axis transient emf only:

$$\begin{aligned} S'_{G,sc} &\approx \frac{(E_q^{nom})^2}{x'_d} = \frac{(1.033)^2}{0.22} = 4.850 \text{ [pu]} \\ &\Rightarrow 4.850 \cdot 3.57 = 17.3 \text{ [MVA]} \end{aligned} \quad (B.26)$$

Calculations of the short circuit (s.c.) capacities for the generator transformer and the resultant short circuit capacity on the 22 kV side of the transformer are shown below:

$$S_{GT,sc} = \frac{(U_{GT}^{nom})^2}{Z_{GT,sc}} = \frac{(U_{GT}^{nom})^2}{z_{sc} \cdot (U_{GT}^{nom})^2 / S_n} = \frac{S_{GT}^{nom}}{z_{sc}} = \frac{3.6}{0.075} = 48 \text{ [MVA]} \quad (B.27)$$

$$S_{G22kV,sc} = \frac{1}{1/S'_{G,sc} + 1/S_{GT,sc}} = \frac{S'_{G,sc} \cdot S_{GT,sc}}{S'_{G,sc} + S_{GT,sc}} = \frac{17.3 \cdot 48}{17.3 + 48} = 12.7 \text{ [MVA]} \quad (B.28)$$

#### B.4 Phasor diagram for generator with round rotor

A phasor diagram for a generator with round rotor is shown in Figure B.6.

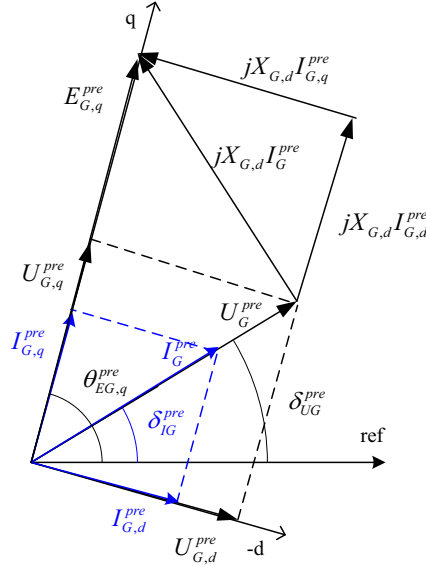
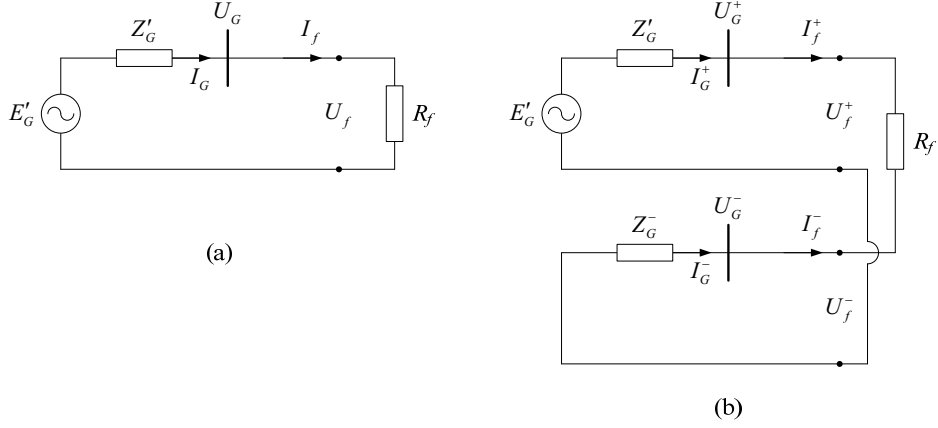


Figure B.6: Phasor-diagram for the DG-unit, in the pre-fault state. Generator with round rotor.

#### B.5 Phase-to-phase short circuit at generator terminals

The equations for calculation of short circuit currents with phase-to-phase faults at the generator terminals can be deduced from the circuits shown in Figure B.7.



**Figure B.7: Equivalent circuit for (a) three-phase short circuit and (b) two-phase short circuit at generator terminals.**

Equation for three-phase short circuit:

$$I_G = \frac{E'_G}{Z'_G + R_f} \quad (\text{B.29})$$

Equation for two-phase short circuit between phase *B* and *C*:

$$\begin{aligned} I_G^+ &= \frac{E'_G}{Z'_G + Z_G^- + R_f} = -I_G^- \\ \Rightarrow I_G^B &= h(hI_G^+ + I_G^-) = h(h-1)I_G^+ = -j\sqrt{3}I_G^+ = \frac{-j\sqrt{3}E'_G}{Z'_G + Z_G^- + R_f} \\ \Rightarrow I_G^C &= h(I_G^+ + hI_G^-) = h(1-h)I_G^+ = j\sqrt{3}I_G^+ = \frac{j\sqrt{3}E'_G}{Z'_G + Z_G^- + R_f} \end{aligned} \quad (\text{B.30})$$

## C Appendix C - Distance-to-fault estimation

### C.1 RMS phasor calculation

The protection and fault localization algorithms require voltage- and current- phasors as inputs. Different ways to obtain the phasors have been explored. Some instantaneous- and phasor- values of the DG-current are plotted in Figure C.1 and Figure C.2. The currents are measured on the 6.6 kV side of the DG-transformer, and the fault is located directly on the 22 kV side of the transformer or 5 km away from the DG-connection point.

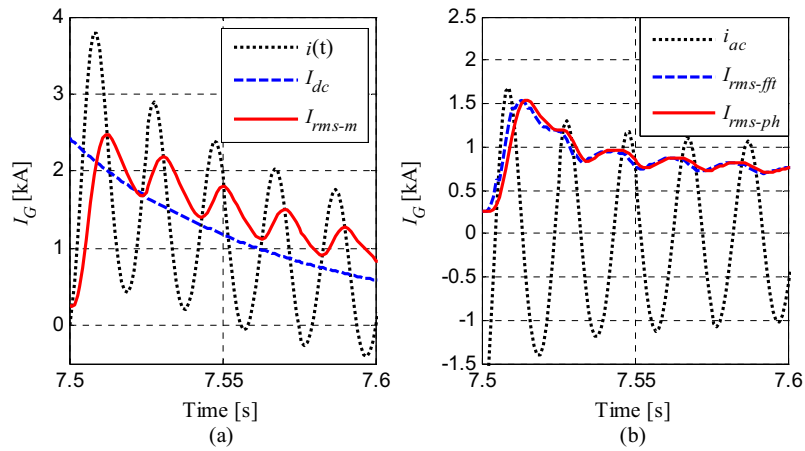


Figure C.1: DG-current for a 3-phase short circuit on the 22 kV side of the generator transformer.

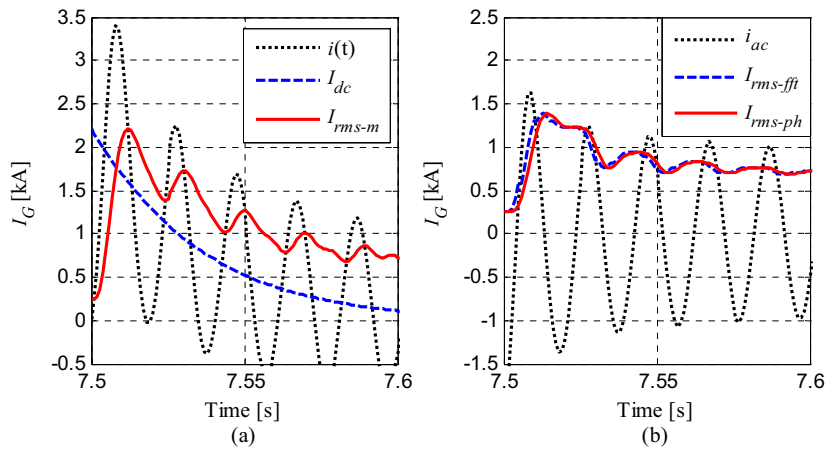


Figure C.2: DG-current for a 3-phase short circuit 5 km away from the DG-connection point on 22 kV level.

Where plotted currents are:

- $i(t)$  - instantaneous value of short circuit current
- $I_{dc}$  - dc-component calculated in Matlab.
- $I_{rms-m}$  - RMS current from the RMS-meter-block in PSCAD.

## Appendix C

$i_{ac}$  - instantaneous value of the short circuit current after the dc-component is removed,  
 $i_{ac} = i(t) - i_{dc}$   
 $I_{rms,fft}$  - RMS value calculated from the FFT-block in PSCAD  
 $I_{rms-ph}$  -RMS value of phasor obtained from fundamental Fourier coefficients calculated in Matlab using a moving time window, as explained in [104].

From the two (a) figures it can be seen that the value obtained from the RMS-meter component in PSCAD is the RMS value of the total current including the dc-component, so it is not convenient to use for protection purposes. The RMS-values calculated with Fourier coefficients and a moving window is very similar FFT-component in PSCAD, as seen in the two (b) figures. Due to this it was chosen to use to FFT-component in PSCAD to obtain RMS phasor values throughout the thesis.

The RMS-value contains ripple in the transient state, and it could be smoothed using a low-pass filter.

### **C.2 Conversion from estimated impedance to distance**

A flow chart for calculating the distance to the fault location from the estimated impedance is shown in Figure C.3. The flow chart is based on a fault on the feeder introduced in Figure 3.1. The estimated impedance to the fault location,  $Z_{in}$ , is input to the algorithm, while the corresponding distance to the fault location,  $d_{out}$ , is the output.

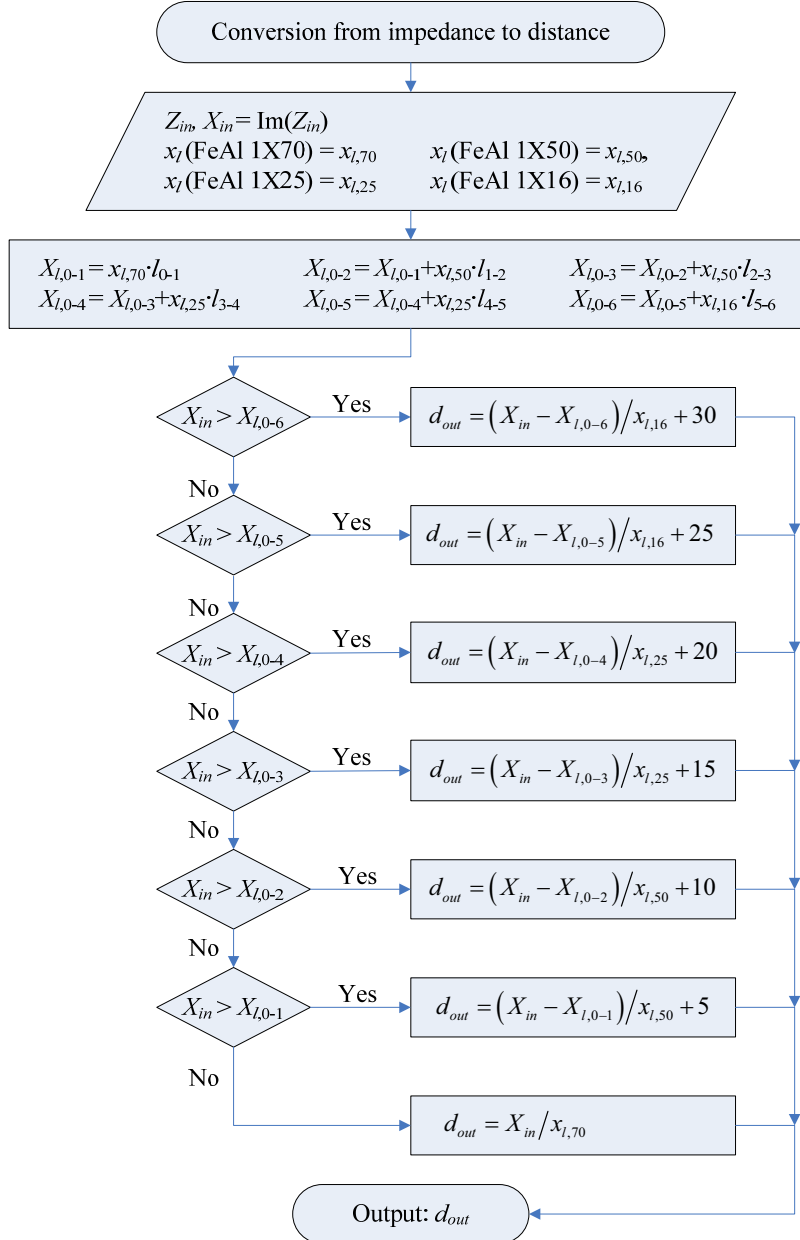


Figure C.3: Flow chart for calculation of distance to fault location from an estimated distance.

### C.3 Impedance to the location of a 2-phase short circuit

The three-phase circuit for a phase-to-phase short circuit between phase *B* and *C* is shown in Figure C.4. The series impedance is the positive sequence impedance of the line.

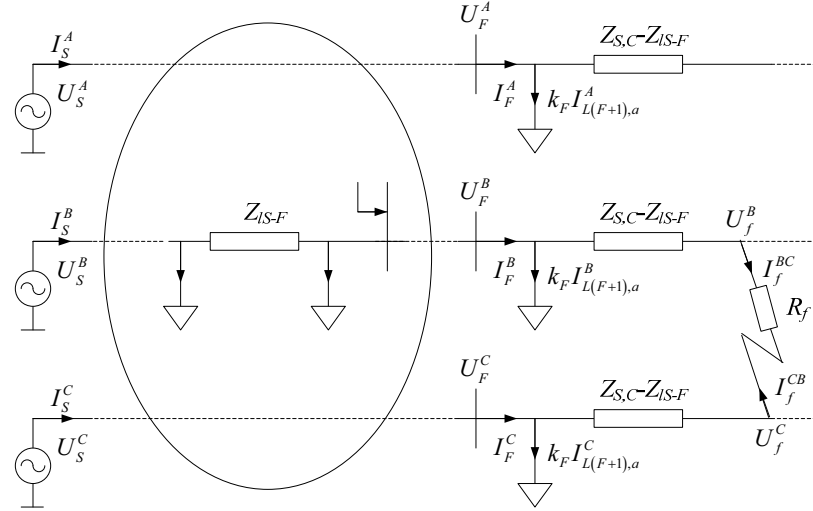


Figure C.4: Equivalent circuit for 2-phase short circuit between phase B and C.

The line impedance  $Z_{IS-F}$  is equal in all three phases, and is the sum of the line impedances in all sections between the substation and node  $F$ . The fault currents in phase B and C are equal, but opposite in direction:

$$I_f^{BC} = -I_f^{CB}$$

$$\Rightarrow h^2 I_f^+ + h I_f^- + I_f^0 = -(h I_f^+ + h^2 I_f^- + I_f^0) \quad (C.1)$$

$$\Rightarrow I_f^+ + I_f^- = 2I_f^0$$

$$\text{Where } h = e^{j\frac{2\pi}{3}}$$

The fault current in phase A is zero:

$$I_f^A = I_f^+ + I_f^- + I_f^0 = 0 \Rightarrow I_f^0 = 0 \quad (C.2)$$

And consequently:

$$I_f^+ + I_f^- = 0 \Rightarrow I_f^- = -I_f^+ \quad (C.3)$$

The voltages in phase B and C are related the following way:

$$U_f^B - \frac{R_f}{2} I_f^{BC} = U_f^C - \frac{R_f}{2} I_f^{CB}$$

$$\Rightarrow (h^2 U_f^+ + h U_f^-) - \frac{R_f}{2} (h^2 I_f^+ + h I_f^-)$$

$$= (h U_f^+ + h^2 U_f^-) - \frac{R_f}{2} (h I_f^+ + h^2 I_f^-) \quad (C.4)$$

$$\Rightarrow U_f^+ - U_f^- = \frac{R_f}{2} \cdot (I_f^+ - I_f^-)$$

The symmetrical component circuit for this type of fault is shown in Figure C.5. The line impedance is equal in the positive and the negative sequence systems.

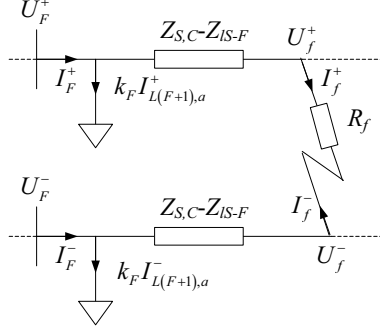


Figure C.5: Sequence network for short circuit between phase B and C.

As a simplification, the loads are neglected in the following calculations. The fault location voltage in (C.4) can be expressed by substation voltage and current:

$$\begin{aligned}
 U_f^+ - U_f^- &= \frac{R_f}{2} \cdot (I_f^+ - I_f^-) \\
 &= \left( U_F^+ - (Z_{S,C} - Z_{IS-F}) (I_F^+ - k_F I_{L(F+1),a}^+) \right) \\
 &\quad - \left( U_F^- - (Z_{S,C} - Z_{IS-F}) (I_F^- - k_F I_{L(F+1),a}^-) \right) \\
 \Rightarrow Z_{S,C} &= Z_{IS-F} + \frac{U_{F,+} - U_{F,-}}{I_F^+ - I_F^- - k_F (I_{L(F+1),a}^+ - I_{L(F+1),a}^-)} \\
 &\quad - \frac{R_f}{2} \cdot \frac{I_f^+ - I_f^-}{I_F^+ - I_F^- - k_F (I_{L(F+1),1+} - I_{L(F+1),1-})}
 \end{aligned} \tag{C.5}$$

The line impedance is equal in the positive and negative sequence system since it is not a rotating component:  $Z_{l1}^+ = Z_{l1}^-$ .

It is desirable to express the compensated impedance as a function of phase-quantities instead of sequence components. The conversion is done using the following relations:

$$\begin{aligned}
 U^+ - U^- &= \frac{1}{3} (U^A + hU^B + h^2U^C) - \frac{1}{3} (U^A + h^2U^B + hU^C) = \frac{h(1-h)}{3} (U^B - U^C) \\
 I^+ - I^- &= \frac{1}{3} (I^A + hI^B + h^2I^C) - \frac{1}{3} (I^A + h^2I^B + hI^C) = \frac{h(1-h)}{3} (I^B - I^C)
 \end{aligned} \tag{C.6}$$

The equation for the compensated impedance then becomes:

$$\begin{aligned}
 Z_{S,C} &= Z_{IS-F} + \frac{(U_F^B - U_F^C)}{(I_F^B - I_F^C) - k_F (I_{L(F+1),a}^B - I_{L(F+1),a}^C)} \\
 &\quad - \frac{R_f}{2} \cdot \frac{(I_f^{BC} - I_f^{CB})}{(I_F^B - I_F^C) - k_F (I_{L(F+1),a}^B - I_{L(F+1),a}^C)} \\
 &= Z_{IS-F} + \frac{\Delta U_F}{\Delta I_F - k_F \Delta I_{L(F+1),a}} - \frac{R_f}{2} \cdot \frac{\Delta I_f}{\Delta I_F - k_F \Delta I_{L(F+1),a}}
 \end{aligned} \tag{C.7}$$

The equation is also valid for faults between phase A and B, and between phase C and A.

For a short circuit fault, the fault resistance is an arc resistance. To avoid impact from the fault resistance on the distance estimate, the reactance part of the impedance ( $X_{S,C}$ ) is commonly utilized for distance estimation.

$$\begin{aligned} X_{S,C} &= \text{Im} \left( Z_{IS-F} + \frac{\Delta U_F}{\Delta I_F - k_F \Delta I_{L(F+1),a}} - \frac{R_f}{2} \cdot \frac{\Delta I_f}{\Delta I_F - k_F \Delta I_{L(F+1),a}} \right) \\ &= X_{IS-F} + \text{Im} \left( \frac{\Delta U_F}{\Delta I_F - k_F \Delta I_{L(F+1),a}} \right) - \frac{R_f}{2} \cdot \text{Im} \left( \frac{\Delta I_f}{\Delta I_F - k_F \Delta I_{L(F+1),a}} \right) \end{aligned} \quad (\text{C.8})$$

The last term proportional to  $R_f$  may have an imaginary part if there is a phase shift between the currents  $\Delta I_f$  and  $(\Delta I_F - k_F \Delta I_{L(F+1),a})$ . In this case the fault impedance appears to have an imaginary part, and may have some impact on the distance estimation based on the reactance. Still, the fault resistance term is neglected in all calculations of the compensated impedance here.

#### C.4 Impedance to the location of a three-phase short circuit

The three-phase circuit for a three-phase short circuit is shown in Figure C.6.

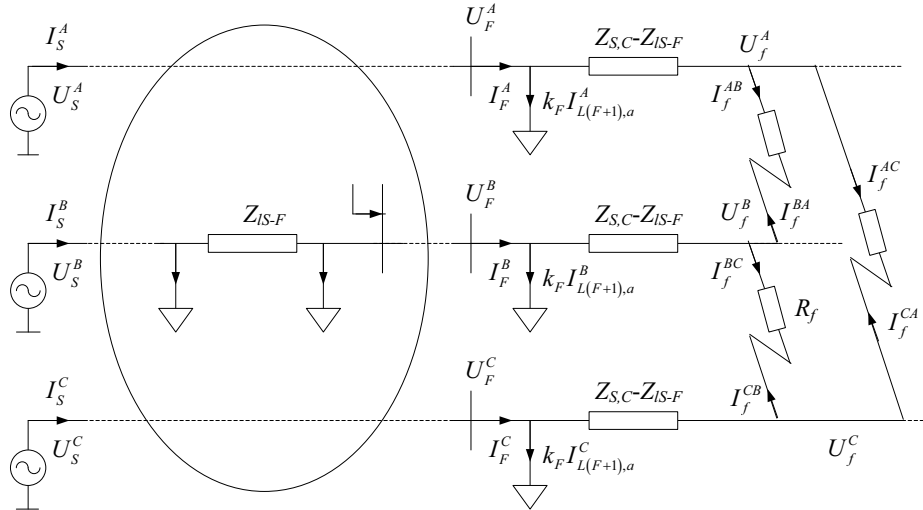


Figure C.6: Equivalent circuit for 3-phase short circuit.

The three-phase short circuit is a symmetrical fault, and only the positive sequence circuit is active. The positive sequence components are equal to the phase components during normal operation. The voltages in the fault location in phase B and C is expressed by:

$$\begin{aligned} U_F^B - (Z_{S,C} - Z_{IS-F})(I_F^B - k_F I_{L(F+1),a}^B) &= U_f^B \\ U_F^C - (Z_{S,C} - Z_{IS-F})(I_F^C - k_F I_{L(F+1),a}^C) &= U_f^C \end{aligned} \quad (\text{C.9})$$

By looking at the voltage drop across the fault resistance between phase B and C, the following expression for the compensated impedance to the fault location can be found:

## Appendix C

$$\begin{aligned}
U_f^B - \frac{R_f}{2} I_f^{BC} &= U_f^C - \frac{R_f}{2} I_f^{CB} \\
\Rightarrow U_F^B - (Z_{S,C} - Z_{IS-F}) (I_F^B - k_F I_{L(F+1),a}^B) - \frac{R_f}{2} I_f^{BC} \\
&= U_F^C - (Z_{S,C} - Z_{IS-F}) (I_F^C - k_F I_{L(F+1),a}^C) - \frac{R_f}{2} I_f^{CB} \\
\Rightarrow Z_{S,C} &= Z_{IS-F} + \frac{U_F^B - U_F^C}{I_F^B - I_F^C - k_F (I_{L(F+1),a}^B - I_{L(F+1),a}^C)} \\
&- \frac{R_f}{2} \cdot \frac{I_f^{BC} - I_f^{CB}}{I_F^B - I_F^C - k_F (I_{L(F+1),a}^B - I_{L(F+1),a}^C)} \\
&= Z_{IS-F} + \frac{\Delta U_F}{\Delta I_F - k_F \Delta I_{L(F+1),a}} - \frac{R_f}{2} \cdot \frac{\Delta I_f}{\Delta I_F - k_F \Delta I_{L(F+1),a}}
\end{aligned} \tag{C.10}$$

The calculations can be done with phase *A*- and *B*- or phase *C*- and *A*- quantities instead, and the result will be the same in all cases. The equation is equal to the one for two-phase short circuits in (C.7). Thus the same equation can be used for calculation of the compensated distance estimate for both two-phase and three-phase short circuits.

### C.5 Pre-fault load estimation on a single feeder section

The pre-fault load in a single feeder section can be estimated from the following equations. The starting point is (5.12).

$$\begin{aligned}
\Rightarrow |U_n^{pre}|^2 &= \left( U_{n-1}^{pre} - Z_{ln} \left( I_{n-1}^{pre} - \left( \frac{S_{Ln,a}^{pre}}{U_{n-1}^{pre}} \right)^* \right) \right) \cdot \left( U_{n-1}^{pre} - Z_{ln} \left( I_{n-1}^{pre} - \left( \frac{S_{Ln,a}^{pre}}{U_{n-1}^{pre}} \right)^* \right) \right)^* \\
\Rightarrow |S_{Ln,a}^{pre}|^2 &+ \left( \left( \frac{U_{n-1}^{pre}}{Z_{ln}} - I_{n-1}^{pre} \right) (U_{n-1}^{pre})^* \cdot e^{j\phi_{Ln}^{pre}} + \left( \frac{U_{n-1}^{pre}}{Z_{ln}} - I_{n-1}^{pre} \right)^* U_{n-1}^{pre} \cdot e^{-j\phi_{Ln}^{pre}} \right) |S_{Ln,a}^{pre}| \\
&+ \left( \frac{U_{n-1}^{pre}}{Z_{ln}} - I_{n-1}^{pre} \right) (U_{n-1}^{pre})^* \cdot \left( \frac{U_{n-1}^{pre}}{Z_{ln}} - I_{n-1}^{pre} \right)^* U_{n-1}^{pre} - \frac{|U_n^{pre}|^2 |U_{n-1}^{pre}|^2}{|Z_{ln}|^2} = 0 \\
\Rightarrow |S_{Ln,a}^{pre}|^2 &+ (K_n + K_n^*) |S_{Ln,a}^{pre}| + K_n K_n^* - \frac{|U_{n-1}^{pre}|^2 |U_n^{pre}|^2}{|Z_{ln}|^2} = 0
\end{aligned} \tag{C.11}$$

Here the complex constant  $K_n$  has been introduced for simplification. The constant can be expressed as a function of the angle between the voltage and current phasors in node *n*-1. Thus the phasor angles of the voltage and current are not required.

$$K_n = \left( \frac{U_{n-1}^{pre}}{Z_{ln}} - I_{n-1}^{pre} \right) (U_{n-1}^{pre})^* \cdot e^{j\phi_{Ln}^{pre}} = \left( \frac{|U_{n-1}^{pre}|}{Z_{ln}} - |I_{n-1}^{pre}| \cdot e^{-j\phi_{n-1}^{pre}} \right) |U_{n-1}^{pre}| \cdot e^{j\phi_{Ln}^{pre}} \tag{C.12}$$

The solution of second order equation is found from:

Appendix C

$$\begin{aligned}
 |S_{Ln,a}^{pre}| &= -\frac{K_n + K_n^*}{2} \pm \sqrt{\left(\frac{K_n + K_n^*}{2}\right)^2 - K_n K_n^* + \frac{|U_{n-1}^{pre}|^2 |U_n^{pre}|^2}{|Z_{ln}|^2}} \\
 &= -\operatorname{Re}(K_n) \pm \sqrt{-(\operatorname{Im}(K_n))^2 + \frac{|U_{n-1}^{pre}|^2 |U_n^{pre}|^2}{|Z_{ln}|^2}}
 \end{aligned}$$